THE UNIVERSITY *of* EDINBURGH

The regulation of endometrial regeneration; mechanisms contributing to repair and restoration of tissue integrity following menses

Fiona Lyndsay Cousins

Medical Research Council

Centre for Reproductive Health

The Queen's Medical Research Institute

47 Little France Crescent

Edinburgh, EH16 4TJ

Thesis submitted to the University of Edinburgh for the degree of Doctor of Philosophy

September 2013

Declaration

This thesis was composed by the author and the studies presented in this thesis were the unaided work of the author, except where acknowledgement is made by reference. The work described in thesis has not been previously accepted for, or is currently being submitted for another qualification.

Fiona Cousins

September 2013.

Acknowledgements

I cannot have had a better supervisor than Professor Philippa Saunders, and I can't thank you enough for your support, patience, guidance and most of all your endless enthusiasm for my PhD project, especially on those occasions when I had none. Thank you for giving me the opportunity to be part of such a great team. Thank you to my second supervisor Professor Hilary Critchley for your input and encouragement over the last three years.

A big part of my PhD was spent in the Animal House and my time there was made easier by the presence of Alison Murray. I will forever be indebted to you, not only for teaching me all I'll ever need to know about mice, but for being a constant source of encouragement and enthusiasm when things didn't go quite right, in and outside of work. Thank you for picking me up and keeping me going.

The Saunders Lab group are a fantastic group of people to be around on a daily basis; Frances Collins, Arantza Esnal, James Martin, Erin Greaves, Douglas Gibson and Yannis Simitsidellis, I thank each and every one of you for all your support over the last three years whether it be technical support, scientific input or just providing me with a bank of great memories.

I would like to acknowledge the technical help of Forbes Howie, as well as Mike Millar who carried out the automated immunohistochemistry. Thank you to Jessica Scanlon who carried out qRTPCR for some of the candidate genes. Thank you to all the staff in the animal unit.

To the other PhD students/postdocs/staff that have been part of the CRH during my time here, thanks for being a supportive and understanding group! To the girls who started with me; Karen Kilcoyne, Fiona Connolly and Lorraine Frew, thank you for the laughs and most of all the fun away from the lab. A big thank you goes to my officemates, Karen and Doug, without you two my PhD would have been a hell of a lot harder. Thank you for everything, your support and friendship has been incredible.

I'd like to thank my family for their continued support; they might not have always understood what it was I did or why my moods were almost always governed by how well my science was going, but they dealt with my ups and downs as best as they could. Thank you to the Inverleith HC Ladies 1s for giving me a reason to leave the lab and for all the fun and laughter over the years. Finally, to the girls; Savannah, Katie, Kat, Lyn, Laura, Moira and Mhairi who have been behind me every step of the way, pushing me towards the end point, I can't thank you enough for everything you have done for me.

I would like to dedicate this thesis to the memory of Dr. Sarju Patel, who sadly passed away before I even began my PhD. Whilst I was still an undergraduate, Sarj told me I should do a PhD as it would be the best thing I would ever do. Perhaps, in time, I might just agree with him.

Abstract

The human endometrium is a dynamic, multi-cellular tissue that lines the inside of the uterine cavity. During a woman's reproductive lifespan the endometrium is subjected to cyclical episodes of proliferation, angiogenesis, differentiation/decidualisation, shedding (menstruation), repair and regeneration in response to fluctuating levels of oestrogen and progesterone secreted by the ovaries. The endometrium displays unparalleled, tightly regulated, tissue remodelling resulting in a healed, scar-free tissue following menses or parturition. Mechanisms responsible for initiation of menses have been well documented: following progesterone withdrawal there is an increase in inflammatory mediators, focal hypoxia and induction and activation of matrix-degrading enzymes. In contrast, the molecular and cellular changes responsible for rapid, regulated, tissue repair at a time when oestrogen and progesterone are low are poorly understood.

Histological studies using human menstrual phase endometrium have revealed that tissue destruction and shedding occur in close proximity to re-epithelialisation/repair. It has been proposed that re-epithelialisation involves proliferation of glandular epithelial cells in the remaining basal compartment; there is also evidence for a contribution from the underlying stroma. A role for androgens in the regulation of apoptosis of endometrial stromal cells has been proposed but the impact of androgens on tissue repair has not been investigated. Studies using human xenografts and primates have been used to model some aspects of the impact of progesterone withdrawal but simultaneous shedding (menses) and repair have not been modelled in mice; the species of choice for translational biomedical research.

In the course of the studies described in this thesis, the following aims have been addressed:

1. To establish a model of menses in the mouse which mimics menses in women, namely; simultaneous breakdown and repair, overt menstruation, immune cell influx, tissue necrosis and re-epithelialisation.
2. To use this model to determine if the stromal cell compartment contributes to endometrial repair.
3. To examine the impact of androgens on the regulation of menses (shedding) and repair.

An informative mouse model of endometrial breakdown that was characterised by overt menses, as well as rapid repair, was developed. Immunohistological evidence for extensive tissue remodelling including active angiogenesis, transient hypoxia, epithelial cell-specific proliferation and re-epithelialisation were obtained by examining uterine tissues recovered

during an “early window of breakdown and repair” (4 to 24 hours after progesterone withdrawal). Novel data included identification of stromal cells that expressed epithelial cell markers, close to the luminal surface following endometrial shedding, suggesting a role for mesenchymal to epithelial transition (MET) in re-epithelialisation of the endometrium. In support of this idea, array and qRTPCR analyses revealed dynamic changes in expression of mRNAs encoded by genes known to be involved in MET during the window of breakdown and repair. Roles for hypoxia and tissue-resident macrophages in breakdown and tissue remodelling were identified.

Treatment of mice with dihydrotestosterone to mimic concentrations of androgens circulated in women at the time of menses had an impact on the timing and duration of endometrial breakdown. Array analysis revealed altered expression of genes implicated in MET and angiogenesis/inflammation highlighting a potential, previously unrecognised role for androgens in regulation of tissue turnover during menstruation.

In summary, using a newly refined mouse model new insights were obtained, implicating androgens and stromal MET in restoration of endometrial tissue homeostasis during menstruation. These findings may inform development of new treatments for disorders associated with aberrant repair such as heavy menstrual bleeding and endometriosis.

Papers relating to this thesis

Cousins FL, Murray A, Esnal A, Gibson DA, Critchley HOD, Saunders PTK. (2014) **Evidence from a Mouse Model That Epithelial Cell Migration and Mesenchymal-Epithelial Transition Contribute to Rapid Restoration of Uterine Tissue Integrity during Menstruation.** *PLoS ONE* **9**(1): e86378. doi:10.1371/journal.pone.0086378

Presentations relating to this thesis

Endometrial repair and regeneration: Studies in a mouse model (1). Poster presented at the Centre for Reproductive Health, QMRI Open Day, Edinburgh, November 2011.

Endometrial repair and regeneration: Studies in a mouse model (2). Poster presented at the Society for Gynaecologic Investigation (SGI) 59th Annual Scientific Meeting, San Diego, USA, March 2012.

Regulation of VEGF by hypoxia during endometrial breakdown and early regeneration in a mouse model of menstruation. Oral presentation at the Society for Reproduction and Fertility (SRF) Annual Meeting, Edinburgh, July 2012.

A role for androgens during endometrial breakdown and early regeneration in a mouse model of menstruation. Poster presented at the Society for Gynaecologic Investigation (SGI) 60th Annual Scientific Meeting, Orlando, Florida, USA, March 2013.

Re-establishment of endometrial integrity following menses- studies in a mouse model. Invited speaker at the endometrial satellite at the Society for Gynaecologic Investigation (SGI) 61st Annual Scientific Meeting, Florence, Italy, March 2014.

Table of Contents

List of Figures

List of Supplementary Figures

List of Tables

List of Supplementary Tables

Abbreviations

8-Br-cAMP	8-bromoadeosine 3'-5'-cyclic adenosine monophosphate
A	androstenedione
Ab	antibody
AF	activation function
Amhr	anto mullerian hormone receptor
Angpt1/2	Angiopoietin 1/2
ANOVA	Analysis of Variance
AP	alkaline phosphatase
Ap-1	activator protein-1
AR/*Ar*	androgen receptor
ARE	androgen response element
BL	basal layer
bp	base pairs
BrdU	bromodeoxyuridine
BSA	bovine serum albumin
cAMP	adenosine 3',5'-cyclic monophosphate
CD31	cluster of differentiation 31/ Platelet endothelial cell adhesion molecule
CD146	cluster of differentiation 146
cDNA	complementary DNA
COX-1/2	cyclooxygenase
CSF-1	colony stimulating factor
c-fms	colony stimulating factor
CSFCS	charcoal stripped foetal calf serum
Ct	cycle threshold
CV	coefficient of variation
CXC/CXCL	chemokine
CYP11A1	cholesterol side chain cleavage cytochrome P450, family 11, subfamily A, polypeptide 1/ P450scc
CYP17	cholesterol side chain cleavage cytochrome P450, family 17, subfamily A, polypeptide 1/ 17α hydroxylase/ C17-20 lyase cytochrome P450
CYP19	cholesterol side chain cleavage cytochrome P450, family 19, subfamily A, polypeptide 1/ aromatase
DAB	3, 3'-diaminobenzidine

ddH2O	double distilled water
DEC	decidualised
DHEA	dehydroepiandrosterone
DHEAS	dehydroepiandrosterone sulphate
DHT	dihydrotestosterone
DNA	deoxyribonucleic acid
DS	decidualised stroma
E2	oestradiol
ECM	extracellular matrix
EGF	epidermal growth factor
EGFP	enhanced green fluorescent protein
EGFR	epidermal growth factor receptor
ELISA	enzyme-linked immunosorbent assay
EMT	epithelial-mesenchymal transition
ERα/*ESR1*	oestrogen receptor alpha
ERβ/*ESR2*	oestrogen receptor beta
Fabpi	fatty acid binding protein 2
FRET	fluorescence resonance energy transfer
FSH	follicle stimulating hormone
FSHR	follicle stimulating hormone receptor
G	gland
GE	genomic elimination
GFP	green fluorescent protein
GnRH	gonadotrophin releasing hormone
GnRHR	gonadotrophin releasing hormone receptor
GR-1	myeloid differentiation factor
H+E	haematoxylin and eosin
H_2O	water
H_2O_2	hydrogen peroxide
h	hours
hrs	hours
HCl	hydrochloric acid
hESCs	human endometrial stromal cells
HIF1α	hypoxia inducible factor 1 alpha
HMB	heavy menstrual bleeding

HPO	hypothalamic pituitary ovarian
HRP	horseradish peroxidase
HSD	hydroxysteroid dehydrogenase
IF	immunofluorescence
IGF	insulin-like growth factor
IGFBP	insulin-like growth factor binding protein
IHC	immunohistochemistry
Ilβ	interleukin beta
kb	kilobases
KCl	potassium chloride
LE	luminal epithelium
LH	luteinising hormone
LRCs	label retaining cells
LHR	luteinising hormone receptor
M	molar
MET	mesenchymal- epithelial transition
ml	millilitre
mM	millimolar
mm	millimetre
MMP	matrix metalloproteinase
mRNA	messenger RNA
MSC	mesenchymal stem-like cell
NAS	normal animal serum
NBF	neutral buffered formalin
ng	nanogram
NGS	normal goat serum
nM	nanomolar
NR	nuclear receptor
NRS	normal rabbit serum
nset	non-surgical embryo transfer device
OVEX	ovariectomy
P	progesterone
P4	progesterone
PBS	phosphate buffered saline
PCOS	polycystic ovarian syndrome

PCR	polymerase chain reaction
PDGFRβ	platelet derived growth factor beta
pg	pictogram
PG	prostaglandin
PGDH	prostaglandin dehydrogenase
PGE2	prostaglandin E2
PGF2α	prostaglandin F2α
PGDH	prostaglandin dehydrogenase
PKA	protein kinase A
PR	progesterone receptor
PRAKO	progesterone receptor-A knock-out
PRKO	progesterone receptor knock-out
qRTPCR	quantitative real time polymerase chain reaction
RIN	RNA integrity number
RLT	RNeasy lysis buffer
RNA	ribonucleic acid
RT	reverse transcription
RU486	mifepristone, progesterone receptor antagonist
s.c.	sub-cutaneous
SC	shed cells
SEM	scanning electron microscopy
Sp-1	specificity protein 1 (transcription factor)
T	testosterone
TAMRA	carboxy-tetramethyl-rhodamine (quencher dye)
TGFα	transforming growth factor alpha
TGFβ	transforming growth factor beta
Tris-HCL	tris(hydroxymethyl)aminomethane-hydrochloric acid
TSA	tyramide signal amplification system
uNK	uterine natural killer cell
µg	microgram
µl	microlitre
µM	micromolar
UPL	universal probe library
VEGF	vascular endothelial growth factor
VIC	Taqman dye label

Chapter 1 Literature Review

1.1 Neonatal and postnatal development of the female reproductive tract

The foundations of the human reproductive tract are laid down between the third and eighth weeks of gestation, at a time when the embryo undergoes a dramatic transformation from a flat plate of cells to recognisable human structures, including; arms, legs and a face.

Humans have a simple uterus, consisting of a single uterine cavity, formed from the fusion of the basement membranes of the two Müllerian ducts during Carnegie stages 22-23 (approximately 8 weeks of gestation) (1–3). The uterus then grows intensively between weeks 16 and 24 of gestation (4), where the mesenchyme differentiates into the endometrial stroma and the myometrium by week 22 of gestation. Superficial glands differentiate from the simple, columnar, luminal epithelium to primordial, glandular epithelial buds (1). Proliferation of cells in the endometrial glands is initiated after birth and continues until the onset of puberty, glands extend from the luminal epithelium towards the myometrium (5–7).

In both male and female embryos the primordial germ cells migrate to the genital ridge before populating the developing gonads around 5 and 6 weeks of gestation (8–12). Sexual differentiation occurs around week 7 (8, 13–15) and thereafter ovarian development is characterised by germ cell proliferation and differentiation into clusters of oocytes, a process which continues until the 22nd week of gestation where the oocytes enter meiotic arrest (16–20).

1.2 Hypothalamic-pituitary-ovarian axis

The female reproductive system is tightly regulated by the hypothalamic pituitary ovarian (HPO) axis. The HPO axis is usually characterised by a linearly organised set of endocrine regulated tissues with a hierarchy, composed of; a subset of hypothalamic neurons, that express the peptide gonadotrophin releasing hormone (GnRH) (21–23), gonadotrope cells of the anterior pituitary and the ovary (composed of two endocrine structures, the follicular complex and the corpus luteum) (24) as depicted in Figure 1-1. Activation of this system commences during puberty, independent of gonadal input (25, 26) and is associated with the onset of pulsatile secretion of GnRH from the hypothalamus. GnRH binds to GnRH receptors (GnRHRs) on the surface of the gonadotropes (27, 28) in the pituitary, triggering the synthesis and secretion of the gonadotrophins, follicle stimulating hormone (FSH) and luteinising hormone (LH). LH and FSH act on the ovary to stimulate the synthesis of the

steroid hormones oestrogens, progestagens and androgens; this will be discussed further in section 1.3.

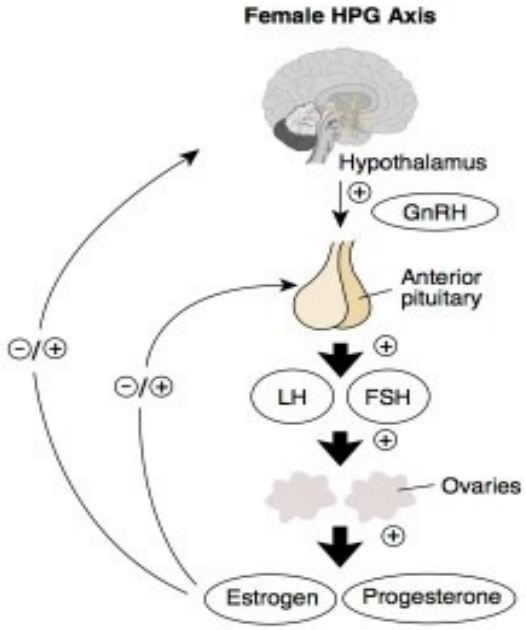

Figure 1-1: Hypothalamic pituitary ovarian axis. The HPO axis is an integrated set of endocrine regulated tissues governed by positive and negative feedback loops. Gonadotrophin releasing hormone (GnRH) stimulates the pituitary to secrete luteinising hormone (LH) and follicle stimulating hormone (FSH) which act on the ovary to drive steroid hormone synthesis. Adapted from (29).

GnRH pulsatility varies across the menstrual cycle (30–32). Pulse frequencies regulate gonadotrophin release from the pituitary, a process which is critical for the controlled generation of an LH surge ensuring correct timing of ovulation (33, 34).

The HPO axis is governed by both positive and negative feedback regulatory loops (35–38). In the female, the effects of the gonadal steroids are dependent upon the stage of the menstrual cycle. Oestrogens exert both negative and positive effects on the hypothalamus. Animal studies, using ovariectomised mice, have indicated that oestrogens are able to suppress the release of gonadotrophin releasing hormone (GnRH) from the hypothalamus during the follicular phase of the menstrual cycle (39). However, studies in ovariectomised pigs show that, during the pre-ovulatory phase oestrogens exert a positive effect on both the hypothalamus and the pituitary (34, 40).

The increase in circulating concentrations of oestrogen levels during the late follicular phases, associated with growth of antral follicles (41), positively stimulates increased secretion of GnRH from the hypothalamus and increased LH secretion from the pituitary (42). Following ovulation, progesterone is released by the corpus luteum which negatively

regulates the HPO axis at all levels. Following the demise of the corpus luteum, oestrogen and progesterone concentrations fall and negative feedback of FSH is removed (reviewed in (43)).

1.3 Ovarian steroid biosynthesis

Sex steroids play a key role in the growth and differentiation of the human endometrium. In women, circulating steroids are derived from the ovary and the adrenal gland. In 1974, Abraham demonstrated that ovarian activity was responsible for fluctuations in the circulating concentrations of oestrogen and progesterone during the normal menstrual cycle (44). Blood plasma concentrations of FSH, LH, oestradiol, progesterone and testosterone fluctuate across the menstrual cycle and are known to vary between women, therefore mean serum concentrations are shown in Table 1-1.

	FollicularPhase			Luteal Phase		
	Early	Mid	Late	Early	Mid	Late
FSH (mIU/ml)	8.02±0.74	10.01±2.13	12.36±1.00	9.8±2.13	5.26±0.87	8.89±2.24
LH (mIU/ml)	7.62±1.41	12.13±0.98	36.52±12.48	18.15±3.66	8.1±1.24	7.02±0.73
E2 (pg/ml)	51±6	80±11	231±40	116±12	147±6.0	39±6.0
P (pg/ml)	903±139	879±88	1144±178	8851±2072	16241±2415	1842±464
T (pg/ml)	601±46	673±39	927±160	743±87	594±40	501±26
free-T (pg/ml)	2.8±0.2	3.4±0.24	3.9±0.41	3.2±0.22	2.7±0.19	2.2±0.09
A (pg/ml)	1264±163	1461±101	1599±83	1377±99	1147±105	1088±73

Table 1-1: Mean serum concentrations (±SEM) of gonadotrophins luteinising hormone (LH) and follicle stimulating hormone (FSH) and the steroid hormones oestradiol (E2), progesterone (P), testosterone (T) and androstenedione (A). Steroid hormone concentrations are shown in picograms per millilitre (pg/ml), n=12. Adapted from (45).

The ovary is composed of two endocrine structures; the follicular complex and the corpus luteum (24). The ovary serves two functions; oogenesis and steroidogenesis. The cellular components of the follicular complex drive steroid hormone production that feeds back to the hypothalamus and pituitary whilst also driving local follicle maturation (46).

The gonadotrophins LH and FSH act on the ovary to stimulate synthesis of the steroid hormones, the most important of which are; testosterone (T), oestradiol (E2) and

progesterone (P4). These steroid hormones are synthesised *de novo* from free cholesterol (reviewed in (47, 48)), which is transported from the liver (49) via the blood to the cytosol of thecal cells in the ovary. Biosynthesis of oestrogen and progesterone requires an enzyme cascade with proteins expressed in both theca and granulosa cells (50, 51), this "two-cell, two-gonadotrophin" model is depicted in Figure 1-2.

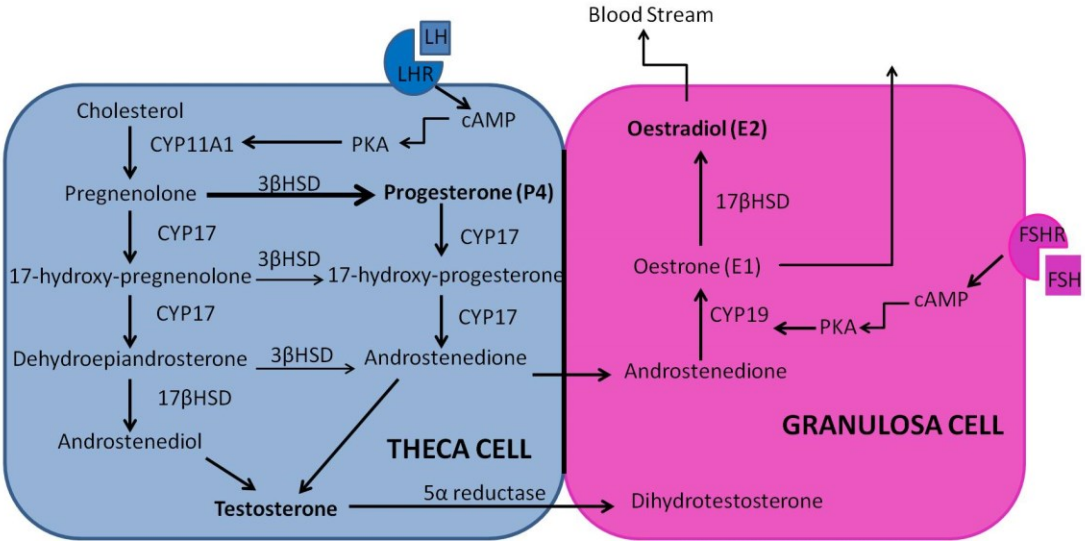

Figure 1-2: Two-cell, two-gonadotrophin model. Steroid hormones testosterone, progesterone and oestradiol are synthesised from cholesterol, via side chain cleavage of cholesterol by CYP11A1 to pregnenolone. Steroid dehydrogenase enzyme activity converts pregnenolone to androstenediol or progesterone. Androstenedione crosses the basement membrane into granulosa cells where it is converted to oestradiol by aromatase (CYP19). CYP11A1; cholesterol side chain cleavage cytochrome P450, CYP17; 17α hydroxylase/C_{17-20} lyase cytochrome P450, CYP19; aromatase, 17βHSD; 17β hydroxysteroid dehydrogenase, 3βHSD; 3β hydroxysteroid dehydrogenase, cAMP; adenosine 3',5'-cyclic monophosphate, PKA; protein kinase A, FSH; follicle stimulating hormone, FSHR; follicle stimulating hormone receptor, LH; luteinising hormone, LHR; luteinising hormone receptor. Adapted from (52, 53).

In brief, LH stimulates biosynthesis of androgens in the theca cells of developing follicles. Binding of LH to a membrane bound G protein coupled receptor (GPCR), LHR, stimulates a second message cascade involving cyclic adenosine monophosphate (cAMP) (54), which in turn stimulates transcription of the *CYP11A* gene. The CYP11a enzyme acts by side chain cleavage, to convert cholesterol to pregnenolone (55). Androstenediol is synthesised by multiple intermediates under the control of 17α hydroxylase (CYP17, encoded by the gene *CYP17A1*) and 17β hydroxysteroid dehydrogenase (17βHSD) (56, 57).

FSH binds to the FSHR (58), which like LHR is also a membrane bound GPCR, on granulosa cells of secondary follicles to initiate a signalling cascade involving cAMP to stimulate aromatase (CYP19) expression (59). CYP19 aromatises theca cell-produced androstenedione, which has crossed the basement membrane (60), to oestradiol. Oestradiol is

then released into the blood stream to act in an endocrine manner on the endometrium and other oestrogen-target tissues.

Oestrogen is the primary hormone synthesised in the ovary during the follicular phase of the cycle, however the pre-ovulatory surge of LH and FSH drives theca and granulosa cell differentiation to form the corpus luteum (61). The first observation of corpora lutea was in the mid-1600s, however the importance of the corpus luteum and its function as an endocrine gland was not confirmed until 1903 by Fraenkel (62) who observed that removal of the corpora lutea resulted in embryo resorption in rabbits.

Corpus lutea formation alters the steroidogenic pathway so that progesterone, not androgens, becomes the main steroid hormone produced by these cells during the secretory phase of the menstrual cycle (61). This is achieved by increased expression of CYP11A1 and 3βHSD to firstly convert cholesterol to pregnenolone then to progesterone, and a decrease in expression of 17α hydroxylase and 17β hydroxysteroid dehydrogenase (63, 64) to reduce oestradiol synthesis.

During the luteal phase of the cycle the size of the corpus luteum increases until it has reached maximal levels of progesterone secretion, this level is maintained during the mid-luteal phase, coinciding with the implantation of a blastocyst. In a conceptus cycle, the corpus luteum is indispensable for establishment of pregnancy (65), whereas in non-conceptus cycle the corpus luteum will undergo luteolysis (structural and functional degradation) (66), resulting in a decrease in oestradiol and progesterone production (65, 67). Suppression of FSH is removed upon progesterone withdrawal and a new cycle of follicle growth and steroid hormone production is initiated (68, 69).

1.4 The human endometrium

The human endometrium is a highly complex and dynamic tissue that lines the inside of the uterine cavity. During a woman's reproductive lifespan the endometrium is subjected to cyclical episodes of proliferation, differentiation, decidualisation, shedding (menstruation), repair and regeneration in response to fluctuating levels of steroid hormones produced from the ovaries (70–77). The endometrium displays unparalleled, controlled, tissue remodelling, resulting in a healed, scar-free tissue following menses or parturition (78–80). Taking into account the declining age of menarche (81), the development of contraception, smaller family sizes and the choice to delay pregnancy until a later age, the average woman undergoes 400 menstrual cycles during her reproductive lifespan (82).

Co-ordinated cell-cell interactions within the endometrium during the menstrual cycle are pivotal to maintaining female fertility. Remodelling of the tissue is essential for maintaining the receptivity of the endometrium to the possible implantation of a blastocyst (83). In the absence of an implanted blastocyst, regression of the corpus luteum is followed by a decrease of progesterone secretion (61, 83–86) that initiates the onset of focal and ischaemic necrosis resulting in shedding of the endometrium (menstruation) and the beginning of a new cycle with the opportunity to re-establish a "receptive" endometrium.

1.4.1 Endometrial composition

The endometrium is morphologically divided into two layers; the upper luminal functional layer and the lower basal layer, adjacent to the myometrium (87–89). The functional layer comprises the upper two thirds of the proliferated endometrium, and it is this layer that is shed during menstruation. It is in the functional layer where the majority of tissue remodelling occurs under tight regulation of the sex steroid hormones oestrogen (secreted from the granulosa cells of the developing ovarian follicles) during the proliferative phase and progesterone (produced from thecal cells of the corpus luteum following ovulation) during the secretory phase. One feature of the functional layer is a striking increase in its depth, with an average thickness of 7mm during the mid-secretory phase, a 14 fold increase in thickness from an initial post-menstruation depth of 0.5mm (90).

Both layers of the endometrium are multi-cellular with well-defined stromal and epithelial compartments. The luminal surface of the functional layer is lined by a single layer of epithelial cells. Embedded within the stroma are glands that are lined with columnar epithelium, extending away from the surface epithelium. Stromal fibroblasts and an extensive vascular compartment are characterised by endothelial cells surrounded by perivascular cells that express contractile proteins such as smooth muscle actin (91–93). The endometrium is also host to a fluctuating immune cell population. T-lymphocytes, eosinophils, mast cells, uterine natural killer cells (uNK) and macrophages are all present through-out the cycle, whilst an influx of leukocytes during the secretory and menstrual phases of the cycle has also been identified (reviewed by (94, 95) and further discussed in section 1.6.3.3.1).

1.5 Steroid hormones and their receptors in the human endometrium

It is well established from studies in women and a range of animal models that oestrogens and progestagens are essential for endometrial function; however there is emerging evidence of a role for androgens in regulating cellular function of the endometrium (96).

Mouse models are often used to study the human endometrium due to the similarity in endometrial structure; the mouse endometrium also displays cyclical changes in cell morphology (97) and steroid receptor expression (98) that parallel those documented in human endometrium during the normal menstrual cycle. Mice are a particularly useful resource due to the availability of transgenics, specifically cell-specific knock out models, which will be discussed in this section. The use of mouse models to study the dynamics of endometrial function will be discussed further in section 1.9.

1.5.1 Steroid hormone receptor structure

Classical actions of sex steroids are mediated via their steroid hormones receptors, which belong to a superfamily of receptors known as nuclear receptors (NR). NRs are an abundant class of transcriptional regulators; ligand binding to NRs has effects on growth, development and homeostasis (99). Analysis of NRs has revealed a common structural organisation of 6 homologous domains (100), named A-F depicted in Figure 1-3.

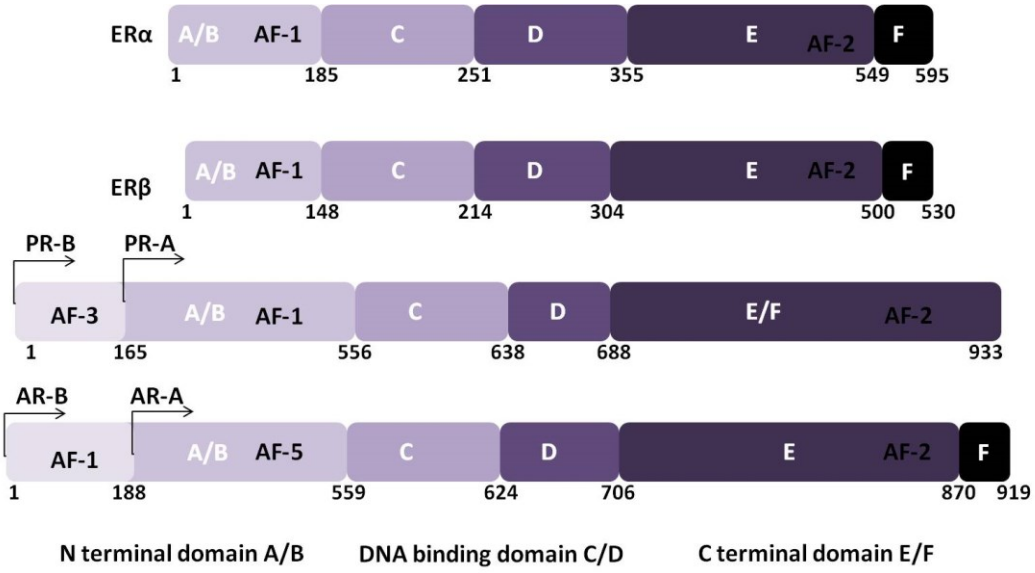

Figure 1-3: Protein structure of the main steroid receptors, oestrogen receptors alpha and beta (ERα/ERβ), progesterone receptors A and B (PR-A/PR-B) and androgen receptors A and B (AR-A/AR-B). AF; activation function. Amino acid lengths for each domain are shown below each protein. Adapted from (101–103).

The N terminal A/B domain differs in length between NR superfamily members and is the least conserved domain of the NR protein. Activation function (AF) sites are located in the A/B region. DNA binding is encoded in domain C (104, 105), which is the most conserved region of the superfamily. Domain E is the hormone binding domain which upon ligand binding participates in dimerisation, translocation and transcriptional activation (106). Domain E also contains the binding site for the heat shock protein hsp90, a chaperone protein (107, 108). This ligand binding domain also contains an additional AF domain, AF-2,

responsible for ligand-dependent activation of the receptor. PR-B contains a third AF in its upstream sequence (109), whilst AR contains AF-5 in its N terminal domain, to allow for ligand-independent binding (101, 110).

1.5.2 Oestrogens in normal endometrial function

Oestrogens regulate the essential processes of normal endometrial function including; proliferation of the functional layer and extensive angiogenesis (111). Oestradiol (E2) is the dominant oestrogen and can be synthesised in the ovary, (as described in section 1.3). However, there is new evidence for local biosynthesis of oestrogens in the normal, cycling endometrium (112) which complements that from studies in disorders including endometriosis (113–115).

Two phases of oestrogen elevation are observed across the menstrual cycle (Table 1-1 and Figure 1-4, E2); the first peak occurs during the late follicular phase prior to ovulation and the LH surge where oestradiol levels rise from around 80pg/ml in the mid follicular phase to approximately 231pg/ml. The second elevation is observed in the mid luteal phase, where E2 peaks around 147pg/ml, studies in mice and women have supported a role for oestrogens during embryo implantation (116–120).

Oestrogens exert their effects on two oestrogen receptors; oestrogen receptor alpha (ERα) and oestrogen receptor beta (ERβ). Both belong to the steroid receptor super-family of nuclear receptors encoded by genes *ESR1* and *ESR2* and are located on chromosomes 6q25.1 and 14q23.2 respectively (106).

In the human endometrium, both ERα and ERβ are temporally and spatially regulated in multiple cell types (98). In the functional layer of the endometrium, ERα and ERβ are both expressed in stromal cells and glandular epithelial cells (121). Studies using mice with cell-specific deletion of ERα (ERKO) have identified a key role for stromal ERα in mediating oestrogen-dependent epithelial cell proliferation (122). However ERβ, not ERα, is expressed in endothelial cells that line the blood vessels (123). ERα and ERβ have been immunolocalised to the perivascular stromal cell (123). Splice variant isoforms of *ESR2,* which lack a ligand binding domain, have been detected in normal endometrium and in endometrial cancer (124). The expression of both ERα and ERβ fluctuate through-out the menstrual cycle and are discussed further in section 1.6.

1.5.3 Progesterone in normal endometrial function

Progesterone concentrations increase significantly during the secretory phase from 1144pg/ml in the late follicular phase to a peak of around 16,241pg/ml in the mid secretory

phase (Table 1-1, P). Progesterone acts via the progesterone receptor (PR), of which there are two main isoforms; PR-A and PR-B (125), encoded by a single gene (*PGR)* located on chromosome 11q22 (126).

Progesterone plays a role in limiting oestrogen-mediated mitogenesis by promoting differentiation of stromal cells (127, 128). For example, progesterone, acting via its cognate receptor inhibits the transcription of the *ESR1* gene (129). Progesterone also stimulates expression of 17β hydroxysteroid dehydrogenase-2 (17βHSD2) which converts oestradiol to oestrone, an oestrogen which has a weaker affinity for the oestrogen receptor (130). In a murine model, when PR was blocked by administration of the antagonist, RU486, a significant decrease in vascular function was noted (131).

Notably, expression of the PR gene and its isoforms are controlled by both oestrogen and progesterone. During the proliferative phase oestrogen stimulates transcriptional activity of the PR gene; however maximal activation of the PR protein is observed during the secretory phase when bioavailable concentrations of the ligand progesterone are at their greatest (132). PR-A is the predominant isoform during the secretory phase, immunolocalised to the stroma and perivascular cells, but absent from the endothelium (98). Selective uterine PR knockout mice (PRKO), for both isoforms, exhibit extensive hyperplasia due to unopposed actions of oestrogen (133). Interestingly, in the uterine cell-selective PR-A knockout (PRAKO), PR-B was sufficient to maintain epithelial mitogenesis (134), indicating that PR-A isoforms are involved in both the opposition of PR-B signalling and oestrogen-dependent proliferation during the secretory phase.

Early studies with selective uterine and ovarian PR knockout mice (PRKO) found that endometrial tissues exhibited a failure in stromal cell decidualisation and were also infertile due to deficient luteinisation of follicle theca and granulosa cells at ovulation (133). More recent studies have highlighted that PR-A is indispensible for decidualisation of the functional endometrium during the secretory phase (96, 135), a process essential for establishment of pregnancy. Artificial stimulation to induce decidualisation in uterine PRAKO mice failed to induce a decidual response (135). This evidence highlights a key role for progesterone and the PR in normal endometrial function.

1.5.4 Androgens in normal endometrial function

Whilst the impact of oestrogens and progestagens on endometrial function has been extensively studied, little attention has been paid to androgens and their actions on the endometrium.

Adult women synthesise about half their circulating androgens in the adrenal and in the ovary, with the other half being synthesised in peripheral sites like the skin (136, 137). Although testosterone is often classed as the "male hormone", because of its key role in the maintenance of the male phenotype, measurement of circulating concentrations of active androgenic ligands reveal that normal women synthesise androgens at a level which is approximately 60% of that of an adult male (138).

Abraham, in 1974, determined the circulating concentrations of androgens (and their metabolites) across the menstrual cycle by taking daily blood samples from 6 women of reproductive age (44). To investigate the relative contributions of the adrenals and ovaries to total serum concentrations blood samples were taken during one normal cycle, then the same women were given a dose of dexamethasone to suppress adrenal production of androgens during the next cycle (44). Abraham observed that ovarian-derived testosterone, androstenedione and dehydroepiandrosterone (DHEA) were maximal during mid-cycle (late proliferative/early secretory phase), whereas concentrations of circulating dihydrotestosterone (DHT) and DHEA sulphate (DHEAS) were maintained across the cycle and were apparently unaffected by menstrual phase. Adrenal contributions of testosterone, androstenedione, DHEA and DHEAS were constant through-out the cycle. More recently, these fluctuations in androgens across the cycle have been confirmed and a decrease in circulating androgens is reported in women with advanced reproductive age (139, 140).

Androgens exert their effects on the androgen receptor (AR) located on the X chromosome at the Xq11-12 locus (141), that consists of 8 exons which encode a protein of 919 amino acids. In the absence of ligand, the AR is bound by heat shock proteins that dissociate upon ligand binding. AR monomers are then transported to the nucleus where they dimerise. The AR has been shown to mediate a range of cellular processes including proliferation, differentiation and apoptosis (142).

The androgen receptor has been immunolocalised to the nuclei of stromal cell fibroblasts of both the functional and basal layer during the proliferative phase (143). However, this expression gradually decreases over the cycle, until a complete lack of expression is observed in the functional layer by day 23 during the late secretory phase (reviewed in (98)). This has been supported by *in vitro* studies, where AR protein levels are suppressed by progesterone in a model of stromal cell decidualisation (96). Using gene data sets, downstream androgen target genes have been shown to have a greater expression during the proliferative phase than in the mid secretory phase (144). This would suggest that that AR

expression is mediated by the fluctuating levels of oestrogen and progesterone through-out the menstrual cycle (145).

The impact of androgens on endometrial function has been investigated. It has been reported that androgens alone cannot initiate a decidual response in primary endometrial stromal cells *in vitro*. However, AR has been shown to regulate expression of genes involved in the maintenance of decidualisation which suggests a role for AR in embryo implantation (96). The inability of AR to initiate decidualisation further underlines the importance of progesterone and PR in regulating endometrial receptivity. Furthermore, in a murine model, androgens (more specifically, DHT) were able to maintain decidualisation of the endometrium after the withdrawal of progesterone support (146). Despite being able to maintain the decidual response *in vivo*, DHT was unable to support foetal development during pregnancy after the removal of progesterone on day 6 of gestation, further evidence for the importance of progesterone in the establishment of pregnancy (146).

1.6 Cyclical changes in the pattern of steroid receptor expression and changes in cellular morphology of the endometrium across the menstrual cycle

The classical morphological changes that occur in the endometrium in response to ovarian steroids were first described by Hitschmann and Adler in 1908 (147). Subsequent studies have described the endometrial morphology of each phase of the menstrual cycle in detail (87, 88, 148–153). A diagrammatic representation of the key changes in the morphology of the functional layer, along with fluctuations in ovarian steroids, is illustrated in Figure 1-4.

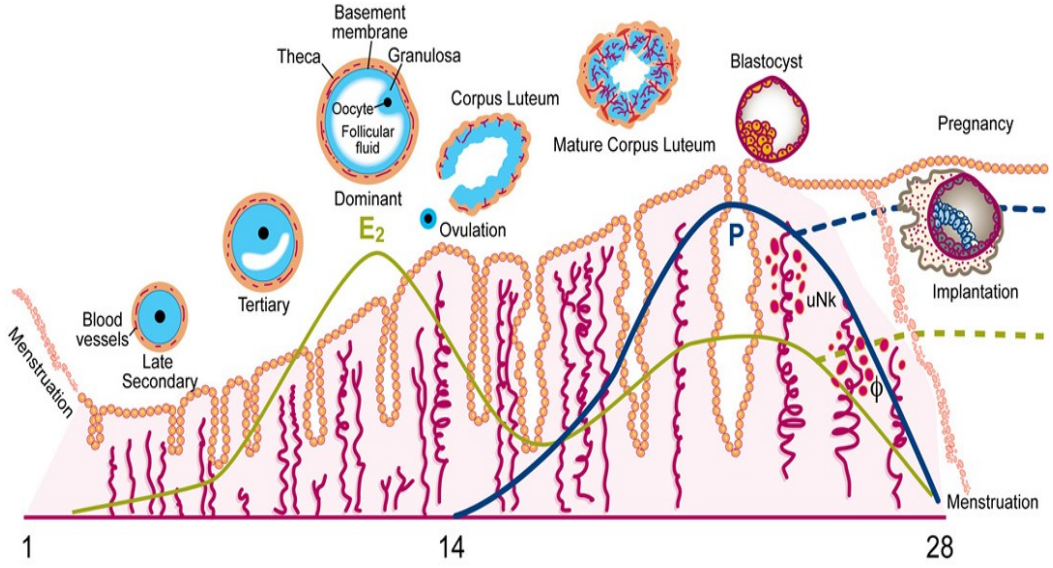

Figure 1-4: Cyclical changes in cellular composition of the functional layer of the human endometrium. The E2 dominant proliferative phase precedes the P4 dominant secretory phase. E2 acting via ERα stimulates cellular proliferation and angiogenesis during days 4-14 of the cycle. Following ovulation the corpus luteum secretes progesterone that in turn mediates the differentiation (decidualisation) of stromal cells in preparation for pregnancy. In the absence of a blastocyst, falling concentrations of progesterone precipitates a cascade of morphological changes culminating in sloughing of the functional layer at the time of menses. In the presence of a blastocyst (pregnancy), progesterone concentrations are maintained (P, dotted blue line) and further decidualisation occurs in the functional layer. Image courtesy of Professor. P. Saunders, unpublished.

Histological evaluation and dating of endometrium during each phase of the menstrual cycle is based on a detailed set of criteria which was first reported in 1950 by Noyes *et al.* This method classifies the cycle into early, mid and late proliferative; early, mid and late secretory; and menstrual phases (89). The following descriptions of the dynamic and temporal changes in cell function of endometrial proliferation and differentiation are based on an average menstrual cycle length of 28 days.

1.6.1 Proliferative phase

During the oestrogen-dominant proliferative phase rising concentrations in serum oestradiol (Figure 1-4; green line; E2), secreted from granulosa cells, stimulate the growth of the functional layer, promoting epithelial and stromal cell proliferation and regrowth of endometrial blood vessels through endothelial cell proliferation (70, 97, 123, 154–156).

Ovarian production of oestrogens begins on approximately day 4 of an average cycle. Oestrogens display different impacts on stromal and epithelial compartments of the endometrium. For example, oestradiol up-regulates the production of insulin-like growth factor-1 (IGF-1) by stromal cells which promotes proliferation of stromal and epithelial cells (157). Epidermal growth factor (EGF) is a potent mitogenic factor, present in the uterine cavity (158). Increasing serum concentrations of oestradiol stimulates the expression of the epidermal growth factor receptor (EGFR) on endometrial epithelial cells, allowing increased ligand binding of EGF (158–160) depicted in Figure 1-5, A. By the mid-proliferative phase (days 8-10) proliferation of cells in both the epithelial and stromal cell compartments results in lengthening of the basal glands and an expansion of the extracellular matrix in the stromal cell compartment (161). Occurring in parallel to these changes, an increase in the number of cilia and microvilli on epithelial cells (161) is observed (Figure 1-5,B). These cilia and microvilli aid distribution of glandular secretions during the secretory phase (148, 162, 163).

Intra-nuclear concentrations of ERα are maximal during the proliferative phase. ERα has been immunolocalised to both the stromal cells and the luminal and glandular epithelium but not in the endothelium (98, 164) (Figure 1-5, C). The full length wild type receptor (ERβ1) and a truncated splice variant (ERβ2) are present in the glandular epithelium, the stroma and endothelium of the proliferative endometrium (123) (Figure 1-5, D). However, the impact of ERβ2 in the endometrium is not well understood. Oestrogen primes the endometrium for the morphological changes that will take place during the secretory phase by inducing expression of the oestrogen-dependent gene *PR* (70, 165, 166).

In the late proliferative phase (11-14 days) pseudostratification of the nuclei of the luminal epithelium cells is thought to contribute to the intra-glandular secretions which occur during the secretory phase to coincide with blastocyst implantation (89). Epithelial mitosis decreases so that proliferation of the functional layer gives way to stromal cell differentiation and decidualisation (161). Notably, PR expression in the glandular epithelium decreases (167).

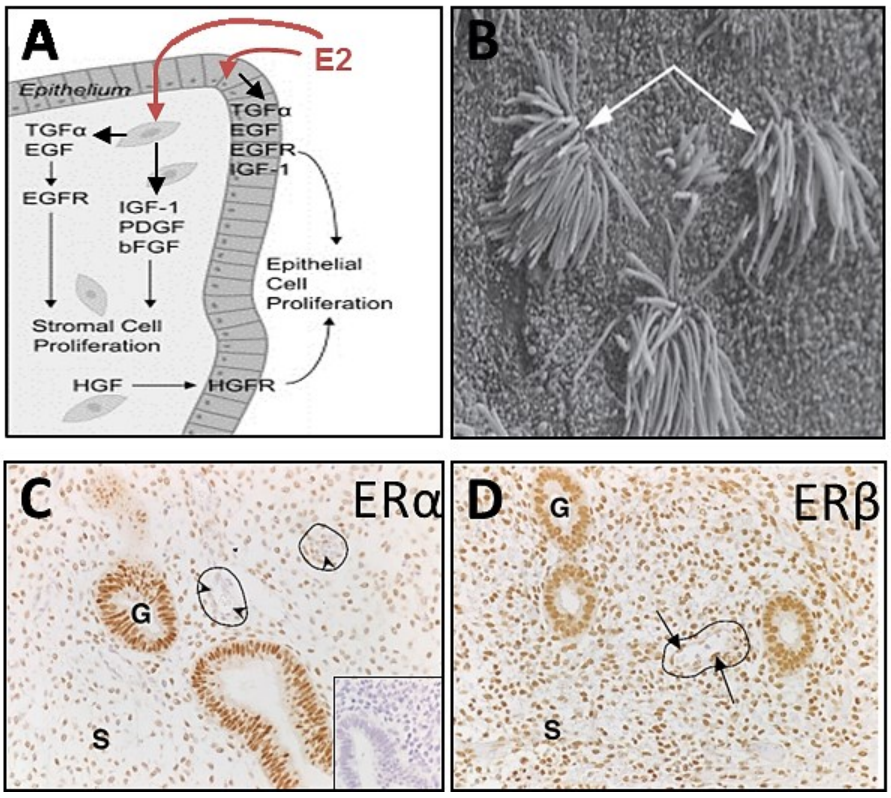

Figure 1-5: Proliferative phase of the human endometrium. A; Oestrogen acts on the epithelium and stroma (red arrows) to stimulate up-regulation of the production of growth factors (bold black arrows) such as insulin-like growth factor (IGF-1) to promote stromal and epithelial cell proliferation. Up-regulation of EGFR by oestradiol allows epidermal growth factor (EGF) to bind and promote epithelial cell proliferation. B; SEM image of the proliferative phase endometrium. Arrows show cilia projecting from the luminal epithelium. C; In the functional layer ERα is immunolocalised to nuclei of the glandular epithelium (G) and stroma (S) but is not found in the endothelium (arrowheads). D; ERβ is immunolocalised to the nuclei of glandular epithelial cells (G), stromal cells (S) and is found in the endothelium (arrows). (Adapted from, (123, 168, 169)).

1.6.2 Secretory phase

Humans display haemochorial placentation during pregnancy, a key feature of this type of placenta is trophoblast invasion and direct contact with the maternal blood supply. It is believed that in order to avoid excessive invasion of the trophoblast, the human endometrium has evolved to accommodate spontaneous and extensive decidualisation typified by differentiation of stromal fibroblasts. It has been reported that incomplete or insufficient decidualisation results in infertility (170).

Spontaneous decidualisation of the endometrium during the secretory phase occurs in preparation for blastocyst implantation. Implantation is a highly co-ordinated event between both the developing embryo and the endometrium (171), with each secreting a number of factors to aid adhesion, invasion and development (172, 173). The endometrium is only receptive to the blastocyst for a limited period of time (173), known as the "window of

receptivity"; therefore it is critical that regulatory molecules are tightly co-ordinated. The "window" is thought to "open" around day 20, when pinopode formation is observed by SEM (174); pinopode formation is dependent upon steroid hormone control (175) and is thought to aid blastocyst implantation (174). Immunolocalisation studies for integrins α4 and β3, adhesion molecules present during secretory phase in human tissues, have shown that the window stays open until around day 23 (174). Gene expression profiles using endometrial biopsies from the proliferative and secretory phase have identified a panel of genes that may be responsible for the regulation of preparation of pregnancy (176, 177).

During the secretory phase, the endometrium is exposed to rising levels of progesterone (Figure 1-4; blue line; P4) secreted from the hormone producing cells of the corpus luteum. Progesterone secretion results in cessation of endometrial epithelial cell proliferation and expression of ERα is down-regulated in both the epithelial and stromal cell compartments (178) (Figure 1-6, B). ERβ is maintained in the stroma during the secretory phase but is insufficient in regulating expression of IGF-1 and other factors (Figure 1-6, C) (123).

Rising levels of progesterone, results in increased expression of PR-A in the stromal cell compartment (Figure 1-6, D) (167). During decidualisation, stromal fibroblasts accumulate collagen (179) and laminin (180), whilst undergoing cellular enlargement to become pre-decidual or decidual cells. Decidualised cells secrete insulin-like growth factor binding protein 1 (IGFBP-1) (Figure 1-6, A) which in turn mediates progesterone-regulated decidualisation (181, 182). During the mid-secretory phase, (day 23) stromal cells initially undergo decidualisation just below the luminal epithelium and around spiral arterioles (183), where progesterone drives the expression of angiopoietin 1, which is a blood vessel stabilisation agent to block excessive angiogenesis (184). Decidualisation then spreads in a "wave-like" motion through-out the endometrium, so that by day 24 (during the late secretory phase of the human cycle); peak secretory activity is observed (Figure 1-6, E). During the late secretory phase, stromal oedema is apparent and the tissue is infiltrated by immune cells including uterine natural killer cells (uNK), macrophages and T cells (83, 185).

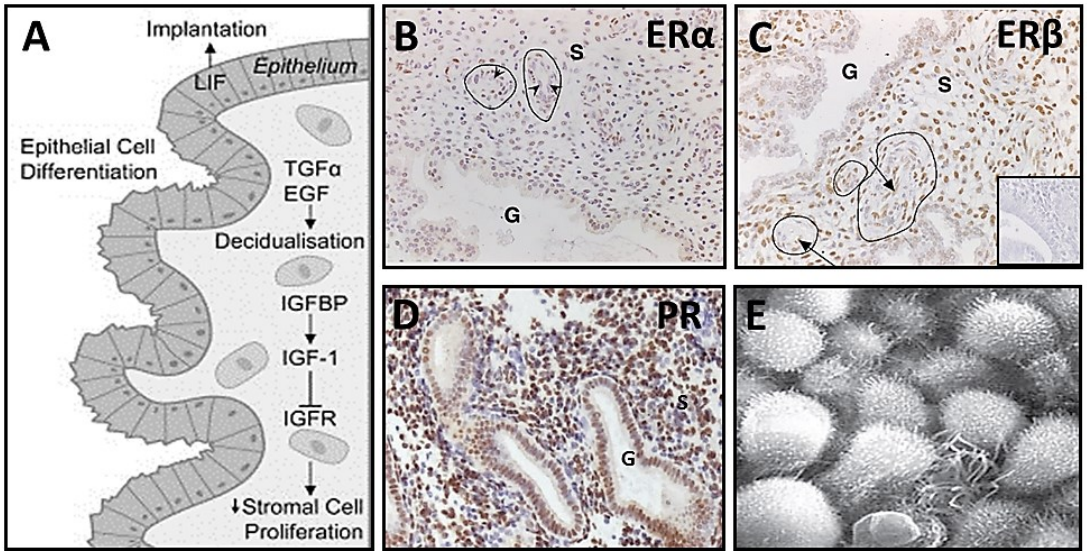

Figure 1-6: Secretory phase of the human endometrium. A; Increasing concentrations of progesterone mediate stromal cell decidualisation via a number of factors including; secretion of insulin-like growth factor binding protein (IGFBP), which decrease stromal cell proliferation. B; In the functional layer ERα is down-regulated in the glandular epithelium (G), stroma (s) and is absent from the endothelium (arrowheads). C; ERβ1 is down-regulated in the glandular epithelium (G), but is maintained in the stroma (S) and in the endothelium (arrows). D; PR is expressed in the stroma and the glandular epithelium of the decidualised, mid-secretory phase endometrium. E; SEM image of the secretory phase endometrium, tall, columnar epithelia are evident. (Adapted from, (123, 148, 168)).

1.6.3 Menstrual phase

In the absence of a developing blastocyst, and therefore the absence of the embryonic signal chorionic gonadotrophin, the corpus luteum regresses resulting in a rapid fall in ovarian-derived steroids and functional progesterone withdrawal (61,63, reviewed by 82). The menstrual phase of the cycle is characterised by the sloughing of the functional layer into the uterine lumen. The shed tissue is then expelled from the uterine cavity via the vagina. Menstrual bleeding itself is the first outward sign of menses; however it is now appreciated that this is the culmination of a cascade of cellular and vascular changes that are initiated following the failure of conception, a summary of this cascade is shown in Figure 1-8.

1.6.3.1 Current concepts of endometrial breakdown

Our current understanding of the cellular changes associated with menstruation is based on the observations by Markee in the 1940s. Markee's studies using auto-transplanted endometrium in the anterior chamber of the eye of rhesus monkeys allowed observations of endometrial function. Markee reported that endometrial bleeding was induced by reduced blood flow to the upper two thirds of the endometrium, followed by a shrinkage in tissue density, then vasoconstriction of the spiral arterioles (186). It has been documented that vasoconstriction is associated with local ischaemia, loss of cell-cell adhesion molecules and

focal disruptions to the endothelium which culminate in a loss of tissue integrity and degradation of the endometrium (84, 169, 187).

Data obtained from detailed high powered analysis of endometrial tissue has revealed that endometrial shedding is a piecemeal process, as shown in Figure 1-7, with areas of shed endometrium (white arrow, exposed basal layer) adjacent to unshed endometrium (black arrow, intact epithelium) (148).

Loss of endometrial integrity has been widely investigated; prostaglandins, enzymatic digestion, matrix metalloproteinases (MMPs), leukocytes, macrophages and fibrinolysis are all implicated in playing a role in tissue breakdown and degradation of only the upper layer of the tissue and the interaction of these factors are shown in Figure 1-8. In normal women, these events are tightly controlled to prevent excessive blood loss and the onset of anaemia.

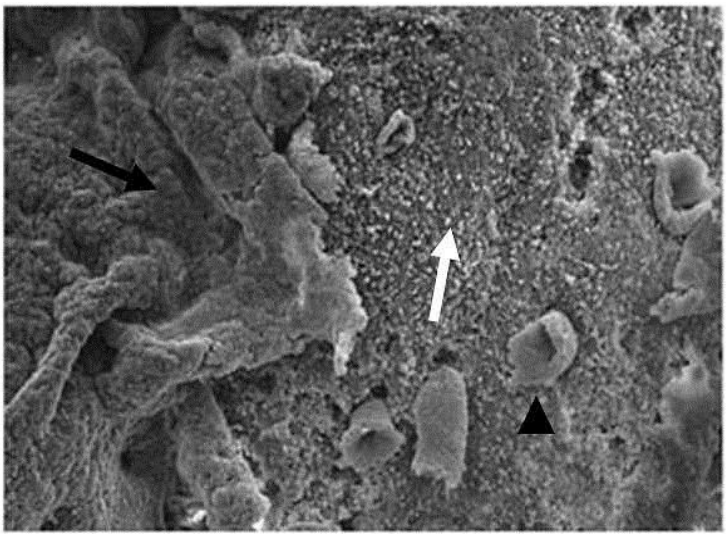

Figure 1-7: Menstrual phase of the human endometrium. SEM image of the endometrium during menses. The endometrium sheds in pieces; areas of unshed endometrium (black arrow) are observed adjacent to a denuded area of the basal layer (white arrow). Exposed basal glands are observed (arrowhead) (adapted from (148)).

1.6.3.2 Hypoxia as a regulating factor during menses

Vasoconstriction of the spiral arterioles prior to the onset of endometrial breakdown is likely to result in local hypoxia in the functional layer of the human endometrium. Initial evidence was proved by the auto-transplantation model used in the rhesus monkey by Markee (186) and reinforced in a mouse model of endometrial breakdown, where the authors reported low oxygen tension within the tissue using a marker of hypoxia (pimonidazole) (188).

Hypoxia inducible factor (HIF1α) is a nuclear protein that regulates a cell's response to hypoxia. In normoxic conditions the protein is rapidly degraded, however when oxygen levels fall the protein is stabilised and the two HIF subunits (HIF1α and HIF1β) dimerise to

initiate transcription of target genes (189). HIF1α protein and mRNA has been identified in the human endometrium during the late secretory and menstrual phases (190), however expression of the protein is independent of mRNA expression consistent with post-transcriptional regulation being key to its function (189).

Hypoxia has been shown to regulate genes involved in angiogenesis (191–193). For example, exposure of endometrial stromal cells to low oxygen tensions *in vitro* is reported to increase concentrations of vascular endothelial growth factor (VEGF) mRNA (193) and decrease expression of the chemokine CXCL12 (191). In a mouse model of breakdown, VEGF has been shown to be essential for re-epithelialisation and angiogenesis of the endometrium following tissue breakdown (188) suggesting that the transient induction of hypoxia, at menses, may provide a key regulatory step in stimulating the rapid repair of the tissue and restoration of tissue homeostasis.

1.6.3.3 Menstruation as an inflammatory event

It was Finn, in 1986, who first linked the events of menstruation to those of an inflammatory response (194). It has been proposed that progesterone maintains uterine quiescence by acting as an anti-inflammatory mediator during the menstrual cycle, in part by, inhibiting the production of pro-inflammatory prostaglandins (PGs) (195–198). For example, in women *in vivo*, it has been reported that progesterone increases the expression of prostaglandin metabolising enzyme 15 hydroxy-prostaglandin dehydrogenase (PGDH) whilst simultaneously suppressing the production of the inducible factor COX-2 in secretory phase endometrium (199). It has also been shown *in vitro,* in human myometrial cells, that progesterone suppresses inter-leukin β (IL-β) derived activation of COX-2, the enzyme that converts arachidonic acid to prostaglandins. Inhibition of IL-β mediated COX-2 suppression is removed upon progesterone withdrawal (200). This allows prostaglandin F2α (PGF2α) facilitated vasoconstriction of the spiral arterioles and smooth muscle contraction to aid shedding, whilst prostaglandin E2 (PGE2) mediates vasodilation (200). PGE2 has also been shown to regulate the expression of hypoxia inducible factor (HIF1α) in Ishikawa cells (an immortalised endometrial epithelial cell line) *in vitro* (190), which in turn up-regulates angiogenic factors which may be involved in vessel stabilisation following tissue degradation (as outlined in Figure 1-8, depicted by the green arrows).

Further anti-inflammatory effects of progesterone include stabilisation of lysosomal membranes and stimulating fibrinolysis. From scanning electron microscopy studies, it has become evident that during the secretory phase progesterone acts to stabilise lysosomal membranes. However, as progesterone concentrations fall lysosomes release lytic enzymes

and acid phosphatases (129, 201) that digest intracellular bridges (as outlined in Figure 1-8, depicted by the pink arrows). A loss of progesterone also stimulates fibrinolysis, where plasminogen is converted to plasmin to aid the breakdown of fibrin in the endothelium of blood vessels (202), so that clotting of the menstrual blood is inhibited (203). Fibrinolysis is an important process in preventing the organisation of fibrin into scar tissue (80, 204), essential to the scar-free healing observed in the endometrium with every menstrual cycle.

1.6.3.3.1 Immune cell influx

As inflammatory mediators, prostaglandins are known to regulate the activity of cytokines and chemokines that play a role in leukocyte recruitment to the endometrium through-out the menstrual cycle (205, 206) (as outlined in Figure 1-8, depicted by the blue arrows). From immunohistochemistry studies, it is proposed that leukocytes comprise up to 40% of the endometrial tissue at the pre-menstrual phase (185). Of the different leukocyte populations present, neutrophils and macrophages appear to be recruited to the endometrium from the blood stream (207–209). In comparison, the majority of the uNK cell population arises from proliferation *in situ* with the remainder recruited from blood stream (210–213). Immunolocalisation for macrophages reveals that they make up approximately 6-15% of the endometrium during the menstrual phase (214) and are proposed to play multiple roles in the regulation of endometrial function; initiation of breakdown, repair and remodelling and preparation for pregnancy. Immunolocalisation studies on fixed tissues and *in vitro* organ culture of endometrial tissues from each phase of the menstrual cycle have revealed that macrophages release matrix metalloproteinases (215) (as outlined in Figure 1-8, depicted by the purple arrows) and hydrolytic enzymes (216) to assist in breaking down collagens and extracellular matrix, respectively, in the endometrium at the time of menses.

Neutrophils are the dominant leukocyte involved in inflammatory processes, with increased numbers localised to the endometrium during breakdown as observed in a mouse model of menstruation, and peak numbers observed during repair (217). *In vitro* culture of human peripheral blood neutrophils and endometrial stromal fibroblasts, revealed that neutrophils activate the secretion MMPs, important mediators of tissue breakdown (as outlined in Figure 1-8, depicted by the purple arrows) (207). In a mouse model of breakdown, neutralisation of neutrophils by antibody administration resulted in a delay of repair of the endometrium (218).

1.6.3.3.2 Matrix metalloproteinases

Matrix metalloproteinases are zinc-dependent endopeptidases that cleave almost all extra-cellular components. The integral role that MMPs play in endometrial tissue breakdown was

first described *in vitro*, in human endometrial explants cultures (219). In the absence of exogenous steroids, tissue necrosis was reported microscopically and increased concentrations of MMPs were observed in the culture media. Administration of inhibitors of MMPs were observed to prevent the lysis of extra-cellular matrix components *in vitro* (219).

The expression of MMPs varies across the menstrual cycle; at menses (consistent with a time of progesterone withdrawal) there is a stark increase in protein expression of MMP-1, -3,-7, -9, -11 and -12 (220–228). Oestradiol and progesterone have been shown to suppress the expression of MMP-1, -3, -7 in culture tissue explants (219), supporting a role for ovarian steroid regulation of MMPs at all stages the menstrual cycle (221, 223, 229). In a mouse model of breakdown, immunolocalisation of MMP-3, -7 and -9 were found to increase in the stroma (MMP-3, -9) and in the epithelium (MMP-7) at the time of tissue breakdown (230), consistent with findings in the human (220, 221, 223, 227). Notably, MMP-3 and -7 were localised close to areas of repairing epithelium and MMP-7 and -9 were co-localised with neutrophils (230). In contrast to findings in women, administration of MMP inhibitors in the mouse model did not have any adverse effect on breakdown of the tissue (230), suggesting that in the mouse MMPs may not be the main contributor to endometrial breakdown.

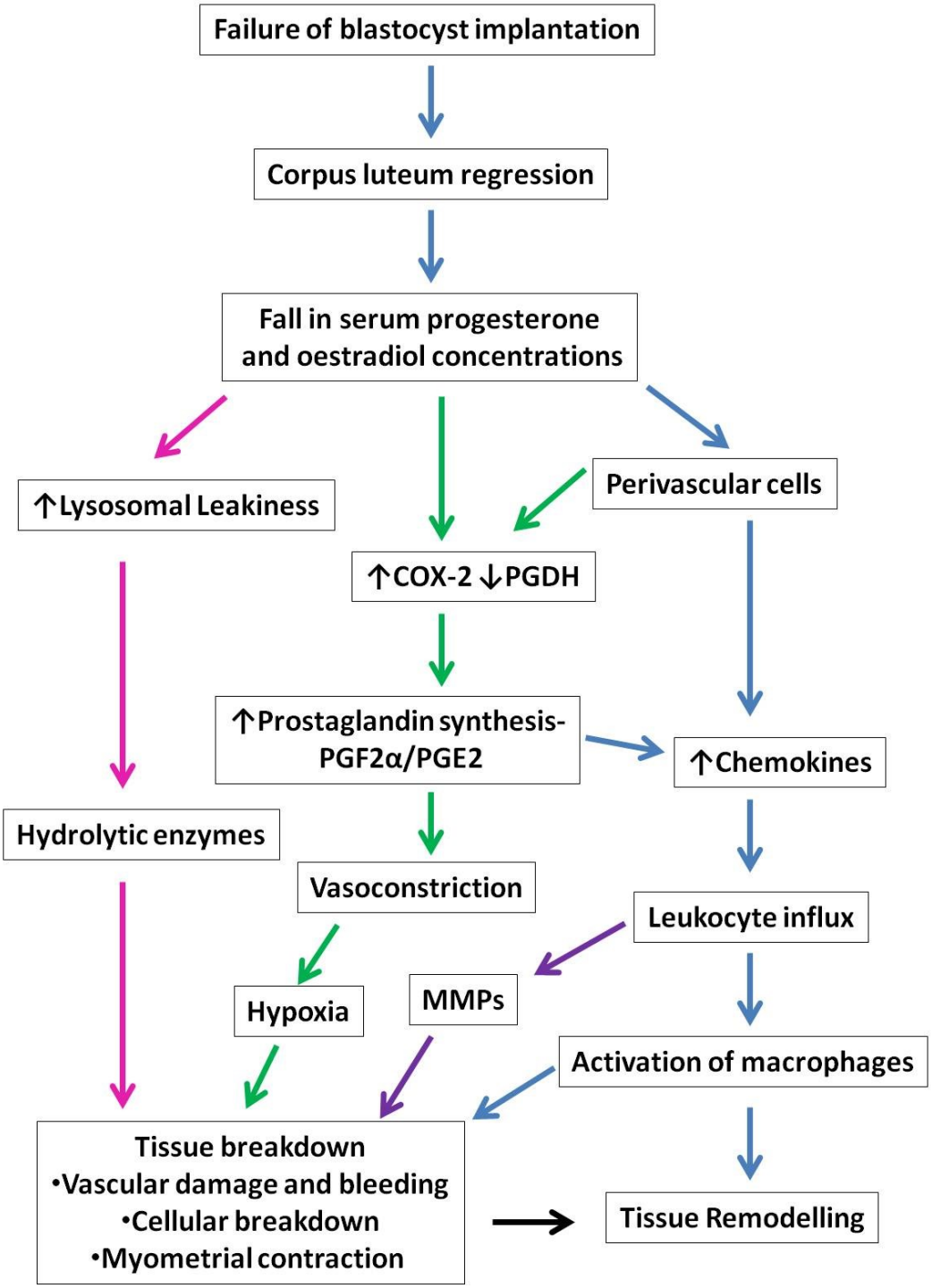

Figure 1-8: Summary of the cascade of events of endometrial breakdown following progesterone withdrawal. Corpus luteum regression results in falling serum progesterone concentrations. This results in a cascade of events culminating in endometrial breakdown. Three main pathways are thought to be involved; 1. An increase in COX-2 and prostaglandin synthesis leads to increased PGF2α causing vasoconstriction and up-regulation of hypoxia inducible factor. COX-2 and PG synthesis also results in increased PGE2 expression (green arrows); 2. An increase in lysosomal leakiness results in hydrolytic breakdown of the tissue (pink arrows); 3. An increase in production of chemokines and immune cell influx (blue arrows). ↑; increase, ↓; decrease, PGF2α; prostaglandin F2 alpha, PGE2; prostaglandin E2, MMPs; matrix metalloproteinases. (Adapted from (72, 83, 187)).

1.7 Endometrial repair and regeneration

The morphological changes that occur during the proliferative, secretory and menstrual phases have been studied by a number of investigators using human tissue, primate and rodent models (72, 132, 148, 169, 201, 231–238), whereas little attention has been paid to endometrial repair.

One striking observation made using human tissue samples was that initial "repair" of the human endometrium is a rapid process, occurring within 48 hours of shedding (237). Elegant scanning electron microscopy (SEM) studies by Ferenczy, in 1975, observed that repair of the human endometrium began on days 2-3 of the menstrual cycle and was completed by days 4-5, as evidenced by a fully reconstructed epithelial cell layer (201, 237). Surprisingly, repair was only observed in areas where the basal glands were exposed to the luminal environment. A recent SEM study by Garry *et al.,* (169) has shown that shedding is a piecemeal process, as evidenced by areas of new epithelium present before shedding is complete. Taken together these observations suggest a co-existence of breakdown and repair processes, which imply a complex regulatory pathway. Therefore, it is important to remember that whilst the menstrual phase, and outward bleeding observed by women, may last up to 5 days or longer, repair processes are already initiated at the start of this process something which is clearly important in limiting the severity of blood loss.

Repair of the endometrium appears to occur in a steroid depleted micro-environment, with low levels of circulating oestrogen and progesterone following the regression of the corpus luteum and prior to significant oestrogen secretion from growing follicles in the ovary. Oestrogen does not appear to be required for the initiation of, or the process of, repair as demonstrated in animal models of endometrial repair (239, 240). For example, an *in vivo* study using a mouse model of breakdown and repair has shown that, in the absence of oestrogen, epithelial, stromal and endothelial cell repair can occur when all exogenous steroids are removed by the administration of letrozole (an aromatase inhibitor), at the time of progesterone withdrawal. Removal of oestrogen did not affect the complete repair of the endometrium following shedding, which was observed within 48 hours (239). Furthermore, a xenograft model using human proliferative phase endometrial explants has also shown that oestrogen is not essential for tissue restoration. Proliferative phase explants were grafted sub-cutaneously onto ovariectomised immunodeficient mice and exposed to exogenous oestrogen and progesterone for 28 days to mimic a human cycle. After steroid removal, tissue destruction was observed. Following breakdown of the tissue on day 31, explants were observed to return to a proliferative phase-like morphology by day 35 in the absence of any

exogenous steroidal support. Repair of the explants in a steroid-depleted micro-environment was confirmed by measuring the circulating concentrations of oestrogens and progesterone in the blood sera (240). A role for oestrogen during endometrial repair has yet to be demonstrated in women.

1.7.1 Epithelial cell proliferation contributes to endometrial repair

The mechanisms that drive endometrial repair after breakdown of the tissue during menses are still a hotly debated topic; epithelial repair has been well described from a morphological view (201, 237) but is still poorly understood from a molecular viewpoint. The most accepted view of repair is that of Novak and Te Linde, who in 1924, proposed that the new luminal epithelium arises from the preserved glandular epithelium of residual glands in the remaining basal layer (241). Histological examination of specimens of menstrual phase tissue, have revealed continuous epithelial extensions arising from basal glands (237) supporting the idea that luminal epithelial cells are derived from the glandular epithelium.

However, an investigation into the mitotic activity of epithelial cells by Baggish *et al.,* in 1967, supports a different view. One where stromal cells undergo cellular transformation to become new surface epithelial cells (242). This hypothesis is supported by recent work by Garry *et al.,* (148, 169) who showed, by SEM, isolated groups of epithelial cells that were not associated with or located near the exposed ends of the basal glands. These authors also report little proliferation of epithelial cells during the repair phase, calling into question the earlier model. The contribution of the stromal cell compartment to epithelial repair has not been widely studied.

1.7.2 Endometrial regeneration by stem cells

The regenerative capacity of the endometrium has also been linked to the presence of adult "stem" (progenitor) cells within the tissue, a concept which was first proposed by Prianishnikov in 1978 (243). Unlike pluripotent foetal stem cells, stem cell progenitors, believed to exist in many adult tissues, are not identified nor defined by the expression of stem cell marker proteins, rather by their functional properties. One example of a tissue that has been identified to have residual adult stem cells is the intestine. The intestine and its niche, the intestinal crypt, have been intensively studied, due to the highly regenerative capacity of the intestine; in an *in vivo* study, where proliferating crypt cells were destroyed, it was discovered that the mouse intestinal epithelium regenerates every three days (244). Studies of the intestine have reported that adult stems and their niche are capable of substantial self-renewal, of differentiation into functional mature progeny and have a high proliferative potential (245–249).

Due to the highly regenerative capacity of the endometrium, it has been proposed that endometrial progenitor stem cells may reside in the base of the glands in the basal layer, due to the monoclonality of the epithelial cells in these glands (250). It is postulated that a rare stem cell population, which might be located in a niche composed of surrounding stromal cells, could give rise to a population of endometrial progenitor cells that will further differentiate into specific endometrial cell types (251). The notion of an adult stem cell niche is not a new concept, having first been described in relation to haematopoietic progenitors by Schofield in 1978 (252). It has been proposed that adult stem cells exist within a tightly controlled micro-environment to ensure they remain undifferentiated but are able to undergo lineage commitment when under special circumstances, such as stress (253). The stem cell niche has been identified in several adult tissues; these include the neural stem cell niche, the epidermal hair follicle niche, the haematopoietic niche and the intestinal crypt stem cell niche (247, 254–256). Each stem cell niche will vary slightly in its cell composition and location, with each being uniquely controlled in order to regenerate their respective organ. Evidence for endometrial progenitors includes establishment of colonies from single cell suspensions of endometrial tissue taken during hysterectomy. These single cell populations proliferate and can form cells with epithelial and stromal cell characteristics in culture (257); these studies indicated a need for stromal-epithelial cell interaction to maintain clonal growth.

“Side populations” of progenitor stem cells have been isolated from human tissues. Side population cells are distinct from the main population of somatic cells in that they display stem cell-like characteristics, one being their ability to efflux dyes, such as Hoechst 33342, through the activity of the ATP-binding cassette pumps localised to their plasma membrane (258). Endometrial side populations for both epithelial and stromal cells have been isolated from living tissues (259) and are capable of reconstructing the human endometrium, when placed under the kidney capsule of mice (260).

A second potential site for an endometrial stem cell population is in a perivascular location within the basal layer. In 2007, Schwab and Gargett identified a population of cells in the human endometrium that displayed similar characteristics to mesenchymal stem cells (MSC). Using two markers; CD146 and platelet derived growth factor receptor β (PDGFRβ) they identified putative pericytes (261), it is postulated that this MSC-like population contributes to the regeneration of both the stromal cell and endothelial cell compartments of the endometrium with each menstrual cycle. More recently, in 2012, Masuda *et al*., (262) have identified W5C5, a single marker that was able to isolate multipotent and self-renewing

MSCs from the endometrium. When exposed to myogenic or angiogenic conditioned media *in vitro*, these cells were able to differentiate into smooth muscle cells and endothelial cells respectively. When placed under the kidney capsule of ovariectomised immunodeficient mice, cells formed stromal cell-like connective tissues, with the support of exogenous oestrogen (262).

A contribution of bone marrow progenitors to the endometrium has also been investigated, following on from a demonstration that haematopoietic stem cells are able to differentiate into hepatocytes (263), neurons (264) and skin (265). In 2004 and later in 2007, the first evidence for a bone marrow contribution to the endometrium was provided. Using a mouse model where bone marrow from male donors was injected into the uterus of recipient mice (266, 267), Y chromosome positive stromal and epithelial cells were observed in the uterus 6 months after bone marrow transplant. This study is supported by work from Cervello *et al.,* (268) who examined the endometrium of women who had undergone a bone marrow transplant for haematological malignancy and had received male-derived bone marrow. The authors observed Y chromosome positive epithelial and stromal cells in the endometrium of these women, however the numbers of cells were very low (0.45%-2.62%). Furthermore, the authors found that the male-derived donor cells were a time-limited population that did not contribute to the endometrial side population (268).

1.8 Disorders associated with endometrial function

1.8.1 Heavy menstrual bleeding

Abnormal uterine bleeding, characterised by heavy and prolonged periods, affects up to one-third of women of child bearing age, leading to social and physical morbidity (269). The mean blood loss per cycle in a normal woman is approximately 30ml (270); however women with heavy menstrual bleeding (HMB) report a mean blood loss of 60-80ml (271) whereas excessive HMB blood loss is reported as greater than 100ml (272).

It is unknown what causes heavy menstrual bleeding; whether it is caused by a delay in repair of the endometrium resulting in a longer bleed or if women with HMB have a thicker, decidualised endometrium resulting in an excess of tissue to be shed. Studies using menstrual effluent from women with HMB and women with normal blood loss have shown a role for prostaglandins in HMB. For example, increased concentrations of mRNAs for COX-1 and COX-2, enzymes that promote the synthesis of prostaglandins, were observed in menstrual effluent (273). HMB is also associated with a shift in the PGF2α/PGE2 ratio, with increased concentrations of PGE2 observed in menstrual effluent (274), which may have an effect on vessel stabilisation during the repair phase. Furthermore, concentrations of *VEGFa*

and active MMP mRNAs were lower in the effluent of women with HMB (275), which may contribute to a delay in epithelial repair. Hypoxia mediated HIF1α regulated VEGF production has been shown in *ex vivo* endometrial tissue cultures, and is thought to contribute to repair of the endometrium (192, 193). It is postulated that a defective hypoxic response may contribute to HMB. Therefore it is imperative to understand the mechanisms that drive the repair phase of the endometrium, in order to develop a therapeutic option for treating HMB.

1.8.2 Endometrial cancer

Endometrial cancer is the most common gynaecological condition in the developed world, and postmenopausal women account for 90% of diagnosed patients (Cancer Research, UK, (276)). Endometrial cancers are divided into two types; type 1 is the oestrogen-dependent endometrioid adenocarcinomas whilst type 2 is oestrogen-independent and carries a poor prognosis due to their intense metastatic phenotype (277–279).

The mechanisms that lead to endometrial cancer are poorly understood; however it is thought that progressive genetic abnormalities (280–283) eventually lead to disruptions in cellular processes that cause increased cell proliferation, a decrease in apoptosis and aberrant angiogenesis (284). It has also been proposed that aberrant inflammatory processes may contribute to endometrial adenocarcinoma (285). Therefore, understanding the mechanisms that control these processes (proliferation, inflammation, apoptosis and angiogenesis) during endometrial repair may provide an insight to the aberrant mechanisms in the development of cancer.

1.8.3 Endometriosis

Endometriosis is the growth of endometrial glands and stroma in sites outside of the uterus, typically on the peritoneum or the ovary (286, 287), and affects 1 in 10 women of reproductive age. Despite the disease first being described in the 1700s, the cause of this condition remains unknown. Endometriosis can cause chronic pelvic pain in some patients, although a direct relationship between pain severity and lesion characteristics has been difficult to demonstrate (288–291).

The most widely accepted theory of why endometriosis develops suggests that endometrial tissue fragments are flushed into the peritoneum at the time of menses and survive by developing a local blood supply (292). The presence of endometriotic tissue in areas outside of the peritoneal cavity (293, 294) and in males (295) appears to contradict this mechanism, and it has been suggested that there are different types of endometriosis that originate from different cell types. For example, there is emerging evidence that endometrial progenitors

shed during menses may contribute to lesion development at ectopic sites (296). Alternative theories include aberrant actions of peritoneal mesothelial cells and stem cells arising from the fallopian tube (reviewed by (297)).

Endometriotic lesions have heterogeneous morphology containing a stromal cell compartment and a glandular epithelium, as well as blood vessels, which closely interact with the mesothelium of the peritoneum to establish blood flow (298) and to ensure lesion development. Lesion development and endometrial repair are likely to share common mechanisms (proliferation, stromal cell organisation, angiogenesis) and therefore studying the repair phase may contribute to the understanding of this disease.

1.8.4 Polycystic ovarian syndrome

Polycystic ovarian syndrome (PCOS) is a complex gynaecological condition that affects approximately 5-20% of the population (299–304). The disease is characterised by endocrine symptoms including amenorrhoea (the absence of menses) and hyperandrogenism that causes outward symptoms including acne and hirsutism (299, 300). It is also linked to metabolic symptoms (305, 306) including peripheral insulin resistance (307) and obesity (308).

Hyperandrogenism in PCOS patients is caused by elevated LH (but not elevated FSH) (309). LH acts on LH receptors expressed on thecal cells stimulating overproduction of androstenedione, stimulating growth of an increased number of follicles and eventual atresia of these follicles which leads to the “cysts” like structures observed by ultrasound (310).

1.8.5 A potential role for androgens in endometrial pathologies

Androgens are not subject to the same fluctuations seen in oestradiol and progesterone (Table 1-1) (44) and therefore it is possible, that at the time of menses, that androgens may contribute to repair of endometrium by an oestrogen-independent mechanism. A role for androgens in endometrial function has not yet been fully elucidated. In a recent study, Marshall *et al.,* has identified a group of androgen-regulated genes in primary human endometrial stromal fibroblasts that appeared to play a role in protecting cells from apoptosis (cell death) and also mediated stromal cell migration (144). This suggests that androgens could play a previously unexplored role in the regulation of endometrial tissue repair.

Notably, aberrations in ovarian androgen production, such as in PCOS, have been shown to result in infertility. Androgens have been implicated in the development of endometrial cancers in post-menopausal women, due to androgens being aromatised to oestrogens to create a hyperoestrogenic state (311). Furthermore, androgens have been shown to promote

the metastatic potential of stromal fibroblasts cells *in vitro* in a model of prostate cancer (312) and could potentially promote prostate cancer cell growth by increasing expression of stromal fibroblast VEGF, as evidenced *in vitro* (313). Therefore, further investigation into androgen actions in the endometrium may elucidate mechanisms that could be targeted for the treatment of endometrial disorders.

1.9 Studying the endometrium

Modelling the dynamic changes observed in the human endometrium through-out the menstrual cycle in animals is challenging because only a few Old World Primates (314, 315) and bat species (316) undergo menstruation. Other mammals, such as rodents, who display cyclical changes in ovarian-derived steroids, do not exhibit endometrial shedding following progesterone withdrawal, rather a process of re-absorption and stromal cell compartment re-organisation (317).

1.9.1 Animal models of menstruation

The endometrium is a multi-cellular tissue with a complex stromal cell compartment that interacts with the epithelial cell compartments. Therefore using individual single cell culture techniques do not enable a full understanding of tissue function, as cell-cell interactions cannot be investigated. Animal models of endometrial function have been developed and successfully used to investigate the mechanisms of progesterone withdrawal and subsequent breakdown of the tissue *in vivo* (231, 233, 234). More recently, models have been used to delineate contributing factors to endometrial repair (188, 217, 239, 318–320). Xenograft models, using human endometrial tissue explants and immunodeficient mice, have allowed investigation of endometrial function *ex vivo* (260, 321–324).

1.9.2 Xenograft models

In vitro cultures of single cell suspensions or endometrial explants have limitations in that they do not have their own blood supply and the immune cell dynamics cannot be studied. Xenograft models using human endometrium, transplanted under the skin or under the kidney capsule of ovariectomised mice, maintain tissue integrity, whilst recreating the steroid micro-environment. Mice are treated with exogenous oestradiol and progesterone to mimic the human cycle. In response to progesterone withdrawal, endometrial explants undergo responses characteristic of menses, including tissue breakdown and immune cell influx (240). Xenograft models have been used to study a role for hypoxia during breakdown (321), immune cell dynamics (240, 325), and the regulation of MMPs during tissue remodelling (325).

1.9.3 Non-human primate models

Menstruating non-human primates, including the macaque, have been used to study endometrial function. Like women, macaques display an average 28 day menstrual cycle and have a similar uterus. As in women, their endometrium can also be morphologically characterised into functional and basal layers (326).

Artificial menstruation can also be induced in ovariectomised rhesus macaques (*Macaca mulatta*) (231). Sequential treatment with oestradiol for 14 days recreates the proliferative phase of the cycle and subsequent treatment with oestradiol plus progesterone mimics the secretory phase of the cycle. Removal of progesterone after 14 days induces a "menses like" event that mimics that of women.

This model has been used to study the mechanisms responsible for the induction of endometrial breakdown, including a role for MMPs during breakdown (231) and a role for fibronectin and integrins in endometrial repair (327). A role for VEGF in endometrial repair has also been highlighted using this model (328). *VEGFa* mRNA concentrations were observed to increase 2 days after progesterone withdrawal, during endometrial breakdown. A further increase in VEGF expression and in the expression of VEGF receptors 1 and 2 was observed during the window of repair (328).

Slayden and Brenner, have identified a critical window of progesterone withdrawal in these animals (329) where menstruation could be reversed if progesterone was withdrawn and then replaced within 36 hours. This study supports the hypothesis by Kelly *et al.,* who postulate that menstruation occurs in two phases (164). The first phase, where falling progesterone concentrations result in increased production in prostaglandins and vasoconstriction can be reversed if progesterone is replaced. This suggests that this phase is primarily controlled by progesterone mediating its effects through the progesterone receptor. However, the second phase of menstruation (tissue breakdown and sloughing) cannot be reversed irrespective of progesterone replacement as the factors that drive these mechanisms are postulated to be progesterone-independent (164).

A second non-human primate model involves sub-cutaneous auto-grafting of macaque endometrium (231). Ovariectomised animals are treated for 14 days with oestradiol, then with oestradiol and progesterone for 8 days. Endometrial grafts were then removed from the uterus, stripped of their functional layer and distributed across the abdominal surface in sub-cutaneous pockets. Animals received oestradiol and progesterone for one month then the progesterone pellet was removed and replaced in two week cycles to recreate recurring

menstrual cycles. These grafts undergo repair, growth and shedding in response to exogenous steroid hormones (231).

1.9.4 Murine models of breakdown and repair

1.9.4.1 Using the mouse to model human endometrial function

As in women, the murine endometrium is subject to cyclical fluctuations in concentrations of ovarian steroids as depicted in Figure 1-9, over a 4 day oestrous cycle. In similarity to women, the mouse undergoes endometrial proliferation during the oestrogen dominant proestrous and oestrous phases. Serum progesterone concentrations increase following ovulation however, the murine endometrium does not undergo spontaneous decidualisation in the absence of a blastocyst, nor does it breakdown at the end of each cycle following the withdrawal of progesterone (330). Despite these shortcomings, the availability of inbred strains and transgenic lines, including those with cell-specific deletions of genes, make mice an attractive model.

The mouse endometrium is similar to the human endometrium in that it can be divided into three layers; the myometrium, the compacted basal layer and the loosely compacted functional stromal compartment (Figure 1-10, A). Like the human endometrium the functional layer of the mouse endometrium contains a loosely packed stromal cell compartment containing endothelial cells and a luminal and glandular epithelium as depicted in Figure 1-10, B.

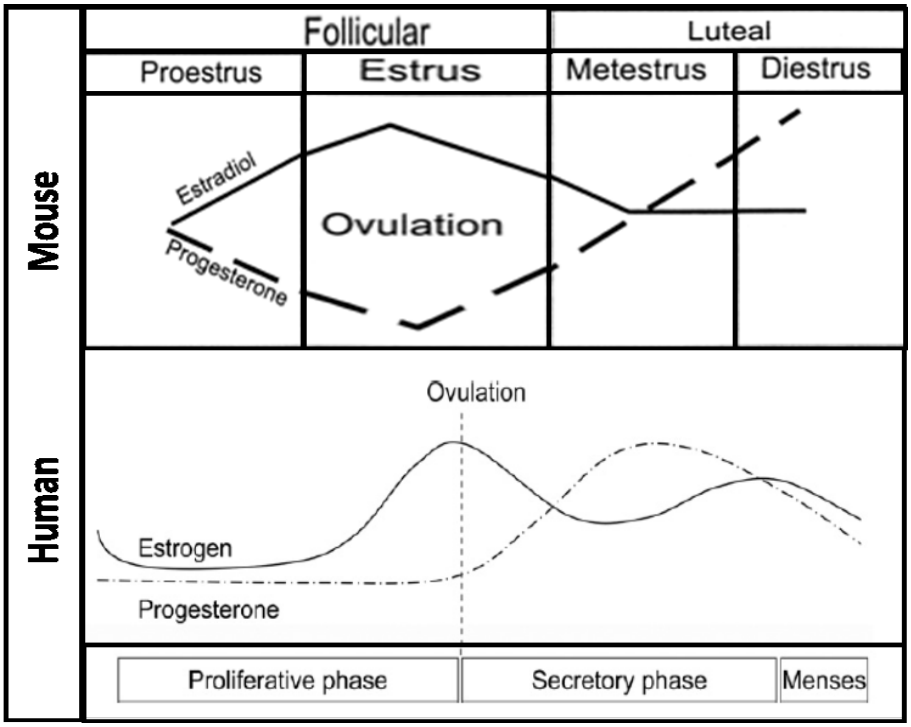

Figure 1-9: Comparison of murine and human steroid hormone fluctuations across a 4 day oestrous cycle (mouse) and a 28 day menstrual cycle (human). Both species are exposed to rising concentrations of oestrogens during the follicular phase, with a peak prior to ovulation. Serum progesterone concentrations increase during the luteal phase, adapted from (168, 330).

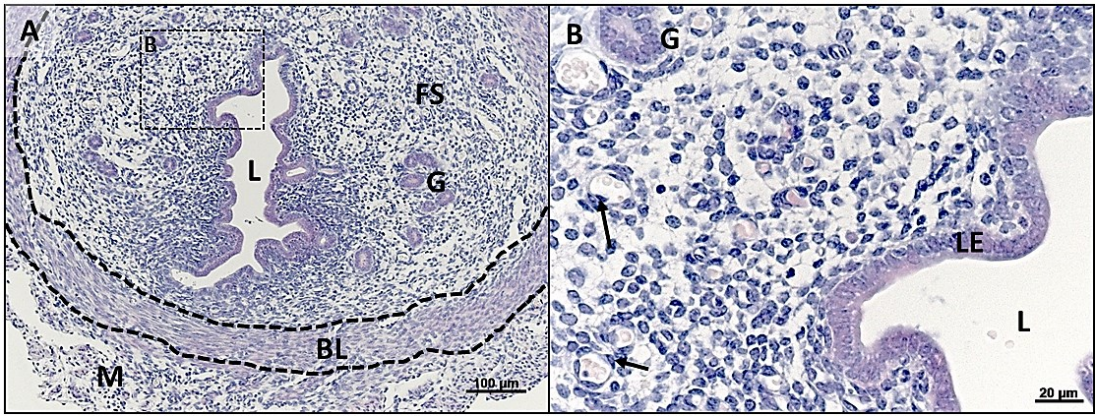

Figure 1-10: The murine endometrium. A; The endometrium is divided into three layers; the myometrium, the basal layer and the functional layer. B; the functional stroma contains a glandular and luminal epithelium and endothelial cells. L; lumen, LE; luminal epithelium, G; glandular epithelium, BL; basal layer, FS; functional stroma, M; myometrium; arrows indicate endothelial cells. Author's own image.

1.9.4.2 Artificial induction of decidualisation and subsequent breakdown in an ovariectomised mouse model

Finn and Pope recognised the need for a small animal model of menses and were the first to describe the artificial induction of decidualisation and menstruation in an ovariectomised albino mouse (234). Finn and Keen had previously developed the artificial decidualisation of the rat endometrium by oil injection in 1967 (331), having identified a defined treatment regime of exogenous steroids to prime the rat endometrium for decidualisation. Finn and Keen experimented with a number of non-water soluble solvents; including fat solvents (ether, benzene and glycerol), polysaccharides, serum, plasma and dextran but none of these solvents induced decidualisation. Decidualisation by oil injection (olive, sesame or paraffin) all led to a decidual response in primed rats, the authors hypothesise that it is the "oiliness" and persistence of these solvents that induces decidualisation by acting like an implanting blastocyst.

Finn and Pope's model uses an optimised schedule of oestradiol and progesterone injections (73) to mimic the oestradiol and progesterone dominant phases of the human menstrual cycle combined with induction of a decidualised cell reaction by oil injection (332). Cessation of progesterone injections results in endometrial breakdown and a "menses like" event; which displays similar characteristics of menses in women including an inflammatory response, tissue necrosis, breakdown and luminal shedding.

Despite the authors describing a "menses like" event this model was not widely used until 2003, when Brasted *et al.,* (233) reinvigorated interest and made further modifications to the Finn and Pope model. Notably, by using silastic progesterone-secreting pellets, rather than daily injections, to ensure a constant delivery of progesterone (333). Also they used the inbred C57BL/6 strain of mice to reduce intra-animal variation. The authors used this model to investigate cellular apoptosis and leukocyte infiltration during breakdown (233), but more importantly their studies were the first to define stages of breakdown in a rodent model. Also they show that "repair", or re-epithelialisation, was complete within 48 hours of the initiation of breakdown (progesterone pellet removal) (233).

This revised version of the mouse menses model has since been used to study a number of factors that might contribute to bleeding and subsequent repair (79, 188, 217, 230, 235, 239, 318, 319, 334). As in primates, a critical window of progesterone withdrawal has been identified in the mouse model; with replacement of progesterone 8-12 hours after the removal of the progesterone pellet (withdrawal) being sufficient to stop bleeding (at 8 hours) or reduce bleeding (at 12 hours) (235). Replacement of progesterone at 8 hours was

sufficient to maintain the decidual cell response, with little cell death observed. Progesterone replacement after 12 hours was unable to prevent cellular apoptosis or bleeding. This study identified a critical window of breakdown in the mouse following artificial decidualisation, with the "first phase" of breakdown complete 12 hours after progesterone withdrawal (235).

A number of studies have used mice to investigate a role for immune cells during endometrial breakdown and subsequent repair (217, 334). Menning *et al.,* investigated the effects of inhibiting all granulocytes using an anti-mouse GR-1 antibody which binds to all cells that are GR-1^+ (bone marrow derived monocytes, capable of differentiation into macrophages and dendritic cells). In GR-1^+ cell depleted mice concentrations of uterine MMPs 3, 9 and 10 were all significantly increased, suggesting that granulocytes may contribute to the regulation of the inflammatory response (334). A second study, which selectively inhibited neutrophils and eosinophils by use of the antibody RB6-8C5 observed delayed repair of the endometrium following breakdown. This antibody has been reported to have no effect on lymphocyte or macrophage numbers. The authors also noted that macrophages, as detected by immunolocalisation for F4/80, were in low abundance and they suggest that they may not contribute to repair of the murine endometrium (217).

Using this model it has been shown that the murine endometrium is capable of re-epithelialisation in the absence of oestrogen (239). This was achieved by removal of all exogenous steroids by use of a soy-free diet, and all effects of any exogenous oestrogens were inhibited using letrozole, an inhibitor of aromatase (the enzyme required for synthesis of oestradiol from androstenedione). Follow up studies have also indicated a role for extracellular matrix and activin in epithelial cell repair (79, 319).

A variation of this established model identified that pharmaceutical blocking of progesterone receptor, with mifepristone, was also adequate to induce a "menses like" event (335), and that breakdown was initiated at 16 hours after progesterone withdrawal. This is in line with the findings of Brasted *et al.,* (233) indicating that the induction of breakdown was not affected by either method of progesterone withdrawal.

1.9.4.3 Pseudopregnancy model of breakdown and repair

The models described in 1.9.4.2 used ovariectomised mouse models, where all hormones were given exogenously by subcutaneous injection (oestradiol) or by secreting pellet (progesterone).

Fan *et al.,* have developed a mouse model without the need for ovariectomy, in which endogenous ovarian hormones contribute to the regulation of uterine tissue (188). Briefly,

intact mice, of the CD1 strain, were mated with vasectomised males and then on day 4 of pseudopregnancy females received an intrauterine injection of oil to induce decidualisation. Steroid withdrawal was then induced 2 days after oil injection by ovariectomy. Endometrial shedding is complete within 24 hours of ovariectomy and re-epithelialisation was observed to occur at 48 hours (188) in the absence of oestradiol and progesterone.

Endometrial repair has been investigated using this pseudopregnancy model. As in the non-human primate model, VEGF was shown to be essential for re-epithelialisation, neo-angiogenesis and vessel stability during the repair phase in the mouse (188). Mice that received an inhibitor of VEGF, the VEGF trap, at the time of steroid withdrawal failed to fully repair, and deficiencies in vasculature were observed. The pseudopregnancy model has also identified a role for the Wnt family signalling molecule Wnt7a in re-epithelialisation, as adenoviral knock downs of Wnt7a resulted in a failure of re-epithelialisation and degradation of basal glands (320).

Using a variation of the pseudopregnancy model, Rudolph *et al.,* developed a mouse model of breakdown in BALB/C mice that displayed overt menstruation, where blood is either visible at the opening to the vagina or following lavage with a small volume of water. In this model, females were given an injection of mifepristone, 2 days after oil injection to block the progesterone receptor and mimic progesterone withdrawal; bleeding was evaluated using vaginal lavage (336).

The authors were the first to record overt menstruation in mice with blood flushed from the murine uterus, raising questions as to why previous mouse models of menses have not shown shedding and clearance of endometrial tissue.

1.10 General conclusions and aims of this study

The human endometrium is a multi-cellular tissue which under the influence of cyclical variations in concentrations of the ovarian steroid hormones oestrogen and progesterone undergoes cycles of growth, differentiation, shedding and repair. In a non-pregnant woman, menstruation, the shedding of the functional layer of the endometrium, is induced by the withdrawal of progesterone due to regression of the corpus luteum. This in turn initiates a cascade of events which cause tissue ischaemia, necrosis and subsequent clearance of the degraded tissue.

Simultaneous shedding and repair of the endometrium occurs, suggesting that repair mechanisms are initiated whilst the tissue is in an oestrogen-depleted state. The mechanisms that drive re-epithelialisation and stromal cell compartment reorganisation are not fully

understood. It is widely accepted that re-epithelialisation occurs through basal gland epithelial cell proliferation; however there is evidence for a contribution from the underlying stroma. It seems likely that the repair of the endometrium will occur through a combination of mechanisms with both the epithelial and stromal cell compartments of the residual basal layer contributing to the new luminal epithelium. A role for androgens has also not been previously explored.

As the endometrium is a multi-cellular tissue, models using tissue explants (xenografts) have been developed to maintain tissue integrity and to complement studies using single cell cultures. Both non-human primates and mice have been used to study menstruation and endometrial repair. These studies have largely focussed on the identification of tissue remodelling factors, including the metalloproteinases, and immune cells, namely leukocytes and neutrophils. However, little attention has been paid to macrophages which are at their highest numbers during menstruation in women, and therefore may be contributing to repair as well as tissue breakdown.

Models using ovariectomised mice, administration of exogenous steroids and oil-induced decidualisation have reported restoration of tissue integrity by 48 hours after progesterone withdrawal. However, studies using this model have not considered that the endometrium will shed and repair simultaneously. Nor have they shown overt menstruation, which has only been shown in a pseudopregnancy mouse model of breakdown.

In the studies outlined in this thesis, the following questions have been addressed:

1. Is it possible to establish a model of menses in the mouse, which mimics menses in women namely; simultaneous breakdown and repair, overt menstruation, immune cell influx, tissue necrosis and re-epithelialisation?
2. Does the stromal cell compartment contribute to endometrial regeneration?
3. Is there a role, if any, for androgens during endometrial repair?

Therefore the hypotheses of this study were; as demonstrated in the human, the stromal cell compartment will contribute to endometrial repair in a murine model of menses and androgens will have an effect on breakdown and repair of the endometrium following progesterone withdrawal.

In the present study, an established mouse model of endometrial breakdown was adapted and optimised to examine an early window of endometrial breakdown. Immunohistological examination of the endometrium was supported by mRNA expression data for candidate

genes hypothesised to be involved in endometrial repair. The effect of androgens on repair was investigated using this mouse model.

The results herein implicate androgens and stromal mesenchymal to epithelial transition in the restoration of endometrial tissue homeostasis during menstruation. These findings may inform development of new treatments for disorders associated with aberrant repair such as heavy menstrual bleeding and endometriosis.

Chapter 2 Materials and Methods

2.1 Animal work

All animal procedures were carried out under the Home Office Animals (Scientific Procedures) Act 1986 under project licence number PPL 60/4208 and personal licence number PIL 60/12992.

All animals were housed in standard conditions with food and water provided *ab libitum* with a constant light cycle of 12 hours.

Wild type C57BL/6 mice were bred in house from available breeding stocks or purchased from Charles River (Charles River Laboratories International, Inc. 251 Ballardvale Street, Wilmington, Massachusetts, USA).

2.1.1 Collection of control murine uterine tissue

To monitor oestrous cycles, adult females of 4-8 weeks of age received daily cervical smears for 14 days. Each vaginal secretion was collected on glass slides, air dried, fixed in methanol, stained with haematoxylin and eosin and viewed under a microscope. Stages of oestrous were identified as diestrus, proestrus, estrus and metestrus seen in Figure 2-1.

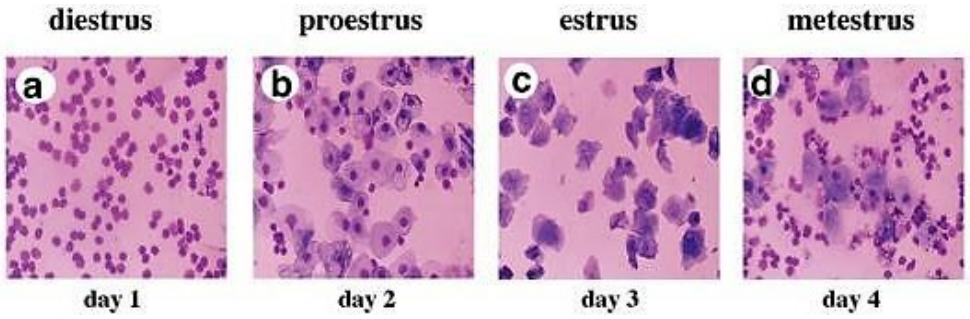

Figure 2-1: Haematoxylin staining of the oestrous cycle of the mouse. Adapted from (337)).

Mice were culled on an appropriate day, so that uterine tissue at each stage could be collected for analysis. One hour prior to culling, mice were injected intraperitoneally with 5-bromo-2'-deoxyuridine (BrdU) (Sigma Aldrich, St Louis, Montana catalogue number) (2.5mg/ml in PBS) to enable identification of actively proliferating cell types at each stage of the cycle.

2.1.2 Transgenic mice- the fms-EGFP mouse line- "The Mac green mouse"

Macrophage colony stimulating factor (CSF-1) regulates differentiation, proliferation and survival of cells of the mononuclear phagocyte system (338). The gene is expressed

selectively in macrophage and trophoblast cell lineages and its activity is mediated by the CSF-1 receptor encoded by *c-fms* proto-oncogene (339, 340).

The generation of these mice has been described previously (340–342). Founder stocks were obtained from Dr. Bernadette Dutia and Professor David Hume (Roslin Institute, University of Edinburgh). Two heterozygous EGFP positive males and two heterozygous EGFP positive females were cross bred with wild type C57BL/6 to form a breeding colony.

2.1.3 Genotyping macrophage green fluorescent protein labelled mice

2.1.3.1 Preparation of digestion buffer

A 50ml stock solution of digestion buffer was prepared using the reagents listed in Table 2-1 and kept at room temperature.

Reagent Stock	Final Concentration	Volume for 50ml stock
KCl 1M	50mM	2.5ml
Tris-HCl pH8.3 1M	10mM	0.5ml
Gelatine 0.2g/ml	0.1mg/ml	25µl
Tween 20 20%	0.45%	1µl
H_2O		46.974ml

Table 2-1: Digestion buffer reagents and volumes for stock solution.

2.1.3.2 Preparation of stock proteinase K

Proteinase K is a serine protease with broad peptide cleavage activity and therefore is used to digest proteins in biological samples.

Stock Proteinase K (Promega, Wisconsin, USA) was re-suspended in 5ml of proteinase K reconstitution buffer (50mMTris-HCl (pH8) and 10mM $CaCl_2$) (Promega) to a working concentration of 20mg/ml and aliquoted and stored at -20°C.

2.1.3.3 DNA extraction from mouse ear biopsy

For each reaction, 50µl of digestion buffer and 200µg/ml of proteinase K were added to each ear clip and then incubated at 55°C for 5 minutes and 95°C for 10 minutes. Suspensions were then stored at -20°C until PCR analysis could be completed.

2.1.3.4 PCR for EGFP transgene in DNA sample from mouse ear biopsy

PCR was carried out to amplify a region of the EGFP transgene using specific primers to EGFP. An internal control, fatty acid binding protein 2 (*Fabpi*), was used as a control for both DNA quality and the success of the PCR reaction.

A final reaction volume of 10µl was prepared from 2x Biomix (Bioline, London, UK), 100µM stocks of EGFP primers (Eurofins mwg operon, Ebersberg, Germany) and 100µM

Fabpi primer stocks (internal control) (Eurofins). Final concentrations, primer sequences and reaction volumes are shown in Table 2-2. Primer sequences for EGFP and *Fabpi* are shown in Table 2-3. A positive (known GFP animal), a negative control (known negative GFP animal) and a no template control (no DNA) were also prepared.

PCR amplification was carried out under the following conditions; 35 cycles of 94°C for 30 seconds; 65°C for 30 seconds; 72°C for 1 minute then 72°C for 7 minutes and finally 10°C for ten minutes. Samples were then kept at 4°C overnight OR at -20°C for later processing.

Reagent Stock	Final Concentration	Volume per 10µl reaction (µl)
2x Biomix	1x	5
EGFP Forward Primer 100µM	100nM	0.1
EGFP Reverse Primer 100µM	100nM	0.1
Fabpi Forward Primer 100µM	100nM	0.1
Fabpi Reverse Primer 100µM	100nM	0.1
H_20		3.6
DNA		1

Table 2-2: PCR mastermix reagents and volumes for 10µl reaction.

Primer	Primer Sequence
EGFP Forward	5' GCA CGA CTT CTT CAA GTC CGC CAT GCC 3'
EGFP Reverse	5' GCG GAT CTT GAA GTT CAC CTT GAT GCC 3'
Fabpi Forward	5' CCT CCG GAG AGC AGC GAT TAA AAG TGT CAG 3'
Fabpi Reverse	5' TAG AGC TTT GCC ACA TCA CAG GTC ATT CAG 3'

Table 2-3: Primer sequences for EGFP and *Fabpi.*

2.1.3.5 Automated analysis of DNA fragments using the QIAxcel system

The QIAxcel system (QIAGEN) is an automated multi-capillary electrophoresis system for separation of DNA fragments with high detection sensitivity even at low concentrations of nucleic acids. The system uses high resolution cartridges capable of detecting fragments as small as 15 base pairs.

2.1.3.6 DNA separation

Samples were added to individual capillaries set in a pre-cast gel cartridge. Negatively charged nucleic acids migrate to the positively charged end of the capillary. As they migrate they pass a detector which measures fluorescence, this emission signal is converted into an electronic data by the photo multiplier (Figure 2-2). Results are displayed as an electropherogram (not shown) or as a gel image, (Figure 2-3).

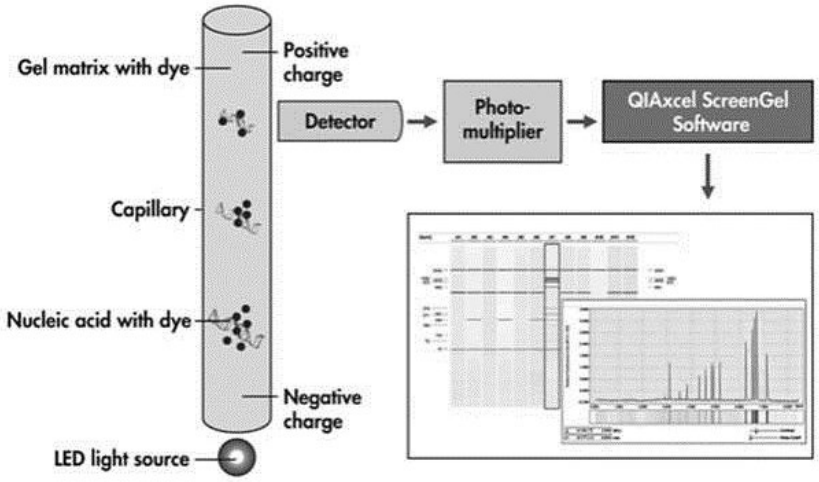

Figure 2-2: Sample separation of DNA fragments using the QIAxcel system adapted from the QIAxcel handbook.

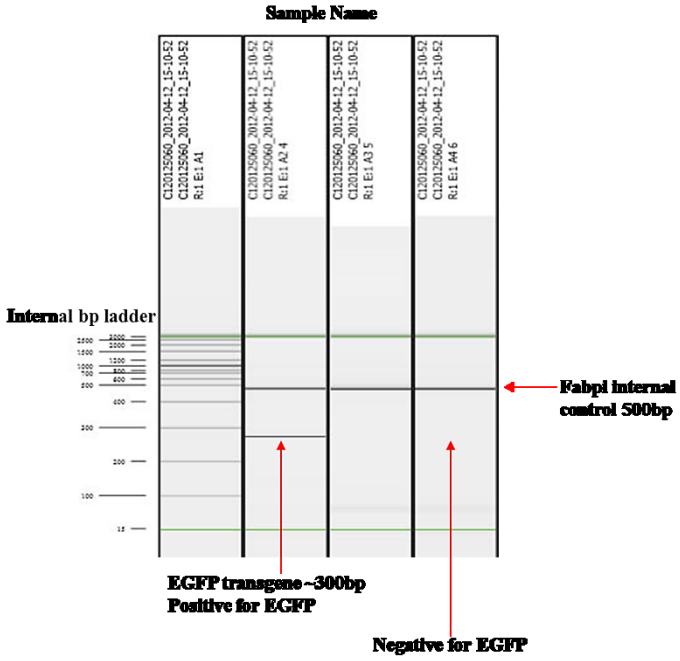

Figure 2-3: Gel image of typical DNA fragment analysis using QIAexcel. Positive sample for EGFP shown in lane 2, negative sample shown in lanes 3 and 4. Internal *Fabpi* control shown at 500bp.

2.1.4 Mouse model of menstruation and regeneration

2.1.4.1 Preparation of steroids for injection

A 1mg/ml stock solution and a 50µg/ml stock solution of β-oestradiol were prepared using crystallised β-oestradiol (E8875, Sigma) and 100% ethanol (VWR Prolabo, France).

Final working concentrations of 1µg/ml and 50ng/ml were prepared using a 1/1000 dilution of stock solutions in sesame seed oil (S3547, Sigma).

2.1.4.2 Preparation of progesterone secreting pellets

Lengths of rubber tubing (Dow corning silastic tubing Cat #508-008, 1.57mm I.D x 3.18mm OD) were washed in 70% ethanol and rinsed in distilled water before air drying. From this tubing, 14mm lengths were cut and one end sealed using adhesive sealant (Dow Corning multipurpose sealant 732). The pellets were then filled with crystalline progesterone (P1030, Sigma) and sealed.

2.1.4.3 Enzyme-Linked Immunosorbent Assay (ELISA) for quantitative determination of progesterone secretion from pellets

Prior to sub-cutaneous insertion, each progesterone pellet was incubated in 1ml of 1% charcoal stripped foetal calf serum (CSFCS) in phosphate buffered saline (PBS) (1%CSFCS:PBS) for a minimum of 48 hours at 37°C. The 1%CSFCS:PBS solution was collected and analysed on the same day. Determination of pellet progesterone secretion was carried out using a progesterone enzyme-linked immunosorbent assay (ELISA) kit (DEMEDITEC diagnostics, Germany). This ELISA is based on the principle of competitive binding where progesterone in the sample of interest competes with a progesterone horseradish peroxidase (HRP) conjugate for binding to a polyclonal anti-progesterone antibody which has been pre-coated to the microtiter wells of the ELISA plate. The amount of bound peroxidase is inversely proportional to the amount of progesterone in the sample.

2.1.4.3.1 Assay procedure

Aspirated 1%CSFCS:PBS solution, along with 6 known standards and 3 control samples (CSFCS media spiked to be “low”, “medium” and “high” for progesterone) (Table 2-4) were dispensed in duplicate in 25µl volumes into microtiter wells pre-coated with a polyclonal anti-progesterone antibody and left to incubate at room temperature for 5 minutes. Progesterone conjugated to HRP, was added to each well in 200µl volumes. The plate was then incubated for 1 hour on a shaking plate to ensure thorough mixing of sample and enzyme conjugate. Wells were rinsed thoroughly 5 times with wash buffer and struck against absorbent paper to remove any residual liquid. A substrate solution containing tetramethylbenzidine was added to each well in 200µl volumes and left to incubate in the dark at room temperature for 15 minutes. The reaction was then stopped by the addition of 100µl of ‘stop solution’ (1N Hydrochloric Acid solution).

Standard/ Known Control	Concentration (ng/ml)
Std 0	0
Std 1	0.3
Std 2	1.25
Std 3	2.5
Std 4	5
Std 5	15
Std 6	40
Low Progesterone	5
Medium Progesterone	15
High Progesterone	30

Table 2-4: Progesterone concentrations of known standards and controls (ng/ml).

2.1.4.3.2 Assay characteristics

The range of the assay was between 0-40ng/ml. Cross reactivity of the antibodies with other steroid hormones were previously tested by the manufacturer and are depicted in Table 2-5.

Steroid	Cross Reaction (%)
Progesterone	100
17α OH Progesterone	0.3
Estriol	<0.1
Estradiol 17β	<0.1
Testosterone	<0.1
11-Desoxycorticosterone	1.1
DHEA-S	<0.02
Cortisol	<0.02
Corticosterone	0.2
Prenenolone	0.35
Cortison	<0.1
11-Desoxycortisol	0.1

Table 2-5: Specificity of antibodies.

Intra assay variation and inter assay variation indicate the precision and repeatability of the assay. Intra assay variation, describes the variation within a data set from on experiment, an intra assay variation of <10 is acceptable. Inter assay variation describes the variation from one assay plate to another, an inter-assay variation <15 is generally acceptable. Intra and inter assay variations shown below in Table 2-6 and Table 2-7 respectively.

Sample	n	Mean (ng/ml)	CV (%)
1	20	0.62	5.4
2	20	4.67	6.99
3	20	10.8	6.86

Table 2-6: Intra assay variation.

Sample	n	Mean (ng/ml)	CV (%)
1	12	0.56	9.96
2	12	4.55	4.34
3	12	10.65	5.59

Table 2-7: Inter assay variation.

2.1.4.3.3 Assay data analysis

The optical density of each well was read at 460nm. Standard curve and average absorbance values were calculated using Masterplex Readerfit (MiraiBio Group, Hitachi Solutions, California, USA).

Pellets that were identified to be secreting ≥10mg/ml of progesterone were chosen for subsequent animal studies.

2.1.4.4 Mouse model of menstruation protocol

A mouse model of menstruation was established in house using a protocol adapted from (233). An overview of the adapted protocol is shown in Figure 2-4.

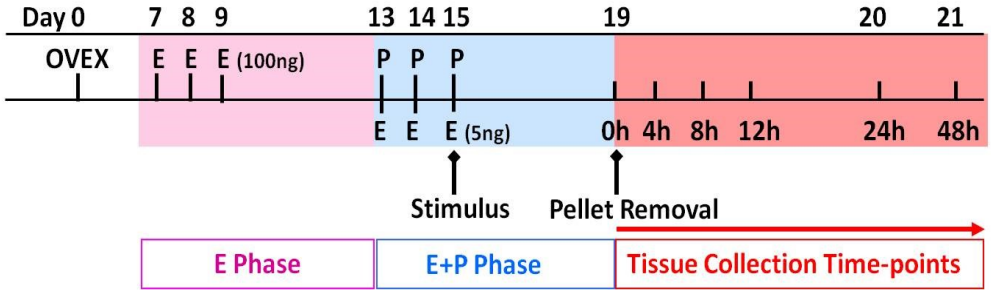

Figure 2-4: Mouse model of menstruation and regeneration. Ovex; ovariectomy, E; β-oestradiol, P; progesterone. β-oestradiol concentrations in brackets.

Female C57BL/6 mice of 8-10 weeks of age were ovariectomised under iso-fluorane induced anaesthesia (Merial), whilst also receiving a post-operative injection of the analgesic, buprenorphine (Vetergesic, 0.1mg/kg, Alstoe animal health). Animals were allowed to recover for seven days following surgery, to allow for depletion of endogenous steroid production. On days 7-9, mice received sub-cutaneous injections (0.1ml) of β-oestradiol in sesame seed oil (1µg/ml), resulting in a final dose of 100ng/100µl. On day 13 after ovariectomy, mice were anaesthetised under iso-fluorane and progesterone secreting pellets were place sub-cutaneously. On days 13-15 mice received daily sub-cutaneous injections (0.1ml) of β-oestradiol in sesame seed oil (50ng/ml), resulting in a final dose of 5ng/100µl. To induce endometrial decidualisation, stimulation of one uterine horn was performed under iso-fluorane induced anaesthesia using a single embryo transfer device (Datesand, Manchester, UK). Twenty microlitres of sesame seed oil was delivered trans-vaginally into the uterine lumen of one horn. The contra-lateral horn was untreated and served as a control.

Progesterone withdrawal was induced when pellets were removed 90 hours after oil injection, designated as time 0. Animals were culled by asphyxiation by carbon dioxide gas at 0, 4, 8, 12, 24 and 48 hours after steroid withdrawal.

Each animal received intra-peritoneal injections of BrdU (2.5mg/ml in PBS) and Hypoxyprobe® (15mg/ml in PBS) 90 minutes prior to culling to measure cellular proliferation and cellular oxygen tension respectively. Hypoxyprobe® is a reagent which forms protein adducts within cells that are at a pO_2 pressure of less than 10mmHg, <1% oxygen and is visualised by as a brown stain following immunohistochemistry. The intensity of immunostaining is directly proportional to oxygen tension. Strong immunostaining is indicative of very low oxygen tensions, cells are exposed to very hypoxic conditions, whereas, the absence of immunostaining indicates cells that are under normoxic conditions (>1% oxygen).

Blood from each animal was collected by venepuncture, centrifuged for 5 minutes at 13,000 rpm and the supernatant serum collected and stored at -20°C for future analysis.

Uteri were dissected, cleaned of fat and weighed. Tissue was cut into pieces and stored in either RNAlater (QIAGEN) at -80°C for subsequent RNA extraction or in 10% neutral buffered formalin (NBF) overnight for histological analysis.

Decidualisation was considered successful where a 400% increase in uterine horn weight as compared to the non-decidualised contra lateral control horn was observed. Any mouse in which the oil treated horn did not meet this criteria was excluded from the study.

2.1.4.4.1 Enzyme immunoassay for quantitative determination of progesterone in sera

Progesterone concentrations in sera were measured to ensure steroid withdrawal had occurred. Determination of progesterone in sera was carried out as described in 2.1.4.3, using 25µl volumes for each sample.

2.2 RNA extraction

Extraction of RNA from either mouse uterine tissue or human cell monolayer extracts was performed using the RNeasy mini kit according to manufacturer's instructions (QIAGEN).

Pieces of mouse uterine tissue previously stored in RNAlater (RNA stabilisation reagent) at -80°C were thawed to room temperature. Each sample was weighed and a 30mg piece cut from the original sample. Any remaining tissue was restored in RNAlater at -80°C.

2.2.1 RNA extraction performed using the RNA easy mini kit

All mouse uterine horn samples were placed in RNeasy Lysis Buffer (RLT) with 1% β-mercaptoethanol and homogenized using metal beads and a tissue lyser (QIAGEN) according to manufacturer's instructions. All cell extracts were placed in RLT+1% (v/v) β-mercaptoethanol and homogenised using QIAshredder spin columns. Seventy percent ethanol was added to all lysates to aid binding conditions and each sample was added to an RNeasy mini spin column. Following a series of wash steps (as detailed in the RNeasy mini kit handbook) total RNA bound to the column whilst all contaminants were washed away. The purified total RNA was then eluted in 30µl of RNase free water.

2.2.2 RNA quantification using Nanodrop

The total concentration of RNA in each sample was determined using a Nanodrop ND-100 Spectrophotometer (Thermoscientific, Delaware, USA), which measured the absorbance of eluted RNA. Each sample was then standardised to a concentration of 100ng/µl using RNase free water and stored at -80°*C*.

2.3 Synthesis of complementary DNA

Reverse transcription of RNA to a single complimentary strand of DNA (cDNA) was performed using the Superscript VILO cDNA synthesis kit (InVitrogen) according to manufacturer's instructions, using the volumes outlined below in Table 2-9.

Reagent Stock	Volume per 40µl reaction (µl)
5x Vilo	8
10x Enzyme	0.5
RNA (100ng/µl)	2
Water	29.5

Table 2-8: Reagent volumes used for synthesis of complementary cDNA.

Each reaction contained a final concentration of 1x VILO reaction mix, 0.125x Superscript enzyme and 100ng/µl of RNA in a final volume of 40µl. Samples were then incubated under the following conditions: 25°C for 10 minutes, 42°C for 60 minutes and 52°C for 5 minutes in a thermal cycler (MJ Research PTC-200 Thermo Cycler, BC-MJPC200).

2.4 Quantitative Real Time PCR- TaqMan method

Quantitative real time polymerase chain reaction (qRTPCR) is used to amplify and quantify specific PCR products whilst significantly reducing any background or false positives.

The TaqMan® method relies on fluorescent probes; in the current study these were supplied from the Universal Probe Library (Roche), to enable detection of specific PCR products after each PCR cycle. The fluorogenic probes have two fluorescent dyes; a 5'-end reporter dye 6-

carboxy-fluorescein (FAM) and a 3'-end quencher dye 6-carboxy-tetramethyl-rhodamine (TAMRA) (Figure 2-5, A) that binds to an amplicon defined by the specific primer pair (Figure 2-5, B). The quencher molecule inhibits the fluorescence emitted by reporter dye via fluorescence resonance energy transfer (FRET). The 5'-3' exonuclease activity of the Taq polymerase cleaves the dual-labelled probe resulting in the release of the reporter dye (Figure 2-5, C). Fluorescence is measured proportionally to the release of the FAM fluorophore.

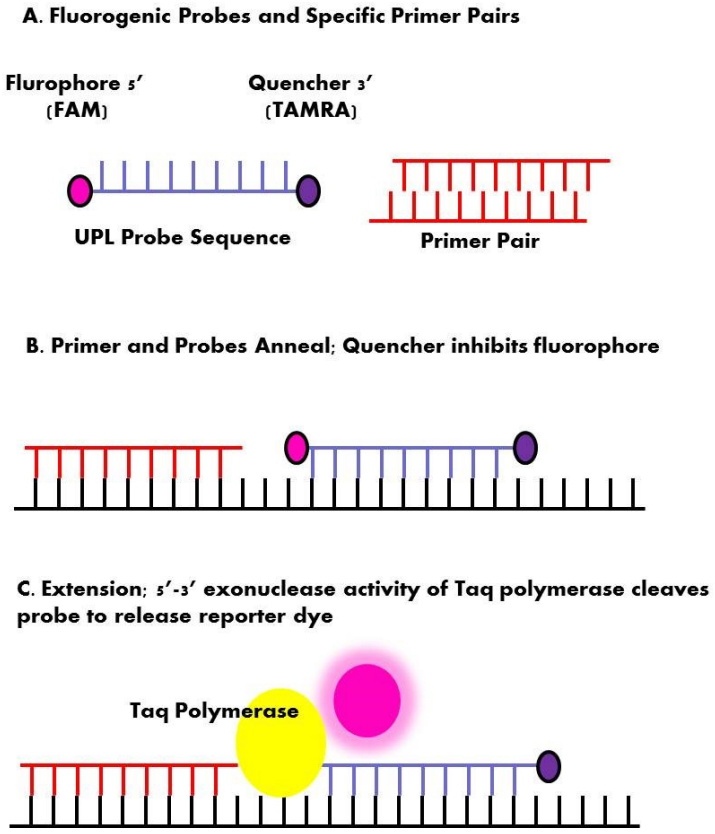

Figure 2-5: Quantitative RTPCR TaqMan Method. A. Fluorogenic probes have two fluorescent dyes; a 5' reporter (FAM) and a 3' quencher (TAMRA). Specific primer pairs for the gene of interest were designed using the Universal Probe Library Assay Design Center (Roche Applied Science). B. Primers and probe bind to the amplicon defined by the specific primer pair. The 3' quencher inhibits fluorescent emissions by the reporter dye. C. The exonuclease activity of Taq polymerase cleaves the dual labelled probe which results in the release of the reporter dye. Fluorescence is measured. (Adapted from (343)).

2.4.1 Quantitative Real Time PCR (qRTPCR)

A final reaction volume of 15µl (Table 2-9) was prepared for each sample that contained qPCR SuperMix with ROX premixed (InVitrogen, California, USA), an internal control gene 18s (VIC- conjugated); forward and reverse primers for the gene of interest (FAM-conjugated). Primers for each gene of interest were designed using the Universal Probe

Library Assay Design Center (Roche Applied Science, Penzberg, Germany) and purchased from Eurofins (mwg operon, Germany). Primer sequences are shown in .

Each reaction was prepared in duplicate and plated onto a 96 well MicroAmp Fast Optical reaction plate (Applied Biosystems, California, USA) and PCR amplification was carried out under the following conditions: 95°c for 10 minutes then 40 cycles of 95°c for 15 seconds then 60°c for 1 minute on a fast real-time PCR System (Applied Biosystems, 7900HT).

Reagent Stock	Final Concentration	Volume per 15µl reaction (µl)
2x Express Supermix	1x	7.5
Forward Primer 20µm	200nM	0.15
Reverse Primer 20µm	200nM	0.15
Probe 10µm	100nM	0.15
Housekeeping gene 18s	primer 10nM, probe 40nM	0.112
DEPC H_2O		4.375
cDNA		1.5

Table 2-9: Reaction volumes for TaqMan qRTPCR

2.4.2 Quantification of gene expression

Quantification of gene expression relies on plotting the detection of fluorescence against the number of cycles on a logarithmic scale. The threshold cycle (Ct) is defined as the number of cycles required for the fluorescent signal to exceed that of the background signal (Figure 2-6).

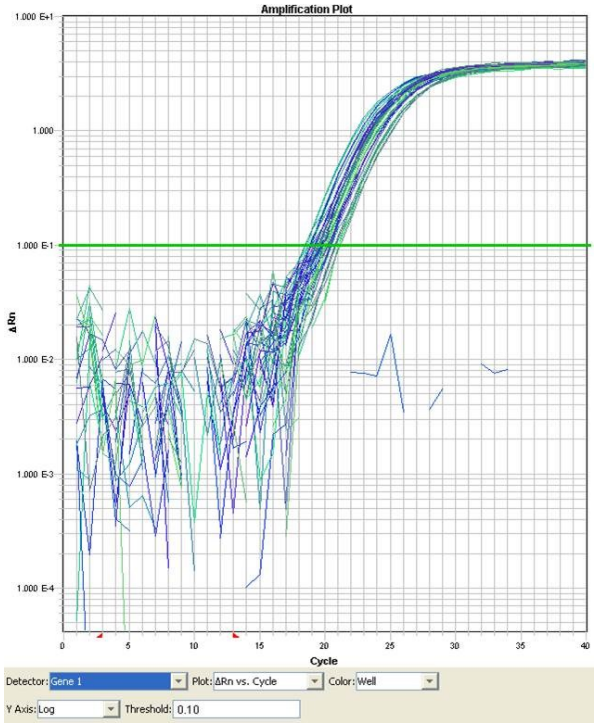

Figure 2-6: Quantification of gene expression. Detection of fluorescence is plotted against the number of cycles (x axis) on a logarithmic scale.

The Ct value is indirectly proportional to the amount of PCR product formed. Analysis was performed using the ΔΔCt method where the fold change is relative to a reference sample as well as an internal control. Sample Cts were normalised to the internal control 18s ribosomal RNA, where ΔCt= Gene of Interest Ct- 18s Ct. The fold change, ΔΔCt, was then calculated as the sample ΔCt – control sample ΔCt.

Gene name	Accession Number	Forward Primer Sequence	Reverse Primer Sequence	UPL Probe Number
Mus musculus prolactin family 8, subfamily a, member 2 *(Prl8a2)*	NM_010088.1	tcagctggacaatttgaaaca	tgtgacattagagtggcagtga	21
Mus musculus estrogen receptor 1 (alpha) *(Esr1)*	NM_007956.4	gctcctaacttgctcctggac	cagcaacatgtcaaagatctcc	97
Mus musculus androgen receptor *(Ar)*	Nm_013476	ccagtcccaattgtgtcaaa	tccctggtactgtccaaacg	58
Mus musculus wingless-related MMTV integration site 4 *(Wnt4)*	NM_009523	ctggactccctccctgtctt	atgcccttgtcactgcaaa	62
Mus musculus wingless-related MMTV integration site 7a *(Wnt7a)*	NM_009527.3	cgctcatgaacttacacaataacg	acaggagcctgacacaccat	78
Mus musculus cadherin 1 *(Cdh1)*	NM_009864.2	atcctcgccctgctgatt	accaccgttctcctccgta	18
Mus musculus cadherin 2 *(Cdh2)*	NM_007664.4	cctccatgtgccggatag	caccagaagcctccacagac	74
Mus musculus Vimentin *(Vim)*	NM_011701.4	tgcgccagcagtatgaaa	gcctcagagaggtcagcaaa	79
Mus musculus keratin 18 *(Krt18)*	NM_010664.2	agatgacaccaacatcacaagg	tccagaccttggacttcctc	78
Mus musculus vascular endothelial growth factor A (*Vegfa*, isoform 1)	NM_001025250.3	aaaaacgaaagcgcaagaaa	tttctccgctctgaacaagg	1
Mus musculus chemokine (C-X-C motif) ligand 12 *(Cxcl12),* transcript variant 3	NM_001012477.1	ctgtgcccttcagattgttg	taatttcgggtcaatgcaca	41
Mus musculus angiopoietin 1 *(Angpt1)*	NM_009640.3	cggatttctcttcccagaaac	tccgacttcatattttccacaa	50
Mus musculus angiopoietin 2 *(Angpt2)*	NM_007426.3	cacactgaccttccccaact	cccacgtccatgtcacagta	82
Mus musculus platelet/endothelial cell adhesion molecule 1 *(Pecam1),* transcript variant 2, mRNA	NM_001032378.1	cggtgttcagcgagatcc	actcgacaggatggaaatcac	45
Mus musculus snail homolog 1 (Drosophila) *(Snai1)*	NM_011427.2	gtctgcacgacctgtggaa	caggagaatggcttctcacc	71

Gene name	Accession Number	Forward Primer Sequence	Reverse Primer Sequence	UPL Probe Number
Mus musculus snail homolog 2 (Drosophila) *(Snai2)*	NM_011415.2	tgcaagatctgtggcaagg	cagtgagggcaagagaaagg	71
Mus musculus Wilm's tumor 1 homolog *(Wt1)*	NM_144783.2	cagatgaacctaggagctaccttaaa	tgcccttctgtccatttca	3
Mus musculus platelet derived growth factor receptor, beta polypeptide *(Pdgfrb),* transcript variant 1	NM_001146268.1	tcaagctgcaggtcaatgtc	ccattggcagggtgactc	67
Mus musculus connective tissue growth factor *(Ctgf)*	NM_010217.2	tgacctggaggaaaacattaaga	agccctgtatgtcttcacactg	71
Mus musculus MAD homolog 3 (Drosophila) *(Smad3)*	NM_016769.4	tccgtatgagcttcgtcaaa	ggtgctggtcactgtctgtc	32
Mus musculus chemokine (C-C) motif ligand 2 *(Ccl2)*	NM_011333.3	catccacgtgttggctca	gatcatcttgctggtgaatgagt	62
Mus musculus colony stimulating factor 1 (macrophage) *(Csf1)*	NM_001113529.1	caggtggaactgccagtataga	gagggtagtggtggatgttcc	12
Mus musculus matrix metallopeptidase 3 *(Mmp3)*	NM_010809.1	ttgttctttgatgcagtcagc	gatttgcgccaaaagtgc	7

Table 2-10: Primer sequences, accession numbers and UPL probe numbers used for genes of interest.

2.5 RT2 Profiler PCR array- SYBR® green method

RT^2 profiler arrays (SABiosciences, Frederick, MD, USA) combine the real time performance of PCR and the ability of a microarray to detect expression of many genes simultaneously. The arrays are designed to contain a panel of 96 primer sets containing housekeeping genes, quality controls and 84 genes that are related to a specific biological pathway. RNA samples used in RT^2 profiler PCR array were subject to quality assessment based on an RNA integrity number (RIN). Samples where RIN<6.0 were excluded.

The RT^2 profiler array uses SYBR® green based detection which differs to the Taqman method. Unlike Taqman, where a specific probe is used for a target sequence, SYBR® green can be added to any sample where it binds to all double stranded DNA present in the sample. During the PCR sequence, DNA polymerase amplifies the target sequence identified by the primers and creates PCR products to which the SYBR® green dye binds. As the PCR progresses, more product is created and an increase in fluorescent intensity is detected proportional to the amount of PCR product produced.

The SYBR® green method can result in false positives as the SYBR® green dye may bind to non-specific double stranded DNA sequences, therefore validation of the array was carried out using the Taqman method, which has a higher specificity.

2.5.1 RNA quantitation using Agilent Technologies

Agilent RNA kits (Agilent Technologies, Waldbronn, Germany) are designed to analyse RNA, using the RNA Integrity Number (RIN) as a measurement of overall RNA quality.

2.5.1.1 Preparing the gel

RNA samples were analysed using the Agilent RNA 6000 Nano Kit (Agilent Technologies, 5067-1511). Briefly, 550µl of the RNA gel matrix was pipetted onto a spin filter and centrifuged at 1500g for 10 minutes. The gel was then aliquoted into 65µl volumes and stored for future use at 4°C.

One microlitre of RNA dye concentrate was then added to one aliquot, mixed well and centrifuged at 13000g for 10 minutes.

2.5.1.2 Loading the Gel dye mix and marker

The gel dye mix was loaded onto the RNA chip as per manufacturer's instructions as detailed in the quick start guide. Five microlitres of the RNA marker were then added to all sample wells.

2.5.1.3 Loading the ladder and samples for analysis

Prior to loading onto the RNA chip, 1.2µl of each RNA sample, extracted as described previously, were denatured at 70°C for two minutes. The ladder was loaded onto the RNA chip as per manufacturer's instructions as detailed in the quick start guide. One microlitre of each RNA samples was added to an individual sample well on the RNA chip. The chip was then vortexed using an IKA vortexer for 1 minute at 2400rpm. The chip was then run on a 2100 Agilent Bioanalyser to measure eukaryote total RNA. RNA quality is displayed as an electropherogram (Figure 2-7) and a gel-like image (Figure 2-8), and as a RIN. A RIN greater than 6.0 was accepted for further analysis by PCR array.

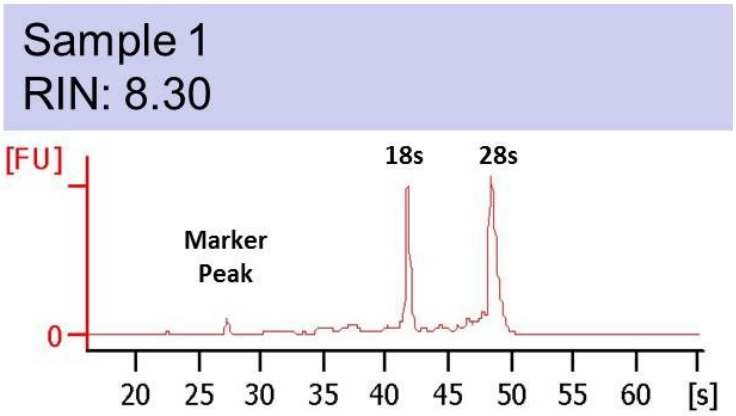

Figure 2-7: Electropherogram shows sharp peaks for the 18s and 28s ribosomal RNA. Time in seconds is displayed along the x axis, where fluorescence is displayed on the y axis.

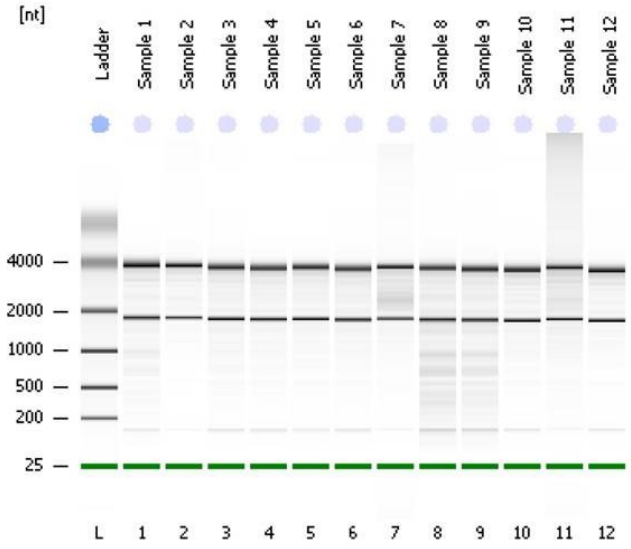

Figure 2-8: Digital gel-like image depicting sharp bands for 18s (~2000) and 28s (~4000) ribosomal RNA. Any sample which had failed the RNA quality control would be highlighted in red.

2.5.2 RNA quantification using Nanodrop

The total concentration of RNA in each sample was determined using a Nanodrop ND-100 Spectrophotometer, which measured the absorbance of eluted RNA. Each sample was then standardised to a concentration of 400ng/µl using RNase free water to be used in the profiler array.

2.5.3 cDNA synthesis using the RT2 first strand kit

Reagents from the RT^2 First Strand Kit were thawed prior to use, centrifuged and set on ice. A genomic elimination (GE) mix was prepared for each sample as outlined in Table 2-11.

RT Component	Volume per 10µl sample
RNA	400ng/µl
Buffer GE	2µl
RNase free water	Variable

Table 2-11: Genomic elimination mix.

Each GE mix was incubated at 42°C for 5 minutes then immediately set on ice for a minimum of 1 minute. The reverse transcription (RT) mix was prepared as outlined in Table 2-12, 10µl of the RT mix was added to each tube containing the GE mix and mixed thoroughly by pipetting. Samples were then incubated at 42°C for 15 minutes then the reaction immediately stopped by incubating at 95°C for 5 minutes, 91µl of RNase free water was then added to each sample and all reactions were then placed on ice.

RT Component	Volume x24 samples
5x Buffer BC3	96µl
Control P2	24µl
RE3 Reverse Transcriptase Mix	48µl
RNase free water	72µl

Table 2-12: Reverse transcription mix.

2.5.4 Real-Time PCR for RT2 profiler PCR arrays

A PCR components mix was prepared for each sample as shown in Table 2-13: . Using a 384 well plate (4x96 well format), 10µl of each sample was added to the appropriate wells. The plate was then sealed using optical adhesive film, and centrifuged for 1 minute at 1000g at room temperature.

Reagent	Volume per sample
2x RT^2 SYBR Green Mastermix	650µl
cDNA synthesis reaction	102µl
RNase free water	548µl

Table 2-13: PCR components mix.

Real time PCR amplification was performed using the Applied Biosystems 7900HT Fast Real-Time PCR system, following the two step cycling programme as detailed in Table 2-14.

Cycles	Duration	Temperature
1	10 minutes	95°C
40	15 seconds	95°C
	1 minute	60°C

Table 2-14: Thermal cycling programme for PCR amplification.

The RT^2 SYBR green mastermix uses hot-start Taq DNA polymerase, which prevents any polymerase activity prior to heat activation which reduces amplification of any non-specific PCR products. SYBR green fluorescence was detected during the annealing step in each cycle and the threshold Ct for each well was calculated.

2.6 Tissue processing

All samples were fixed in NBF overnight at room temperature, rinsed in 70% ethanol and then stored in 70% ethanol before tissue processing in a core facility according to standard protocols (www.crh.ed.ac.uk/surf).

Uterine samples were orientated in the wax blocks so that transverse sections of the uterine horn could be cut.

Serial 5µm sections were cut using a Leica RM2125RT microtome onto X-tra adhesive pre-cleaned micro slides (Surgipath, Leica Biosystems, Peterborough, UK) and incubated overnight at 57°C. Slides were stored at room temperature until future use.

2.7 Histological examination of murine uterine sections

2.7.1 Haematoxylin and eosin staining

Haematoxylin and Eosin staining (H&E) is a commonly used histological staining method. Haematoxylin colours the nucleus of a cell blue, whilst eosin colours cytoplasmic structures in varying shades of pink to red.

On serial sections mounted on slides, H&E staining was carried out on sections 300µm apart to determine a working area of uterus for further immunohistological analysis.

Tissues sections were dewaxed in xylene (VWR Prolabo) for 10 minutes (two 5 minute washes) before being rehydrated at 20 second intervals through descending concentrations of alcohol. Sections were washed in distilled water before submersion in Mayer's haematoxylin for 3 minutes. Following a further wash in water slides were dipped in 1% acid alcohol then followed by another wash in water. Slides were then passed through Scott's tap water for 10 seconds, washed in water then passed through eosin for 10 seconds before a final wash in water. Slides were then dehydrated through ascending concentrations of alcohols before a

final immersion in xylene to remove any alcohol on the slides. Slides were then mounted using Pertex (CellPath) and coverslips (VWR Prolabo).

2.7.2 Immunohistological examination of proteins

Immunohistochemistry (IHC) is a multistep method by which proteins are detected in tissues by exploiting the use of antibodies which bind to specific antigenic regions on proteins against which they are raised (primary antibodies).

Antigens can either be detected by enzyme mediated chromogenic detection (IHC method) or by fluorochrome detection (immunofluorescence (IF) method) using a secondary antibody raised against the IgG of the species in which the primary antibody was prepared (Figure 2-9).

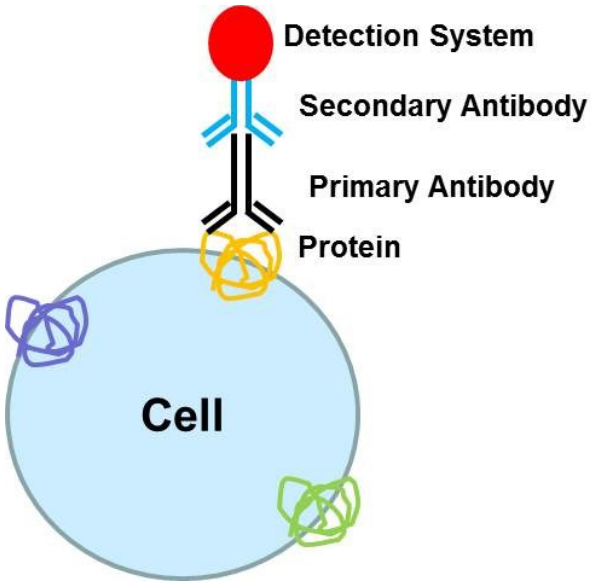

Figure 2-9: Immunohistological examination of proteins.

Unless otherwise stated, the detection method of each antigen was performed using a standard protocol. Unless otherwise stated, all wash steps were carried out twice for 5 minutes at room temperature.

2.7.2.1 Dewaxing and rehydrating of tissue sections

Tissue sections were dewaxed in xylene and rehydrated in descending concentrations of alcohol as previously described.

2.7.2.2 Antigen retrieval

Antigen retrieval is a technique employed to tackle the loss of immunoreactivity to some proteins which occurs during tissue fixation. Formalin fixation remains the fixative of choice, despite formalin fixation resulting in protein cross-linking (344), which "masks" or

"cloaks" the protein limiting the ability of protein epitopes to bind to their complementary antibodies. Antigen retrieval allows for the breaking of these cross-linkages, precipitation of protein and rehydration of tissue sections (345).

Key to the method of antigen retrieval is the exposure to heat (346) in an acidic or alkaline retrieval buffer (347, 348). Conditions are selected to denature but not destroy proteins within the tissue and are particularly recommended for proteins within the nucleus, e.g. steroid receptors. Unless otherwise stated all antigens were retrieved in citrate buffer (pH6).

Briefly, fixed sections mounted on slides were immersed in 0.01M citrate buffer, (pH6) and were exposed to heat using a decloaking chamber (Biocare Medical, CA, USA) on a set programme where the temperature of the citrate buffer was slowly risen to 124°C then decreased to 90°C over a 10 minute period. Slides were slowly brought back to room temperature by the addition of tepid water.

2.7.2.3 Endogenous peroxidase blocking

An endogenous peroxidase blocking step is included to reduce non-specific background staining that may be caused by the HRP-conjugate binding to endogenous peroxidases in the tissue of interest.

Sections were blocked in 3% hydrogen peroxide (H_2O_2) (VWR Prolabo) in methanol (Fisher Chemical) for 30 minutes then washed twice in TBS (IHC method) or PBS (IF method) for 5 minutes.

2.7.2.4 Serum blocking

Normal serum from the species that the secondary antibody was raised in was used to prevent non-specific binding of the secondary antibody.

Sections were blocked in 20% normal animal serum (NAS; 20% animal serum +TBS +0.05% bovine serum albumin (BSA)) for 30 minutes at room temperature then washed in the appropriate wash buffer.

2.7.2.5 Primary antibody application

Primary antibodies were added at an optimised dilution in NAS and left to incubate overnight at 4°C. Controls included a positive tissue control, a tissue negative control as well as an antibody negative control where the primary antibody was replaced with 20% normal serum. A complete list of primary antibodies and their working dilutions are shown below in Table 2-15.

Antibody Name	Supplier & Cat. No.	Dilution IHC	Dilution IF	Serum Block
Polyclonal sheep anti-**BrdU**	Fitzgerald 20-BS17	1/4000	1/5000	Rabbit
Rabbit polyclonal anti-**CD31**	Abcam 28364		1/1500	Goat
Mouse monoclonal anti-**Hypoxyprobe®**	hpi clone 4.3.11.3	1/100		Goat
Mouse monoclonal anti-**Pan cytokeratin**	Sigma C2562	1/2000	1/4000	Goat
Rabbit monoclonal anti-**Vimentin**	Cell Sigalling Tech #5741		1/600	Goat
Rabbit polyclonal anti-**Snail/Slug***	Abcam 63371	1/750		Horse
Rabbit polyclonal anti-**WT-1**	Santa cruz sc-192	1/1000		Goat
Rabbit monoclonal anti-**Androgen receptor**	Spring bioscience clone SP107	1/400		Goat
Rabbit monoclonal anti-**Green fluorescent protein†**	Invitrogen A11122	1/250		

Table 2-15 Primary antibodies and their suppliers and concentrations.

2.7.2.6 Secondary antibody application

Following overnight incubation of primary antibodies, sections were washed and then incubated at room temperature with either biotinylated secondary antibodies (IHC method) or with peroxidase-conjugated secondary antibodies (IF method) diluted 1/500 in NAS for 30 minutes. A complete list of secondary antibodies are shown below in Table 2-16.

Antibody Name	Supplier & Cat. No.
Rabbit anti sheep biotinylated	Vector BA 6000
Rabbit anti sheep peroxidase	AutogenBioclear ABN001HRP
Rabbit anti goat biotinylated	DAKO E0466
Rabbit anti mouse biotinylated	DAKO E0464
Rabbit anti mouse peroxidase	DAKO P0260
Goat anti rabbit biotinylated	Vector BA1000
Goat anti rabbit peroxidase	Vector PI1000
Goat anti mouse biotinylated	Vector BA9200
Goat anti mouse peroxidase	Abcam 6823

Table 2-16: Secondary antibodies and their suppliers.

2.7.2.7 Antigen detection

2.7.2.7.1 Enzyme mediated chromogenic detection- immunohistochemistry method

Enzyme mediated chromogenic detection involves the addition of enzyme which binds to the secondary antibody and then a substrate of that enzyme is introduced to form a visible reaction product in the form of a precipitate. The most commonly used enzymes for chromogenic detection are streptavidin-horseradish peroxidase (HRP) or streptavidin alkaline phosphatase (AP). For single antigen detection, unless otherwise stated, streptavidin-HRP was used.

Sections were incubated with streptavidin horseradish peroxidase (Vector, SA-5004), diluted in TBS, for 30 minutes at room temperature. Positive signals were visualised using the chromogen 3, 3-diaminobezidine (DAB) (Vector, Peterborough, UK) which formed a brown precipitate (Figure 2-10). Reactions were stopped by immersing the sections in water.

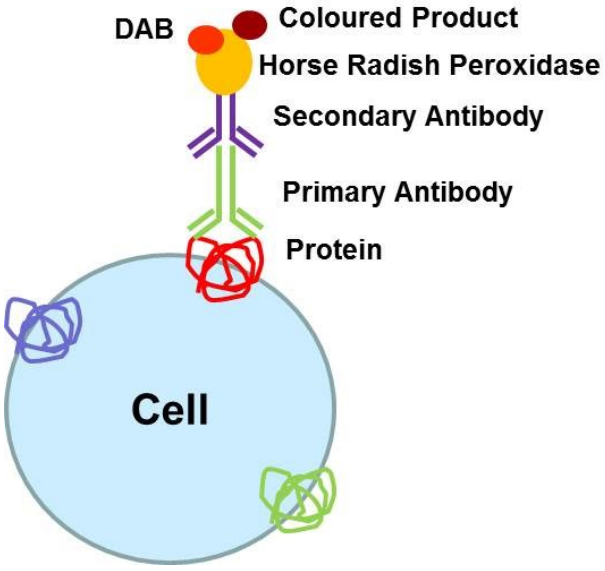

Figure 2-10: Enzyme Mediated Chromogenic Detection- Immunohistochemistry Method. After incubation with primary and secondary antibodies, sections are incubated in streptavidin horse radish peroxidase (Strep-HRP) and positive signals visualised by DAB.

2.7.2.7.2 Fluorochrome detection- Immunofluorescence method

Fluorochrome detection is commonly used to identify multiple antigens in the same tissue and also to determine if any co-localisation of target antigens has occurred. The Tyramide Signal Amplification (TSA^{TM}) system (PerkinElmer, Massachusetts, USA) allows for signal amplification and enables sub-cellular localisation of low abundance antigens. This results in increased sensitivity without an increase in background staining. Signal amplification by tyramide is activated by the catalytic activity of HRP, which converts tyramide into a

reactive intermediate that covalently bind to electron rich moieties to generate high-density labelling of the target protein.

Following incubation with secondary antibodies, sections were washed and incubated for 10 minutes in the dark with the Tyramide kit (Figure 2-11), diluted 1/50 in the kit diluent. In the case of a double stain, the red cyanine-3 fluorophore were used first as the green cyanine-5 fluorophore is more sensitive to photobleaching. All following steps were carried out with minimal light exposure. To prevent photobleaching, slides were covered with foil during all wash steps and incubated in the dark.

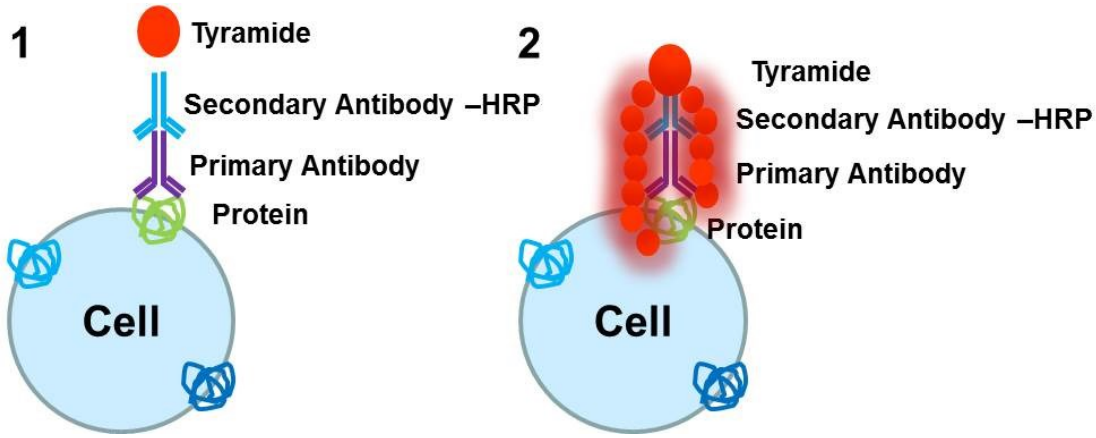

Figure 2-11: Enzyme Mediated Chromogenic Detection- Immunofluorescence Method. 1. After incubation with primary and secondary antibodies, sections are incubated with the tyramide signal amplification kit for 10 minutes. 2. Tyramide enables sub-cellular, high density labelling.

2.7.2.8 Nuclear counterstaining

2.7.2.8.1 Nuclear counterstaining- Immunohistochemistry method

Sections were counterstained in haematoxylin for 3 minutes and dipped in 1% acid alcohol (1% hydrochloric acid in 70% ethanol) before a thorough wash in water. Sections were then passed through ascending concentrations of alcohol; 70%, 80%, 95%; before immersion in xylene. Slides were then mounted with coverslips (VWR Prolabo) using Pertex (Cell Path).

2.7.2.8.2 Nuclear counterstaining- Immunofluorescence method

DAPI (4', 6-diamidino-2-phenylindole) is a fluorescent stain that passes through the cell membrane to bind to the A-T rich regions in DNA. Its emission wavelength is 461nm, therefore staining nuclei blue.

Following washes in PBS, sections were counterstained with DAPI (Sigma, D9542), diluted 1/1000 in PBS, for 10 minutes at room temperature. Sections were washed thoroughly in PBS, and then mounted with coverslips using the aqueous mounting medium permafluor (Immunotech, Marseille, France).

2.7.2.9 Modifications to the standard immunohistochemistry method

*The Snail/Slug antibody cross-reacts with both proteins; antigen retrieval was carried out at pH9, slides were blocked in 3% hydrogen peroxide for 30 minutes and then blocked in 2.5% horse serum for 30 minutes. The primary antibody was diluted in 2.5% horse serum and incubated overnight at 4°C. The ImmPRESS™ polymerised reporter enzyme detection system was used, where one drop of the anti-rabbit IgG was applied to each slide for 30 minutes. This detection system was used to increase sensitivity and reduce the background that had been previously observed using the standard protocol. Sections were washed and positive signals were visualised by DAB. Sections were counterstained, dehydrated and mounted as previously described.

† For green fluorescent protein (GFP), automated immunohistochemistry was performed using the Bond-max immunostaining machine (Leica Microsystems, UK). This automated system carries out a standard protocol as per manufacturer's instructions including; antigen retrieval, wash steps and peroxidase blocking before incubating with the primary antibody. A polymer refine detection kit is utilised to increase sensitivity. Positive signals were visualised by DAB.

2.7.2.10 Image analysis

DAB positive sections were imaged using AxioVision 4.8 Software (Carl Zeiss, Cambridge, UK) and a PROVIS microscope (Olympus Optical, London, UK) with an attached Canon DS126131 camera.

Fluorescent sections were imaged using Zen 2009 software (Carl Zeiss, Cambridge, UK) and a Zeiss LSM 510 Meta Confocal microscope (Carl Zeiss, Cambridge, UK).

2.8 Statistical Analysis

Serum progesterone concentrations were analysed by One Way ANOVA using the standard error of the mean, using Bonferroni post hoc testing to compare each time-point to the 0 hour time-point and then each other time-point.

mRNA concentrations for candidate genes were investigated across all time-points by One Way or Two Way Analysis of Variance (ANOVA) using the standard error of the mean. In Chapters 3 and 4 in each One Way ANOVA, Bonferroni post hoc testing was used to first compare all time-points to the 0 hour time-point before column to column analysis, which is indicated on each graph. In Chapter 5 where treatment with DHT was investigated, each Two Way ANOVA compared no treatment v treatment for each time-point by Bonferroni

post hoc testing as indicated. Data was analysed using Graphpad Prism 5, where significance was accepted where $p<0.05$.

For the SABioscience PCR arrays, analysis was performed using SABiosciences web portal, (http://pcrdataanalysis.sabiosciences.com/pcr/arrayanalysis.php); data analysis was performed using the ΔΔCt as described previously. Each time-point (8 and 24 hours) was compared to the 0 hour time-point by *Student t test*. Array validation by Taqman qRTPCR was performed by One Way or Two Way ANOVA as described in the figure legends.

Chapter 3 Establishment of a mouse model of menses for use as a functional model of endometrial breakdown and repair

3.1 Introduction

The human endometrium displays a remarkable ability of cyclical regeneration and remodelling, a process which can occur up to 400 times during a women's reproductive lifespan (82). Endometrial proliferation, differentiation and shedding occur under tightly controlled conditions, governed by the ovarian steroid hormones; oestrogen and progesterone (72). The cellular and molecular mechanisms that occur during the normal cycle have been widely studied (72, 87, 148–150); however mechanisms governing the repair and re-establishment of tissue homeostasis following menses have yet to be fully elucidated. Understanding these mechanisms is essential if we are to devise new therapies for endometrial pathologies, such as heavy menstrual bleeding, endometrial cancer or endometriosis.

The cascade of events that culminates in tissue destruction, loss of cell integrity and subsequent shedding of the upper functional layer of the endometrium at the time of menses (186) is generally accepted to be precipitated by the withdrawal of progesterone following the regression of the corpus luteum (62, 72, 349). Notably, some recent microscopy studies have revealed that shedding of the endometrium is a locally occurring, progressive process, with areas of partially shed, shed and regenerating endometrium observed in close proximity within the tissue (148). This observation would suggest that progesterone withdrawal not only initiates the onset of tissue breakdown but may also contribute to a molecular cascade stimulating endometrial repair. In the endometrium, restoration of tissue integrity is very rapid, with complete re-epithelialisation of the denuded basal layer of the endometrium occurring within 48 hours (201), thereby limiting the amount of blood loss from the exposed basal vasculature. Aberrations in the efficient regulation of this initial repair process may be a cause of the gynaecological complaint of heavy menstrual bleeding (HMB) (350).

It is well established that proliferation and differentiation of the functional layer of endometrium during the menstrual cycle is sex steroid-dependent being entrained by fluctuations in concentrations of ovarian steroid hormones in the general circulation (44). However, the rapid phase of endometrial regeneration, during which the tissue undergoes re-epithelialisation, neo-angiogenesis and vessel remodelling occurs whilst circulating

oestrogen and progesterone concentrations are low (44). This suggests that initial repair is not governed directly by ovarian derived steroid hormones. Notably, in an ovariectomised mouse model (239), restoration of endometrial integrity was observed to occur after shedding of the tissue, even in the absence of ovarian derived oestrogen action. However in contrast to mice, women are known to have significant circulating adrenal steroids (44). If, consistent with data from mice, the human endometrium is capable of restoration of tissue integrity in the absence of oestrogens, then other mechanisms must be pivotal in regulating the early repair of the epithelium and the remodelling of the stromal cell compartment after shedding of the functional layer.

Studies of the processes involved in the regulation of menses and repair face major challenges because only a few Old World Primates (315) and bat species (316) undergo physiological menstrual cycles. Other mammals, such as mice, who also display cyclical changes in both steroid hormone production and in their endometrial cell morphology, do not experience endometrial shedding following progesterone withdrawal, rather a process of re-absorption and stromal cell re-organisation (317). Therefore, in order to study the human endometrium, models must either be *in vivo* animal models that aim to mimic menstruation and subsequent repair (231, 233, 234) (described in section 1.9) or *in vitro* studies using human tissue explants (219, 221, 225, 351, 352), as studies using isolated human cells are less relevant because of the loss of intercellular signalling and architecture.

Due to their close relationship and existence of menstrual cycles a few non-human primate animal models have been used to study endometrial cycling. The macaque is the main non-human primate used to study endometrial function; the cynomolgus monkey (*Macaca fascicularis*) and the rhesus macaque (*Macaca mulatta*) are used to study endometrial cancer (353, 354) and menstruation (235, 329, 355, 356) respectively**.** The baboon (*Papio anubis*) (357–359) and the rhesus macaque (360–362) have been used to study endometriosis. However, there are drawbacks in using non-human primate models, including handling and housing costs, as well as low reproduction rates (363). A mouse model has the advantage of shorter generation times, larger litter sizes, increased genetic similarity in inbred strains to reduce animal variation and the option to use genetically modified transgenic animals; over-expression, knockout or cell specific targeting (364). The mouse uterus, like the human, has both basal and apical compartments within the uterine lining as well as developed uterine glands, stroma and a vascular compartment. The mouse endometrium also displays cyclical

changes in steroid receptor expression (98) and cellular morphology (97) during the oestrous cycle that parallel those reported in human endometrium during the normal menstrual cycle.

In 1984, Finn and Pope (234) were the first to describe a protocol for the artificial induction of endometrial decidualisation and endometrial breakdown in the mouse, using a timed schedule of hormonal injections. In their model, stromal cell decidualisation had to be induced by oil injection as in rodents, unlike in women, decidualisation only occurs naturally in response to blastocyst implantation (365, 366). Progesterone support was then withdrawn from these animals to mimic luteal regression. The success of this model was evident when features of menstruation normally seen in women were observed in the murine uterus, these included immune cell infiltration and tissue degeneration (234). The model was later improved by Brasted *et al.,* (233) who used an inbred strain of mice to reduce intra-animal variation, and altered the modes of delivery of the steroid hormones to include the use of a progesterone-secreting pellet. In their study, uteri were harvested at 0, 16, 20, 24, 36 and 48 hours after the withdrawal of progesterone. Based on haematoxylin and eosin sections they showed endometrial breakdown at 16 hours and complete restoration of endometrial architecture by 48 hours. This revised model has been used to study leukocyte infiltration (233), extracellular matrix dynamics (79), re-epithelialisation (318), and matrix metalloproteinases (230). Notably, all these studies focussed on a window of 12-48 hours after the withdrawal of progesterone during which 16 hours was classed as the time-point where menstruation begins, 24 hours as the time-point where re-epithelialisation was occurring and 48 hours classed as the time-point where complete repair and regeneration has occurred.

Pseudopregnancy models of endometrial breakdown have been developed, in which endogenous ovarian hormones contribute to endometrial regulation (188, 334, 336). Briefly, intact mice are mated with vasectomised males, on day 4 of pseudopregnancy the endometrium is artificially decidualised by oil injection, then 48 hours later ovariectomy induces steroid withdrawal and initiates endometrial shedding. Endometrial shedding is reported to be complete by 24 hours after steroid withdrawal, with complete restoration of tissue integrity by 48 hours (188, 336). Rudolph *et al.,* also reported overt menstruation using the pseudopregnancy model (336), which had not been previously reported in the Finn and Pope or Brasted models using exogenous steroid hormones.

Menses in women is characterised by overt bleeding, simultaneous breakdown and repair, immune cell influx, tissue necrosis and re-epithelialisation. Recent SEM studies into

endometrial breakdown and repair in women have revealed that tissue breakdown and repair occur concurrently (148) and so repair mechanisms must be initiated early and prior to full breakdown and clearance of the tissue. Therefore, in previous mouse models of endometrial breakdown and repair, the time-points chosen to investigate repair (24 hours in the ovariectomy model, 36 hours in the pseudopregnancy model) may be too late to study early repair mechanisms. Overt menstruation has only been reported in the pseudopregnancy model of breakdown, highlighting a limitation to the ovariectomy model.

With these observations in mind, the purpose of the studies described in this chapter was to develop a mouse model of breakdown and repair capable of identifying specific time-points for tissue breakdown, early repair and tissue remodelling.

3.1.1 Aims of the chapter

1. To establish a model of menses in the mouse which mimics menstruation in women; namely a model which exhibits overt menstruation and simultaneous breakdown and repair.
2. To study an "early" window of endometrial repair using this mouse model of menstruation.
3. To identify specific time-points where tissue destruction, re-epithelialisation and endometrial cell proliferation occur.
4. To investigate the dynamics of re-epithelisation of the endometrium during the early repair window.

Chapter 3. Establishment of a mouse model of menses for use as a functional model of endometrial breakdown and repair.

3.2 Materials and methods

3.2.1 Mouse model of menstruation

A mouse model of menstruation was established in house using a protocol adapted from Brasted *et al.,* (233). Table 3-1 outlines the adaptations made to the Brasted protocol. The full protocol is described in section 2.1.4 and outlined in Figure 2-4.

3.2.2 Tissue processing and immunohistochemistry

All samples were fixed in NBF overnight at room temperature, rinsed in 70% ethanol and then stored in 70% ethanol before tissue processing as described in section 2.6.

Immunohistochemistry was carried out using the standard protocol outlined in section 2.7.2 using the antibodies outlined in Table 2-15 and Table 2-16.

Images were analysed as detailed in section 2.7.2.10.

3.2.3 Enzyme immunoassay for quantitative determination of progesterone secretion in sera

Determination of progesterone secretion in blood sera was carried out using a progesterone enzyme-linked immunosorbent assay (ELISA) kit (DEMEDITECH diagnostics, Germany) as described in section 2.1.4.4.1.

3.2.4 RNA extraction

RNA extraction was carried out as detailed in section 2.2.

3.2.5 Synthesis of complementary DNA using VILO cDNA synthesis kit

Reverse transcription of RNA to cDNA was performed using the Superscript VILO cDNA synthesis kit (InVitrogen) according to manufacturer's instructions, using the volumes outlined below in Table 2-8. Samples were then incubated under the conditions detailed in section 2.3

3.2.6 Quantitative Real Time PCR

Quantitative real time PCR was carried out as detailed in section 2.4**.**

Statistical analysis was performed as detailed in section 2.8.

Protocol	Exogenous Hormone Schedule	Time Between Last E2 & Dec	Dec Method	Time Allowed for Dec	Success Rate	Tissue Collection TP	Observations
Finn and Pope, 1984	E2, s.c. delivery, 0.1ml, 100ng. Vehicle: Arachis oil. Days 7,8 P4, s.c. delivery, 0.1ml 500µg, Vehicle: Arachis oil, Days 12,13,14 E2, s.c. delivery, 0.1ml, 10ng. Vehicle: Arachis oil. Days 12,13,14	4-6 hours	Surgical flank incision 20µl arachis oil injected into lumen	70 hours	N/A		Protocol included in table to show adaptations made by Brasted *et al.*
Brasted et al., 2003	E2, s.c. delivery, 0.1ml, 100ng. Vehicle: Arachis oil. Days 7, 8, 9 Crystalline P4 pellet, incubated for 16h in 1% CSFCS in PBS at 37°C prior to sub cutaneous implantation. Days 13-17. E2, s.c. delivery, 0.1ml, 5ng. Vehicle: Arachis oil. Days 13, 14, 15	2 hours	Surgical flank incision 20µl sesame oil injected into lumen	49 hours	0 n=9	0 hours	No decidualisation observed after 49 hours Suggested change; vehicle delivery

Protocol	Exogenous Hormone Schedule	Time Between Last E2 & Dec	Dec Method	Time Allowed for Dec	Success Rate	Tissue Collection TP	Observations
Adaptation 1- Vehicle Delivery	E2, s.c. delivery, 0.1ml, 100ng. Vehicle: sesame oil. Days 7,8,9 Crystalline P4 pellet, incubated for 16h in 1% CSFCS in PBS at 37°C prior to sub cutaneous implantation. Days 13-17. E2, s.c. delivery, 0.1ml, 5ng. Vehicle: sesame oil. Days 13, 14, 15	2 hours	Surgical flank incision 20µl sesame oil injected into lumen	49 hours	1 n=11	0 hours	Slight pinkness observed in one horn, possible beginnings of decidualisation Suggested change; length of decidualisation time
Adaptation 2- Dec Time	E2, s.c. delivery, 0.1ml, 100ng. Vehicle: sesame oil. Days 7, 8, 9 Crystalline P4 pellet, incubated for 16h in 1% CSFCS in PBS at 37°C prior to sub cutaneous implantation. Days 13-19. E2, s.c. delivery, 0.1ml, 5ng. Vehicle: sesame oil. Days 13, 14, 15	3 hours	Surgical flank incision 20µl sesame oil injected into lumen	90 hours	12 n=24	0, 24 hours	Partial decidualisation observed in both horns. Suggested change; P4 secretion from pellet, decidualisation method

Protocol	Exogenous Hormone Schedule	Time Between Last E2 & Dec	Dec Method	Time Allowed for Dec	Success Rate	Tissue Collection TP	Observations
Adaptation 3- P4 secretion & Dec method	E2, s.c. delivery, 0.1ml, 100ng. Vehicle: sesame oil. Days 7, 8, 9 Crystalline P4 pellet, incubated for 48 hours in 1% CSFCS in PBS at 37°C prior to sub cutaneous implantation. Days 13-19. E2, s.c. delivery, 0.1ml, 5ng. Vehicle: sesame oil. Days 13, 14, 15	3 hours	Vaginal delivery by nset 20µl sesame oil	90 hours	60 n=91	0, 4, 8, 12, 24 hours	Full decidualisation observed in the stimulated uterine horn Blood cells observed in lumen at 4 hours.

Table 3-1: Establishment of a mouse model of menstruation that mimics human menstruation. Adaptations made to the Brasted model are shown in red as outlined in Adaptations 1, 2 and 3. Key; s.c. sub-cutaneous injection, dec; decidualisation, E2; oestradiol, P4; progesterone, TP: time-point, CSFCS; charcoal stripped foetal calf serum. Success rate: the number of mice fully decidualised at 0 hours or evidence of decidualisation then breakdown at the later time-points.

3.3 Results

3.3.1 Establishment of a mouse model that mimics menstruation in women

In order to establish a functional model of breakdown and repair, a number of adaptations were made to the model described by Brasted *et al*., as outlined in Table 3-1. The first minor adjustment (Table 3-1, adaptation 1) was to change the type of oil used to deliver the exogenous oestradiol, as first observations were that the arachis (peanut) oil did not stay in solution and therefore may have had an adverse effect on oestrogen priming and decidualisation, as no mice had undergone decidualisation. Following this change observation of the uterine horns after 49 hours suggested that decidualisation had begun but was not complete (one mouse was observed to have undergone partial decidualisation).

In keeping with the length of decidualisation described by Finn and Pope (234), (70 hours), the length of time allowed for decidualisation was extended to 90 hours (Table 3-1, adaptation 2). Partial decidualisation of the uterine horn was observed in 50% of the mice, where small sections of the horn had decidualised but other areas of the horn were comparable to the non-decidualised horn. Artificial decidualisation of one uterine horn had been performed via a flank incision, then injection of oil through the myometrium into the lumen. A number of limitations were observed whilst carrying out this procedure; it was difficult to orientate the syringe exactly into the lumen itself, without piercing straight through the opposite uterine wall, furthermore, whilst injecting the oil a proportion of the oil would reflux back out of the point of syringe entry.

These observations led us to adopt vaginal delivery of oil (Table 3-1, adaptation 3) using a non-surgical embryo transfer device, which allowed direct delivery of oil into one horn and also eliminated an invasive surgical technique. Progesterone pellet incubation was also lengthened from 16 hours to 48 hours to ensure that progesterone secretion had been stimulated prior to pellet implantation. Upon dissection, after 90 hours of decidualisation, one uterine horn was decidualised and was significantly larger and heavier than the contra-lateral non-decidualised horn (evidence of which is shown in section 3.3.4).

A set of time-points were selected specifically to focus on investigation into early breakdown and repair; 0 hours (classed as the time of pellet removal and the initiation of steroid withdrawal), 4 hours, 8 hours, 12 hours and 24 hours. A small number of mice were collected at 48 hours after the withdrawal of the progesterone pellet (n=6).

3.3.2 Evidence of endometrial shedding

Evidence of endometrial breakdown was initially investigated by observing the vagina for blood and by carrying out a vaginal smear of each animal, as described in section 3.2.1. The percentage of mice bleeding at each time-point was calculated and is displayed in Figure 3-1.

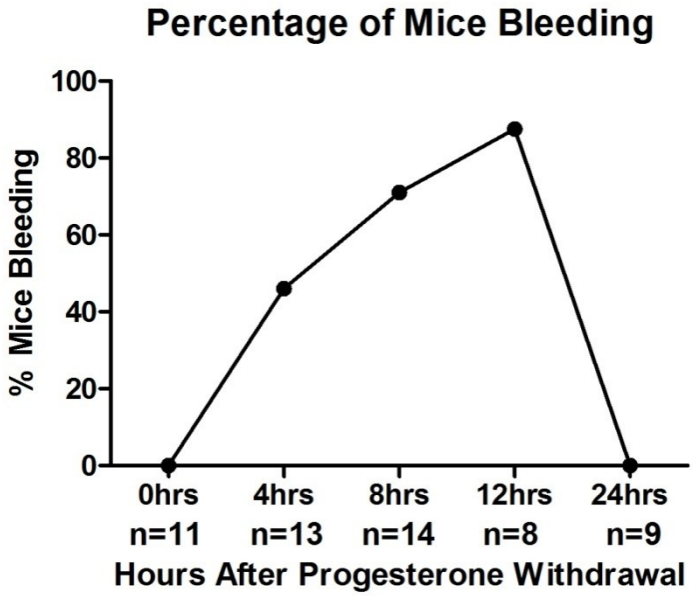

Figure 3-1: Percentage of mice bleeding following progesterone withdrawal. The percentage was calculated as those that were identified to be bleeding at each time-point from the total number of mice investigated for each time-point.

No mice were found to have blood cells in their vaginal smear at 0 hours (time of pellet removal and induction of progesterone withdrawal). As early as 4 hours after the withdrawal of progesterone, blood cells were detected in the vaginal smear of 46% of the mice. Blood was also observed at 8 hours (71%) and 12 hours after progesterone withdrawal, with 87.5% of mice having a blood positive smear at 12 hours (Figure 3-3, A). By 24 hours the consistency of the blood had changed with no blood present in the vaginal smears, but blood-containing material still present in the uterine horn when they were dissected. These mice were classed to have ceased bleeding by 24 hours.

3.3.3 Evidence that hormonal withdrawal initiates endometrial shedding

To confirm that the uterus was undergoing endometrial breakdown due to the withdrawal of progesterone, serum progesterone levels were measured by ELISA, and are depicted in Figure 3-2. Progesterone concentrations were significantly ($p<0.001$) decreased from 0 hours (12±3ng/ml) to 4 hours (2.6±4ng/ml) after withdrawal. Serum concentrations at the later time-points were also significantly decreased ($p<0.001$) in comparison to the 0 hour time-

point. The lowest concentration was observed at 8 hours ($p<0.001$, 1.5±1.0ng/ml) after the removal of the progesterone secreting pellet, no significant differences were found between the latter time-points. These results are consistent with progesterone withdrawal observed in women at the time of menses.

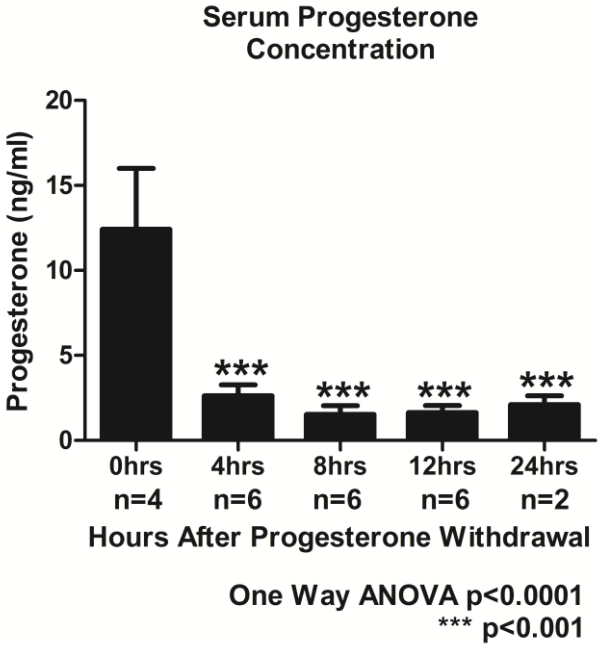

Figure 3-2: Serum progesterone concentrations following withdrawal of progesterone. Progesterone concentrations (ng/ml) were detected to decrease following withdrawal of the progesterone pellet at 0hrs. Statistical analysis was carried out by One Way ANOVA followed by Bonferroni post hoc testing, where stars indicate comparison between each time-point and the 0 hour time-point.

3.3.4 Gross morphology of the uterus upon dissection following progesterone withdrawal

Consistent with the adaptations described in section 3.3.1 the use of a non-surgical trans-vaginal stimulus versus surgical insertion for initiation of decidualisation resulted in full decidualisation of one uterine horn (Figure 3-3, B), observed alongside its contra-lateral control horn (non-decidualised). Notably, blood cells were visually detectable in the vagina (Figure 3-3, A) and lumen (Figure 3-3, C) of the non-decidualised horn following vaginal lavage but 24 hours after progesterone withdrawal, breakdown of tissue within the decidualised horn was obvious (Figure 3-3, D). Endometrial tissue that had shed from the uterine horn and leaked out through the cervix during dissection is also shown in Figure 3-3, D.

Mean uterine horn weights for non-decidualised and decidualised horns at each time-point are shown in Figure 3-4. Consistent with successful induction of decidualisation, at the time of progesterone withdrawal, the weight of the decidualised horn (black bars) was significantly greater ($p<0.001$) than that of the non-decidualised horn (white bars). Progesterone withdrawal did not have any effect on the mean weight of the non-decidualised horn (white bars) and the weight of the decidualised horn was significantly greater than that of the non-decidualised horn ($p<0.001$) at 0, 4, 8 and 12 hours after progesterone withdrawal. No significant difference was observed at 24 hours.

To confirm that the uterine horns, classed as "decidualised horns", had undergone a decidual response, mRNA concentrations for prolactin (*Prl8*), a marker of decidualisation (367), were examined by qRTPCR. Relative mRNA concentrations at each time-point are displayed in Figure 3-5. At the 0 hour time-point the mRNA concentration for prolactin in the decidualised horn was shown to be 2000 fold higher than that of the non-decidualised control; mRNA concentrations for *Prl8* were detected to significantly decrease following progesterone withdrawal ($p<0.05$, 4 hours; $p<0.001$, 8-24 hours). The lowest *Prl8* mRNA concentration was detected 24 hours after progesterone withdrawal ($p<0.001$). The rapid and significant reduction in *Prl8* mRNA ($p<0.001$) at 12 hours was in marked contrast to the maintenance of uterine wet weight at this time.

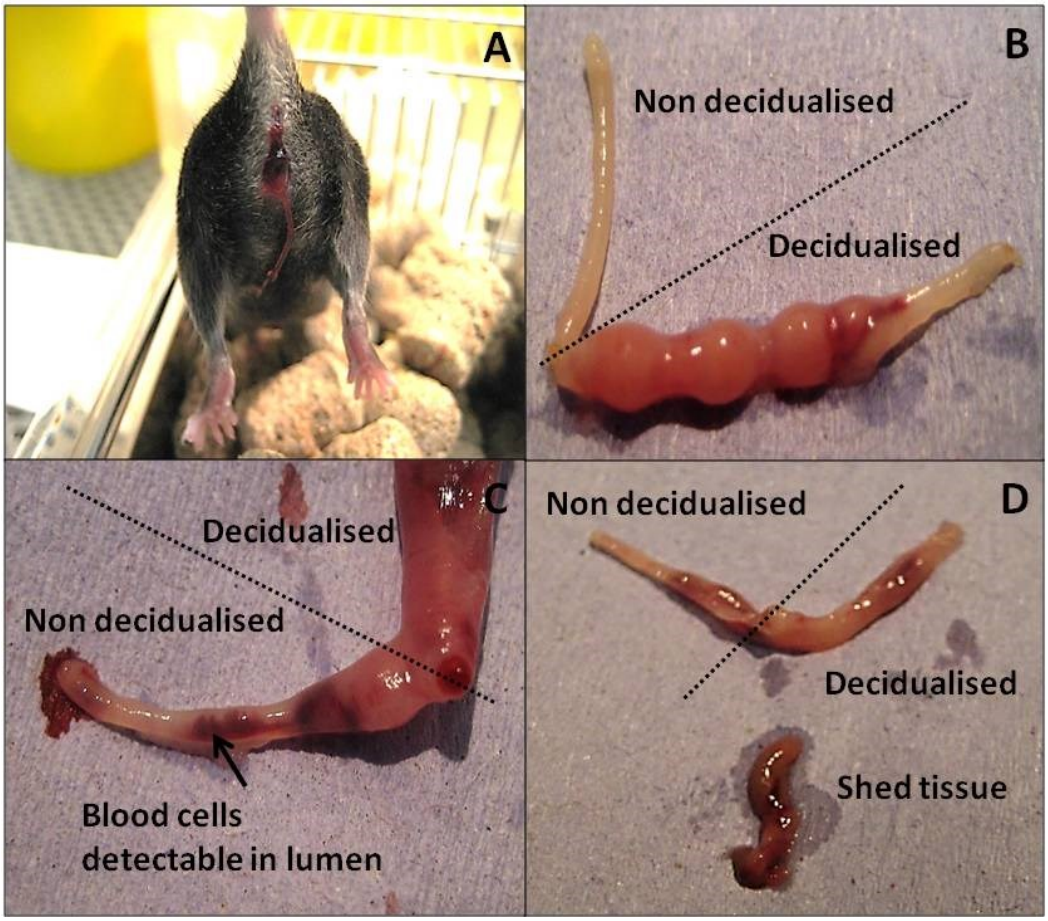

Figure 3-3: Morphology of the uterus following decidualisation and progesterone withdrawal. A; Blood detected in the vaginal smear, 12 hours after withdrawal. B; The non decidualised control (left) and the decidualised horn (right) upon dissection (12 hours after withdrawal). C; Blood cells were detectable in lumen of the non decidualised horn following vaginal lavage (24 hours after withdrawal). D; Shed tissue expelled from cervix (24 hours after withdrawal), decidualised horn shows regression.

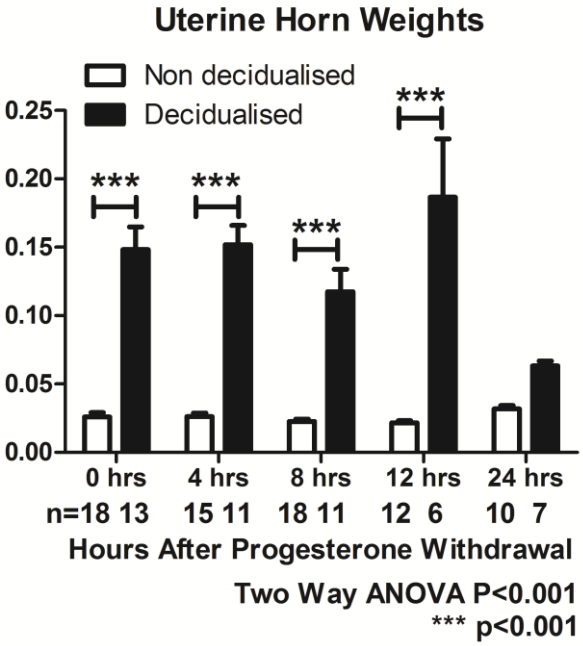

Figure 3-4: Mean uterine horn weights following progesterone withdrawal. Non-decidualised horns (white bars) showed no significant differences in uterine weight (g). Decidualised horns were significantly heavier than their non-decidualised controls at 0, 4, 8, 12 and 24 hours ($p<0.001$). No significant difference was observed between non-decidualised and decidualised horns at 24 hours. Statistical analysis was performed by Two Way ANOVA and Bonferroni post hoc testing.

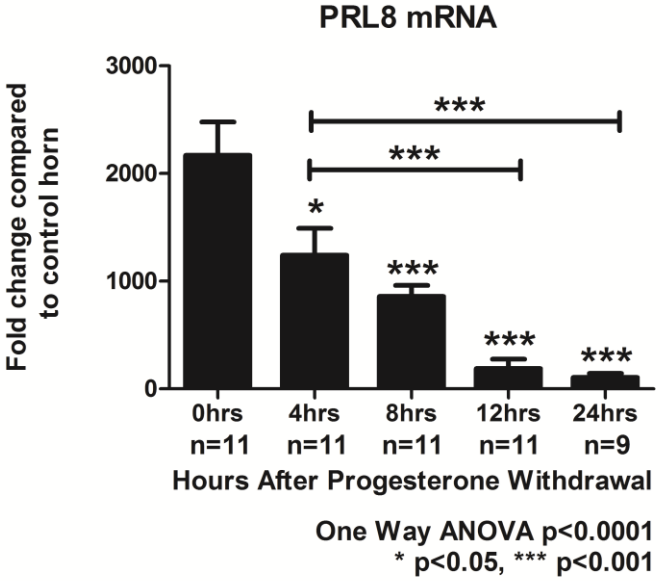

Figure 3-5: qRTPCR for prolactin8 (*Prl8*), a marker of decidualisation, following withdrawal of progesterone. mRNA expression for the decidualised horn (black bars) normalised against the 0hr non-decidualised control horn. Statistical analysis was performed by One Way ANOVA and Bonferroni post hoc testing, where each time-point was first compared to the 0 hour time-point and then to each other time-point.

3.3.5 Histological examination of endometrial breakdown and repair following progesterone withdrawal

Uterine morphology in the control (non-decidualised) horn at 0 hours is shown in Figure 3-6 as an illustration of tissue morphology in the absence of decidualisation. In the non-decidualised uterine horn (Figure 3-6, A), an intact epithelium lines the lumen, which can be clearly seen in the centre of the tissue. The functional and basal layers of the tissue are clearly detected due to the greater stromal density of the basal compartment (outlined by the dashed lines). The outer myometrial muscular layers can be seen surrounding the uterine horn. At a higher magnification, (Figure 3-6, B) glandular structures (G) lined by epithelial cells can be seen within the loosely packed stromal cell compartment of the functional layer (FS).

The decidualised horn at the time of progesterone withdrawal (0 hours) was observed to have undergone extensive stromal cell remodelling during the 90 hour decidualisation period, as shown in Figure 3-6, C and D. Large nuclei were observed within the decidualised cell mass (Figure 3-6, F) which filled in the centre of the uterine horn (DS), with a compacted stromal compartment in the outer basal layer (BL) (Figure 3-6, E). Flattened epithelial cells (as detected by immunohistochemistry for pan-cytokeratin) were observed lining the lumen (Figure 3-6, E) which was much reduced in volume in comparison to the 0 hour control horn (Figure 3-6, B).

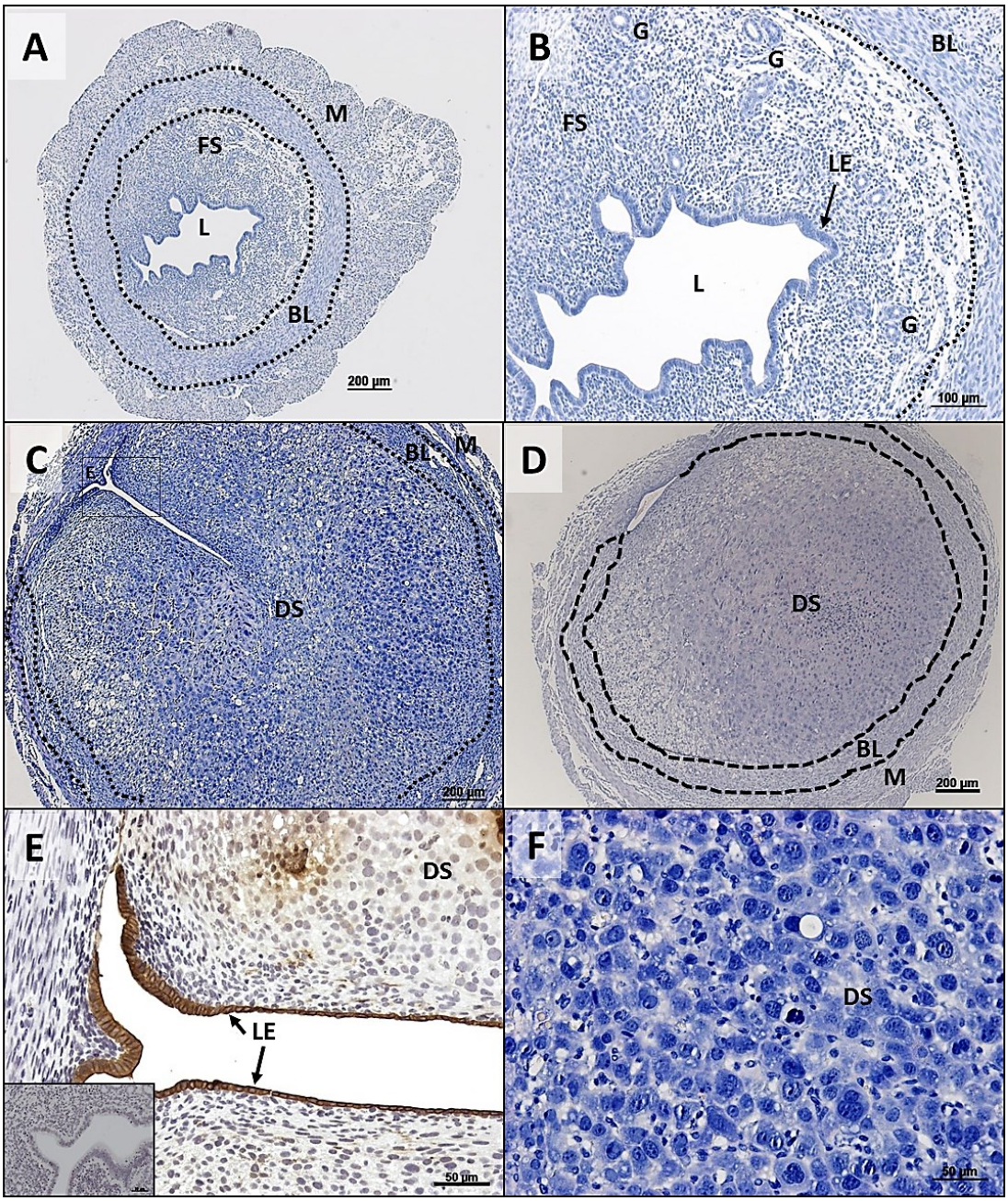

Figure 3-6: Morphology of the non-decidualised (A-B) and decidualised (C-F) uterine horns at the time of progesterone withdrawal. Dashed lines depict the different cellular compartments that comprise the endometrium, transverse section. A; Non-decidualised horn at 0 hours. B; An intact epithelium lines the lumen, a loosely packed stromal compartment (FS) is observed in the functional layer, compared to the basal layer (BL). C+D; Given animal variability, two representative uteri are shown in images C and D. C-D; Stromal remodelling was observed in decidualised horn, identified by densely packed stromal compartment (DS). E; A flattened, intact epithelium, as indicated by brown staining for epithelial marker pan-cytokeratin, lines the condensed lumen. Inset, negative control. F; Decidualised stromal cells display large rounded nuclei. M; myometrium, BL; Basal layer, LE; luminal epithelium, DS; decidualised stroma, FS; functional stroma, G; glands. Scale bars as indicated. Images are representative of 3 animals.

As in humans, variation was found to occur in the morphology of the murine uterine tissues following pellet removal. However, this is the first report of striking morphological changes occurring in the decidualised horn within 4 hours of progesterone withdrawal (Figure 3-7, A and B) with the decidualised cell mass observed to have started to shed into the lumen (Figure 3-7, D) by 4 hours. Immunohistochemistry for epithelial marker pan cytokeratin allows identification of luminal and glandular epithelial cells (Figure 3-7, C and D). The leading edge of the decidualised cell mass is lined by luminal epithelial cells (arrowheads). Initial breakdown of the decidualised stroma into the lumen was also detected (Figure 3-7, D).

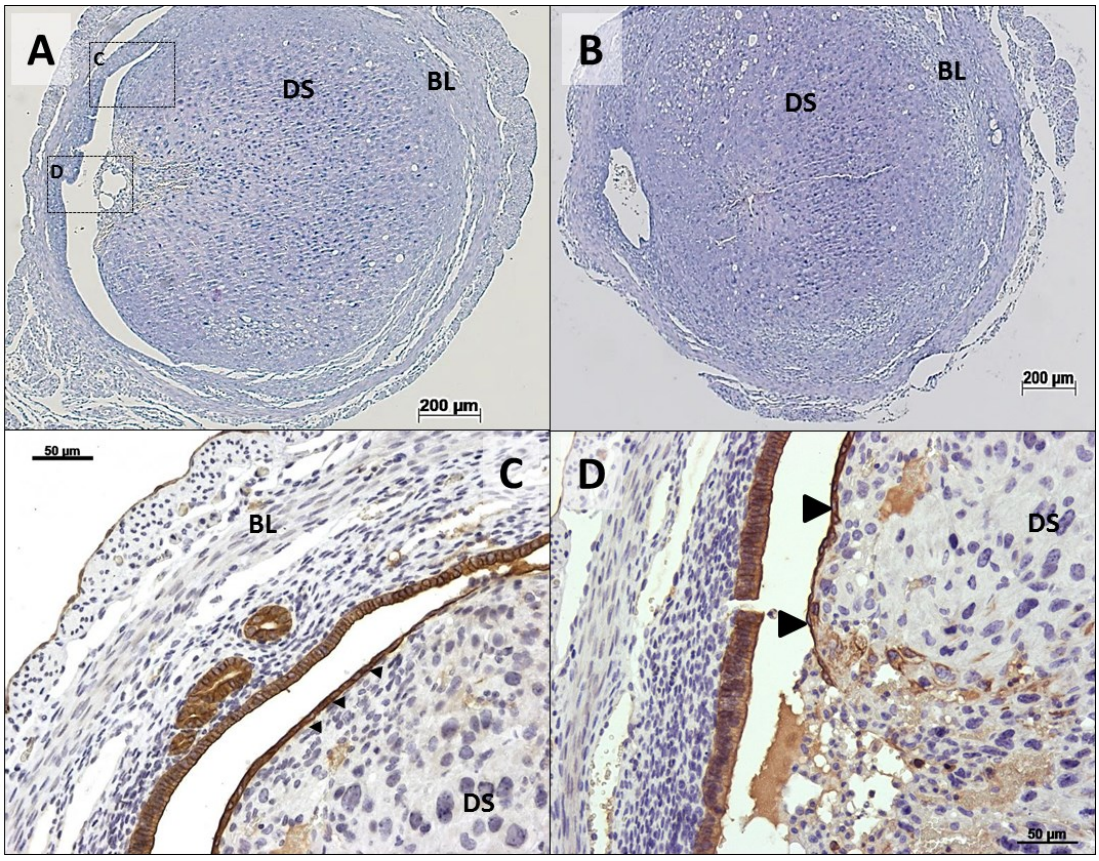

Figure 3-7: Morphology of decidualised uterus 4 hours after progesterone withdrawal. Given animal variability, two representative uteri are shown in images A and B. A+B; Morphology of uterus 4 hours after progesterone withdrawal. C; Immunohistochemistry for pan cytokeratin (epithelial marker) demonstrates that the leading edge of the decidual cells is lines by luminal epithelial cells (arrowheads) D; Decidualised cells begin to shed into the lumen. Leading edge of the decidualised cells are stained for cytokeratin (arrowheads). M; myometrium, BL; Basal layer, LE; luminal epithelium, DS; decidualised stroma. Scale bars as indicated. Images are representative of 3 animals.

By 8 hours after withdrawal of progesterone support (Figure 3-8, A, B), a mass of decidualised cells that had become detached from the underlying uterine tissue were clearly visible in the centre of the uterine lumen (Figure 3-8, A and B). An area of exposed basal stroma was observed in Figure 3-8, C, (ES) where the decidualised functional layer had detached. Notably, in this region the absence of an epithelial cell layer was noted. In Figure 3-8, D, an epithelial cell layer, positive for epithelial marker pan cytokeratin, can be seen lining the lumen, and glands (G) were observed in the basal layer in sites close to the luminal epithelium.

By 12 hours, the time-point which was identified to have the highest percentage of mice with vaginal blood, sections of basal tissue adjacent to the shed decidualised cell mass appeared to be denuded of epithelium, as demonstrated by a lack of cells positive for pan cytokeratin (Figure 3-9, B, arrowheads). In contrast, other areas of the tissue in the same section had round epithelial cells lining the lumen (Figure 3-9, A, arrows) and glands were detected in the basal layer (G). Blood vessels were also detected in sites close to the luminal epithelium (Figure 3-9, A, arrowheads).

In uterine horns retrieved at 24 hours after the removal of the progesterone secreting pellet, some variation was observed with some uteri having a few regions of recently shed decidua and incomplete epithelialisation of the luminal surface (Figure 3-10, A). Round epithelial cells can be observed lining the luminal surface (pan cytokeratin staining, Figure 3-10, C, arrowheads). In other uterine samples (Figure 3-10, B) an intact, invaginated luminal epithelium was present (Figure 3-10, D) consistent with re-epithelialisation of the endometrium being completed.

Histological examination of uterine horns collected at 0, 4, 8, 12 and 24 hours demonstrated that endometrial breakdown begins within 4 hours of progesterone withdrawal, as evidenced by blood in the vaginal lavage. Breakdown and shedding of the functional stromal layer occurred within 8-12 hours and re-epithelialisation was observed to occur, or had occurred, by 24 hours. Evidence of round epithelial cells at 24 hours suggests that repair mechanisms have already been initiated. Therefore the set of time-points chosen are adequate for further investigation into the mechanisms that contribute to repair and re-establishment of tissue integrity.

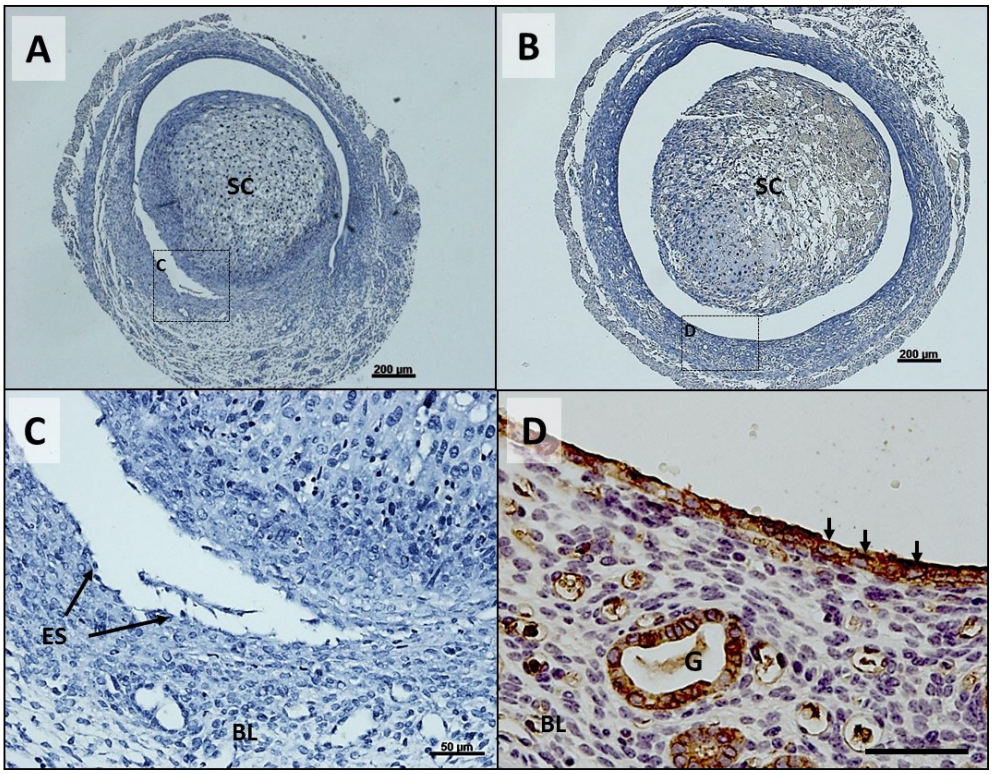

Figure 3-8: Morphology of decidualised uterus 8 hours after progesterone withdrawal. Given animal variability, two representative uteri are shown in images A and B. A+B; Decidualised cells that have detached from the basal layer are observed in the lumen. C; Area of denuded endometrium following detachment of the decidualised cells from the basal layer. The exposed stroma apparently lacks an epithelial cell layer. D; Pan cytokeratin staining identifies flattened epithelial cells observed lining lumen. Glands appear in basal layer, close to luminal epithelium. M; myometrium, BL; Basal layer, LE; luminal epithelium, G; glandular epithelium, ES; exposed stroma. Scale bars as indicated, scale bar in D, 20um. Images are representative of 4 animals.

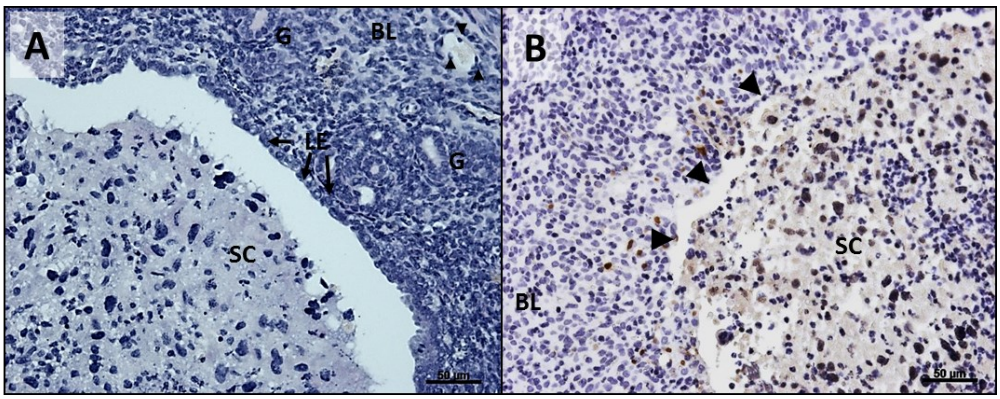

Figure 3-9: Morphology of decidualised uterus 12 hours after progesterone withdrawal. A; Round epithelial cells observed lining the lumen (LE), near basal glands (G) and blood vessels (arrowheads). B; The decidualised cell mass detaches from basal layer exposing the basal layer (BL) to the lumen, immunohistochemistry for pan cytokeratin highlights that there are no epithelial cells lining the lumen at this time (arrowheads). BL; Basal layer, LE; luminal epithelium, G; glandular epithelium. Scale bars as indicated. Images are representative of 2 animals.

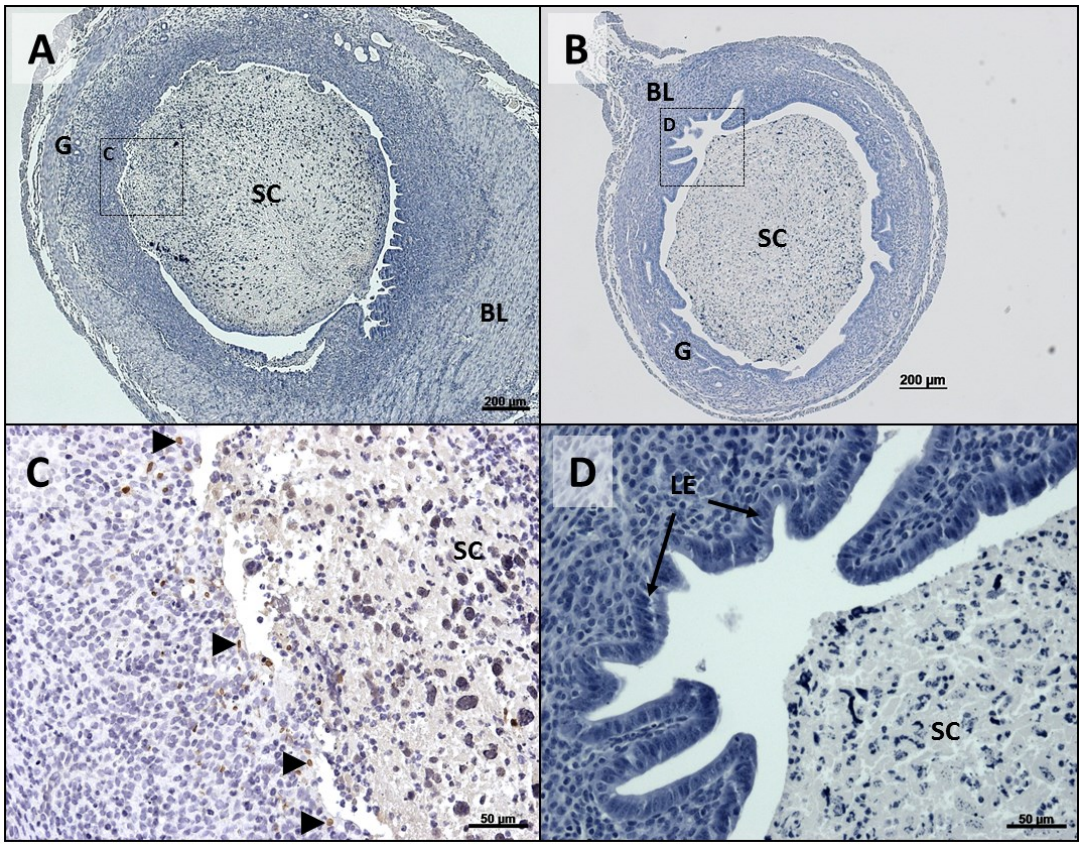

Figure 3-10: Morphology of decidualised uterus 24 hours after progesterone withdrawal. Given animal variability, two representative uteri are shown in images A and B. A+B; Shed cells from the decidualised functional layer are present in the uterine lumen of both animals. C; Immunohistochemistry for pan cytokeratin highlights an area of recently exposed basal stromal compartment with round epithelial cells present on the luminal surface (as indicated by arrowheads). D; An intact luminal epithelium containing columnar epithelial cells are observed. LE; luminal epithelium, G; glandular epithelium. Scale bars as indicated. Images are representative of 4 animals.

3.3.6 Re-epithelialisation of the endometrium

3.3.6.1 Evidence for re-epithelialisation by epithelial cell proliferation

To investigate epithelial cell proliferation and its contribution to re-epithelialisation and restoration of an intact endometrium, mice were injected with bromodeoxyuridine (BrdU) 90 minutes prior to culling (see section 2.1.4.4). BrdU is a synthetic nucleoside that incorporates into replicating DNA during the S phase of the cell cycle. Administration of BrdU at this time was used to label cells that were actively proliferating at the time of culling.

Incorporation of BrdU was detectable in uterine tissues at all time-points. BrdU positive cells were detected in both the functional and basal layers of the endometrium in tissues collected at the time of progesterone withdrawal (Figure 3-11, A). BrdU positive cells were detected in the decidualised stroma (Figure 3-11, B), however decidualised cells in the centre of the decidualised cell mass were largely BrdU negative (Figure 3-11, A). Stromal cells in the basal layer were also BrdU positive (Figure 3-11, C), as were a number of luminal epithelial cells (Figure 3-11, D).

BrdU positive cells were detected in the endometrium 4 hours after withdrawal of progesterone (Figure 3-12, A). A number of BrdU positive cells in the luminal epithelium were detected (Figure 3-12, B and F), BrdU positive cells were also detected in the decidualised stroma (Figure 3-12, C-E). BrdU positive cells were largely localised to the non-decidualised cells in the basal layer adjacent to the decidualised stroma (Figure 3-12, C-F).

Microscopic observations suggested that the highest numbers of BrdU positive epithelial cell nuclei were identified 12-24 hours after the withdrawal of progesterone, however quantification is required. At 12 hours after withdrawal, the luminal epithelium contained a number of cells positive for BrdU (Figure 3-13, A and B). Notably, stromal cells in the basal layer adjacent to a region of exposed endometrium lacking a proliferative epithelial cell layer were also identified to be BrdU positive (Figure 3-13, C, arrowheads). Flat epithelial cells positive for BrdU are observed lining sections of the lumen (Figure 3-13, C, arrows). Stromal cells in the basal layer close to glandular structures were BrdU positive (Figure 3-13, D), whilst the glandular epithelium of glands in the basal layer was BrdU negative (Figure 3-13, D-F). In Figure 3-13, E, sections of the endometrium appeared ‘ragged’, following shedding of the functional layer; however a few BrdU positive, flat epithelial cells are present. In another area of the tissue in the same cross-section (Figure 3-13,F), round

epithelial cells positive for BrdU were identified in what appeared to be a more 'intact' epithelium compared to that in Figure 3-13, E.

Luminal epithelial cell proliferation was still evident at the 24 hour time-point (Figure 3-14, A). However, due to animal variation in the length of time taken to repair, BrdU positive luminal epithelial cells were not detected in every sample (Figure 3-14, D). BrdU positive cells appeared to be lining vascular structures (Figure 3-14, B, arrowheads) as well as an possible increase in the number of BrdU positive epithelial cells (Figure 3-14, B and C). In some samples, cells in the basal glandular epithelium were also found to be positive for BrdU (Figure 3-14, D), a finding which was not detected at the earlier time-points.

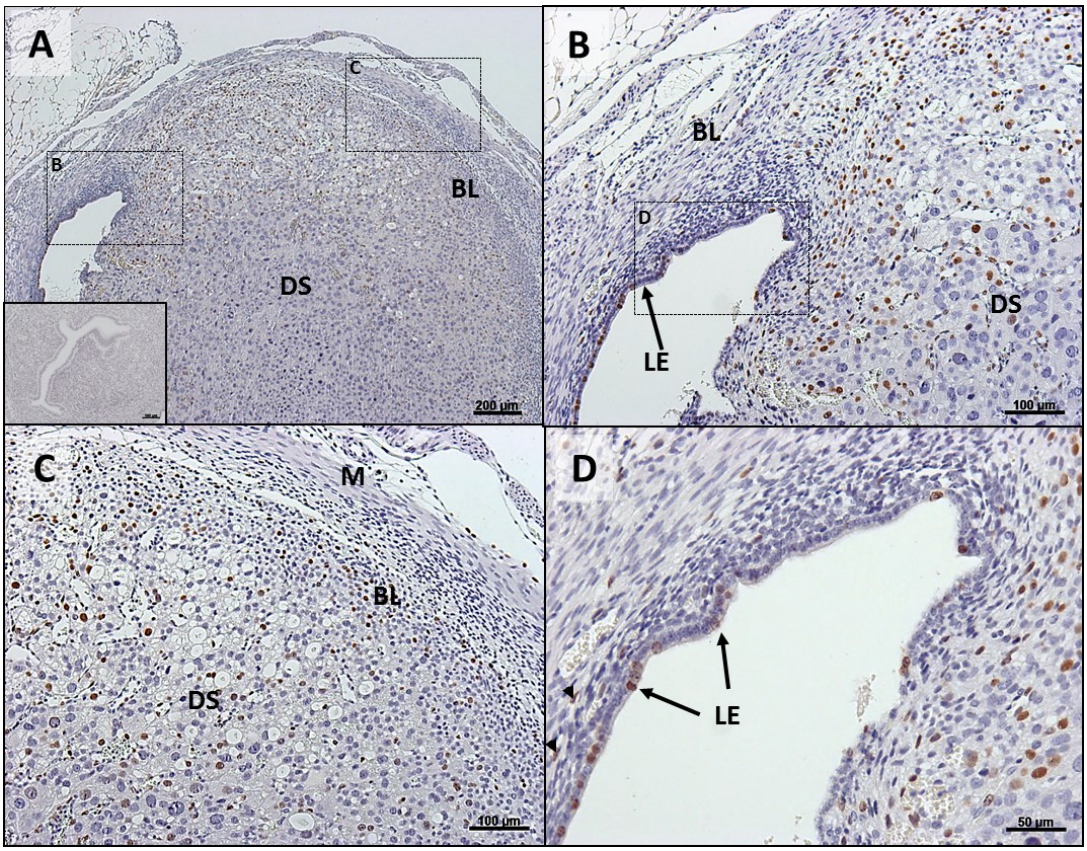

Figure 3-11: Endometrial cell proliferation at the time of progesterone withdrawal (0 hours). A; BrdU positive cells (brown staining) were identified at 0 hours, in the basal layer, decidualised stroma and in the luminal epithelium, inset negative control. B; BrdU positive cells are observed in the decidualised stroma adjacent to the basal layer. C; Decidualised cells towards the centre of the lumen are largely BrdU negative, a large number of cells in the basal stroma are BrdU positive. D; Luminal epithelial cells are BrdU positive. M; myometrium, BL; Basal layer, LE; luminal epithelium, DS; decidualised stromal cells. Scale bars as indicated. Images are representative of 4 animals.

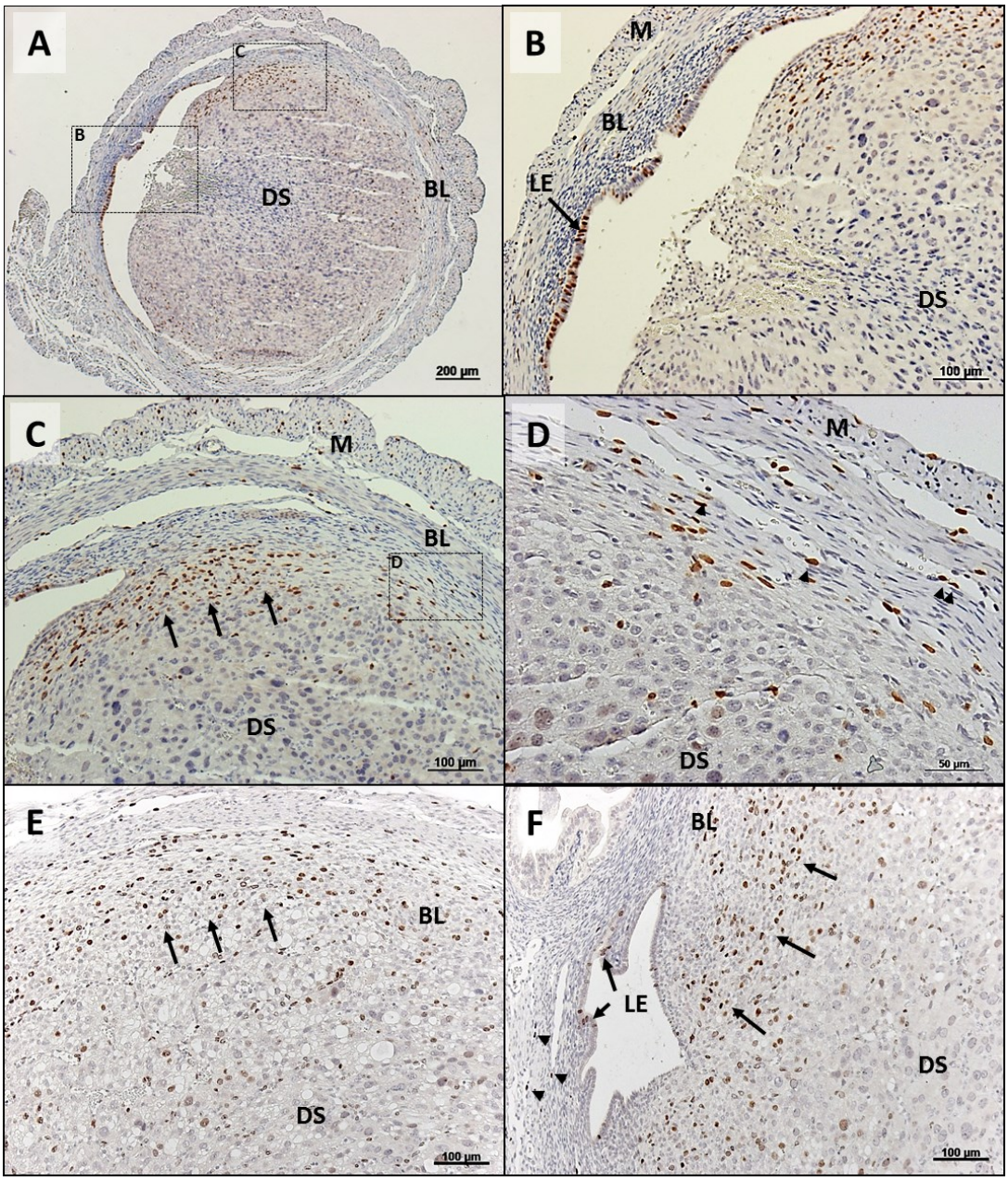

Figure 3-12: Endometrial cell proliferation 4 hours after progesterone withdrawal. Two representative uteri are shown in A-D and E-F. A; BrdU positive cells (brown staining) were localised to the basal stroma, the decidualised functional stroma and in the luminal epithelium. B; BrdU positive cells in the luminal epithelium. C; BrdU positive cells in the basal layer adjacent to the decidualised cells appeared to be more densely populated. D; BrdU positive cells were associated with the vasculature of the basal layer and outer myometrial layer (arrowheads). E; In another sample, BrdU positive cells were localised to the basal layer (arrows). F; BrdU positive cells were localised to the basal stroma (arrows), luminal epithelium and the vasculature (arrowheads). BL; Basal layer, LE; luminal epithelium, DS; decidualised stromal cells, M; myometrium. Scale bars as indicated. Images are representative of 3 animals.

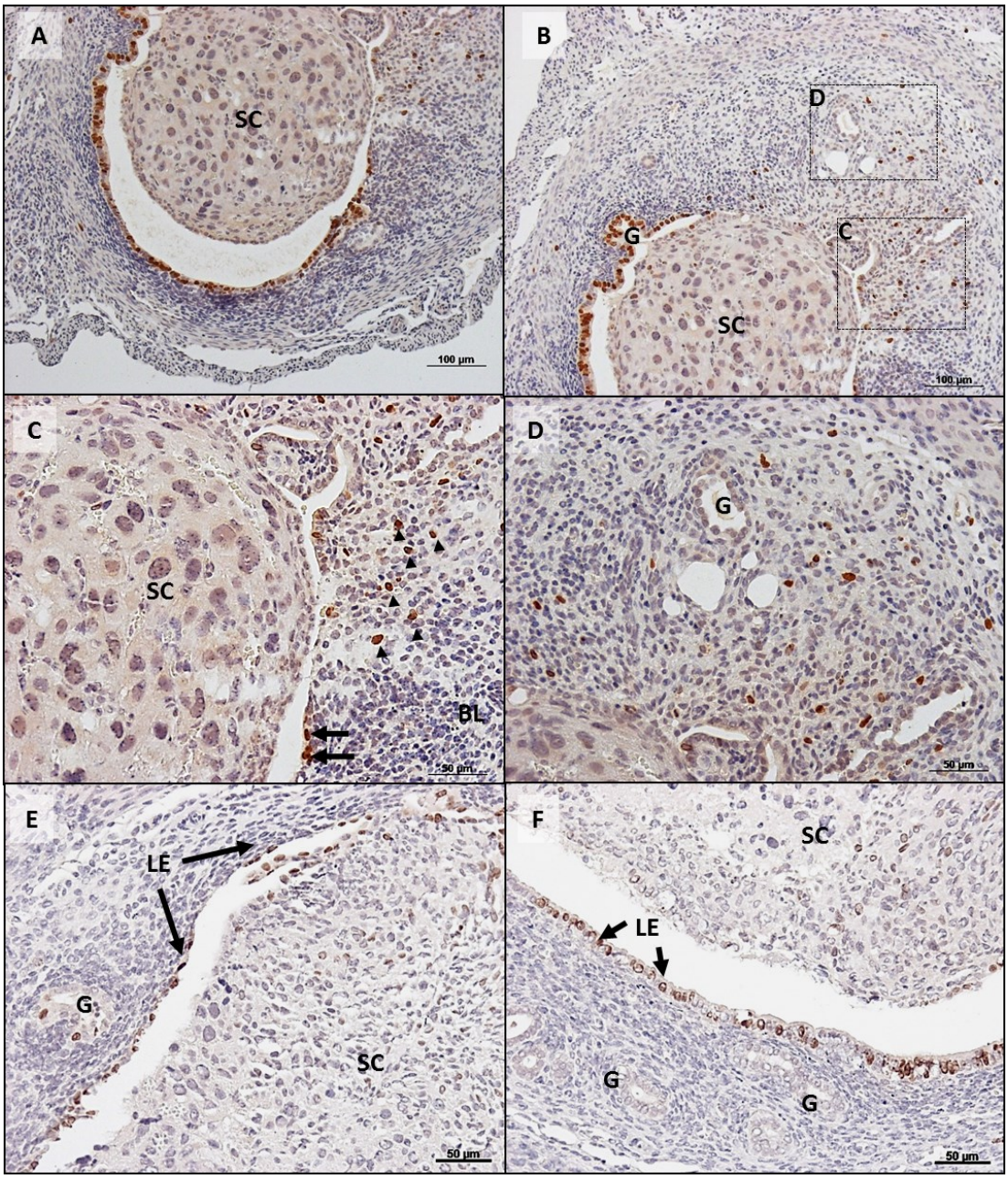

Figure 3-13: Endometrial cell proliferation 12 hours after progesterone withdrawal. Two representative uteri are shown A-D and E-F. A; BrdU positive cells (brown staining) were observed in the luminal epithelium. B; BrdU positive cells were localised to sites in the basal stroma. C; Stromal cell in close proximity to an area of denuded endometrium are positive for BrdU (arrowheads). Flat epithelial cells were identified lining the lumen (arrows). D; Stromal cells in the basal layer were positive for BrdU, however the glandular epithelium was negative (G). E; In another sample, BrdU positive flat epithelial cells are observed lining the lumen, the glandular epithelium is negative for BrdU. F; The glandular epithelium is negative (G), round luminal epithelial cells are BrdU positive. BL; Basal layer, LE; luminal epithelium, SC; shed cells, G; glandular epithelium. Scale bars as indicated. Images are representative of 4 animals.

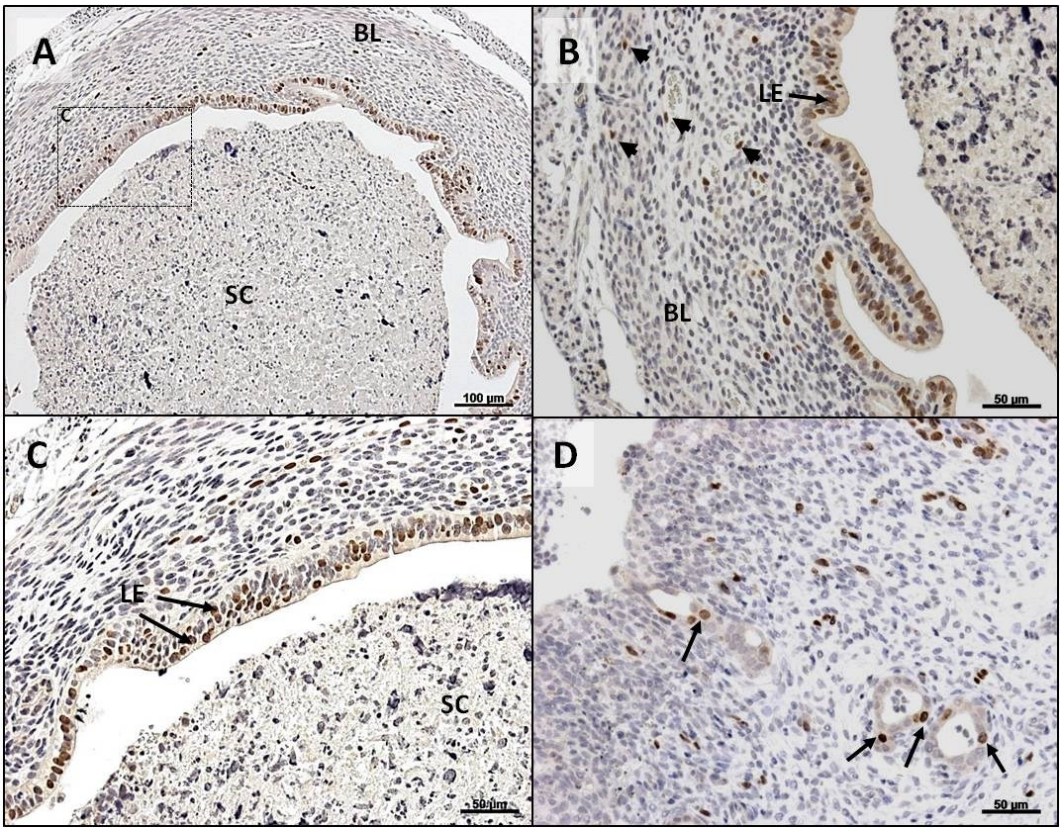

Figure 3-14: Endometrial cell proliferation 24 hours after progesterone withdrawal. Two representative uteri are shown A-C and D. A; Large proportions of the luminal epithelial cells are positive for BrdU. B; Cells associated with the vasculature are BrdU positive (arrowheads). C; Luminal epithelial cells are stacked on top of each other, and are also BrdU positive. D; In another sample, BrdU positive stromal cells are observed to be "scattered" through the stromal cell compartment. Notably, the glandular epithelium contains BrdU positive cells (arrows). BL; Basal layer, LE; luminal epithelium, SC; shed cells. Scale bars as indicated. Images are representative of 2 animals.

3.3.6.2 Evidence for re-epithelialisation by epithelial cell migration

To complement and extend preliminary observations based on histological evaluation (section 3.3.5) immunohistochemistry for pan-cytokeratin was used to monitor the location of epithelial cells in the endometrium 8-24 hours after removal of the progesterone pellet.

At the 8 hour time-point in this model, the endometrium has begun to detach from the underlying basal stromal compartment (Figure 3-15, A). The protruding edge of the decidualised cell mass was lined with epithelial cells (Figure 3-15, B, arrowheads). At this time-point areas of denuded endometrium were observed in the remaining basal layer of the tissue (Figure 3-15, A and C, arrowheads), as evidenced by the absence of pan-cytokeratin positive cells. Note that in Figure 3-15, D, positive immunostaining for pan-cytokeratin was detected in the luminal epithelium adjacent to an area of denuded endometrium highlighted by the arrowheads.

By 24 hours after the withdrawal of progesterone, the decidualised functional stroma has detached from the underlying basal layer (Figure 3-16, A). An area of denuded endometrium was observed (Figure 3-16, B and C, arrowheads). Adjacent to this region were a layer of pan-cytokeratin positive epithelial cells (Figure 3-16, C), of which the 'leading edge' of these cells appeared to be made up of round epithelial cells (Figure 3-16, D). These cells appeared to be "rolling" towards an area of denuded endometrium.

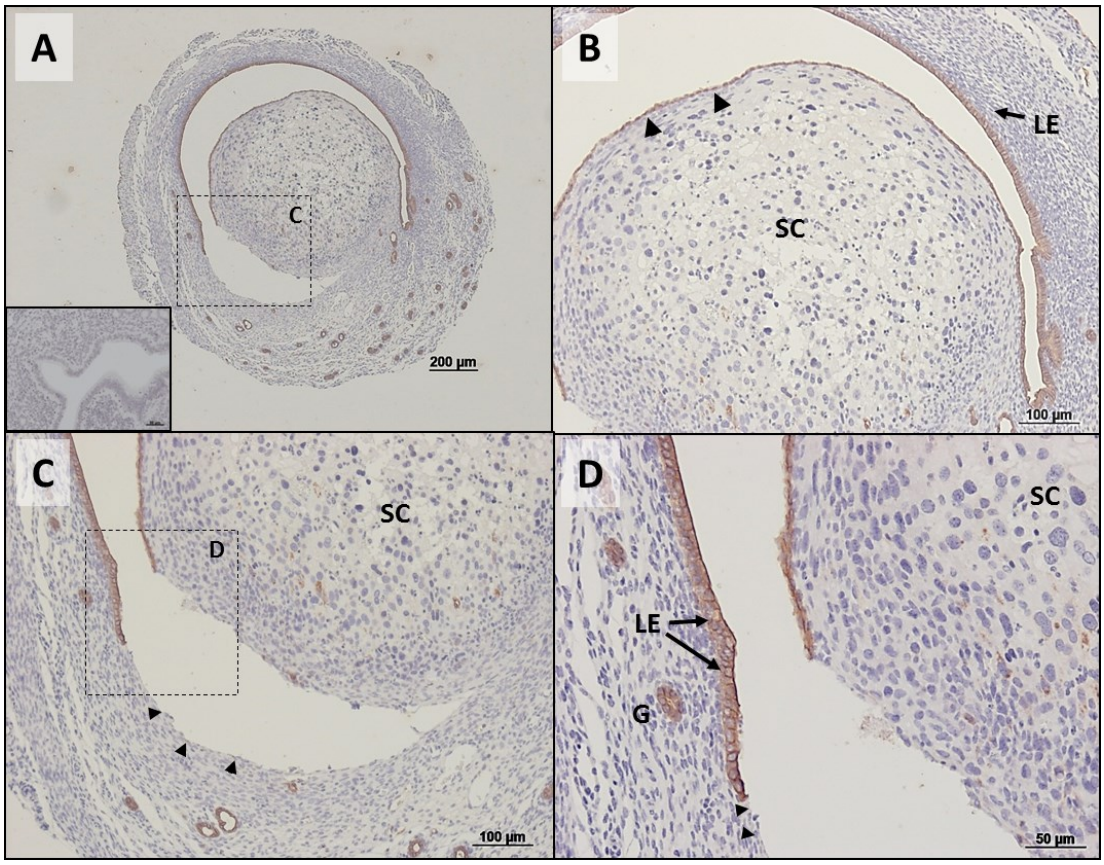

Figure 3-15: Staining for pan-cytokeratin revealed partial re-epithelialisation of the endometrium, 8 hours after progesterone withdrawal. A; The decidualised cell mass is observed to be detaching from the underlying stromal cell compartment, inset negative control. B; The epithelium of the protruding edge of the decidualised stroma remains positive for pan-cytokeratin (arrowheads). C; The decidualised stroma has detached from underlying basal stroma, resulting in an area of denuded endometrium (arrowheads) as evidenced by the lack of positive staining for pan-cytokeratin. D; An area of remaining luminal epithelium is positive for pan-cytokeratin, adjacent to an area of denuded endometrium (arrowheads). Cytokeratin positive glandular epithelial cells are also observed in the basal layer. BL; Basal layer, LE; luminal epithelium, G: glandular epithelium, SC; shed cells. Scale bars as indicated. Images are representative of 2 animals.

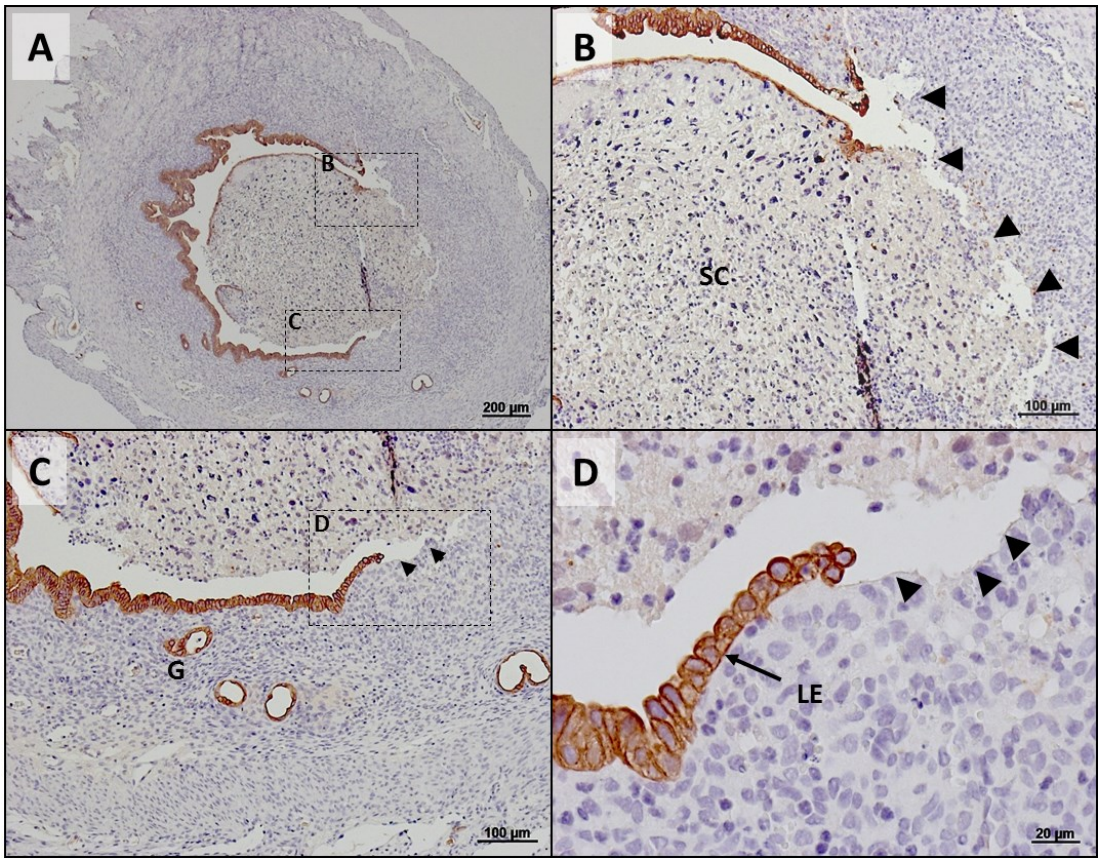

Figure 3-16: Staining for pan-cytokeratin revealed epithelial cell dynamics, 24 hours after progesterone withdrawal. Epithelial cells (pan-cytokeratin positive) were detected in the luminal and glandular epithelial cell compartments. A; The shed decidualised cell mass is observed to be detaching from the underlying stromal cell compartment. B; The denuded, underlying stroma is observed as indicated by the arrowheads next to a region of luminal epithelial cells. C; The luminal epithelium is observed next to an area of denuded basal stroma (arrowheads). D; Round epithelial cells were observed to be "rolling" along an area of the denuded basal stroma. LE; luminal epithelium, G: glandular epithelium, SC; shed cells. Scale bars are as indicated. Images are representative of 3 animals.

3.3.6.3 Evidence of stromal and epithelial cell dynamics during breakdown and repair

To complement these observations, qRTPCR was performed for genes that had been previously described to encode proteins for mesenchymal (stromal cell) markers; *Cdh2* (N cadherin), *Wnt4* and vimentin *(Vim)*, and epithelial cell markers; *Cdh1* (E cadherin), *Wnt7a* and cytokeratin 8 (*Krt8*). Concentrations of mRNAs for these genes across the breakdown and repair window are depicted in Figure 3-17.

Concentrations of mRNAs for *Cdh2* were significantly up-regulated 4 hours ($p<0.001$) after progesterone withdrawal when compared to the 0 hour time-point, mRNA concentrations then significantly decreased from 4 hours ($p<0.01$, $p<0.001$) so that by 12 and 24 hours, concentrations were similar to that of 0 hours. *Wnt4* mRNA concentrations in the decidualised horn were increased by 10 fold when compared to the control horn and were maintained until 12 hours where mRNA concentrations were significantly decreased ($p<0.05$) from the time of progesterone withdrawal. Concentrations further decreased at 24 hours ($p<0.001$). Concentrations of mRNAs for vimentin were significantly up-regulated at 4 and 8 hours after the withdrawal of progesterone (4 hours; $p<0.001$, 8 hours; $p<0.01$), and displayed a similar trend to that of *Cdh2*, with the greatest concentration detected at 4 hours, then a steady decrease towards the 24 hour time-point.

Concentrations of mRNAs for *Cdh1* were significantly up-regulated at 24 hours ($p<0.001$) in comparison to the 0 hour time-point. No significant difference in mRNA concentrations were observed between 0-12 hours. Concentrations of *Wnt7a* mRNA displayed similar dynamic changes to *Cdh1*, where a trend of an increase was detected at 4 hours and 12 hours before a significant increase was detected at 24 hours ($p<0.001$). Concentrations for keratin 18 (*Krt18*) mRNA steadily increased from the 0 hour time-point, with significant increases observed at 24 hours ($p<0.01$).

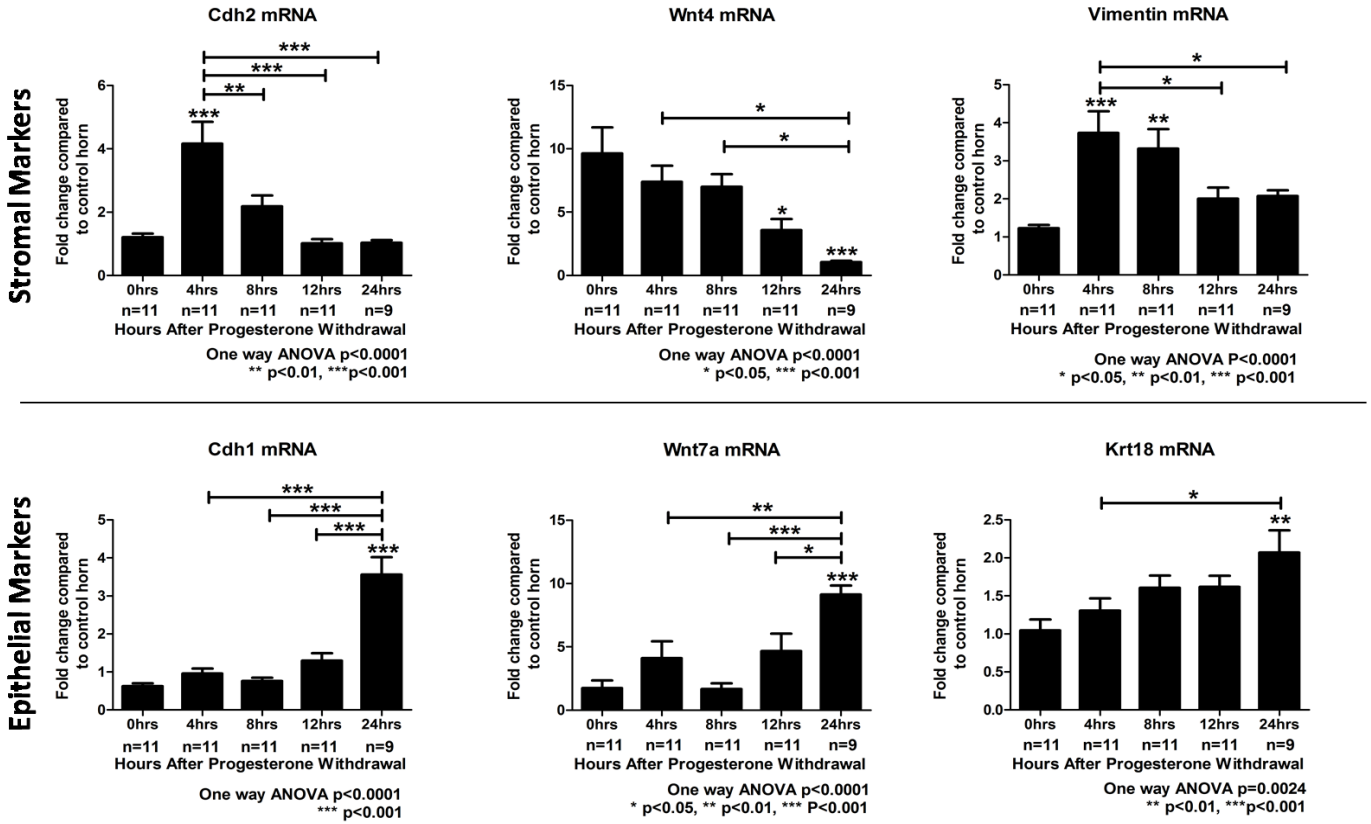

Figure 3-17: Evidence of stromal and epithelial cell dynamics during the window of breakdown and repair. mRNA concentrations for genes that encode proteins for known stromal (*Cdh2, Wnt4*, vimentin) and epithelial cell markers (*Cdh1, Wnt7a* and *Krt18*). mRNA concentrations for the decidualised horn (black bars) were normalised against the 0 hour control horn. Statistical analysis was performed by One Way ANOVA and Bonferroni post hoc testing, comparing each time-point to the 0hr decidualised time-point and then to each time-point.

3.3.7 Evidence for re-epithelialisation of the endometrium by stromal cell differentiation

Immunohistochemistry for pan-cytokeratin was initially carried out to locate epithelial cells at the luminal surface and in the basal glands. Surprisingly, pan cytokeratin positive cells were also documented in the stromal cell compartment (Figure 3-18, A-F).

Notably, pan-cytokeratin positive stromal cells (arrowheads) were localised to areas adjacent to the denuded, luminal surface of the endometrium (depicted by arrows), where the decidualised functional stroma (SC) had detached from the underlying basal layer.

In Figure 3-18, A, two separate areas of the endometrium contained subsets of pan-cytokeratin positive stromal cells. In Figure 3-18, C and F a small number of stromal cells were positive for pan-cytokeratin, in comparison to Figure 3-18, D, which shows a cluster of pan-cytokeratin positive stromal cells adjacent to the lumen.

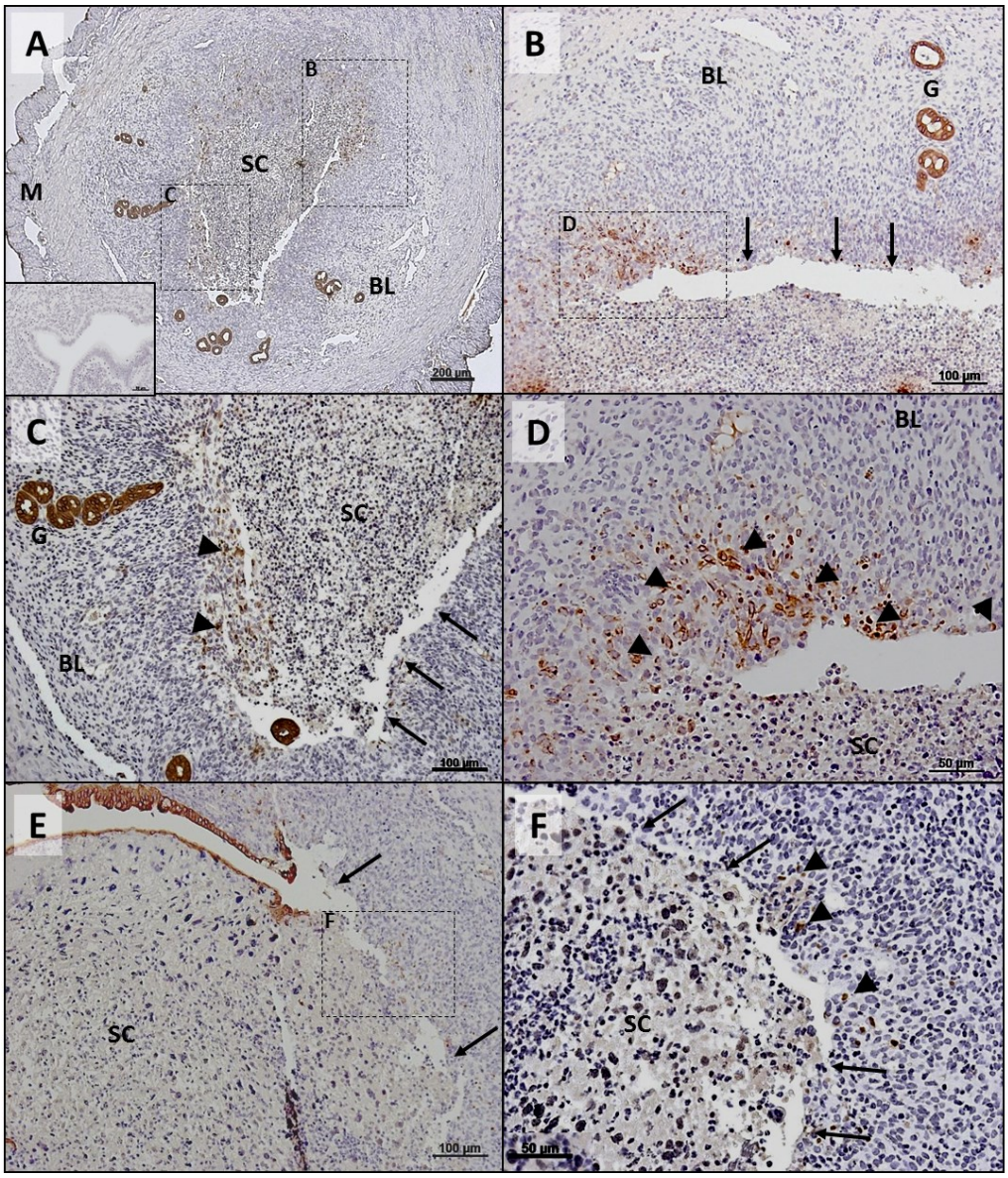

Figure 3-18: Evidence of pan cytokeratin positive stromal cells. Pan-cytokeratin, used as a marker for epithelial cells, was observed in a subset of cells in the underlying stromal cell compartment at 24 hours after progesterone withdrawal. Two representative uteri are shown A-D and E-F. A; Shed decidualised cells are observed in the lumen, next to areas of denuded basal stroma. B; Pan-cytokeratin positive glandular epithelial cells (G) are detected in close proximity to the denuded luminal surface (illustrated by the arrows). C; Positive immunostaining for pan-cytokeratin is detected in glandular epithelial cells and in stroma cells adjacent to the lumen (arrowheads). D; A subset of stromal cells adjacent to the luminal surface are pan-cytokeratin positive (arrowheads). E+F; In another sample, positive pan-cytokeratin stromal cells (arrowheads) were detected adjacent to the luminal surface of a denuded area of endometrium (arrows). BL; basal layer, G: glandular epithelium, SC; shed cells. Scale bars as indicated. Images are representative of 3 animals.

3.4 Discussion

The current study used a new mouse model to investigate cellular and molecular events that occur during endometrial breakdown and repair. Studies using human tissue samples have highlighted evidence for synchronous breakdown and repair of the endometrium during menses (148). Previously described mouse models have been used to study a number of factors that may be involved in endometrial repair, however we believe that these do not allow for investigation of early repair mechanisms. For ease in descriptive purposes, previously described models and our own are outlined in Table 3-2.

A previously described mouse model of menses (Brasted model) failed to focus on time-points relevant to this time period choosing instead to examine breakdown at 16 hours after progesterone withdrawal, and epithelial repair at 24 hours, with complete restoration observed by 48 hours (233). An alternative model that relied on induction of pseudopregnancy and subsequent anti-progestin treatment (mifepristone) (Rudolph model) resulted in protracted breakdown occurring between 0-48 hours after the actions of progesterone were blocked (336). An extended repair phase was also recorded, with repair initiated at 48 hours and complete by 120 hours after administration of mifepristone treatment (336).

Hormone Administration	Decidualisation Method	Method of Progesterone Withdrawal	Publications
Ovariectomy then exogenous hormones by sub-cutaneous injection	Oil injection via flank	Cessation of hormone injections	Finn and Pope, 1984 (234)
Ovariectomy then exogenous hormones by sub-cutaneous injection and progesterone pellet	Oil injection via flank	Pellet removal	Brasted et al., 2003 (233); Kaitu'u-Lino et al., 2005, 2007, 2009, 2010 (230, 239, 318, 319, 368); Evans et al., 2011 (79); Menning et al., 2012 (334); Wang et al., 2013 (235)
Ovariectomy then exogenous hormones by sub-cutaneous injection and progesterone pellet	Oil injection via flank	Mifepristone	Xu et al., 2007 (218)
Ovariectomy then exogenous hormones by sub-cutaneous injection and progesterone pellet	***Oil injection via vagina***	***Pellet removal***	***Cousins, 2014*** (369)
Pseudopregnancy to harness endogenous ovarian-derived steroids	Oil injection via flank	Ovariectomy	Fan et al., 2008, 2012 (188, 320)
Pseudopregnancy to harness endogenous ovarian-derived steroids	Oil injection via flank	Mifepristone	Rudolph et al., 2012 (336)

Table 3-2: Previously described mouse models of menses. Our newly refined model is in italics.

3.4.1 Model adaptation and selection of dissection time-points for a window of early breakdown and repair

Unlike humans, mice do not undergo spontaneous decidualisation and therefore do not naturally menstruate (317, 365, 366). The first description of the artificial induction of endometrial decidualisation and breakdown in the mouse was by Finn and Pope in 1984 (234). This method was subsequently refined by Brasted *et al.,* (233) and has been used to study re-epithelialisation (318), leukocyte infiltration at the onset of breakdown (233), extracellular matrix dynamics during repair (79) and a role for metalloproteinases during repair (230). Other models which relied on endogenous steroid hormone production induced by pseudopregnancy **(**described in section 1.9.4.3) have been used to study hypoxia at the onset of endometrial breakdown and immune cell dynamics in a prolonged breakdown and repair window (188, 320).

The protocol described in this study, was adapted in-house from a previously described protocol (233). Notably, we extended the period of decidualisation from 49 to 90 hours. This adaptation was made following a pilot study where we observed only partial decidualisation of the stimulated horn (where the wet weight of decidualised horn was not significantly greater than the control horn) at 49 hours. In their pioneering study, Finn and Pope describe decidualisation as a progressive response to artificial stimuli (234) and in their original method, stimulation was carried out 4-6 hours after the last progesterone injection, and decidualisation was recorded up until 70 hours later (234).

Another notable change, from the Brasted model, included induction of artificial decidualisation using oil stimulus delivered via the vagina rather than by puncturing the wall of the uterus. This method is more physiologically relevant to the natural process of decidualisation which occurs in the presence of a blastocyst in the mouse. It also eliminates the possibility of any other inflammatory responses that may occur during flank incision and injection of oil through the myometrium as adopted by other groups.

After a decidualisation period of 90 hours, mean decidualised horn wet weights were greater at 0 hours than those previously published by Brasted *et al*., (233) (~0.15g v~ 0.07g), however by 24 hours had decreased to a weight similar to the 24 hour time-point reported in the original publication (~0.07g) (233). Consistent with the findings recorded by Brasted *et al.,* we noted an increase in the mean wet weight of the decidualised horn during breakdown (8-12 hours) which then decreased by 24 hours consistent with shedding and subsequent restoration of normal uterine architecture.

In the current study tissues recovered at 4, 8 and 12 hours after the withdrawal of the progesterone pellet were examined in detail and as complete restoration of endometrial integrity was observed in the majority of mice at 24 hours, this was used as the last time-point for our investigation of early repair mechanisms.

3.4.2 Evidence for endometrial breakdown and shedding during an early window of breakdown and repair

In the current study, evidence of endometrial breakdown occurred by 4 hours after progesterone withdrawal, as evidenced by blood cells in the vaginal smear (Figure 3-1). This finding is in contrast to previously described mouse models, where 8 hours was identified as the earliest time-point where blood cells were observed in the vaginal smear (334), with authors reporting maximal bleeding 24 hours after withdrawal. A study by Xu *et al.,* (218), who used the ovariectomy model and mifepristone administration, reported no vaginal bleeding before 16 hours. In a more recent paper Rudolph *et al.,* (336) used the pseudopregnancy model and mifepristone administration and reported bleeding at 24 hours.

In the current study, vaginal bleeding was detected at the 4 hour time-point and was also detected 8 hours later at the 12 hour time-point, suggesting that bleeding persists for at least 8 hours after the onset of bleeding, a finding consistent with previous studies (218). Mean uterine horn weights for the non-decidualised and decidualised horns were significantly different at 0, 4, 8, and 12hours (Figure 3-4). However, the mean uterine wet weight of the decidualised horn at 24 hours after the withdrawal of progesterone was not significantly different than the non-decidualised horn, suggesting that a degree of regression of the uterine horn had occurred due to shedding and repair of the endometrium.

Consistent with a previous report using a mouse model of menstruation (233), in our study removal of the progesterone pellet led to a rapid fall in serum levels of progesterone from a mean value of 12.4332ng/ml at 0 hours to 2.62ng/ml by 4 hours, continuing to decrease to 2.1ng/ml by 24 hours. To confirm decidualisation of the functional stroma in response to oil injection, prolactin mRNA concentrations were measured and were detected to be down-regulated from maximal concentrations at 0 hours to the lowest concentration at 24 hours. To our knowledge this is the first study to report molecular and histological evidence of decidualisation of the functional layer in a mouse model of menses. Degradation of the decidualised cell mass was observed microscopically and confirmed by decreasing concentrations of prolactin mRNA.

The striking difference in uterine phenotype observed in the non-decidualised control horn and the oil treated decidualised horn at 0 hours (Figure 3-6) was consistent with previous reports (79, 218, 230, 233). Evidence for early breakdown of the endometrium, as observed by red blood cells in the lumen, was consistent with histological evaluation which revealed shedding of the decidual cell mass into the lumen as early as the 4 hour time-point (Figure 3-7).

Previous studies that used the ovariectomy and pseudopregnancy mouse models to examine breakdown and repair within the uterus selected time-points at 24 hours intervals (79, 188, 218, 230, 318, 336), and have not considered that a number of molecular and morphological changes may occur within one 24 hour period. In our study, tissue collection at 4 hour intervals revealed changes within the uterus which have not been previously reported.

For example, we observed that after the withdrawal of the progesterone pellet, breakdown of the decidualised cell mass occurs within 4 hours. By 8 hours the decidual cell mass was observed to "bud" out into the lumen, whilst progressively detaching from the underlying basal stroma to reveal a partially denuded endometrium, whilst still being attached to another area of the basal layer. By 12 hours the functional layer was observed to have has fully detached, and 12 hours later (24 hours after progesterone withdrawal) re-epithelialisation was nearly or totally complete.

Complete re-epithelialisation was observed in most animals by 24 hours, but due to some animal variation some animals were still undergoing repair of their epithelium at this time (Figure 3-10). This is consistent with reports in other mouse models (233, 318, 336) and similar to the variance in duration of menstruation recorded in women.

It is important to note that in this model, as in women, endometrial repair is occurring in steroid-depleted conditions, as demonstrated by the clearance of progesterone (Figure 3-2). These findings would be consistent with data reported in a mouse model by Kaitu'u-Lino *et al.,* (239) who administered a dose of letrozole (an aromatase inhibitor) at the time of progesterone withdrawal, to suppress any effects of exogenous oestrogens, and observed complete restoration of endometrial integrity within 48 hours of progesterone withdrawal and letrozole administration.

3.4.3 Endometrial re-epithelialisation occurs during an early window of breakdown and repair via two possible mechanisms

In women, histological evaluation suggests that menstruation and loss of the functional layer of the tissue results in exposed regions of the basal compartment with naked stroma and

glands. The current dogma is that regeneration of the functional layer of the endometrium requires rapid re-epithelialisation, and was first described in human endometrial samples taken during the menstrual phase by Novak and Te Linde in 1924 (241). They stated that the new epithelium arose from stumps of the glands located in the basal layer of the endometrium (Figure 3-19, A). Based on results in subsequent studies, conducted using samples from women and mouse models, notably by Gargett and colleagues, it has been postulated that these basal glands contain endometrial stem cells residing in a tightly controlled stem cell niche (91) and that this population plays a key role in formation of the new epithelium following menses. Studies by Cervello *et al*., (259, 260) identified side population cells within the human endometrium as putative stem cells capable of generating endometrial-like tissues when transplanted into immuno-deficient mice. However, recent evidence by Garry *et al.,* (169) revealed that Ki67 expression (a marker of cellular proliferation) was minimal in the stromal cell compartment of samples taken from women during the menstrual phase and virtually undetectable in the glandular epithelium during days 1-3 of menstruation even though re-epithelialisation was documented. The authors postulated that another mechanism must contribute to the new epithelial cell layer (Figure 3-19, B) and suggested that a subset of cells close to the denuded luminal surface differentiate to give rise to the new epithelium. This differentiation process of mesenchymal-epithelial transition (MET) and its reverse process of epithelial-mesenchymal transition (EMT) have been extensively studied in embryonic development (370, 371) and in the formation of tumours (372–374). However, whether it plays a key role in endometrial repair is yet to be tested in model systems.

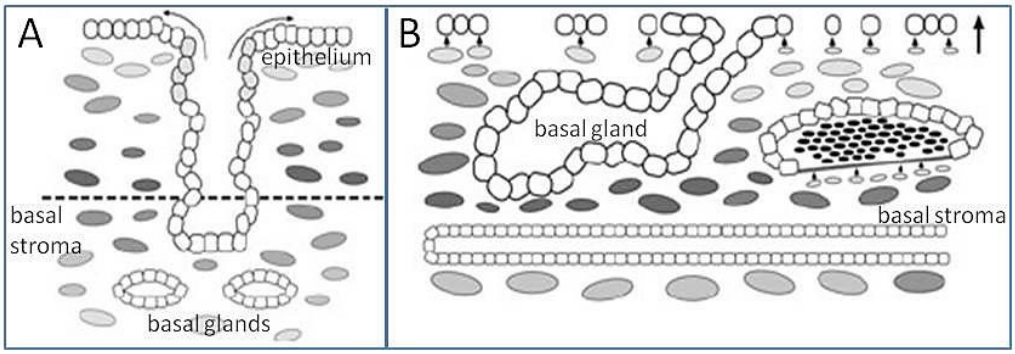

Figure 3-19: Potential mechanisms for re-epithelialisation. A. The current theory of re-epithelialisation; mitotic division of epithelial cells in the basal glands followed by progressive migration of these new cells across the denuded stromal surface. B. New cells arise from small, undifferentiated cells near the luminal surface. Stromal-derived cells may also contribute to the glandular epithelium. Adapted from (169).

In the current study, we used the mouse model to investigate the potential for each of these two mechanisms in re-epithelialisation of the uterine compartment.

3.4.4 Re-epithelialisation by mitotic division of epithelial cells

In our mouse model of menses epithelial proliferation was quantified by staining for BrdU, incorporated into cells immediately prior to tissue recovery. Cells positive for BrdU were observed in both the stromal cell compartment of the basal layer and in the luminal epithelium at 4, 8, 12 and 24 hours after the withdrawal of progesterone. Peak proliferative activity within the epithelium was documented subjectively at 12 and 24 hours. Notably, epithelial cells within the glands were not immunopositive at 0, 4, 8 or 12 hours (consistent with the proliferation studies in women described by Garry et al., (169) described in section 3.4.3).

The first observation of basal glandular epithelial cell proliferation was not detected until 24 hours after progesterone withdrawal at a time when the luminal epithelium was intact in most animals (Figure 3-14, F). This may suggest that luminal re-epithelialisation is initiated by proliferation of unshed luminal epithelial cells, whilst basal glandular epithelial cell proliferation contributes to re-establishment of the glandular compartment alone. Subsets of stromal cells close to the luminal surface, and perivascular cells were also observed to be BrdU positive at 12 and 24 hours highlighting the complex nature of the tissue.

An absence of glandular epithelial proliferation documented in our new model is in contrast to a recent study by Kaitu'u-Lino *et al.,* who, using their own mouse model of menses, observed that glandular epithelial cell proliferation was maximal at 48 hours after the withdrawal of progesterone (318). The percentage of proliferating glandular epithelial cells (~20.8%) was also greater than the percentage of proliferating luminal epithelial cells (~18%). However, direct comparisons to our own data are difficult as in their study, mice were injected with BrdU on 4 consecutive days during their putative proliferative phase (oestrogen stimulation alone) and therefore their analysis was based on cells that had retained their BrdU label over a 9 day period. This injection regime was used to identify a population of slow cycling cells, which the authors believe to be epithelial progenitors present in the glands (318). This is in contrast to our own study where BrdU incorporation was documented in cells that hadn't undergone multiple divisions and were proliferating at the time of dissection, rather than those that had been proliferating for many days. In addition our observation of epithelial cells "rolling" across the denuded stroma at the leading edge of the luminal epithelium (Figure 3-16, D) implicates a combination of luminal

epithelial cell proliferation and migration as key processes involved in the early repair of the tissue.

Consistent with the observation of an apparent increase in luminal epithelial cell proliferation at 12 and 24 hours, additional investigation into the transcription of genes encoding proteins for epithelial cell markers revealed that these were also significantly increased during this time. Concentrations for mRNAs for *Cdh1*, *Wnt7a* and *Krt18* were all up-regulated at 12 hours, and further increased at 24 hours when compared to the 0 hour time-point.

3.4.5 Re-epithelialisation by stromal cell differentiation

In the current study, the possible contribution of cells within the stromal cell compartment to the new luminal epithelium was first investigated by immunohistochemistry, using pan-cytokeratin to identify any cells expressing this classic epithelial cell marker.

Subsets of stromal cells close to the luminal surface were observed to be cytokeratin positive (Figure 3-18). This new finding supports a hypothesis by Garry *et al.,* who postulate that stromal cells may contribute to the new epithelial layer, and that these cells will reside close to the luminal surface and not deep in the basal layer (148). The discovery of pan-cytokeratin positive stromal cells at the 24 hour time-point, but not at 12 hours, may suggest that stromal cell differentiation, if occurring, is activated at the end of the repair window.

The observation of these clusters of pan-cytokeratin positive cells may suggest that these cells are in a transition state from a mesenchymal to epithelial phenotype. Our findings are consistent with previous studies that have utilised mouse models of post-partum repair (375) and pseudopregnancy models of decidualisation and breakdown (376), where cytokeratin positive stromal cells were identified in the endometrium at time-points associated with repair after progesterone withdrawal.

The studies presented in this chapter revealed that dynamic changes in mRNA concentrations for mesenchymal and epithelial markers were detected during the window of breakdown and repair (Figure 3-17). One striking observation is that the trends for each set of genes (stromal v epithelial) are mirror images of each other, as stromal cell markers decrease epithelial cell markers increase. Specifically, the total mRNA concentrations of stromal cell specific proteins are increased during breakdown of the tissue (4-8 hours) consistent with an increase in stromal cell proliferation detected in the basal layer of the tissue at this time (Figure 3-12). However, consistent with the observation of breakdown and

shedding of the decidualised stromal mass and initiation of re-epithelialisation, an increase in concentrations of mRNAs encoding epithelial markers (in parallel with a decrease in stromal markers) was detected in parallel with an increase epithelial cell proliferation in uterine tissue recovered at 12 and 24 hours (Figure 3-13 and Figure 3-14). This switch of stromal to epithelial proliferation, changes at the molecular level and the observation of pan-cytokeratin positive stromal cells adjacent to sites of denuded endometrium all suggest that our hypothesis of the stromal cell compartment contributing to the repair of the luminal epithelium may be occurring. MET is regulated by a number of key genes and downstream transcription factors (377–379), and in the next chapter we conducted a more detailed examination of the activity of these genes during our window of breakdown and repair.

3.4.6 Summary

In the current study a newly refined mouse model of menstruation was optimised and adapted from previously published protocols. Using this model we established novel time-points for the investigation of endometrial breakdown and re-epithelialisation of the tissue and shed new light on the processes operating during this critical time window.

In our model we report that the onset of breakdown of the tissue is rapid, occurring within 4 hours after progesterone withdrawal. Endometrial shedding was complete within 12 hours, whilst re-epithelialisation was occurring or was complete by the 24 hour time-point. We believe that this set of time-points is more indicative of those observed in women, where repair of the tissue is a rapid process, and occurs simultaneously with tissue breakdown (148).

Having established a window of breakdown and repair, this model was used to investigate re-epithelialisation as a mechanism of repair. In our model, proliferation of the residual luminal epithelium was present during the repair phase, whilst basal glandular epithelium proliferation was minimal. This finding, along with evidence of luminal epithelial cell motility, suggests that residual luminal epithelial cells, not shed during breakdown contribute to the new luminal layer of cells. Furthermore, the presence of pan-cytokeratin positive stromal cells adjacent to denuded areas of recently shed endometrium is suggestive of MET as a potential mechanism of re-epithelialisation. From the evidence in this study, it is possible that both mechanisms; mitotic division of epithelial cells and mesenchymal-epithelial transition contribute to the re-establishment of endometrial integrity.

The results herein provide a novel description of the breakdown and re-epithelialisation in a mouse model of menstruation. In Chapter 1 (section 1.6.3) the cascade of events observed

during menstruation in women was described, including; induction of local hypoxia via arteriole vasoconstriction and immune cell influx. Using our new model of breakdown and repair, the following chapter will investigate a role for hypoxia in initiation of repair mechanisms and angiogenesis, a role for the endometrial macrophage in tissue remodelling and further investigation into MET as a potential repair mechanism. A role for androgens during menses will be discussed in Chapter 5.

Chapter 4 Mechanisms that contribute to the restoration of endometrial integrity following menses

4.1 Introduction

In women extensive endometrial remodelling occurs during menses and the subsequent repair phase of every reproductive cycle. Due to its multi-cellular composition, in order to restore tissue homeostasis, the endometrium must undergo; re-epithelialisation, stromal cell remodelling and endothelial cell proliferation and stabilisation during this repair phase in preparation for steroid-derived proliferation and differentiation.

4.1.1 Re-epithelialisation of the exposed stroma

Re-epithelialisation is a crucial process in endometrial repair. Any delay can lead to prolonged bleeding which can cause anaemia in women. A widely accepted model of endometrial regeneration, based on observations made by Novak and Te Linde, in 1924, suggests that a new population of glandular and luminal epithelial cells arise from the epithelium of glands that are retained in the basal layer after shedding of the functional layer (241).

Recent data suggest that this model of endometrial repair needs to be revisited with recent advances in stem cell research having highlighted them as a potential resource involved in tissue regeneration. For example, recent work on human endometrial stem cells (262, 380) circulating progenitor cells (mouse and human) (266, 267, 381, 382) and human endometrial side population cells (259, 260, 268, 383, 384) implicate all of them as playing a role in repair of the tissue following menses. Notably, label retaining cells (LRCs) have been identified in both the stromal and epithelial cell compartments of the mouse endometrium (385, 386) during post natal development and these are postulated to be stem-like cells that contribute to the growth of the tissue. A mouse model used in studies prior to those described in Chapter 3 documented stem-like label-retaining cells in the endometrium in the basal glands. Clonogenic (stem-like) cells have also been identified in both the stromal and epithelial cell compartments of the human endometrium (251, 257, 387).

Another possible mechanism involved in endometrial re-epithelialisation is cellular transdifferentiation. Recent scanning electron microscopy (SEM) studies have implicated stromal cell differentiation to epithelial cells as a possible mechanism for repair (148, 169). In Chapter 3, using a newly refined mouse model of breakdown and repair, stromal cells adjacent to areas of shed endometrium were found to be immunopositive for the epithelial

marker cytokeratin. These novel findings led us to speculate that these cells were undergoing a morphological change and may be contributing to the new epithelial layer, and therefore prompted further studies as described in this chapter. Our preliminary findings would be consistent with data from Garry *et al.,* who observed new epithelial cells on the luminal surface of the endometrium that were not connected to, or extensions of, the glandular epithelium (148).

4.1.2 Mesenchymal to epithelial cell transition

Mesenchymal to epithelial transition (MET) is a biological process by which mesenchymal cells lose their migratory and invasive phenotype, transforming into polarised epithelial cells which are anchored by cell adhesion molecules to the basement membrane (388, 389). In tissues the occurrence of MET is generally reported to be less common than epithelial to mesenchymal transition (EMT). EMT has been widely studied in the context of prenatal development and organogenesis (389–391) and cancer metastasis (372, 377, 379, 392–397). EMT has also been implicated in maintenance of tissue homeostasis in tissues such as the heart (398, 399), intestine (400, 401) and the mammary gland (402). MET has been studied in the context of hepatic stem cell differentiation (403); a role for MET has not previously been investigated in the context of restoration of endometrial homeostasis.

Studies on EMT and MET in a variety of tissues/conditions have reported data demonstrating involvement of multiple molecular processes including activation of transcription factors, reorganisation of cytoskeletal proteins and changes in cell-surface expression markers (372, 377–379, 404). Recent reviews have summarised the cell surface expression markers that are used as markers for mesenchymal versus epithelial cell phenotypes *in vivo* (Figure 4-1). It is generally accepted that cells expressing *both* mesenchymal and epithelial markers are in an “intermediate” or “transition” state.

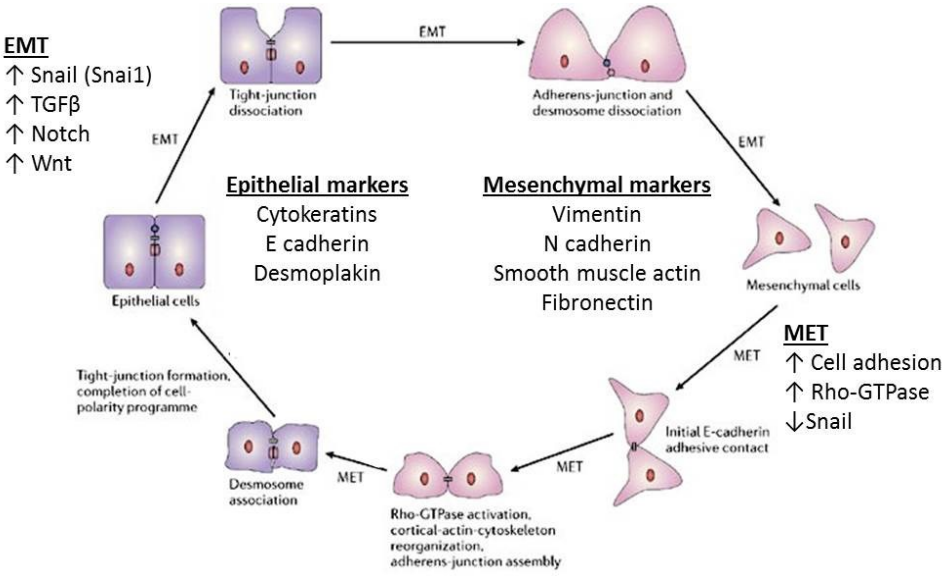

Figure 4-1: Mesenchymal to epithelial transition (MET) and its reverse process epithelial to mesenchymal transition (EMT). MET is driven by an up-regulation of adhesion molecules between mesenchymal cells, followed by cytoskeletal reorganisation and desmosome association. The polarity of cells is altered and tight junctions form, cells begin to express epithelial markers including cytokeratins (Adapted from (405–407)).

A number of key genes and downstream transcription factors involved in the regulation of both processes have been identified. Wilms' tumour 1 (WT1) is located on chromosome 11 and encodes 36 protein isoforms (408). WT1 acts as a transcription factor for Snail (*SNAI1*) and Slug (*SNAI2*) (404). WT1 is essential during gastrulation and organogenesis; in a knock-out mouse model with targeted ablation of WT1, the kidneys, gonads, spleen and adrenal glands fail to form and homozygous embryos die at mid-gestation (409, 410). WT1 has also been shown to be activated upon tissue injury (407).

The transcription factors Snail and Slug have been shown to be repressors of expression of the epithelial cell protein E cadherin in tumour models, driving EMT over MET to support tumour formation (411–413).

MET has been studied in a number of tissues, including the kidney (414–416), and skin (417). *In vitro* studies have demonstrated that renal fibroblasts can be driven towards an epithelial phenotype (415, 416). *In vitro* studies in different tissues have documented that during MET Snail is down-regulated in mesenchymal cells releasing its inhibition on E-cadherin. An increase in E-cadherin expression drives an increase in cell-cell adhesion molecules (417). Mesenchymal cells begin to express epithelial cell markers during this intermediate step; becoming less motile and anchored to the basement membrane and desmosome formation follows. Increased E cadherin drives tight junction formation (414,

417), finally cells undergo polarisation from a front-rear axis of polarity of mesenchymal cells to the apical-basal polarity seen in all epithelial cells (reviewed by (418)).

A role for MET during postpartum repair of the endometrium has been investigated in two mouse models. In the first study, uterine tissues were collected from an *Amhr2-Cre* knock in mouse line, whose myometrium was labelled for β-galactosidase. Uterine tissues were collected prior to pregnancy, at which time β-galactosidase was localised exclusively within the myometrium and stromal cells. Tissues were then collected 2 hours post-partum (day 0), one day post-partum (day 1) and three days post-partum (day 3). Dual staining for β-galactosidase and cytokeratin was detected in the luminal epithelium 1 day post-partum and the glandular epithelium 3 days post-partum, raising the possibility that cells from the stromal cell compartment had contributed to the repair of the luminal epithelium and to the formation of the new glands (375).

A second study utilised a pseudopregnancy model (as described in section 1.9.4.3), in which females were mated with vasectomised males and artificially decidualised before endometrial breakdown was induced by removal of the ovaries. In uterine samples removed during the breakdown and repair window, the authors detected cells dual stained for pan-cytokeratin and vimentin in the stromal cell compartment adjacent to the myometrial-stromal border at 24 hours; and also adjacent to the shed cells/exposed stromal cell compartment at 48 hours after ovariectomy (376). Another fate mapping study conducted during postnatal development was carried out using an Amhr2-Cre; Rosa26-EYFP mouse model in which EYGP was expressed in all cells derived from the mesoderm (mesenchymal cells). At postnatal day 25, in virgin females, EYFP was not expressed in the glandular or luminal epithelium. However, after 3 pregnancies, EYFP was expressed in both the glandular and luminal epithelium, suggesting that stromal-derived cells do contribute to endometrial remodelling in the post-partum period in a non-menstruating species (376).

4.1.3 A role for hypoxia during endometrial repair

In vitro studies using human endometrial explants (419, 420) and *in vivo* studies in non-human primates (188, 328) have reported that active angiogenesis occurs during the proliferative phase of the menstrual cycle, at a time when expansion of the functional layer of the endometrium is driven by rising concentrations of circulating oestrogens. Endothelial cell proliferation is suppressed during the secretory phase and vessel maturation and coiling occur (232) to prepare the endometrium for implantation and pregnancy. Despite oestrogen

and progesterone being the key regulators of endometrial growth and differentiation, it is thought that they may not directly regulate VEGF-dependent angiogenesis (421).

Progesterone withdrawal precipitates a cascade of molecular changes including increased expression of the enzyme COX-2, a key regulator of prostaglandin biosynthesis (422) resulting in the biosynthesis of prostaglandins which induce myometrial contractions and vasoconstriction of the spiral arterioles (reviewed by 48). The net result of these changes is the generation of a hypoxic environment in the upper, decidualised, functional layer of the tissue which is typical of that associated with tissue necrosis and ischaemic injury (186). Hypoxia is associated with stabilisation of HIF, a key regulator of hypoxic response genes which are expressed in endometrial tissues during menses (190, 192, 193).

Hypoxia has been shown to promote stromal and epithelial cell secretion of VEGF in human endometrial stromal cells i*n vitro* (193), suggesting that hypoxia may be a key regulator of endothelial cell proliferation and stability during endometrial repair. Regulation of endothelial cell stability and remodelling is essential to the successful repair of the tissue. Neo-angiogenesis is likely to occur during menses and will involve a variety of pro-angiogenic and anti-angiogenic factors the full details of which require further study.

4.1.4 Immune cell influx and contribution to repair

A diverse population of immune cells is present in the human endometrium, including neutrophils, macrophages and mast cells with their numbers fluctuating dependent upon cycle stage. Notably, leukocytes are reported to comprise up to 40% of endometrial tissue during endometrial breakdown (185, 214), consistent with the acceptance that menstruation is an inflammatory event.

Tissue resident endometrial macrophages have been postulated to have many roles in the endometrium including; initiation of menses (71), tissue breakdown and clearance (148) and remodelling of the functional layer during early repair phases of the endometrium (423).

Immune cell influx during endometrial breakdown and repair has been investigated using mouse models that include induced endometrial breakdown (217, 334). These studies reported that uterine natural killer cells (uNKs), macrophages, neutrophils and T cells are all present in the decidualised mouse endometrium prior to breakdown of the tissue. After progesterone withdrawal, one study reported that neutrophil numbers appear to increase whilst other immune cells types decrease (217). Inhibition of neutrophils by a monoclonal antibody, RB6-8C5, delayed repair of the murine endometrium suggesting a role for this cell

type in breakdown and remodelling (217). Macrophage numbers were reported to increase during the repair phase, at a time when neutrophil numbers decreased (334), implicating a role for macrophages during remodelling of the mouse endometrium, at least in this model. These data are consistent with immunolocalisation studies in human endometrial samples from the menstrual phase, where an increase in neutrophils, eosinophils, T cells, B cells, macrophages and uNK cells was recorded upon progesterone withdrawal (185, 209, 214, 424). Immunolocalisation studies in human tissues and *in vitro* cultures indicate that neutrophils are the dominant leukocyte during breakdown (207, 424), whereas macrophages are postulated to be key to tissue remodelling during the repair phase (215).

In summary, the human endometrium is a multi-cellular tissue that undergoes a tightly regulated cycle of proliferation, differentiation, breakdown and repair; however the mechanisms that contribute to tissue restoration following menses are poorly understood. It is likely that a combination of interchanging mechanisms contribute to restoration of tissue integrity. We believe that studies in our novel mouse model can provide insights into regulatory events during this critical time window.

4.1.5 Aims of the chapter

1. To investigate a role for mesenchymal to epithelial transition during re-epithelialisation of the endometrium.
2. To investigate immune cell influx, specifically macrophages during breakdown and repair.
3. To determine a role for hypoxia during endometrial breakdown.

Chapter 4. Mechanisms that contribute to the restoration of endometrial integrity following menses.

4.2 Materials and methods

4.2.1 Mouse model of menstruation

The mouse model established in Chapter 3 and described in section 2.1.4.4 was utilised to investigate mechanisms contributing to endometrial repair. The protocol is outlined in Figure 2-4.

4.2.2 Transgenic *fms*-EGFP mouse line- "The Mac green mouse"

Generation of the Mac green mouse is described in Chapter 2.1.2. Founder stocks were generously provided by Dr. Bernadette Dutia and Professor David Hume (University of Edinburgh). Genotyping for EGFP positive mice was carried out as described in section 2.1.2. Mac green mice were included in the menses model and dissected at each of the designated time-points.

4.2.3 Immunohistochemistry

All samples were fixed in NBF overnight at room temperature, rinsed in 70% ethanol and then stored in 70% ethanol before tissue processing as described in section 2.6.

Immunohistochemistry was carried out using the standard protocol outlined in section 2.7.2 using the antibodies outlines in Table 2-15 and Table 2-16. Modifications to the standard protocol were required for Snail/Slug and green fluorescent protein (GFP). Deviations to the standard protocol are outlined in section 2.7.2.9.

Images were analysed as detailed in section 2.7.2.10.

4.2.4 RNA extraction

RNA extraction was carried out as detailed in section 2.2.

4.2.5 Synthesis of complementary DNA using VILO cDNA synthesis kit

Reverse transcription of RNA to cDNA was performed using the Superscript VILO cDNA synthesis kit (InVitrogen) according to manufacturer's instructions, using the volumes outlined below in Table 2-8. Samples were then incubated under the conditions detailed in section 2.3

4.2.6 Quantitative Real Time PCR

Quantitative real time PCR was carried out as detailed in section 2.4**.**

Statistical analysis was performed as detailed in section 2.8.

4.2.7 RT2 Profiler PCR array

RT^2 profiler arrays contain a panel of genes containing housekeeping genes, quality controls and 84 genes that are related to a specific biological pathway. RNA samples used in RT^2 profiler PCR array were subject to quality assessment based on RIN. Samples were RIN<6.0 were excluded. Two gene arrays were utilised in this study; Mouse Epithelial to Mesenchymal Transition Array (SABiosciences, PAMM-090Z) and Mouse Angiogenesis Array (SABiosciences, PAMM-024Z).

RNA quantitation was performed as detailed in section 2.5.1. A RIN greater than 6.0 was accepted for further analysis by PCR array. cDNA synthesis was performed following the protocol outlined in section 2.5.3. Real time PCR was performed as detailed in section 2.5.4.

PCR data analysis was performed using the SABiosciences web portal as detailed in section 2.8.

4.2.7.1.1 Putative pathway analysis by MetaCore™

MetaCore™ is an integrated software that utilises a manually curated database of known species specific interactions between protein-protein, protein-DNA and protein-RNA. MetaCore™ was used to map potential signalling and metabolic pathways of candidate genes investigated by PCR array.

4.3 Results

4.3.1 Evidence from a mouse model that re-epithelialisation of the endometrium involves mesenchymal to epithelial transition.

Following an initial observation of cytokeratin positive cells in the stromal cell compartment of repairing endometrium in Chapter 3**,** further evidence for MET during endometrial repair was investigated by immunofluorescence, using double staining for the mesenchymal marker vimentin and the epithelial marker cytokeratin.

During breakdown of the tissue (0-8 hours after P withdrawal), no co-localisation of vimentin and cytokeratin was observed (Figure 4-2, A and B) with vimentin localised exclusively within the stromal compartment of the basal layer and cytokeratin is only detected in the glandular and luminal epithelium. At 12 hours, a few dual labelled cells (yellow) were detected in the basal layer close to the myometrium (Figure 4-2, D; arrowheads) and interestingly, stromal cells in the basal layer were also strongly stained for cytokeratin (Figure 4-2, E). At 24 hours, in tissue samples exhibiting repair (Figure 4-2, F), the area of exposed stroma is highlighted by the white arrows, and is found adjacent to the shed functional layer (SC) present in the lumen. A higher powered image of one area in Figure 4-2, G, shows co-localisation of vimentin and cytokeratin in stromal cells adjacent to the lumen (white arrowheads). These cells are expressing both epithelial and mesenchymal markers and therefore can be considered as an intermediate phenotype that occurs in the process of MET.

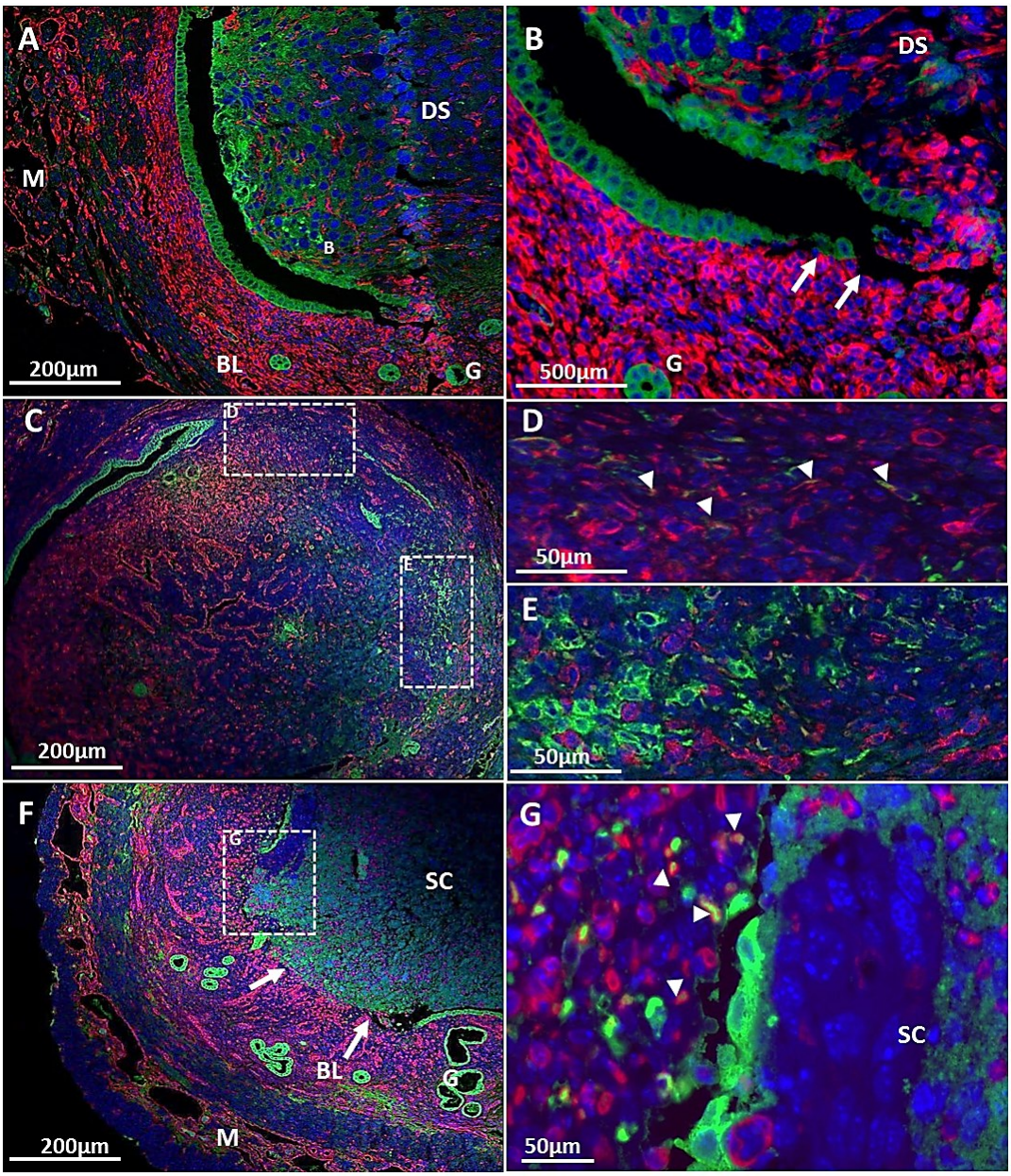

Figure 4-2: Epithelial cells stained for cytokeratin (green) and mesenchymal cells stained for vimentin (red) in the mouse endometrium. A and B; 8 hours after progesterone withdrawal, the decidualised cells begin to detach from the underlying stroma (white arrows). The stromal cells of the underlying basal stroma were positive for vimentin (red), the glandular epithelium (G) and the encroaching luminal epithelium were positive for cytokeratin (green). No co-localisation for cytokeratin and vimentin was observed. C; 12 hours after progesterone withdrawal, vimentin positive decidualised cells were observed, budding into the lumen. D; Vimentin and cytokeratin positive cells were observed in the basal layer, close to the myometrium (arrowheads). E; stromal cells in the basal layer were positive for cytokeratin. F and G; 24 hours after progesterone withdrawal. An area of shed endometrium (indicated by white arrows) was observed. Co-localisation of vimentin and cytokeratin (white arrowheads) was detected close to the surface of the underlying basal layer. DS; decidualised stroma, M; myometrium, BL; basal layer, G: glandular epithelium, SC; shed cells. Scale bars as indicated. Images representative of 3 animals.

4.3.1.1 MET array analysis

To complement the observation of dual-labelled cells close to the luminal surface, additional evaluation of MET was investigated using a PCR array that profiles 84 key genes that are known to be involved in the EMT pathway (and therefore its reverse process MET). The cDNAs detected by the array include cell surface receptors, cell adhesion markers, extracellular and cytoskeleton genes and genes involved in migration, motility and morphogenesis, as well as key transcription factors of this process. The full gene list can be found in the Supplementary Table 1.

Samples from three time-points were chosen for analysis; 0 hours as the time-point prior to breakdown, 8 hours after progesterone withdrawal (blood in vagina), as this was a time when the tissue is observed to be breaking down, and 24 hours after progesterone withdrawal, as in our model the endometrium was undergoing or had completed re-epithelialisation. Those genes in which a significant change in fold regulation was documented are shown in Table 4-1, Table 4-2 and Table 4-3.

Notably, at both the 8 hour and 24 hour time-points a greater proportion of genes were up-regulated than down-regulated when compared with the 0 hour time-point; n=20 v 4 and n=43 v 5 respectively. Of the 21 gene changes that occurred between 8 and 24 hours, 12 were up-regulated whereas 9 were down-regulated.

A number of the changes detected in the mouse mirrored those reported in human tissue at time of menses (224, 226, 425), including a striking up-regulation in expression of *Mmp-3* (a 3 fold increase at 8 hours, and a 61 fold increase at 24 hours) and evidence of dynamic differences occurring between 8 and 24 hours. *Mmp-9* was also significantly up-regulated between 8 and 24 hours (11 fold increase).

Other notable changes included expression of the epithelial markers *Krt7* (4 fold increase at 8 hours and 28 fold increase at 24 hours when compared to the 0 hour time-point) and *Cdh1*(E cadherin) (5 fold increase between 0 and 24 hours). Cell adhesion molecules *Dsc2* (desmocollin2) and *Spp1* (osteopontin) were also significantly up-regulated. *Spp1* increased 4 fold at 8 hours and 23 fold at 24 hours when compared to the 0 hour time-point. *Dsc2* increased 4 fold between 0 and 24 hours. Intracellular junction protein desmoplakin (*Dsp*) increased 9 fold at 24 hours when compared to the 0 hour time-point. Snail homolog *Snai3*, increased 5 fold at 8 hours and 15 fold at 24 hours. Platelet derived growth factor receptor beta *(*PDGFRβ) increased 2 fold at 8 hours and 4 fold at 24 hours.

Gene Name	p value	Fold Regulation
Col5a2	0.014999	1.3733
Fzd7	0.004084	2.112
Gng11	0.027026	-2.0012
Igfbp4	0.007334	1.8312
Il1rn	0.000873	2.0872
Ilk	0.027785	1.4167
Itgb1	0.001503	1.4681
Krt19	0.000383	1.9973
Krt7	0.001239	4.8209
Mmp2	0.008265	2.0402
Mmp3	0.013284	3.0056
Mtap1b	0.021019	1.7783
Pdgfrb	0.030445	2.1571
Plek2	0.001445	2.1191
Rgs2	0.001027	-2.7773
Snai2	0.018714	-2.1138
Snai3	0.006822	5.6312
Spp1	0.001467	4.3785
Stat3	0.001286	1.5821
Steap1	0.000673	2.3442
Tfpi2	0.008769	-1.8252
Timp1	0.015419	1.6154
Tmeff1	0.000078	2.3973
Wnt11	0.000277	3.4224
Number of genes significantly up-regulated	20	
Number of genes significantly down-regulated	4	

Table 4-1: Significant changes in gene expression 8 hours after progesterone withdrawal, as displayed by up- or down- fold regulation when compared against the 0 hour group, n=6.

Gene Name	p value	Fold Regulation
Akt1	0.004507	1.6241
Bmp1	0.001376	1.7233
Bmp7	0.04878	1.8035
Cald1	0.006957	2.2812
Camk2n1	0.04425	4.8329
Cav2	0.03615	1.7465
Cdh1	0	5.1764
Cdh2	0.046312	1.4957
Dsc2	0.000383	4.734
Dsp	0.000257	9.5533
Esr1	0.032215	1.5223
Fn1	0.007739	3.0108
Fzd7	0.011578	2.2833
Gng11	0.016563	-2.7033
Gsc	0.039591	2.8029
Gsk3b	0.046881	1.4052
Ilk	0.004121	1.8766
Itgb1	0.006007	1.6552
Jag1	0.002575	3.4856
Krt19	0.000053	7.5293
Krt7	0.000018	28.178
Mitf	0.001484	-2.1751
Mmp2	0.00544	2.7303
Mmp3	0.001871	61.2906
Msn	0.000728	1.8437
Mtap1b	0.000492	2.1494
Notch1	0.031693	1.6165
Ocln	0.005327	11.2243
Pdgfrb	0.000015	4.5738
Plek2	0.044301	1.6349
Ptp4a1	0.002475	1.8968
Rgs2	0.001014	-4.2015
Smad2	0.005844	1.3823
Snai3	0.011681	15.8243
Spp1	0.000141	23.2021
Stat3	0.00232	1.8157
Steap1	0.000283	4.6399
Tcf4	0.001468	1.4002
Tfpi2	0.002632	-2.1709
Tgfb1	0.004964	1.783
Tgfb2	0.004658	-1.497
Tmeff1	0.000001	4.1575
Tmem132a	0.00069	2.8066
Tspan13	0.00039	3.2687

Gene Name	p value	Fold Regulation
Twist1	0.00125	3.294
Vim	0.001135	1.7446
Vps13a	0.035245	1.5401
Zeb1	0.000009	2.4496
Number of genes significantly up-regulated	43	
Number of genes significantly down-regulated	5	

Table 4-2: Significant changes in gene expression 24 hours after progesterone withdrawal, as displayed by up- or down- fold regulation when compared against the 0 hour group, n=6.

Gene Name	p value	Fold Regulation
Ahnak	0.036678	0.5404
Cdh1	0.004232	2.0487
Dsc2	0.038234	2.2635
Dsp	0.007373	3.0514
Egfr	0.002567	0.5275
Gng11	0.04006	0.4894
Igfbp4	0.015997	0.5351
Jag1	0.035072	1.9634
Krt19	0.044665	2.492
Krt7	0.014579	3.8638
Mitf	0.043177	0.3895
Mmp3	0.010098	13.4799
Mmp9	0.024631	11.2996
Mst1r	0.049177	0.6576
Ocln	0.047848	3.1545
Plek2	0.041571	0.51
Pppde2	0.006287	0.6375
Rgs2	0.038365	0.437
Spp1	0.023751	3.5029
Tgfb2	0.008919	0.3996
Tgfb3	0.025285	0.5698
Number of genes significantly up-regulated	12	
Number of genes significantly down-regulated	9	

Table 4-3: Significant changes in gene expression 24 hours after progesterone withdrawal, as displayed by up- or down- fold regulation when compared against the 8 hour group, n=6.

4.3.1.2 Dynamics of gene expression during the breakdown and repair window

To complement and extend these observations, additional experiments focussed on examining the dynamics of expression of genes, previously described to be critically involved in regulation of MET and its reverse process EMT, across all of the time-points investigated in our model. Gene expression was quantified by qRTPCR (Figure 4-3). Concentrations of *Wt1* mRNA in total uterine tissue extracts displayed dynamic changes

across the window of breakdown and repair (4-24 hours). For example, the total concentration of *Wt1* mRNA showed a trend of an increase at the 4 hour time-point when compared to the 0 hour time-point occurring at a time when breakdown of the tissue was first observed; concentrations were observed to decrease at 8 hours before being significantly decreased at 12 hours ($p<0.01$) and 24 hours ($p<0.01$) when compared to the 4 hour time-point.

Concentrations of Snail mRNA exhibited a similar pattern to that of *Wt1*, with a trend of an increase at 4 hours before a decrease of expression towards 24 hours, however no significant changes in mRNA concentrations were observed. Concentrations of the second snail homolog, Slug, showed no significant changes between 0 and 24 hours, however a trend of a decrease was observed at 8 hours which is consistent with data obtained from the array. Concentrations of the third Snail homolog Smuc (*Snai3*) were observed to be inversely regulated compared to *Snai1*. mRNA concentrations did not significantly change between the 0 and 12 hour time-points, however a significant increase in mRNA concentrations was observed between 12 and 24 hours ($p<0.001$), coincident with re-epithelialisation of the tissue. A significant increase between 0 and 24 hours is consistent with the increase observed in the array.

Protein expression of WT1 and Snail (Snai 1 and 2) were evaluated by immunohistochemistry, and the localisation of these proteins is shown in Figure 4-4. Consistent with the mRNA data, the most intense immunostaining of WT1 was detected 4 hours after progesterone withdrawal localised to both the decidualised stromal cells in the functional layer and the stromal fibroblasts in basal layer (Figure 4-4, A). WT1 immunoexpression appeared to be less intense in the shed cells (SC) 12 hours after withdrawal of progesterone (Figure 4-4, B). Notably, WT1 was not expressed in the luminal (LE) or glandular (G) epithelium, and weaker immunostaining for WT1 was observed in the basal stromal cell compartment at 12 hours when compared to the 4 hour time-point. Endothelial cells were also observed to be WT1 immunonegative (Figure 4-4, B, inset image, black arrowheads).

The homologs of Snail (Snail and Slug) were immunolocalised, by an antibody that recognised both proteins, to stromal cells as well as the glandular epithelium during breakdown at 8 hours after progesterone withdrawal (Figure 4-4, C). More intense immunoexpression of Snail/Slug was observed in the luminal epithelium and the surrounding

stroma during repair, (Figure 4-4, D), in tissues recovered 24 hours after progesterone withdrawal.

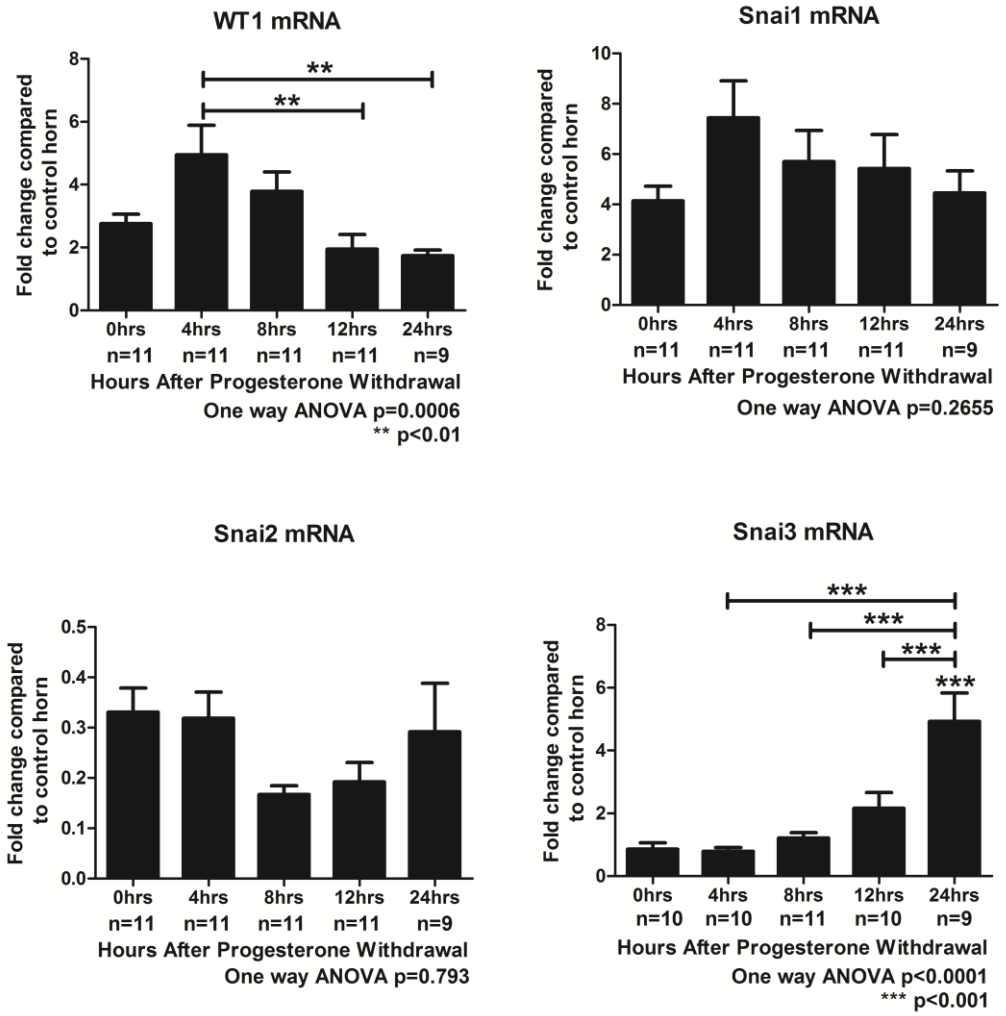

Figure 4-3: mRNA concentrations for candidate genes involved in mesenchymal to epithelial transition; *Wt1*, Snail (*Snai1)*, Slug *(Snai2),* Smuc *(Snai3)* following progesterone withdrawal. mRNA expression for the decidualised horn (black bars) was normalised against the control 0 hour horn. Statistical analysis was performed by One way ANOVA and Bonferroni post hoc testing, where each time-point was compared to the 0 hour time-point and then each other time-point, where * p<0.05, ** p<0.01, ***p<0.001.

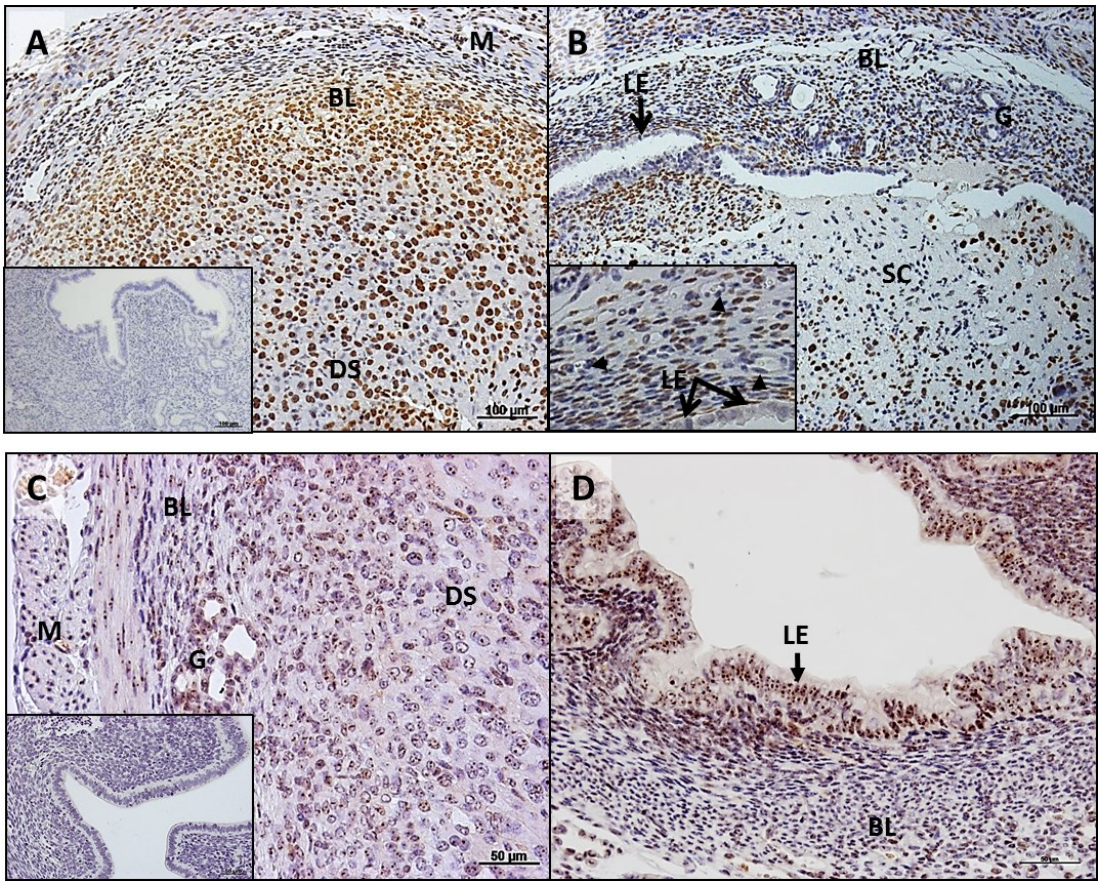

Figure 4-4: WT1 (A and B) and Snail/Slug (C and D) localisation in the mouse endometrium during breakdown and repair. A; WT1 is immunopositive in decidualised stromal cells and also expressed in the stroma of the functional and basal layers at 4 hours after progesterone withdrawal (inset image is the negative control). B; WT1 is absent from the luminal epithelium (LE) and the glandular epithelium (GE) at all time-points. WT1 appears to be down-regulated in the basal layer and is largely absent from the shed cells in the lumen, 12 hours after progesterone withdrawal. Inset; endothelial cells are WT1 negative. C; Snail/Slug is expressed in the stromal cells and epithelial cells at 8 hours after progesterone withdrawal. D; staining for Snail/Slug was observed in the luminal epithelium and the adjacent stromal cells at 24 hours after progesterone withdrawal. BL; basal layer, G: glandular epithelium, SC; shed cells, DS; decidualised stroma, LE; luminal epithelium, M; myometrium. Scale bars as indicated. Images representative of 2 animals per time-point.

4.3.1.3 Network analysis of the MET pathway

To understand the potential interactions between the genes detected as being changed in both the array and in the MET regulatory genes (*Wt1, Snai1, Snai2, Snai3*), a basic gene network was generated using MetaCore™ (Thomson Reuters) software. To filter data, the full gene array list was input into the software, any gene that was found to have no interaction to any of the other 83 genes was removed from the network. As WT1 has been previously demonstrated as a master regulator of the Snail homologs those genes that are downstream of WT1 were highlighted to identify candidates for further investigation. The results of this analysis are depicted in Figure 4-5. Direct interactions between genes, known to be involved in ***EMT*** in other tissues, are depicted using arrows; green arrows denote stimulatory actions, whereas red lines denote inhibitory actions, a key for the symbols used in the array can be found in Supplementary Figure 1. A full list of gene names highlighted in the network can be found in Supplementary Table 1.

From the network analysis it is evident that multiple cell compartments are involved in regulation of MET and that multiple interactions occur between each compartment. According to this network analysis, changes in expression of WT1 may play a role in modulating expression of MMP-9; this is consistent with data reported in the array, where no significant changes were observed in expression of *Mmp-9* during breakdown (0-8 hours) at a time when *Wt1* is increased (Figure 4-3). However, as expression of *Wt1* is decreased (12-24 hours) and therefore its putative inhibitory impact reduced, an 11 fold increase in *Mmp-9* was reported in the array between the 8 hour and 24 hour time-point. During EMT, WT1 has been reported to have direct stimulatory effects on Snail, whilst inhibiting Slug, E cadherin and *Tgfb* (399, 404, 426). In the current data, Slug mRNA was decreased at 8 hours, consistent with data reported in Figure 4-3. Increased mRNA concentrations of *Wt1* were also coincident with low mRNA concentrations of E cadherin (*Cdh1*) reported in Figure 3-17, during breakdown. Although the relative contributions of *Wt1*, *Snai1 and Snai2* in EMT may be complex, it was notable that as *Wt1* mRNA concentrations decreased increases in *Tgfb* and E cadherin were detected in the array.

Genes upstream of E cadherin and N cadherin, common epithelial and mesenchymal markers used for cellular phenotyping, are also depicted in Figure 4-5. Interestingly, *Mmp-2* and *Mmp-9* have been reported to exhibit inhibitory actions on E cadherin (427–430), which may account for the low fold changes observed in E cadherin in the array.

In summary, dynamic gene changes associated with regulation of cell identity are observed during breakdown (0-8 hours) and repair (8-24 hours). Of note, striking increases in epithelial markers (*Krt7* and *Cdh1*), tissue remodelling factors (MMPs), cell adhesion molecules (*Spp1* and *Dsc2*) and intracellular junction proteins (*Dsp*) were observed 24 hours after withdrawal of progesterone during the window of endometrial repair. This suggests a net effect of MET over EMT. Network analysis, using known gene interactions, demonstrates that MET is a complex regulatory pathway involving multiple cellular compartments. Candidates for further investigation were identified from the network analysis and include; Mmp-2 and Mmp-9, PDGFRβ and Twist.

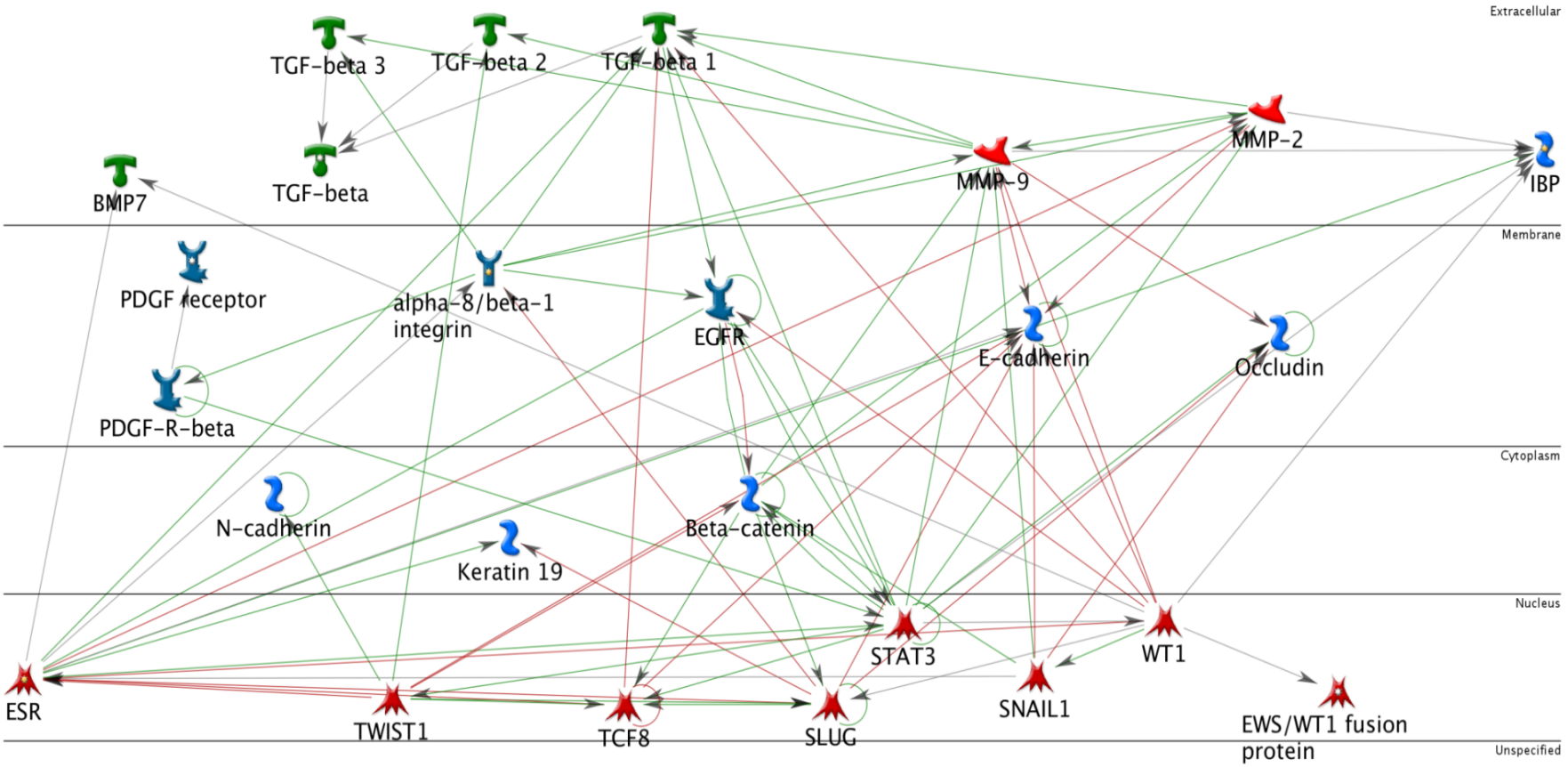

Figure 4-5: Known interactions of genes downstream of WT1, Snail and Slug. Arrows indicate direct effects on other genes in the pathway. Green arrows indicate activation, whereas red arrows show inhibitory action. Pathway generated using MetaCore™ software. Gene symbols are outlined in Supplementary Figure 1.

4.3.2 A role for macrophages during endometrial breakdown and repair

4.3.2.1 Identification of monocytes in the Mac green mouse

Mice with EGFP-labelled cells of the monocyte lineage, the "Mac green mouse" (341), were used in the model of menstruation with tissues recovered at multiple time-points. Immunohistochemistry for EGFP was used to identify tissue resident macrophages during breakdown and repair so as to assess the numbers and locations of cells during uterine tissue remodelling.

At the time of full decidualisation (0 hours, Figure 4-6), EGFP positive cells (putative tissue macrophages) were localised in the decidualised stroma (Figure 4-6, A), in blood vessels (Figure 4-6, B) the stromal cell compartment of the basal layer (Figure 4-6, C) and in the luminal epithelium (Figure 4-6, D). By 12 hours after progesterone withdrawal, a time when the decidual cells were observed to be detaching from the underlying basal layer (Figure 4-7), macrophages appeared to have infiltrated the basal layer and were localised to areas adjacent to regions of shedding (Figure 4-7, C). Additionally, a significant population of macrophages were detected adjacent to the luminal epithelium (Figure 4-7, B, arrowheads). Figure 4-7, D, shows a portion of tissue where detachment of the decidual cells from the basal layer is well advanced. Macrophages are evident in the remaining basal layer, but also in the tissue mass that had been shed into the lumen and was in the process of breaking down (Figure 4-7, D, arrowheads).

By 24 hours, the diameter of the uterus had reduced (Figure 4-8, A), and the luminal epithelium was continuous consistent with full repair. However, EGFP positive macrophages were still detected in the tissue at this time. In contrast to the 0 hour and 12 hour time-points, it was notable that macrophages were largely absent from the basal layer of the tissue (Figure 4-8, B and C) but appeared to be localised within the stromal cell compartment immediately adjacent to the luminal epithelium (C, arrows) with some floating in the lumen (Figure 4-8, D).

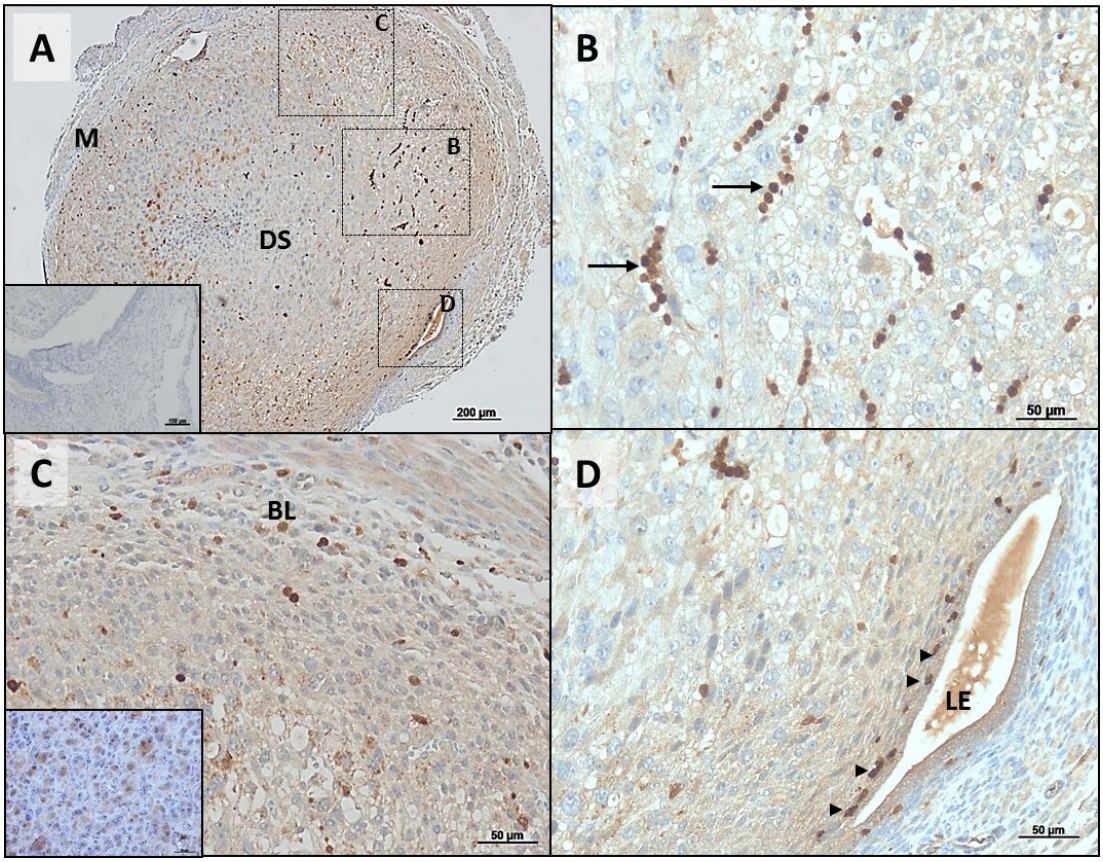

Figure 4-6: Localisation of EGFP positive cells (putative tissue macrophages) in fully decidualised tissue at the time of progesterone withdrawal (0 hours) in the mac green mouse. Macrophages were identified by immunohistochemistry for green fluorescent protein (GFP) as indicated by brown staining. A; Macrophages were observed in the decidualised stroma, the basal layer and the luminal epithelium. B; EGFP positive cells are localised in the blood vessels (arrows) and the decidualised stroma. C; Positive immunostaining for macrophages detected in the basal layer of the endometrium. D; Macrophages were identified in the luminal epithelium. Elongated EGFP positive cells were detected adjacent to the luminal epithelium (arrowheads). BL; basal layer, DS; decidualised stroma, LE; luminal epithelium, M; myometrium. Scale bars as indicated. Images representative of 2 animals.

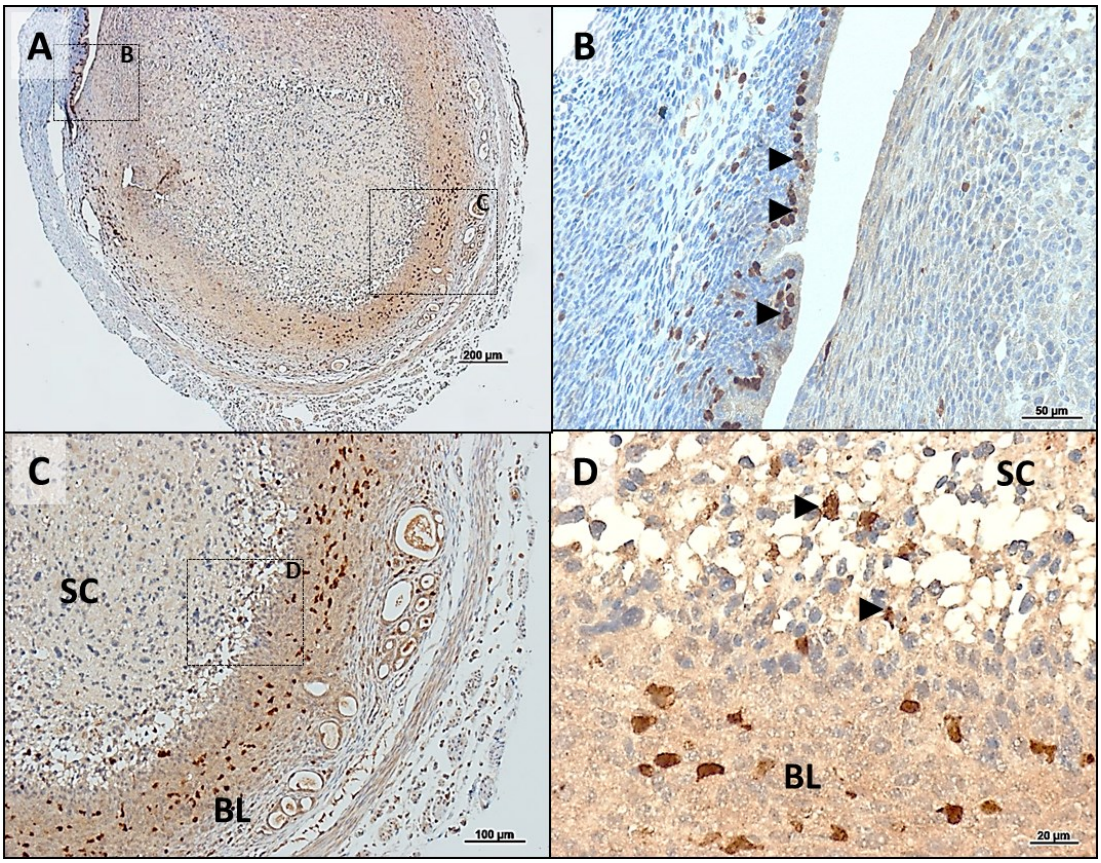

Figure 4-7: Localisation of EGFP positive cells (putative tissue macrophages), 12 hours after progesterone withdrawal. Macrophages were identified by immunohistochemistry for green fluorescent protein (GFP) as indicated by brown staining. A; Macrophages were observed in the basal layer and surrounding the luminal epithelium. B; Macrophages were observed adjacent to luminal epithelial cells (arrowheads). C; Immunopositive staining for macrophages observed in the basal layer of the endometrium. D; Macrophages were localised to the basal layer, but also shed during detachment of the functional stroma. SC; shed cells. BL; basal layer. Scale bars as indicated. Images representative of 3 animals.

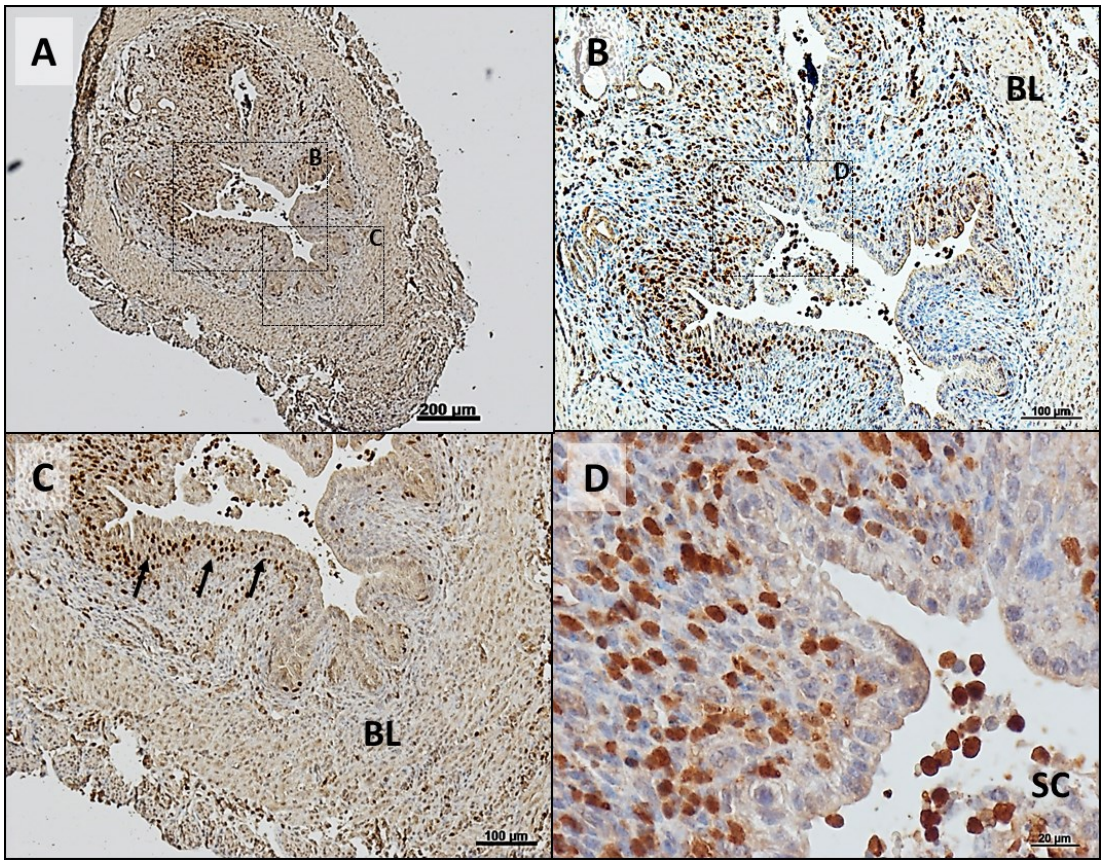

Figure 4-8: Localisation of EGFP positive (putative tissue macrophages), 24 hours after progesterone withdrawal. Macrophages were identified by immunohistochemistry for green fluorescent protein (GFP) as indicated by brown staining. A; Macrophages were localised primarily to the stromal cell compartment surrounding the luminal epithelium. B; Macrophages were observed adjacent to luminal epithelial cells. C; Macrophages were localised to regions adjacent to the luminal epithelium (arrows). Macrophages were largely absent from the basal layer of the tissue. D; Macrophages were also detected in the shed cells in the lumen. SC; shed cells. BL; basal layer. Scale bars as indicated. Images representative of 2 animals.

4.3.2.2 Expression of genes involved in macrophage recruitment

To complement these observational studies, qRTPCR was performed for genes that had been previously described as encoding proteins involved in macrophage recruitment, differentiation or proliferation (208, 423, 431–435), gene expression is outlined in Figure 4-9. Concentrations of the chemokine *Ccl2* did not change significantly during the window of breakdown (0-8 hours), however a significant increase in concentrations of *Ccl2* mRNA was detected at at 24 hours ($p<0.001$). Concentrations of connective tissue growth factor (*Ctgf*) followed a similar pattern, with no change observed at the 4-12 hour time-points. A significant increase in concentrations of *Ctgf* was detected at 24 hours after progesterone withdrawal ($p<0.001$). No significant changes in concentrations of *Smad3* mRNA were detected across the window of breakdown and repair. Similarly, no significant changes were observed for macrophage colony stimulating factor (*mCsf*), however a trend of a decrease in concentrations was observed from 0 hours through to the 12 hour time-point.

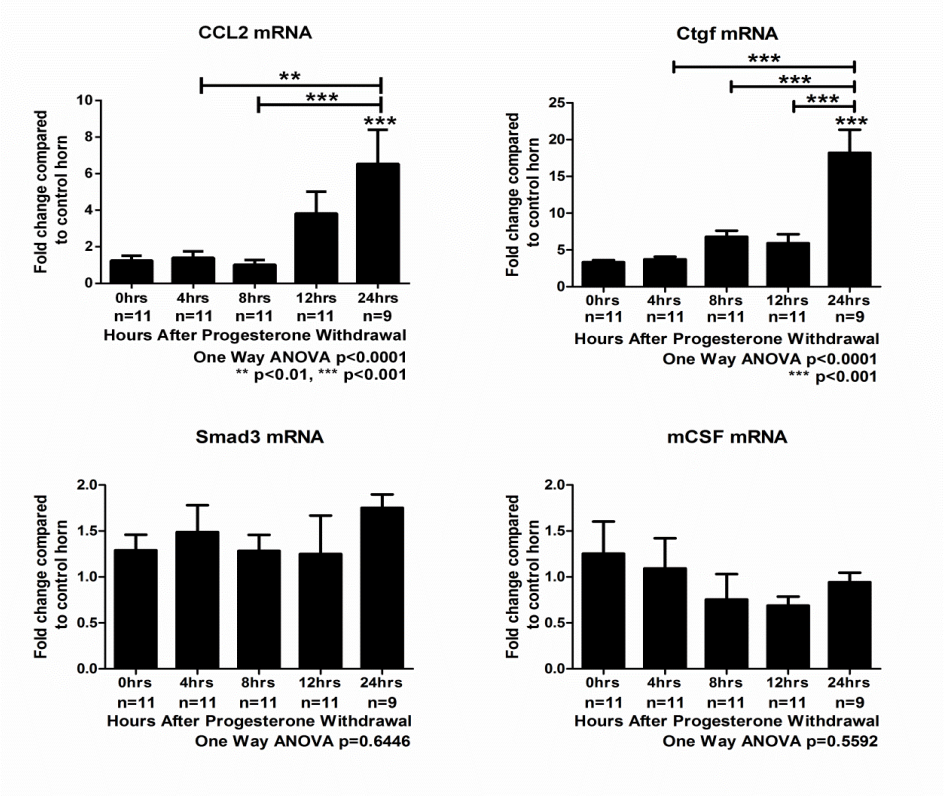

Figure 4-9: mRNA concentrations for candidate genes involved in macrophage influx or differentiation; *Ccl2, Ctgf, Smad3* and *mCsf* following progesterone withdrawal. mRNA expression for the decidualised horn (black bars) was normalised against the control 0hr horn. Statistical analysis was performed by One way ANOVA and Bonferroni post hoc testing, comparing each time-point to the decidualised 0hr time-point, and then each other time-point, where ** $p<0.01$ and *** $p<0.001$.

4.3.3 A hypoxic gradient exists during endometrial breakdown that may drive neo-angiogenesis during endometrial repair

Evidence of hypoxia was investigated using the Hypoxyprobe® labelling system, where pimonidazole was injected intra-peritoneally 90 minutes prior to culling. This reagent forms protein adducts within cells that are at a pO_2 pressure of less than 10mmHg, <1% oxygen and is visualised by as a brown stain following immunohistochemistry. The intensity of immunostaining is directly proportional to oxygen tension. Strong immunostaining is indicative of very low oxygen tensions, cells are exposed to very hypoxic conditions, whereas, the absence of immunostaining indicates cells that are under normoxic conditions (>1% oxygen).

Weak immunostaining, consistent with a low level of hypoxia, was detectable across the uterine horn at the time of progesterone withdrawal (Figure 4-10, A-D) regardless of whether a decidual mass was present (C and D) or not (A and B). For example, positive immunostaining was localised to the stromal cell compartment immediately adjacent to the luminal epithelium in the non-decidualised control horn (A and B). In contrast, when a decidual mass was present, positive immunostaining for hypoxia appeared more intense in the decidualised stromal cells and was also detected in cells adjacent to the basal layer (Figure 4-10, C and D).

In tissue recovered 4 hours after progesterone withdrawal there was very intense immunostaining localised to the decidualised stromal cells within the central tissue mass. In the tissue section illustrated in Figure 4-10 the myometrium and the basal layer remained unstained suggesting that they remained normoxic (Figure 4-10, E and F). Weak immunostaining was also detected in perivascular regions (F, arrowheads).

By 8 hours, in samples where the central decidual mass had fully detached from the underlying endometrium, shed cells in the lumen (Figure 4-11, A and B) appeared to have very low oxygen levels, indicated by intense immunostaining. Positive immunostaining, consistent with hypoxia, was also observed in the stromal cells adjacent to the lumen (Figure 4-11, B). A similar pattern of staining was also observed at 12 hours following progesterone withdrawal (C and D) however the intensity of immunostaining was not as strong as at 8 hours. By 24 hours (Figure 4-11, E and F), weaker staining was evident in the shed cells, however the luminal epithelium and the stromal cell layers immediately adjacent to the lumen was positively stained.

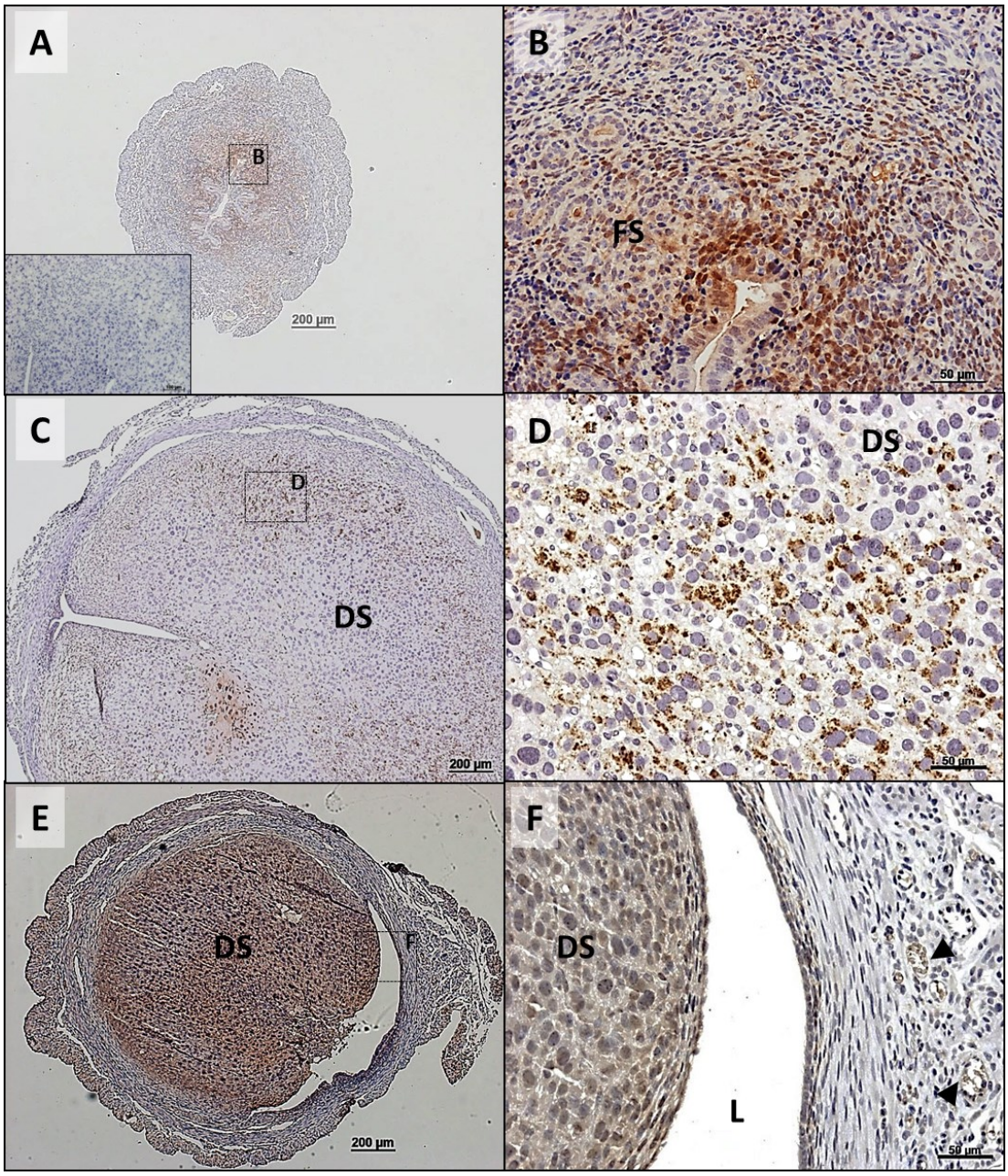

Figure 4-10 A hypoxic gradient exists during endometrial breakdown and repair, 0-4 hours after progesterone withdrawal. Hypoxia was visualised using the Hypoxyprobe® labelling system. A; Weak immunostaining, indicative of low oxygen levels (brown staining) was localised to the stromal cells of the functional layer in the non-decidualised, contra-lateral control horn at the time of progesterone withdrawal, inset negative control. B; Positive immunostaining for hypoxia was localised to the stromal cells adjacent to the luminal epithelium at 0 hours in the non-decidualised horn. C; Weak immunostaining was detected in the decidualised cell mass at the time of progesterone withdrawal. D; Evidence of hypoxia in decidualised stroma cells. E; Strong immunostaining, indicative of very low oxygen levels was detected in the decidualised stromal cells 4 hours after progesterone withdrawal. F; Positive immunostaining for hypoxia was observed in blood vessels close to lumen. DS; decidualised stroma, FS; functional stroma, L; lumen. Scale bars as indicated. Images representative of 3 animals per time-point.

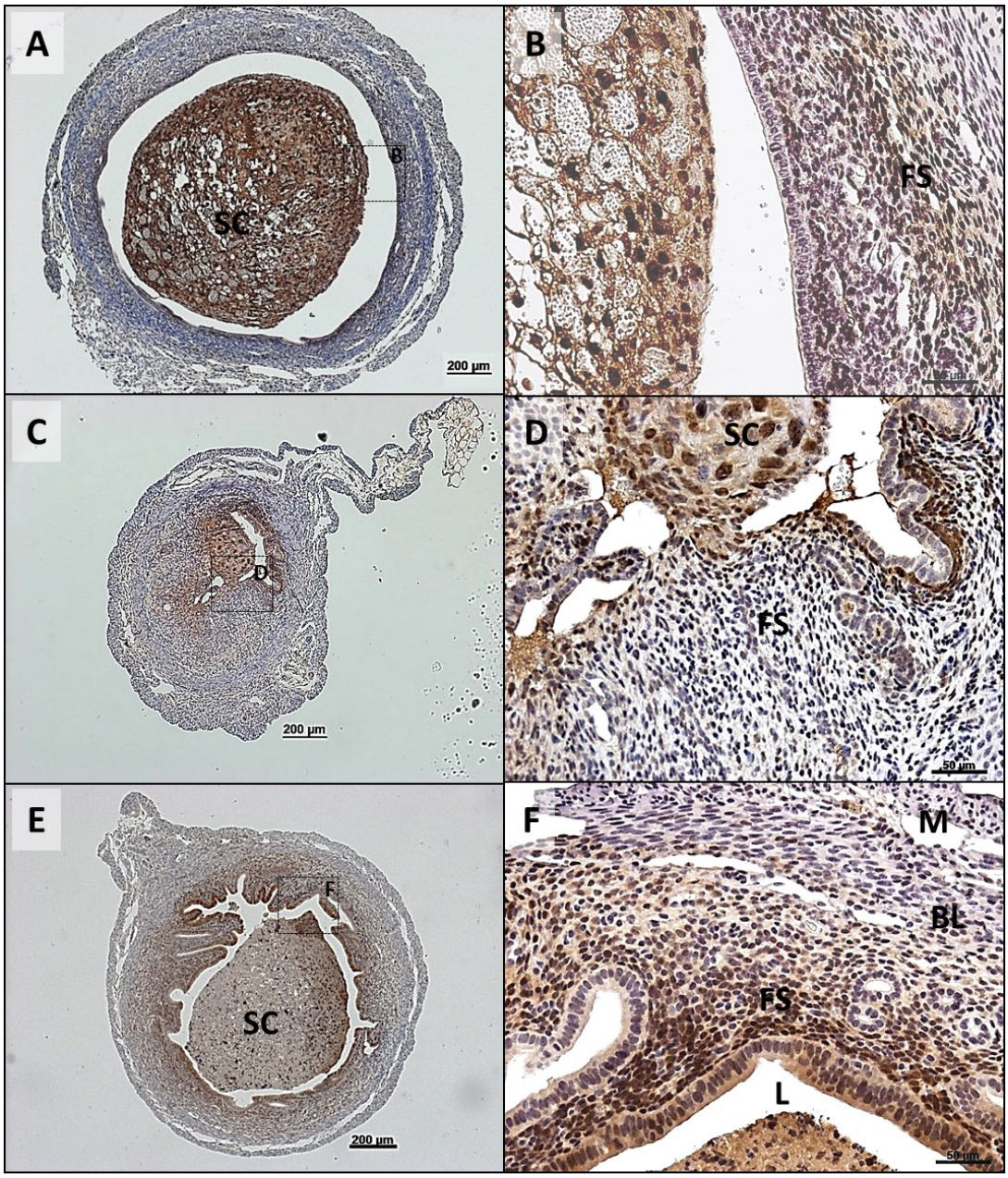

Figure 4-11: A hypoxic gradient exists during endometrial breakdown and repair, 8-24 hours after progesterone withdrawal. Hypoxia was visualised using the Hypoxyprobe® labelling system. A; Strong immunostaining for hypoxia (brown staining), indicative of very low oxygen levels was detected in the shed cells in the uterine lumen 8 hours after progesterone withdrawal. B; Strong immunostaining was detected in the shed cells and in the adjacent luminal epithelium. C; Strong immunostaining is localised to the shed cells and in the luminal epithelium 12 hours after progesterone withdrawal. D; Strong immunostaining observed adjacent to luminal epithelium. E; 24 hours after progesterone withdrawal hypoxia is restricted to the luminal epithelium and stromal cells adjacent to the luminal epithelium. Underlying basal layer cells are under more normoxic conditions, illustrated by the absence of positive immunostaining. F; The luminal epithelium and proximal stromal cells are still under hypoxic conditions. SC; shed cells, FS; functional stroma, BL; basal layer, M; myometrium, L; lumen. Scale bars as indicated. Images representative of 3 animals per time-point.

4.3.3.1 Key genes that are involved in angiogenesis and endothelial cell stability appear to be regulated by hypoxia

To investigate whether induction of hypoxia had an impact on the expression of genes previously reported to be regulated by low oxygen tension *in vitro,* gene expression was quantified using qRTPCR of total tissue extracts (Figure 4-12). Vascular endothelial growth factor (*Vegfa*) mRNA was significantly up-regulated at 8 hours ($p<0.001$) and 12 hours ($p<0.05$). The increase in mRNA concentrations observed at 8 hours is consistent with the strong staining for hypoxia observed at this time-point. In contrast to this, the chemokine *Cxcl12* (also known as stromal cell derived factor 1) was significantly up-regulated at 24 hours ($p<0.001$). *Pecam-1*, also known as the endothelial cell marker CD31, mRNA concentrations were also found to be significantly increased at 4 hours ($p<0.001$) after progesterone withdrawal consistent with an increase in hypoxia. *Pecam-1* mRNA concentrations were significantly down-regulated by 24 hours ($p<0.05$).

Expression of angiopoietins 1 and 2 (which are factors involved in endothelial cell stability and endothelial cell remodelling and breakdown respectively) also showed dynamic changes during the window of breakdown and repair. Angiopoietin 1 (*Angpt1*) showed a trend of an increase at 4 hours after withdrawal; before mRNA concentrations were significantly down-regulated from 4 hours to 12 ($p<0.01$) and 24 hours ($p<0.01$) after withdrawal of steroidal support. Angiopoietin 2 (*Angpt2*) mRNA concentrations were maintained until 8 hours after withdrawal, but were then significantly down-regulated at 12 hours ($p<0.001$) and 24 hours after withdrawal ($p<0.001$).

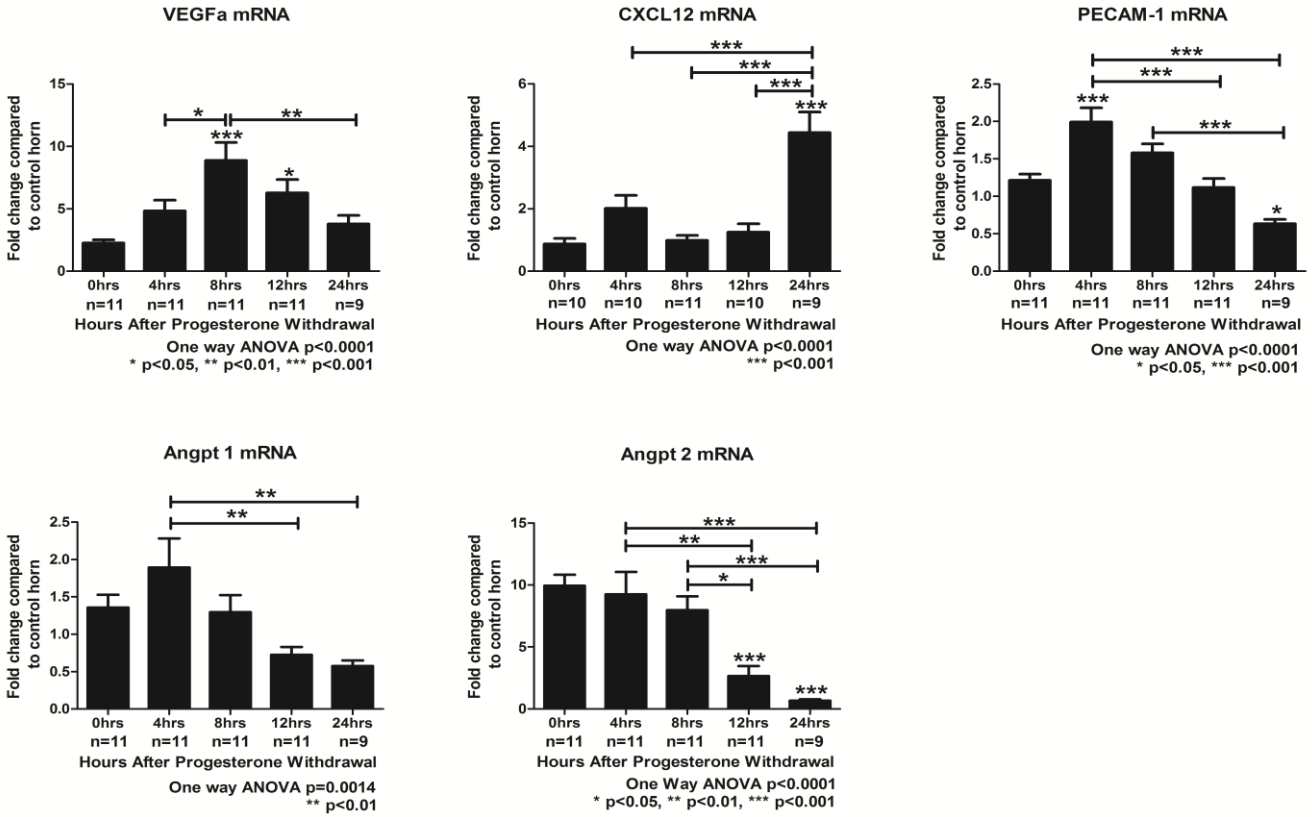

Figure 4-12: mRNA concentrations for candidate genes, *Vegfa, Cxcl12, Pecam-1, Angpt1* and *Angpt2,* that may be regulated by hypoxia during the window of breakdown and repair following withdrawal of progesterone. mRNA expression for the decidualised horn (black bars) normalised against the 0hr non decidualised control horn. Statistical analysis was performed by One Way ANOVA and Bonferroni post hoc testing, comparing each time-point to the 0hr time-point and each other time-point, where * p<0.05 ** p<0.01 and *** p<0.001.

4.3.4 Endothelial cell dynamics during breakdown and repair

Further evaluation of the regulation of angiogenesis during breakdown and repair was investigated by immunofluorescence.

Endothelial cell proliferation was investigated by immunofluorescence for BrdU (as a marker of cells undergoing proliferation) and CD31 (PECAM-1). At the 0 hour time-point, endothelial cells in the basal layer were positive for BrdU (Overleaf, Figure 4-13, A and B). At the 4 hour time-point a number of BrdU positive endothelial cells were identified in the decidualised stroma (Overleaf, Figure 4-13) and in the basal layer (Overleaf, Figure 4-13, D). No $CD31^{+}BrdU^{+}$ cells were observed at 8 hours, a time when blood vessels in the stromal cell compartment were exposed to the lumen (Overleaf, Figure 4-13, E, white arrowheads), or at 12 hours after progesterone withdrawal suggesting a switch from endothelial cell proliferation to endothelial cell stabilisation at this time (Overleaf, Figure 4-13, F). At 24 hours, where re-epithelialisation has been shown to occur (Overleaf, Figure 4-13, G and H), $CD31^{+}BrdU^{+}$ cells were detected in the basal layer; however there appeared to be fewer BrdU positive endothelial cells at this time-point in comparison to the 0 or 4 hour time-points, however quantification is required to confirm this observation.

Overleaf, Figure 4-13: Endothelial cell proliferation and stability during breakdown and repair. Endothelial cells (red) and proliferating BrdU positive cells (green). A and B; At 0hrs, BrdU positive endothelial cells are identified in the basal layer and in the decidualised stroma (arrows). C and D; 4 hours after withdrawal, BrdU positive endothelial cells (white arrows) reside near the lumen and in the decidualised cell mass. E; 8 hours after withdrawal, exposed blood vessels in the stromal cell compartment are adjacent to the lumen (white arrowheads). F; 12 hours after withdrawal, endothelial cells close to the exposed stroma do not appear to be proliferating. G and H; 24 hours after withdrawal, endothelial cells of small vessels are BrdU positive, white arrows. BL; basal layer, DS; decidualised stroma, SC; shed cells. All scale bars as indicated. Images representative of 2 animals per time-point.

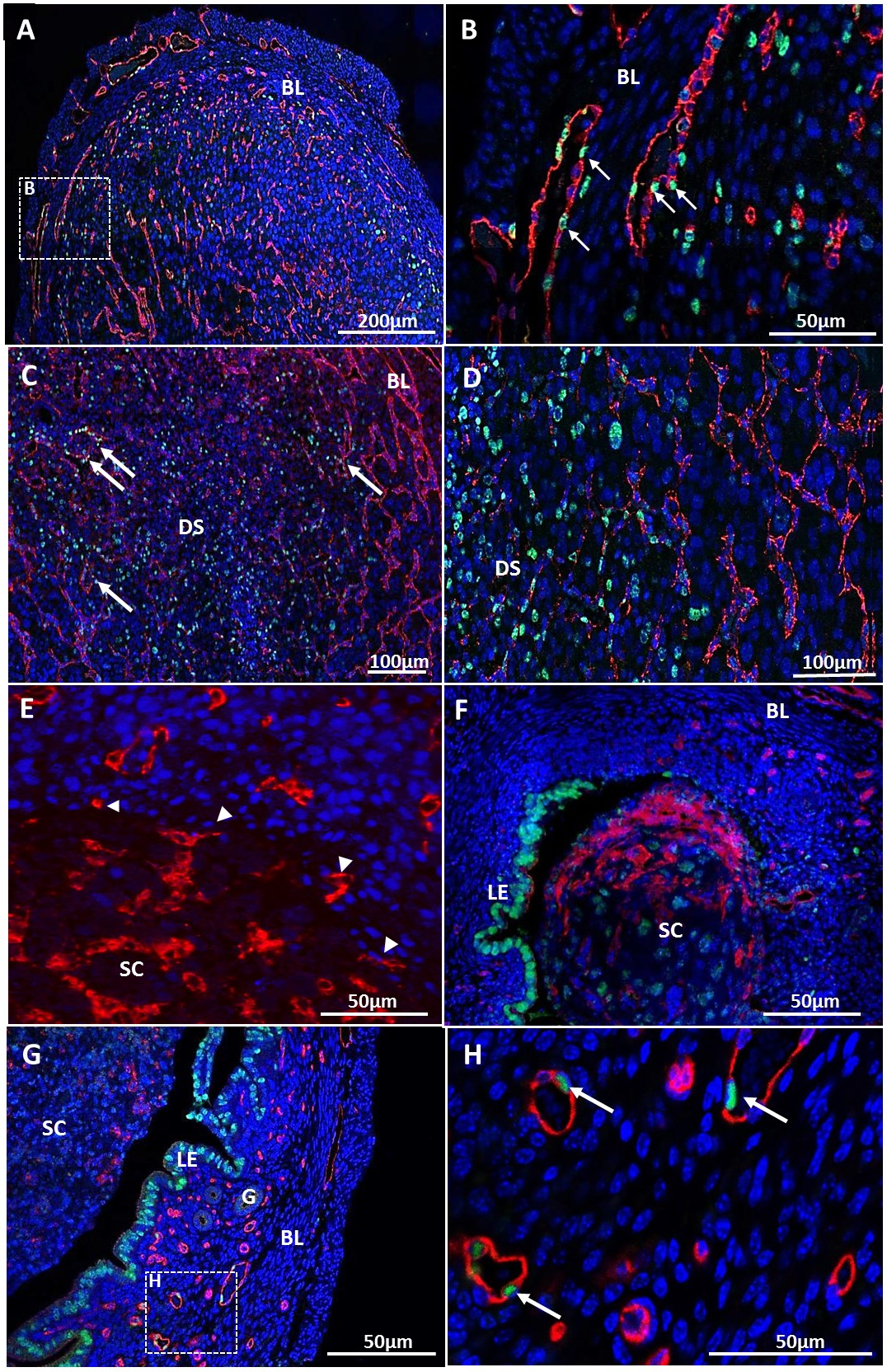
A
BL
B
200µm
B
BL
50µm
C
BL
DS
100µm
D
DS
100µm
E
SC
50µm
F
BL
LE
SC
50µm
G
SC
LE
G
BL
H
50µm
H
50µm

4.3.4.1 Angiogenesis array analysis

Additional evaluation of angiogenesis was investigated using a PCR array that profiles 84 key genes that are involved in angiogenesis, including growth factors, cell adhesion molecules, proteases, cytokines and transcription factors. The full gene list can be found in the Supplementary Table 2.

Samples from the three key time-points (0, 8 and 24 hours) were utilised. The differences in fold regulation of gene expression were analysed using the ΔΔCT method, where the 8 hour and 24 hour time-points were compared to the 0 hour time-point. Additionally the fold regulation between the 8 hour and 24 hours groups was analysed. Those genes in which a significant change in fold regulation was observed are shown in Table 4-4, Table 4-5 and Table 4-6.

In contrast to the MET array, at both the 8 hour and 24 hour time-points a greater proportion of genes were down-regulated than up-regulated when compared to the 0 hour time-point; n=29 v 11 and n=26 v 19 respectively. A number of striking gene changes were detected, including; up-regulation of the chemokines *Cxcl1* (4 fold increase; 0 hours versus 8 hours, 56 fold increase; 0 hours v 24 hours and 11 fold increase; 8 hours v 24 hours), *Cxcl2* (4 fold increase; 0 v 8), *Cxcl5* (10 fold increase; 0 v 24, 11 fold increase; 8 v 24), and *Ccl2* (7 fold increase; 0 v 24, consistent with mRNA concentrations detected by qRTPCR shown in Figure 4-9).

Down-regulation of leukocyte cell derived chemotaxin (*Lect1*) was detected at 8 hours (6 fold decrease) and 24 hours (51 fold decrease) when compared to the 0 hour time-point, with evidence of dynamic regulation occurring between 8 and 24 hours (10 fold decrease). Interestingly, HIF2α (*Epas1*) was down-regulated at 8 hours (~4 fold decrease) and at 24 hours (~9 fold decrease). Consistent with data presented in Figure 4-9, angiopoietin 2 (*Angpt2*) was down-regulated at 8 hours (~5 fold decrease) and 24 hours (~23 fold decrease). Consistent with reports in human tissue at menses, endothelin (*Edn1*) was up-regulated at 24 hours (6 fold increase). A number of changes were detected at 24 hours when compared to the 0 hour time-point including; granulocyte colony stimulating factor (*Csf3*) (~32 fold increase), transforming growth factor a (*Tgfa*) (6 fold decrease), signalling molecule *Sphk1* (11 fold decrease) and tumour necrosis factor (*Tnf*) (24 fold increase).

Gene Name	p value	Fold Regulation
Akt1	0.000137	-2.5842
Angpt2	0.00299	-4.9175
Bai1	0.048497	-2.5934
Cdh5	0.012848	-4.0682
Csf3	0.025896	2.5198
Cxcl1	0.004732	4.1928
Cxcl2	0.006045	4.4648
Efnb2	0.001374	-2.8566
Egf	0.005832	-3.4239
Eng	0.001554	-2.2298
Epas1	0.000331	-3.9733
Ephb4	0.00026	-1.8575
Erbb2	0.000141	-2.1867
Fgfr3	0.00048	-2.539
Flt1	0.009749	-1.804
Ifng	0.031845	-2.258
Igf1	0.000008	-3.1822
Il1b	0.00072	4.8631
Il6	0.041614	1.7567
Itgav	0.015424	-1.6608
Kdr	0.000342	-1.7111
Lect1	0.000234	-6.116
Mapk14	0.00171	-1.3964
Mmp9	0.001015	2.1744
Nos3	0.006183	-1.4661
Pecam1	0.0097	-1.5109
Plau	0.022668	2.7188
Plg	0.000315	3.5833
Ptgs1	0.000024	-1.6422
Ptk2	0.016074	-1.269
Sphk1	0.000006	-4.9733
Tek	0.000448	-1.4716
Tgfa	0.000068	-3.4111
Thbs1	0.010501	2.4701
Tie1	0.006365	-1.4041
Timp2	0.028328	-1.1885
Tnf	0.003052	2.3139
Vegfa	0.003885	2.1533
Vegfb	0.038244	-1.2515
Vegfc	0.004284	-1.8048
Number of genes significantly up-regulated		11
Number of genes significantly down-regulated		29

Table 4-4: Significant changes in gene expression 8 hours after progesterone withdrawal, as displayed by up- or down- fold regulation when compared against the 0 hour group, n=6.

Gene Name	p value	Fold Regulation
Angpt1	0.046288	-1.7594
Angpt2	0.000001	-22.9351
Ccl11	0.02758	2.2697
Ccl2	0.032995	7.0443
Cdh5	0.004155	-3.0425
Csf3	0.01885	31.9636
Ctgf	0.035697	1.9539
Cxcl1	0.004845	56.8512
Cxcl5	0.001852	10.6539
Edn1	0.006193	6.0435
Efna1	0.043344	1.5754
Efnb2	0.003062	-2.6326
Egf	0.018678	-1.9777
Eng	0.026026	-1.8363
Epas1	0.000012	-8.9365
Ephb4	0.041566	-1.7025
F3	0.001286	4.2343
Fgfr3	0.000062	-3.4944
Flt1	0.006391	-2.0237
Hgf	0.006579	2.1842
Igf1	0.000002	-3.1035
Il6	0.01492	1.9559
Jag1	0.00324	1.6671
Kdr	0.00011	-2.471
Lect1	0.000004	-51.9476
Mapk14	0.011274	-1.4252
Mmp14	0.038408	1.4948
Mmp9	0.00972	28.7339
Nos3	0.003536	-2.0241
Pdgfa	0.000588	2.8488
Pecam1	0.000247	-2.0313
Plau	0.007907	3.6989
Plg	0.00004	4.7103
Ptgs1	0.000002	-2.6514
Ptk2	0.013642	-1.5107
S1pr1	0.000788	-1.6036
Sphk1	0	-11.2585
Tek	0.010909	-2.0434
Tgfa	0.000001	-6.0818
Tgfb2	0.000026	-2.7031
Tgfb3	0.025882	-1.9838
Thbs2	0.000037	4.5008

Gene Name	p value	Fold Regulation
Tie1	0.00304	-2.1991
Timp1	0.040893	-1.9155
Tnf	0.003514	24.461
Number of genes significantly up-regulated		19
Number of genes significantly down-regulated		26

Table 4-5: Significant changes in gene expression 24 hours after progesterone withdrawal, as displayed by up- or down- fold regulation when compared against the 0 hour group, n=6.

Gene Name	p value	Fold Regulation
Cxcl1	0.011036	11.4046
Cxcl5	0.018181	11.2299
Epas1	0.035205	-2.6741
F3	0.000182	3.3533
Lect1	0.022018	-10.0984
Mmp9	0.019236	11.1146
Pdgfa	0.012495	1.9942
Pecam1	0.012721	-1.5984
Ptgs1	0.006979	-1.9196
S1pr1	0.011802	-1.6882
Sphk1	0.031526	-2.6915
Tgfb2	0.002581	-2.6708
Tgfb3	0.020302	-2.1296
Thbs2	0.007458	4.175
Tie1	0.049309	-1.8621
Timp1	0.009032	-2.6922
Tnf	0.009709	8.8916
Vegfa	0.024635	-2.9003
Number of genes significantly up-regulated		7
Number of genes significantly down-regulated		11

Table 4-6: Significant changes in gene expression 24 hours after progesterone withdrawal, as displayed by up- or down- fold regulation when compared against the 8 hour group, n=6.

4.3.4.2 Network analysis of the angiogenesis pathway

As in the MET array, a basic gene network was generated using MetaCore™ in order to identify targets for future investigation, the network is depicted in Figure 4-14 and the symbol key can be found in Supplementary Figure 1. From the network analysis, the first observation is that, like the MET array, multiple cell compartments are involved in the angiogenesis pathway. From the network, it is evident that HIF1α is a main regulator of this pathway; HIF1α is up-stream of 22 genes (Figure 4-15) and has been shown to regulate activation of key genes including VEGFa, angiopoietin 2, MMP-2, endothelin and TNFα.

Another gene that may be a key regulator of endometrial vessel repair/stabilisation is MMP-9. Network analysis shows that MMP-9 has known stimulatory actions on VEGF and endothelin, whilst inhibiting collagen IV, VEGFR-1 and fibronectin. From the network analysis TGFβ, fibronectin, MMP-9, MMP-2 were identified as candidates for future investigation.

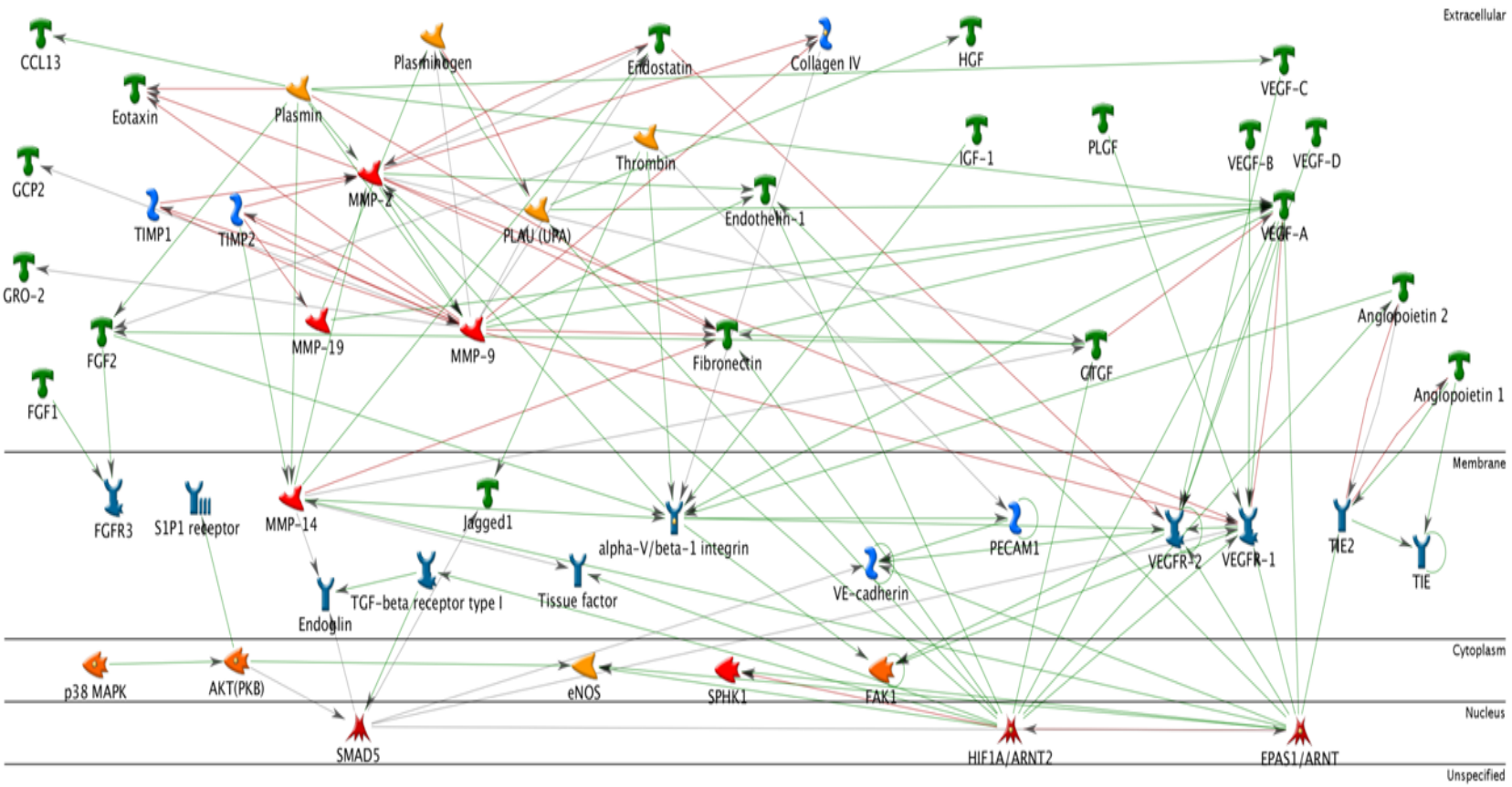

Figure 4-14: Interactions of key genes involved in angiogenesis. Arrows indicate direct effects on other genes in the pathway. Green arrows indicate activation, whereas red arrows show inhibitory action. Pathway generated using MetaCore™ software. Gene symbols are outlined in Supplementary Figure 1.

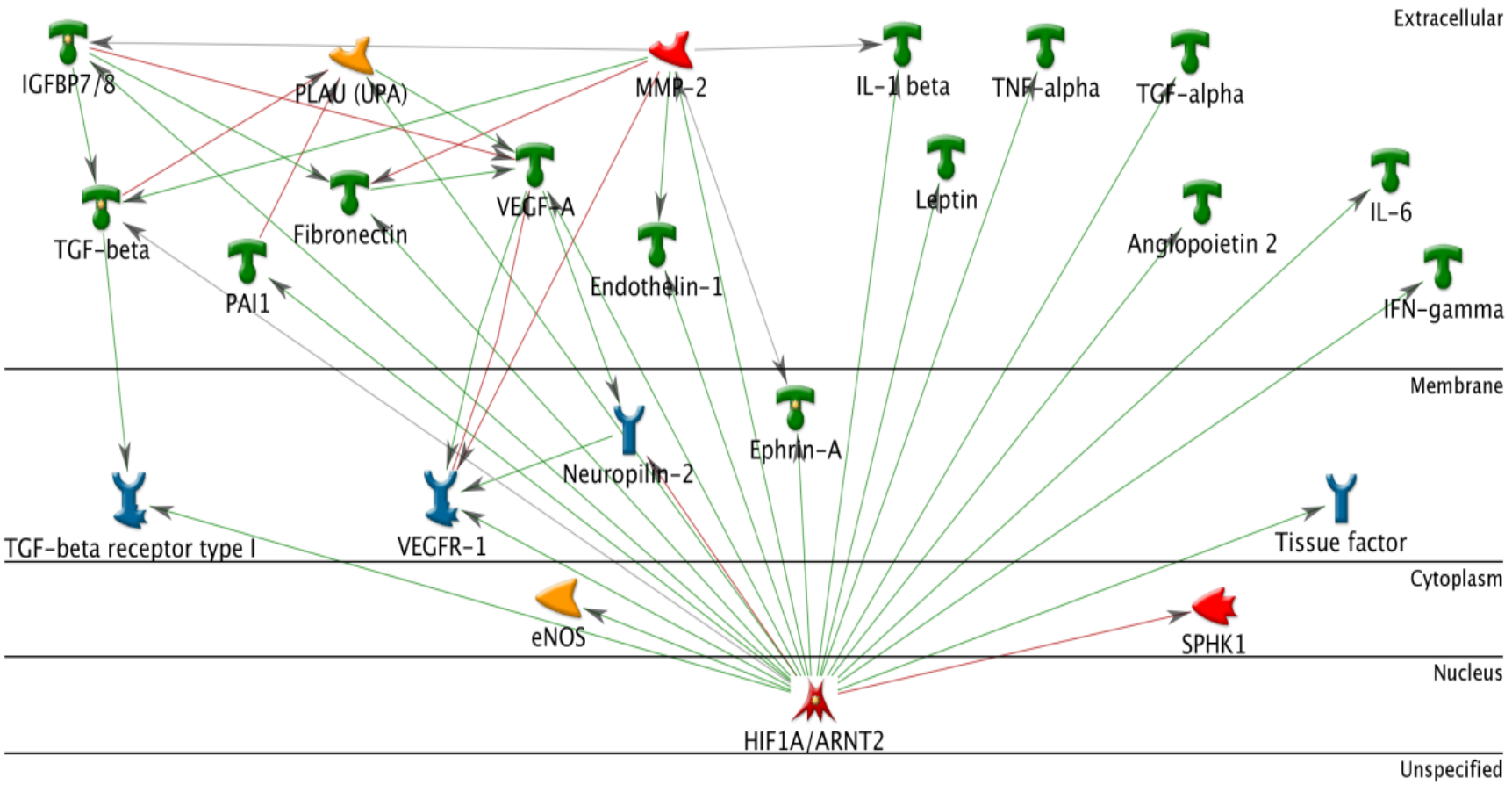

Figure 4-15: Downstream targets of HIF1α, a known regulator of angiogenesis. Green arrows indicate activation, whereas red arrows show inhibitory action. Pathway generated using MetaCore™ software. Gene symbols are outlined in Supplementary Figure 1.

4.4 Discussion

4.4.1 Contribution of the stromal cell compartment to endometrial repair

It is likely that a number of mechanisms contribute to the repair of the endometrium, including; epithelial cell proliferation, stromal cell transformation, stem cell differentiation, vessel remodelling and remodelling by immune cells. The data reported in this chapter provides evidence of a role for the stromal cell compartment in endometrial repair.

4.4.1.1 MET as a mechanism of re-epithelialisation

It has been proposed that a primary mechanism responsible for endometrial repair is the proliferation of the glandular epithelium of the residual basal glands; however recent studies by scanning electron microscopy have questioned this hypothesis. The re-appraisal of tissue repair by Garry *et al.,* (148, 169), has suggested that new epithelial cells might also arise from transformation of cells in the stromal cell compartment.

Mesenchymal to epithelial transition in the endometrium has not been widely studied. However, two mouse models have proposed a role for MET during post-partum remodelling and after artificial decidualisation. Both studies suggest that during homeostasis of the mouse endometrium, stromal and epithelial compartments are maintained by cells within their own compartment. However, post-partum, where extensive remodelling of the endometrium takes place, stromal fibroblasts differentiate and incorporate into the new epithelium (375, 376).

In our mouse model of endometrial breakdown and repair, we have identified a subset of cells in the basal layer of the repairing endometrium that express both epithelial and mesenchymal markers (cytokeratin and vimentin respectively) (Figure 4-2). These dual labelled cells were localised to the stromal cell compartment of the residing basal layer of the endometrium, just 12 hours after the withdrawal of progesterone (Figure 4-2, C-E). By 24 hours, dual labelled cells were identified in the stromal cell compartment adjacent to the luminal surface (Figure 4-2, F and G). These cells were localised to regions where the stroma is exposed to the lumen (following shedding) and were not close to areas of proliferating luminal epithelial cells. These findings implicate a role for early repair mechanisms that are initiated prior to the shedding and dissociation of the functional layer, as well as a role for a stromal cell contribution to the new epithelium in areas of denuded endometrium.

In their pseudopregnancy model of breakdown, Patterson *et al.,* describe dual labelled pan-cytokeratin and vimentin positive cells close to the myometrial-stromal border 24 hours after steroid withdrawal, and also adjacent to the lumen 36 hours post ovariectomy (376). Their

findings are consistent with our own; however we believe the current study provides a better insight into the mechanisms of breakdown and repair as it more clearly mimics the repair processes in women, including overt menstruation and rapid repair processes.

In the current study, the dynamic changes in mRNA concentrations and protein expression for Wilms' tumour 1, Snail and Slug reported during the window of breakdown and repair (Figure 4-3) are consistent with a novel role for MET during repair of the epithelium after endometrial shedding. A role for MET in endometrial epithelial repair may indeed be a new concept, but its role in repair mechanisms in other tissues has been widely investigated, in the kidney, liver and lung ((415, 436, 437) and Daris, unpublished). This study is the first to investigate the potential molecular mechanisms of MET in the endometrium using a mouse model of endometrial repair.

Complementary to these findings, using a focussed PCR array, we discovered striking changes in the expression of a number of genes known to regulate MET by comparing tissue recovered at 8 hours during breakdown and at 24 hours at a time when repair was complete or nearly so. Despite small fold increases in Snail and vimentin at the 8 hour and 24 hour time-points, which may suggest that EMT is occurring, epithelial cell markers, cell adhesion markers and intracellular junction proteins were all greatly up-regulated at 24 hours consistent with maturation of epithelial cells. It is important to note that the array was carried out on whole tissue extracts and therefore increases in epithelial markers may be attributable to an increase in epithelial cell number as well as stromal cell differentiation. These preliminary studies have demonstrated that dynamic changes in cellular morphology occur during endometrial repair phases, and that molecular mechanisms may be driving repair of the epithelium through stromal cell differentiation. Lineage tracing studies using this mouse model would complement the data reported.

4.4.1.2 Contribution of immune cells to endometrial repair and remodelling

Menstruation is accepted to be an inflammatory event, with a diverse population of immune cells present in the endometrium during breakdown (207, 208, 214, 217, 438, 439). Macrophages are proposed to play multiple roles in the regulation of endometrial function including; breakdown, repair and remodelling (reviewed by (94)).

The use of monocyte lineage labelled mice (the Mac green mouse) enabled investigation of macrophage number and localisation in the endometrium during the breakdown and repair window. In contrast to a previous study, where neutrophils were determined to be the predominant immune cell present during repair (217), large numbers of EGFP-positive cells

(putative tissue macrophages) were detected in the endometrium at the 24 hour time-point, a time where the endometrium is undergoing or has undergone repair. EGFP positive cells were mainly localised to the basal layer adjacent to areas of degenerating endometrium during breakdown. However, during repair, large numbers were observed adjacent to the luminal epithelium. This would suggest that macrophages may be playing two roles; tissue breakdown during the early time-points and tissue remodelling during later time-points. This is consistent with repair mechanisms in other tissues, for example in the lung, where alveolar macrophages contribute to epithelial repair in the later stages of an inflammatory response (440), driving anti-inflammatory mechanisms.

The techniques used for the generation of the Mac green mouse involved targeted insertion of the EGFP gene downstream of the *c-fms* gene promoter. The *c-fms* gene encodes the receptor for macrophage colony stimulating factor (m-CSF-1) and is selectively expressed in all macrophages. *c-fms* mRNA and protein is normally absent from mature granulocytes (i.e. neutrophils) however the targeting strategy means that expression of the EGFP reporter gene *may be* retained in progeny from the common bone marrow progenitor. Therefore, a very small number of the EGFP-positive cells detected in the mouse endometrium may not be macrophages, and could be granulocytes or lymphocytes. Further investigation with dual staining techniques is required to definitively confirm that tissue resident EGFP positive cells are macrophages. In this study, uterine tissues were fixed in neutral buffered formalin, which was not conducive to staining with F4/80, a marker used by previous groups (217, 334, 341, 441). Dual staining of EGFP and a neutrophil marker such as Ly-6B.2 would determine whether some EGFP positive cells are neutrophils available to participate in both breakdown and repair.

Using mouse models of breakdown and repair (217, 334) it has been reported that endometrial repair is merely delayed, not inhibited, by neutrophil neutralisation indicating that another immune cell must be able to contribute to, and complete, repair. Based on our new data we believe that immune cell is the macrophage.

4.4.1.3 Secretion of factors from the stromal cell compartment contributing to endometrial repair

CCL2 and connective tissue growth factor (CTGF) have been implicated in the process of endometrial repair (208, 423, 438) in women. CCL2, also known as monocyte chemotactic protein (MCP-1), is a chemoattractant for macrophages, NK cells, basophils and

lymphocytes (442–446). The protein expression of CCL2 has been shown to vary across the human menstrual cycle, with peak expression observed during menses (205, 208, 447).

In the current study, using our mouse model, we detected low concentrations for mRNAs for *Ccl2* during breakdown however these were markedly increased during the repair phases (Figure 4-9, 12-24 hours) consistent with an apparent increase in numbers of macrophages in the endometrium at 24 hours (Figure 4-8). CCL2 is not a chemoattractant for neutrophils (448), therefore would have no direct action of neutrophil infiltration at this time. CCL2 has been reported to be secreted from human endometrial stromal fibroblasts (449–451) and macrophages (452) *in vitro*, hence the increase in macrophages observed during the repair phase may contribute to increase in total mRNA. We speculate that, during breakdown, fibroblasts and macrophages in the basal layer may secrete CCL2 in order to recruit macrophages from the blood stream in preparation for repair. During repair, resident macrophages may secrete increased levels of CCL2 to drive *in situ* proliferation.

Connective tissue growth factor is an important growth factor involved in wound healing in the skin (453) and also displays cycle and cell-specific immunostaining in the endometrium (423, 454), where stromal cell expression of CTGF was greater during the secretory phase than in the proliferative phase (454), with the greatest expression reported during the menstrual phase (423). CTGF is reported to be expressed by macrophages and its expression is regulated by hypoxia (423). In an *in vitro* human epithelial cell culture model, exposure to hypoxia significantly up-regulated CTGF mRNA and protein in a time-dependent manner (423). This finding is consistent with those in our model, where *Ctgf* mRNA concentrations were detected to increase in the uterus at the 8 hour time-point, coincident with exposure to strong hypoxic conditions (as demonstrated by strong immunostaining for the Hypoxyprobe®) at 4-8 hours after steroid withdrawal (Figure 4-10). CTGF has been reported to promote stromal fibroblast proliferation in an *in vitro* model using rat kidney fibroblasts (455), as well as promoting differentiation of human mesenchymal stem cell into fibroblasts *in vitro* (456), and therefore may play a role in remodelling of the stromal cell compartment during repair.

From the data reported herein it is unclear as to the cellular localisation of CCL2 and CTGF, for example whether macrophages or stromal cells are involved in the transcription of these genes. Further investigation, by immunohistochemistry, would identify the cell types that express both of these factors.

Macrophages have been shown to secrete a number of factors that may contribute to the repair of the endometrium. For example, it has been reported that alveolar macrophages secrete TNFα, a potent epithelial mitogen (440). Increased concentrations of mRNA encoding *Tnfa* were detected in the angiogenesis array at the 24 hour time-point, a time where endometrial repair and epithelial cell proliferation can be detected, coincident with peak numbers of macrophages. Murine endometrial macrophages have been reported to secrete osteopontin (*Spp1*), a cell adhesion molecule that contributes to endometrial remodelling during the early phases of pregnancy (457). Consistent with this finding, a 23 fold increase in *Spp1* was detected in the MET array at the 24 hour time-point, whilst the endometrium was undergoing repair.

It is possible that macrophages play a dual role in human endometrial breakdown and repair. For example, despite a low number of macrophages detected in the tissue during breakdown, human macrophages have been reported to secrete VEGF (452) which may contribute to endothelial cell stability during breakdown; in our mouse model, *Vegfa* mRNA concentrations are up-regulated during the breakdown phase. During repair however, those macrophages localised to the basal stroma and those adjacent to the luminal epithelium may be secreting factors that aid re-epithelialisation such as TNFα or osteopontin.

4.4.1.4 Contribution of endometrial "stem" progenitor cells

Activation and proliferation of endometrial stem cells has been proposed as another potential mechanism of endometrial repair following shedding. A number of different sites have been postulated as sources for endometrial stem cells including; a basal gland epithelial stem cell niche, perivascular stem cells and bone marrow progenitors.

Bone marrow derived cells have been identified in the stromal cell and epithelial cell compartments of the human endometrium (268) suggesting a potential role for these cells in endometrial regeneration. *In vitro* studies using haematopoietic progenitor cells (HPC) highlight a role for CXCL12 in chemotaxis and mobilisation of HPCs from the bone marrow to peripheral tissues (458, 459). HPCs can differentiate into multiple cell types *in vitro* including hepatocytes and neurons (263, 264), suggesting that the increase in *Cxcl12* transcription detected during repair of the mouse endometrium (Figure 4-12) may therefore be driving mobilisation of HPCs to the endometrium, to contribute to endometrial stromal or epithelial cells. Furthermore VEGF has been reported as a chemoattractant for endothelial progenitor cells from the bone marrow (460) whilst also promoting their differentiation. *Vegfa* mRNA concentrations were increased 4-24 hours after the withdrawal of progesterone

(Figure 4-12) so endothelial cell progenitor migration may be another mechanism in repair of the tissue, which merits further investigation.

Putative perivascular mesenchymal stem cells have been identified in the human endometrium using two markers; CD146 and PDGFRβ (261). Isolated CD146+ PDGFRβ+ cells were multipotent and able to differentiate into four mesenchymal lineages, and are postulated to be pericytes which are able to give rise to both stromal and endothelial cell compartments of the endometrium (261). An increase in transcription of *Pdgfrb* was detected in our mouse model of breakdown at 8 hours and 24 hours. In the human endometrium PDGFRβ is localised to the stromal fibroblasts and perivascular regions, whilst being absent from the epithelium (461). A pilot study, using PDGFRβ-GFP labelled lineage tracing mice, has identified PDGFRβ positive cells in the luminal epithelium of the mouse endometrium during the normal oestrous cycle (Simitsidellis, unpublished), suggesting that mesenchymal stem cells may contribute to overall tissue homeostasis.

4.4.2 Degenerating functional layer contributes to repair of the underlying basal layer

Another contributor to re-epithelialisation and remodelling of the basal layer may, in fact, be the degenerating functional layer shed during menses. Laser capture studies on human tissues, taken during menses, have revealed that the shed functional stroma expresses gene products associated with extracellular matrix synthesis, prostaglandin synthesis and high levels of IL-8, which may be involved in the recruitment of leukocytes to the endometrium during repair phases (462).

A pilot study, using conditioned media from primary human decidualised stromal cells undergoing progesterone withdrawal (1,2 and 4 days after withdrawal), had no significant effect on human endometrial endothelial cell proliferation when compared to control media in a network formation assay (Cousins, unpublished). However, as little endothelial cell proliferation was observed during the repair phase in the mouse model, it is possible that secreted factors from the degenerating functional stroma do not promote proliferation of endothelial cells, but may promote stability. Furthermore, it would be of interest to investigate the effect, if any, of progesterone withdrawal conditioned media in a wound healing assay of primary epithelial cells to determine if secreted factors from the degenerating functional stroma contribute to epithelial cell repair.

4.4.3 A role for hypoxia in the regulation of endometrial repair

4.4.3.1 Hypoxia and angiogenesis

It has been recognised that hypoxia is involved in tumour development, ischaemic injury and during endometrial breakdown (186, 189, 190, 192, 193, 393, 439, 463–470). Hypoxia-inducible factor (HIF) is a dimeric protein complex which has been shown to be a key regulator of a cell's response to low oxygen tensions. Under hypoxic conditions, the beta and alpha subunits dimerise to bind to hypoxia response elements which activate transcription of target genes (463). Candidate genes investigated in the angiogenesis PCR array were analysed for HIF-dependent regulation; those genes that are known to be regulated by HIF1α are shown in Figure 4-15.

An apparent gradient consistent with transient hypoxia was observed during the window of breakdown and repair in the mouse model. To complement this novel finding, candidate genes, including *Vegfa*, *Cxcl12* and the angiopoietins were regulated in parallel to staining for hypoxia during this window (Figure 4-10, Figure 4-11 and Figure 4-12). Of these candidate genes, endometrial expression of VEGF has been shown to be directly regulated by hypoxia (191, 193, 471) by a HIF1α dependent mechanism (193, 472). *Vegfa* mRNA concentrations were up-regulated at 4 and 8 hours, consistent with strong staining for hypoxia in the endometrial stroma and epithelium (Figure 4-10 and Figure 4-12). VEGF is a key regulator of angiogenesis (473); endothelial cell proliferation was observed at the 4 and 8 hour time-points consistent with an increase in *Vegfa* expression (Overleaf, Figure 4-13, B and C).

Angiopoietin 2 has been shown to play a dual role in endometrial repair; Angiopoietin 2 drives tissue remodelling in the presence of high VEGF concentrations (474), whilst it contributes to vessel destabilisation in low VEGF concentrations (475). These data are consistent with our findings, where *Angpt2* mRNA concentrations were maintained during initial breakdown of the endometrium (0-8 hours) (Figure 4-12) in the presence of increased *Vegfa* mRNA concentrations (Figure 4-12). Endothelial cell proliferation was also detected (Overleaf, Figure 4-13, B and C) at these time-points suggesting that Angpt 2 may be contributing to endothelial cell remodelling at this time.

In women, *ANGPT1* and *ANGPT2* mRNA concentrations are observed to be at their highest during the secretory phase of the human cycle (475), consistent with our findings in mice where *Angpt1* and *Angpt*2 were at their highest mRNA concentrations levels in the decidualised tissue prior to removal of progesterone and breakdown (0 hours). Endometrial

expression of ANGPT 2 has been shown to be regulated by hypoxia, (476, 477) by both HIF-dependent (478) and HIF-independent mechanisms (479).

CXCL12, (also known as stromal-derived factor) is a chemokine that has been shown to regulate several functions, including angiogenesis (191, 469, 470), haematopoietic stem cell mobilisation (460) and monocyte chemotaxis (480, 481). CXCL12 was initially investigated in this study for its role in angiogenesis. mRNA concentrations of *Cxcl12* were detected as being down-regulated during breakdown of the mouse endometrium (0-8 hours), but concentrations increased at 12 and 24 hours, consistent with a decrease in staining for hypoxia. Regulation of CXCL12 by hypoxia has been demonstrated *in vitro*, where endometrial primary stromal cell expression of CXCL12 was down-regulated when exposed to hypoxia (191). In contrast to this, hypoxia up-regulates the receptor for CXCL12, CXCR4, in endothelial cells, monocyte derived macrophages and in cancer cells (469, 482).

Recently, the proliferative capacity of CXCL12 has been investigated *in vitro*, with CXCL12 promoting endometrial epithelial and stromal cell proliferation in an oestrogen dependent manner (483). In our model, *Cxcl12* was observed to increase, in the absence of both oestrogen and progesterone, 12 hours after the withdrawal of steroidal support. It is possible that in our model, VEGF drives initial angiogenesis and vessel stabilisation under hypoxic conditions, at a time where we detected endothelial cell proliferation. However as breakdown ensues, and oxygen tensions return to more normoxic levels, VEGF concentrations decrease coincident with an increase in CXCL12, which may support vessel stabilisation over vessel proliferation; which can be observed during foetal development (484–486). Macrophages have been reported to secrete CXCL12 *in vitro* (452), which may account for the increase in the concentrations of *Cxcl12* mRNA during repair phases as this was at a time when an increased number of macrophages were detected.

In the current study, very little endothelial cell proliferation was detected during the repair phase; this is consistent with findings from Kaitu'u-Lino *et al.,* who, in their mouse model, detected a greater number of proliferating endothelial cells during decidualisation of the mouse endometrium in comparison to the repair phase (368). However, it is likely that during the repair phase, VEGF-dependent angiogenesis by endothelial cell proliferation is not the most critical event with endothelial cell sprouting or branching likely to be key to vessel stabilisation in preparation for the proliferative phase of the next cycle.

4.4.3.2 Hypoxia and monocyte recruitment

A role for hypoxia in monocyte recruitment has been identified in pathological conditions including tumours, wound healing and ischaemic inflammatory sites (441, 487–489). High numbers of macrophages are associated with endometrial cancers (490, 491), where hypoxia inhibits expression of CCR2, the receptor for CCL2, to limit macrophage migration (492) so that they remain as tumour-associated macrophages. Hypoxia has been reported to increase concentrations of *CCL2* in a HIF-dependent manner in *in vitro* models of cancer (493, 494), airway inflammation (495) and ischaemic brain injury (489). HIF-dependent down-regulation of CCL2 has been reported in a model of murine renal fibrosis (496). In mice with specific myeloid cell HIF activation, inflammation was suppressed due to inhibition of receptors for chemokine receptors including CCR2 (496). These findings indicate that HIF regulation of inflammatory responses is context dependent. A role for hypoxia in macrophage migration during menses has not been reported and merits further investigation.

In our mouse model of breakdown and repair, mRNA concentrations for *Ccl2* maintained at a low level during endometrial breakdown, a time where the immunostaining for hypoxia was most intense. However an increase in mRNA concentrations for *Ccl2* was detected at 12 and 24 hours during the repair phase of the tissue, when immunostaining for hypoxia was at its weakest. This might suggest that in normal function, hypoxia may limit macrophage activation and migration from the bone marrow during endometrial breakdown, in favour of another immune cell, but when the tissue returns to more normoxic conditions, during repair, macrophages are able to infiltrate to aid scavenging and tissue remodelling.

4.4.4 Summary

In the current study, using our refined mouse model of endometrial breakdown and repair, a role for stromal cell differentiation, macrophage infiltration and hypoxia during endometrial repair was investigated.

The identification of dual labelled cytokeratin and vimentin positive cells in the stromal cell compartment adjacent to the lumen supports our hypothesis that MET contributes to re-epithelialisation during the repair window. Analysis of genes known to be involved in EMT and MET were investigated by a PCR array; dynamic changes were observed at both the 8 hour (breakdown) and 24 hour (repair) time-points. Up-regulation of epithelial cell markers and adhesion molecules during the repair phase suggest a net effect of MET over EMT. Lineage tracing studies would complement these data.

A hypoxic gradient was observed across the uterine horn during the window of breakdown and repair, which coincided with dynamic changes in mRNA concentrations of genes involved in angiogenesis, vessel stabilisation and remodelling and monocyte chemotaxis. Investigation of the uterine macrophage population revealed an influx of macrophages during the repair phase, which is likely to contribute to remodelling of the tissue after breakdown and shedding.

From the results presented in this chapter, it is clear that a number of factors will contribute to the restoration of tissue integrity. These studies support the hypothesis that hypoxia plays a key role in the initiation of repair processes, either by driving angiogenic factors or regulating the influx of macrophages which cumulatively contribute to re-establishment of an intact endometrium following menses.

Chapter 5 A role for androgens in endometrial function

5.1 Introduction

The regulation of endometrial function by ovarian derived oestrogens and progestagens has been extensively studied, whilst the full impact of androgens on endometrial function is yet to be elucidated.

5.1.1 Circulating androgens and receptor expression

The main sources of androgens in women are the ovary and the adrenal, which together account for approximately 50% of total androgen synthesis. Peripheral sites like the skin or adipose tissue account for the other 50% of androgen synthesis (136, 137) .

A study by Abraham, in 1974, determined relative circulating concentrations of androgens in women during their menstrual cycle. Two pro-androgens, (classed as those which have no androgenic effect unless they are metabolised to testosterone), androstenedione and dehydroepiandrosterone (DHEA) were found to peak during the late proliferative/early secretory phase, in parallel with peak oestradiol concentrations (44). A third pro-androgen, DHEA sulphate (DHEAS) was observed to be maintained across the menstrual cycle. The potent androgen testosterone exhibited fluctuations through-out the menstrual cycle with its lowest concentrations observed during the early proliferative phase, a mid-cycle peak, before decreasing during the secretory phase, to concentrations that were still higher than during the proliferative phase. The amount of non-aromatisable androgen dihydrotestosterone (DHT) was low in peripheral circulation, which is in line with reports that the majority of DHT is synthesised locally in target tissues by the conversion of testosterone to DHT by 5α reductase (497, 498). Two isozymes of 5α reductase are present in the human endometrium (499) suggesting that DHT may play a role in endometrial function.

The second part of Abraham's study involved suppression of ovarian-derived androgen production using dexamethasone, to determine adrenal contributions of testosterone, DHEA, DHEAS and androstenedione. This confirmed that androgens from the adrenals do not fluctuate during the menstrual cycle and that ovarian-derived androgens are likely to be under endocrine regulatory feedback loops (44). A later study in 1986, demonstrated that elevated concentrations of testosterone (delivered intravenously to cycling women) altered LH pulsatility, in this study aromatisation of androgens to oestrogens was inhibited by testolactone (an aromatase inhibitor) (500).

Androgens exert their primary effects on gene expression via the androgen receptor (AR) (101, 104, 110, 501) (as discussed in section 1.5.4). Immunolocalisation studies have identified AR in the nuclei of stromal fibroblasts in both the functional and basal layers of the human endometrium, with most intense immunoexpression during the proliferative phase. Expression in the stroma of the functional layer gradually decreases during the secretory phase (98, 143). AR has also been immunolocalised to the glandular epithelial cell compartment of the basal layer during the proliferative phase (502), with a decrease in expression detected during the secretory phase until no immunostaining for AR is observed by the late secretory phase (143). In the functional layer, AR is immunolocalised to the glandular epithelium in the mid-late secretory phase (144). AR expression has been shown to be up-regulated in women who are treated with anti-progestins (503).

5.1.2 A role for androgens during endometrial function

A possible role for androgens in endometrial function has been demonstrated *in vivo* in a murine model of decidualisation. In this model 1mg of testosterone or DHT (in combination with oestradiol) on days 6-8 of the protocol was able to maintain the decidual mass, in the absence of progesterone, following artificial decidualisation by oil injection on day 5 (146). However, androgens alone could not initiate the decidual response (146), which requires exposure to progesterone, thereby highlighting the importance of progesterone during this process. These results suggest that androgens may play a supporting role during decidualisation. Two *in vitro* models using human endometrial stromal cells have demonstrated that both DHT and testosterone are able to stimulate biosynthesis of prolactin (a decidualisation marker) in the absence of progesterone (504, 505). Prolactin production was enhanced when testosterone and progesterone were administered in combination, supporting the suggestion that androgens may contribute to endometrial decidualisation in women and may therefore be involved in preparing the endometrium for pregnancy.

An anti-proliferative effect of androgens has been documented in a number of studies, including those in female to male transsexuals, where long term use of androgens results in endometrial atrophy (506–508). Furthermore, in a study in post-menopausal women, treatment with testosterone alone had no effect on endometrial thickness or proliferation (509). In comparison, treatment with oestrogen or oestrogen and testosterone resulted a significant increase in the number of proliferating cells and in endometrial thickness (509). An *in vivo* study in the macaque has highlighted the possible anti-oestrogenic potential of androgens (503) which might complement the role of progestins in limiting excessive endometrial proliferation.

In contrast to oestradiol and progesterone, whose serum concentrations fluctuate across the menstrual cycle, circulating concentrations of testosterone are maintained (Table 1-1). Despite circulating concentrations of testosterone being much greater than those of oestradiol at both the late secretory and early proliferative phases, a role for androgens in tissue breakdown at menses or in tissue remodelling during repair phases has not been investigated.

An *in vitro* study using human endometrial stromal cells treated with DHT revealed a subset of genes that were androgen-regulated. These genes were related to two pathways; the regulation of apoptosis and stromal cell migration (144), which could implicate androgens in the regulation of endometrial repair. In recent studies, Kajihara and colleagues have suggested that androgens may promote resistance to oxidative stress (504) and increase formation of gap junctions (510) both of which are important for cellular transformation of decidualised stromal cells.

5.1.3 Androgens, the androgen receptor and endometrial disorders

Increased circulating androgens have been linked to a decline in endometrial function and fertility. For example, increased serum androgen concentrations have been detected in women with recurrent miscarriage (511), where both circulating concentrations of testosterone and androstenedione were significantly greater compared to control women. Observed increases in testosterone concentrations across the menstrual cycle in women with recurrent miscarriage were correlated with a decrease in placental protein 14 (a marker of decidualised endometrium) (511), suggesting that increased androgens have a detrimental effect on the receptivity of the endometrium.

Polycystic ovarian syndrome (PCOS) is associated with hyperandrogenism (305), caused by overproduction of androstenedione from ovarian thecal cells. This overproduction results in an increased number of growing follicles which then become atretic (309, 310). Women with PCOS tend to display sub-fertility and amenorrhoea. A study measuring expression of AR in women with PCOS has revealed that endometrial AR expression is significantly greater in glandular and luminal epithelial cells, at both proliferative and secretory phases when compared to control women (no PCOS) (512). Furthermore, mRNA concentrations for AR are significantly up-regulated in PCOS women compared to control women (512). Additionally, endometrium from PCOS women had delayed or no protein expression of integrin αvβ3, a marker of endometrial receptivity (512). Women with PCOS exhibit unopposed oestrogens due to chronic anovulation, which may also lead to endometrial hyperplasia (513, 514). Women with PCOS are thought to be at a higher risk for endometrial cancer, though a definitive link is still to be established.

The post-menopausal ovary is hormonally active, contributing to circulating testosterone levels (515–517). The conversion of testosterone to oestrogens to create a hyperoestrogenic state is implicated in the development of endometrial cancers, where women with endometrial malignancies have increased expression of aromatase (518). Expression of androgen receptor has been described in endometrial cancer (499, 502, 519, 520) and Ishikawa cells, derived from a well differentiated endometrial adenocarcinoma, are also AR positive (521).

The AR contains a CAG polymorphic repeat in exon 1 (522, 523), the length of this repeat is directly correlated to the transcriptional activity of AR, in that the longer the repeat the lower the transcriptional activity (524, 525). Receptors with longer repeats also have decreased binding to androgens (522, 525).

Furthermore, PCOS and endometrial cancer have also been linked to the length of the CAG repeat. PCOS women have a shorter CAG in comparison to "normal" control women (526–528) suggestive of a more active form of the protein, whereas an increase in CAG repeat length has been reported in women with endometrial cancer compared to healthy controls (529, 530). However, other studies have questioned the role of AR polymorphisms in endometrial cancer (531, 532).

The anti-proliferative effects of androgens have highlighted them as one therapy choice in the treatment of endometriosis, an inflammatory condition where endometrial glands and stroma grow outside of the uterus (287). Endometriosis is often associated with infertility implicating endometrial dysfunction (286). Danazol (an androgenic compound), promotes atrophy of the endometrium and endometrial lesions as well as reducing pain associated with endometriosis (533, 534), however its use as a treatment for endometriosis has been discontinued in some countries due to its androgenic side effects, including weight gain and hirsutism.

In summary, the human endometrium is exposed to fluctuations in both oestradiol and progesterone across the menstrual cycle, regulating cell proliferation and cellular differentiation. In contrast to oestradiol and progesterone, concentrations of androgens such as testosterone and androstenedione are maintained across the cycle. Aberrant androgen concentrations are associated with endometrial disorders; however a role for androgens in "normal" function has not been fully explored. From previous studies it is likely that the AR plays an anti-proliferative role which may regulate tissue dynamics through-out the cycle.

5.1.4 Aims of the chapter

1. To investigate a role for androgens in restoring endometrial integrity after breakdown using a mouse model of menses
2. More specifically, to investigate if androgens have an effect on re-epithelialisation and angiogenesis.

5.2 Materials and methods

5.2.1 Mouse model of menstruation

The mouse model established in Chapter 3 and described in section 2.1.4.4 was utilised to investigate mechanisms contributing to endometrial repair. Mice underwent the protocol as detailed in section 2.1.4.4 with one minor deviation. On day 19 mice received a single, 0.1ml, sub-cutaneous injection of 2mg/ml dihydrotestosterone-proprionate (A2570-000, Steraloids, Rhode Island, USA) in sterile PBS. At the same time the progesterone pellets were removed to induce progesterone withdrawal (pellet withdrawal was designated as 0 hours). The protocol is outlined in Figure 5-1.

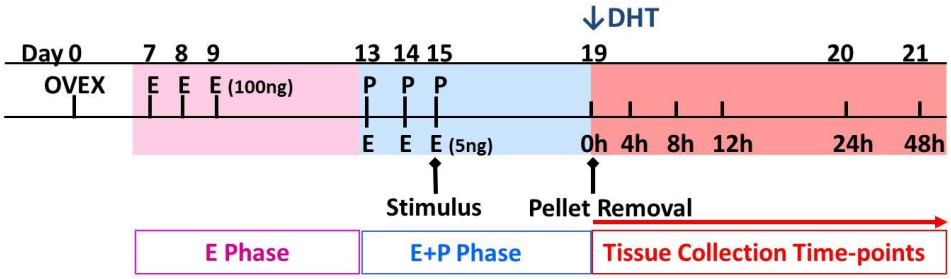

Figure 5-1: Mouse model of menstruation and repair. Ovex; ovariectomy, E; β-oestradiol, P; progesterone, DHT; dihydrotestosterone-proprionate. β-oestradiol concentrations in brackets.

5.2.2 Tissue processing and immunohistochemistry

All samples were fixed in NBF overnight at room temperature, rinsed in 70% ethanol and then stored in 70% ethanol before tissue processing as described in section 2.6.

Immunohistochemistry was carried out using the standard protocol outlined in section 2.7.2 using the antibodies outlined in Table 2-15 and Table 2-16.

5.2.3 RNA extraction

RNA extraction was carried out as detailed in section 2.2.

5.2.4 Synthesis of complementary DNA using VILO cDNA synthesis kit

Reverse transcription of RNA to cDNA was performed using the Superscript VILO cDNA synthesis kit (InVitrogen) according to manufacturer's instructions, using the volumes

outlined below in Table 2-8. Samples were then incubated under the conditions detailed in section 2.3

5.2.5 Quantitative Real Time PCR

Quantitative real time PCR was carried out as detailed in section 2.4**.**

Statistical analysis was performed as detailed in section 2.8.

5.2.6 RT2 Profiler PCR Array

RT^2 profiler arrays contain a panel of genes containing housekeeping genes, quality controls and 84 genes that are related to a specific biological pathway. RNA samples used in RT^2 profiler PCR array were subject to quality assessment based on RIN. Samples were RIN<6.0 were excluded. Two gene arrays were utilised in this study; Mouse Epithelial to Mesenchymal Transition Array (SABiosciences, PAMM-090Z) and Mouse Angiogenesis Array (SABiosciences, PAMM-024Z).

RNA quantitation was performed as detailed in section 2.5.1. A RIN greater than 6.0 was accepted for further analysis by PCR array. cDNA synthesis was performed following the protocol outlined in section 2.5.3. Real time PCR was performed as detailed in section 2.5.4.

PCR data analysis was performed using the SABiosciences web portal as detailed in section 2.8.

5.2.6.1.1 Putative pathway analysis by MetaCore™

MetaCore™ utilises a manually curated database of known species specific interactions between protein-protein, protein-DNA and protein-RNA. MetaCore™ was used to map potential signalling and metabolic pathways of candidate genes investigated by PCR array.

5.2.6.1.2 Multi-genome analysis of positions and patterns of elements of regulation (MAPPER)

MAPPER is a large, computational database that allows identification of transcription factor binding sites (TFBS) within a known human, mouse or Drosophila gene/uploaded sequence. The search engine combines data from two online databases, TRANSFAC® AND JASPAR, along with Markov models that calculate the probability of TFBS within a gene.

Candidate genes were investigated for putative androgen receptor/androgen response elements (ARE) along with tethering molecules Sp-1 and Ap-1 within 500 base pairs of their transcription start site.

5.3 Results

5.3.1 DHT delays the onset of menses

A key observation made using vaginal lavage was that DHT treated animals began to bleed at a later time-point when compared to their matched untreated animals. Figure 5-2 shows the percentage of untreated (-DHT) (black line) and DHT treated (blue line) animals bleeding at each time-point. As previously shown in the untreated animals, bleeding began in 46% of the animals at 4 hours with the highest percentage of bleeders observed at 12 hours (87.5%), with no blood detected in the vaginal lavage by 24 hours, suggesting re-epithelialisation had occurred. In the DHT treated animals, blood cells were only detected in the lavage of one mouse at 4 hours (16%), whereas this number had increased by 8 hours to 50%, a percentage similar to the untreated 4 hour time-point (46%). The number of mice with vaginal bleeding increased to 100% at 24 hours. These data suggest that administration of DHT was delaying the onset of menses, and was also likely to be delaying repair as all of the mice were still bleeding at 24 hours.

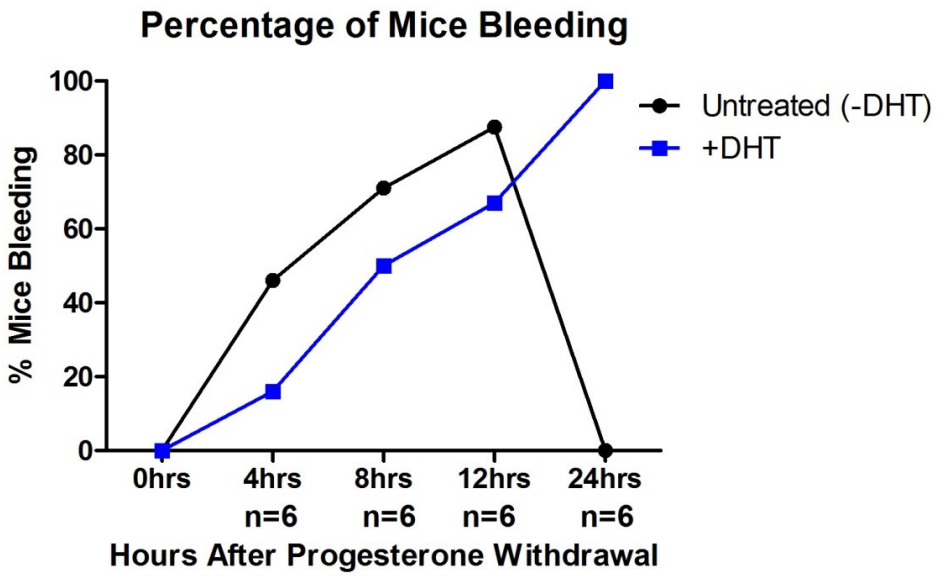

Figure 5-2: DHT delays the onset of bleeding. The percentage of mice bleeding at each time-point following the addition of DHT at 0 hours was plotted (blue line) against untreated animals (black line) (data previously shown in figure 3-2). N numbers for DHT treated animals are shown.

To complement these findings, the effect of DHT was further evaluated by investigating mRNA concentrations for prolactin 8 (*Prl8*), a marker of decidualisation (535), during the breakdown and repair window (Figure 5-3).

Prl8 mRNA concentrations in DHT treated animals (blue bars) were significantly up-regulated at 4 ($p<0.001$), when compared to the matched, untreated time-point (black bars). Concentrations of mRNA for *Prl8* in the 4 hour DHT group were significantly greater than its equivalent untreated group, but were also greater than the 0 hour untreated group (not shown), which suggests that DHT may not only be maintaining decidualisation in the absence of progesterone but may also be enhancing the decidual response. A downward trend in *Prl8* mRNA concentrations was observed towards the 24 hour time-point, and it was notable that *Prl8* concentrations in the 24 hour DHT group were similar to that of the untreated 8 hour group.

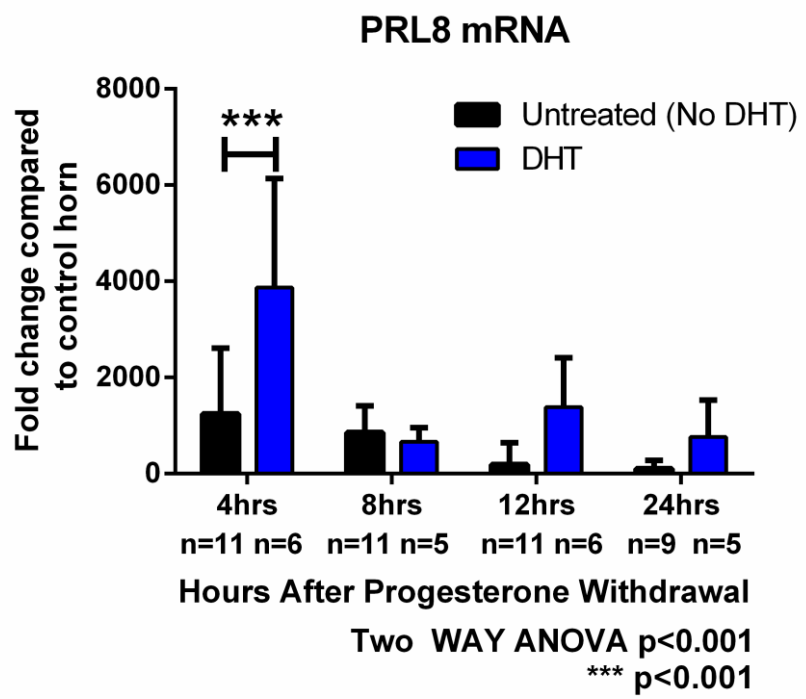

Figure 5-3: *Prl8* mRNA expression in DHT treated animals (blue bars) compared to untreated animals (black bars). mRNA expression for the decidualised horns were normalised against the 0 hour non decidualised horn. Statistical analysis was performed by Two Way ANOVA and Bonferroni post hoc testing, comparing each DHT time-point to their matched untreated time-point where *** $p<0.001$.

It was suspected that one potential impact of DHT might be to compensate for the decline in progesterone by maintaining the decidual tissue, delaying the onset of menses in our mouse model. To further investigate this, mRNA concentrations for ERα were measured. In the uterus, expression of ERα is normally down-regulated by progesterone, and therefore would be expected to increase once the inhibition by progesterone was removed following removal of the progesterone pellet. In the untreated group, mRNA concentrations for ERα were found to significantly increase 4 hours after the withdrawal of progesterone ($p<0.001$) and stayed significantly higher than the 0 hour time-point until the 24 hour time-point ($p<0.05$) (not shown). In the DHT treated animals (Figure 5-4), ERα mRNA concentrations were significantly decreased at 4 hours ($p<0.001$) when compared to the matched 4 hour untreated time-point. By 8 hours no significant difference was detected between untreated and DHT treated mice.

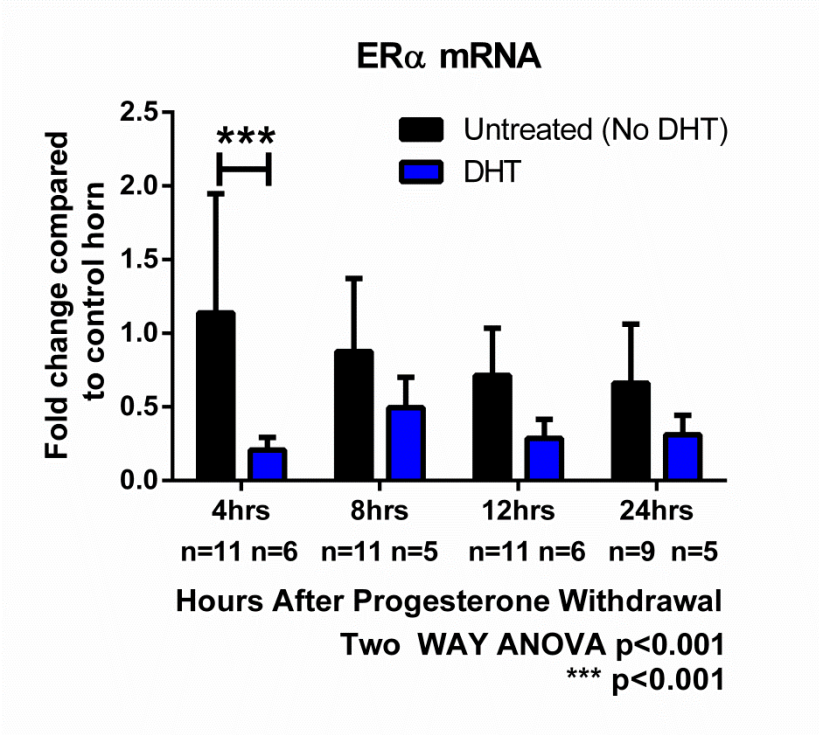

Figure 5-4: ERα (*Esr1*) mRNA expression in untreated (black bars) and DHT treated (blue bars) animals. mRNA expression for the decidualised horns were normalised against the 0 hour non decidualised horn. Statistical analysis was performed by Two Way ANOVA and Bonferroni post hoc testing, comparing each DHT time-point to their matched untreated time-point where *** $p<0.001$.

5.3.2 DHT delays the onset of tissue breakdown

Uterine morphology at each time-point is depicted in Figure 5-5and Figure 5-6. In the DHT treated animals, recovered 4 hours after the removal of the progesterone pellet (Figure 5-5, B), the gross morphology of the uterine horn resembles that of the untreated (-DHT) 4 hour time-point (Figure 5-5, A). An intact luminal epithelium was observed (Figure 5-5, C), along with decidualised stromal cells in the centre of the horn (Figure 5-5, D). In the DHT treated uterus recovered at 8 hours after progesterone withdrawal (Figure 5-5, F) the beginning of breakdown was observed (Figure 5-5, H) in the decidualised stroma. However, in comparison to the untreated tissue (Figure 5-5, E) shedding of the functional layer into the lumen had not occurred. Maintenance of the decidual response was observed in another area of the tissue (Figure 5-5, G).

At 12 hours (Figure 5-6, A-D), decidualised cells in the centre of the uterine lumen, appeared to be apoptotic, adjacent to these cells was an area of stroma that appeared to be breaking down (Figure 5-6, C). Unlike in untreated tissues, breakdown of the functional layer into the lumen was not observed.

By 24 hours (Figure 5-6, E-H), the entire functional stroma appeared apoptotic, due to the changes in cell morphology and loss of haematoxylin counterstain, but had not detached from the underlying basal layer (Figure 5-6 G and H), as demonstrated in the untreated uterus recovered at 12 hours after progesterone withdrawal (Figure 5-6, A).

Overleaf, Figure 5-5: Morphology of the DHT treated uterine horn 4 hours (A-D) and 8 hours (E-H) after the withdrawal of progesterone. A; Uterine morphology 4 hours after progesterone withdrawal in untreated mice. B; Uterine morphology of DHT treated mice at 4 hours. C; An intact epithelial layer is observed (LE). D; Decidualised stromal cells are observed in the centre of the horn. E; Morphology of the uterus 8 hours after progesterone withdrawal in untreated mice. F; Morphology of the uterus un DHT treated mice. G; The maintenance of the decidual response is observed in another area of the same section. H; The beginnings of breakdown was observed in an area of decidualised functional stroma (arrowheads). DS; decidualised stromal cells, LE; luminal epithelium, BL; basal layer. Scale bars as indicated. Images representative of 3 animals per time-point.

Figure 5-6: Morphology of the DHT treated uterine horn 12 hours (A-D) and 24 hours (E-H) after the withdrawal of progesterone. A; Uterine morphology 12 hours after progesterone withdrawal in untreated mice. B; Uterine morphology in DHT treated mice. C; An intact epithelial layer still lines the lumen. D; Cells appear to be breaking down to the left of this image. E; Uterine morphology 24 hours after progesterone withdrawal in untreated tissues. F; Uterine morphology 24 hours after progesterone withdrawal in DHT treated tissues. G and H; Decidualised cells have not yet detached from the underlying basal layer . SC; shed cells, BL; basal layer. Scale bars as indicated. Images representative of 3 animals per time-point.

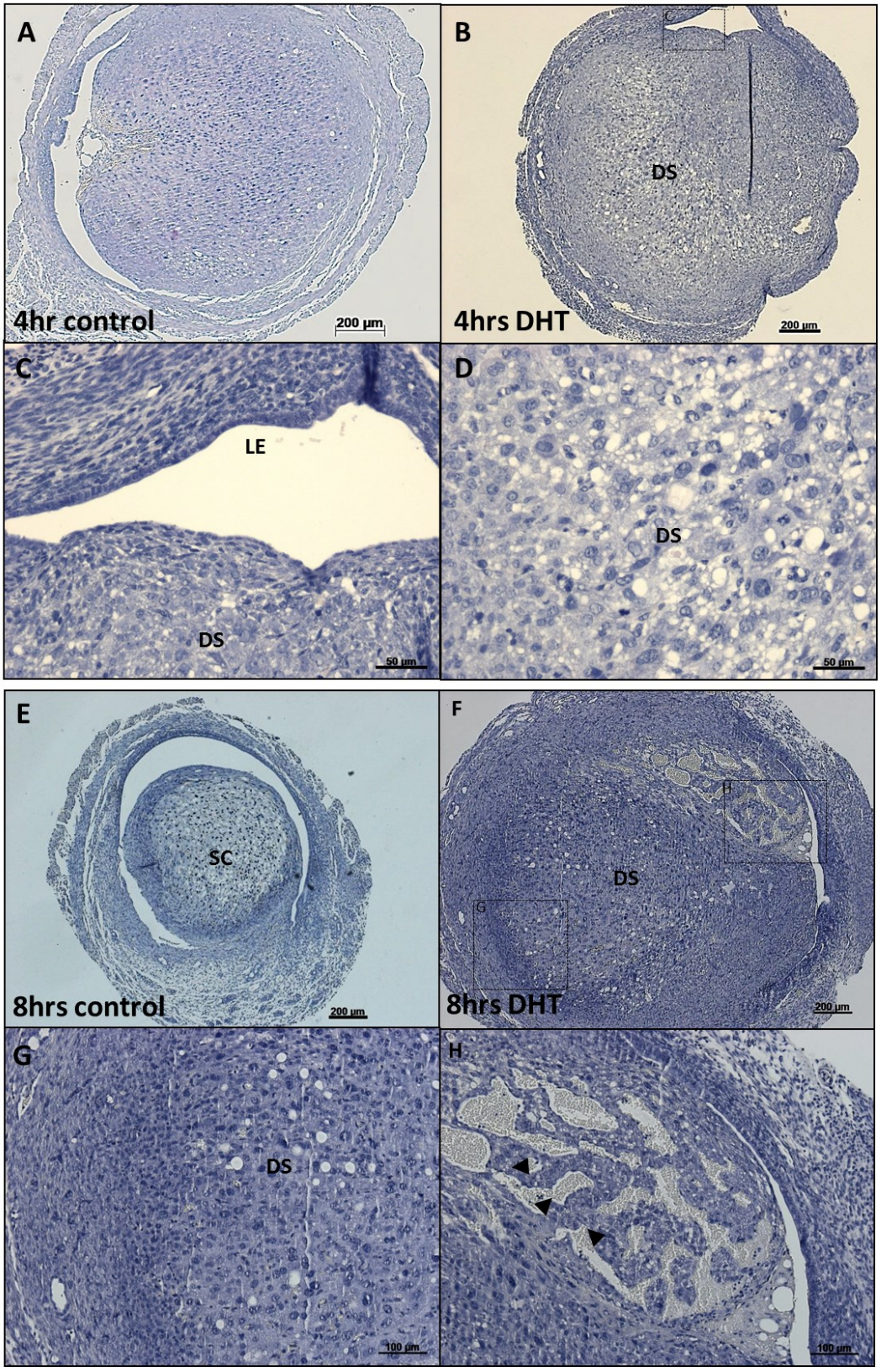

Figure 5-5: Morphology of the DHT treated uterine horn 4 hours (A-C) and 8 hours (D-F) after the withdrawal of progesterone.

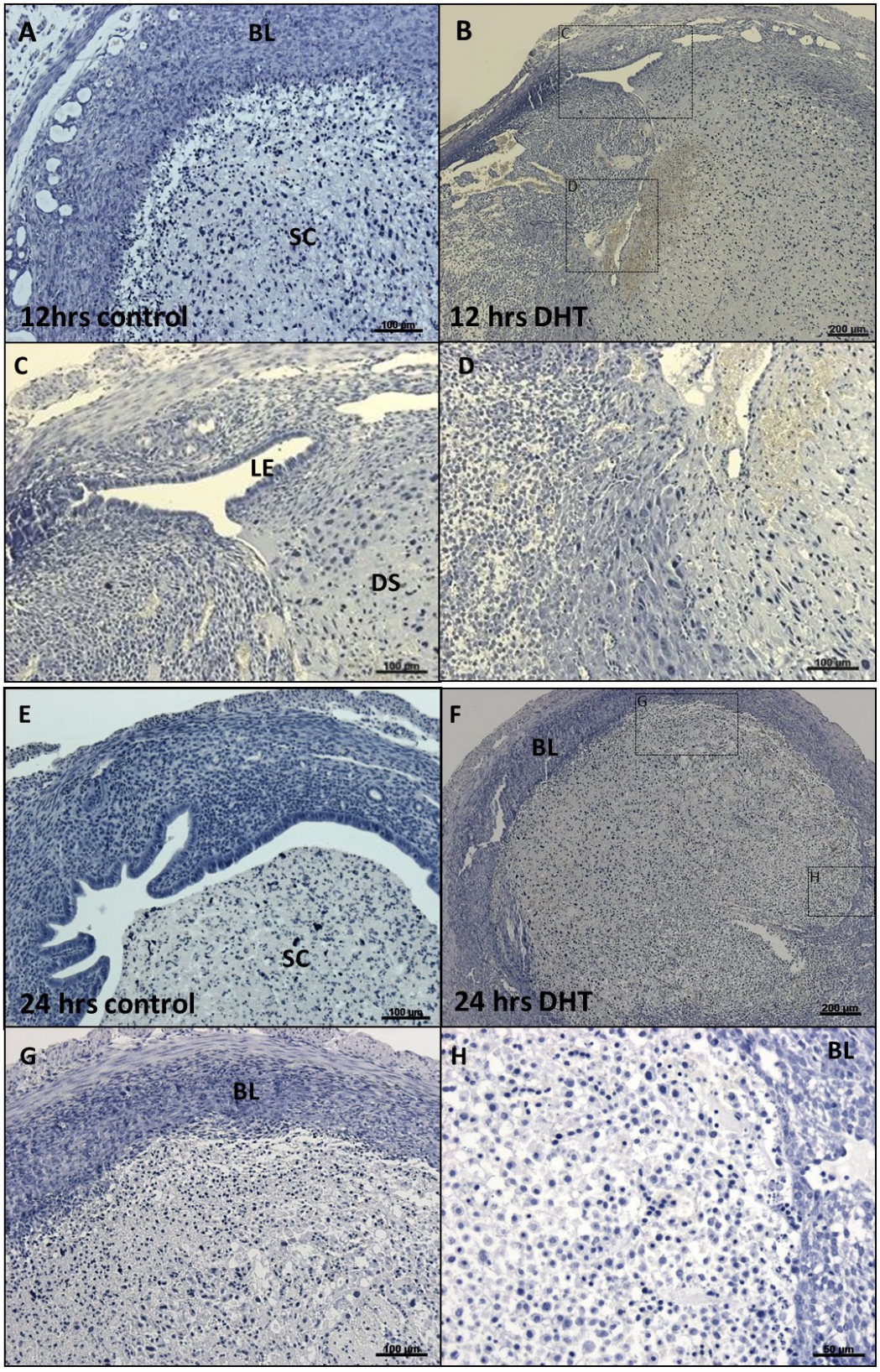

Figure 5-6: Morphology of the DHT treated uterine horn 12 hours (A-C) and 24 hours (D-F) after the withdrawal of progesterone.

5.3.3 Treatment with DHT appears to alter androgen receptor expression during breakdown

To understand whether DHT could be regulating the delay in breakdown via its cognate receptor, the androgen receptor, AR expression was compared in uteri recovered at 4 and 24 hours in both untreated (-DHT) and DHT treated (+DHT) samples.

At 4 hours (Figure 5-7, A and B), androgen receptor protein was immunolocalised to the nuclei of decidualised stroma cells and stromal fibroblasts in the basal layer. AR expression was not detected in the luminal epithelium. In the DHT treated animals, there appeared to be an increase in the intensity of immunostaining for AR (Figure 5-7, B) in both the decidualised stromal cells and in the stromal cells adjacent to the luminal epithelium, consistent with ligand-induced stabilisation of the protein.

At the 24 hour time-point (Figure 5-7, C and D), in the untreated animals (C), expression of AR was sparsely distributed throughout the stromal cell compartment. In DHT treated animals, (Figure 5-7, D) immunostaining for AR appeared to be more intense in the basal layer and was localised to the stromal cells adjacent to the luminal epithelium.

Transcriptional regulation of AR (*Ar*) was investigated by qRTPCR to determine mRNA concentrations at each time-point (Figure 5-8). At 4 hours mRNA concentrations of *Ar* were lower than that of their untreated counterparts (ns, $p>0.05$), however a trend of an increase was observed at 8 hours. *Ar* mRNA concentrations appeared to increase from the 12 hour to the 24 hour time-point, but were not significantly greater than the untreated tissues.

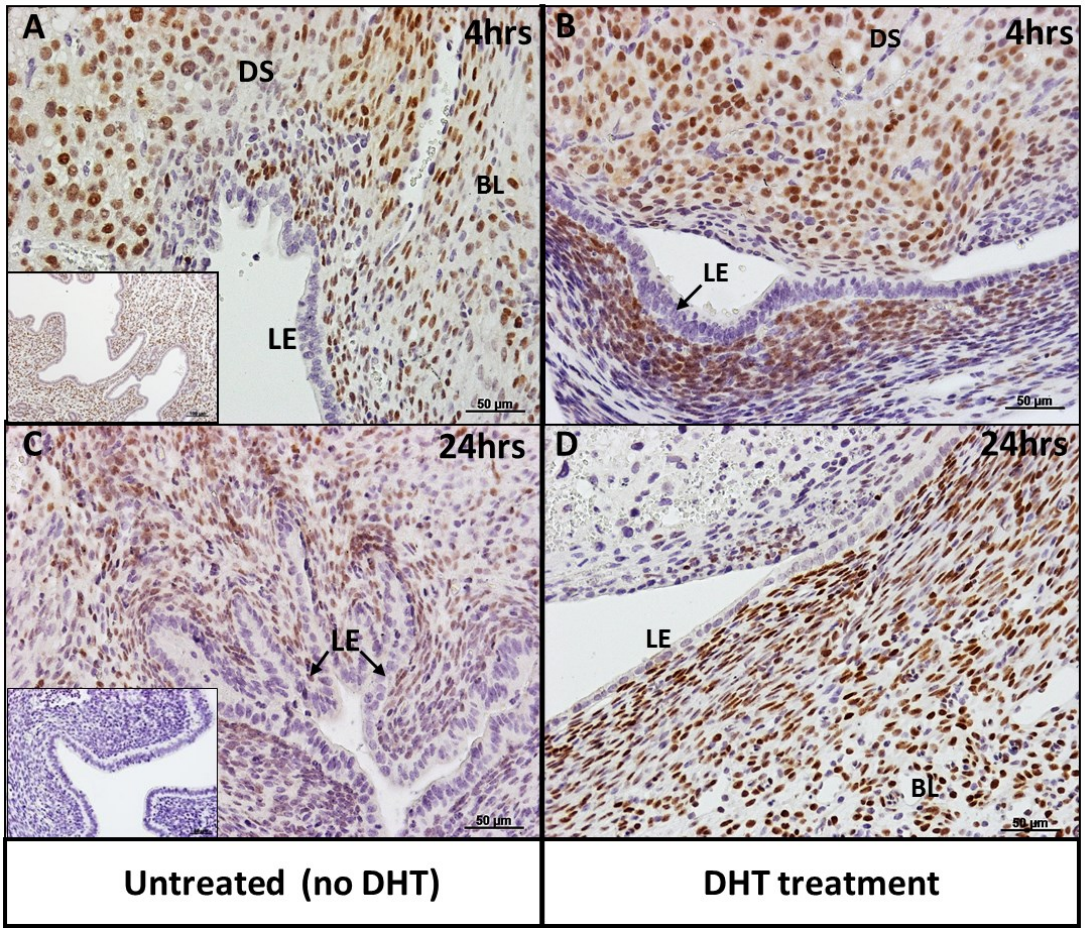

Figure 5-7: Androgen receptor (AR) expression in untreated and DHT treated animals (4 hours, A and B, and 24 hours, C and D after the withdrawal of progesterone). A; At 4 hours, AR was detected in the decidualised stromal cells and stromal cells in the basal layer, whilst it was absent in the epithelium, inset AR in intact mouse endometrium. B; At 4 hours after progesterone withdrawal in the DHT treated animals, there appeared to be an increase in AR expression in the decidualised stroma and in the stroma adjacent to the luminal epithelium. C; By 24 hours weak immunostaining for AR is present on the stromal cell compartment, inset negative control. D; In the DHT treated animals, strong immunostaining for AR is present in the stromal cells adjacent to the luminal epithelium. DS; decidualised stromal cells, LE; luminal epithelium, BL; basal layer. Scale bars as indicated. Images representative of 2 animals per time-point.

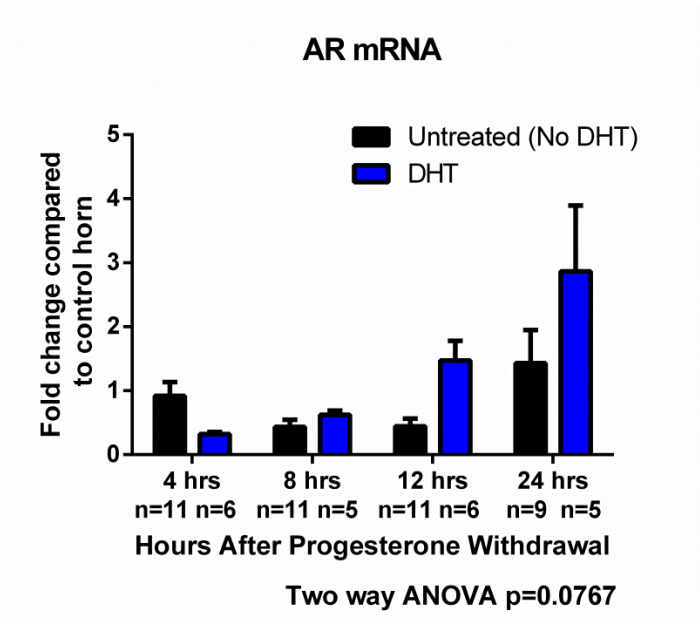

Figure 5-8: Androgen receptor (*Ar*) mRNA concentrations in untreated (black bars) and DHT treated animals (blue bars). mRNA expression for the decidualised horns were normalised against the non-decidualised 0hr horn. Statistical analysis was performed by Two WAY ANOVA and Bonferroni post hoc testing, comparing each DHT time-point to its respective untreated time-point.

5.3.4 Administration of DHT delays repair of the endometrium by inhibiting MET

A role for MET in endometrial repair was discussed in Chapter 4, after dynamic regulation of genes involved in the MET pathway were discovered during the window of breakdown and repair in our mouse model. Following the initial observation that a single injection of DHT delayed the onset of breakdown, the effect of DHT on MET was investigated.

In uterine samples recovered from mice not treated with DHT (-DHT), evidence of dual labelled, vimentin and cytokeratin positive cells were first observed at the myometrial border at the 12 hour time-point and at the luminal surface at the 24 hour time-point (see Figure 4-3). In contrast, dual labelled cells were only detected in the DHT treated animals at the 24 hour time-point (Figure 5-9, A and B). Unlike in untreated tissues where these cells were clustered together, in some DHT treated samples, dual labelled cells were sparsely distributed through-out the basal layer adjacent to an area where the decidualised stromal cells had not detached from the underlying basal stroma (Figure 5-9, A and B). However these were not observed in every animal (Figure 5-9, C). In contrast to data reported in chapter 4, no dual labelled were detected in areas near the luminal epithelium (Figure 5-9, D).

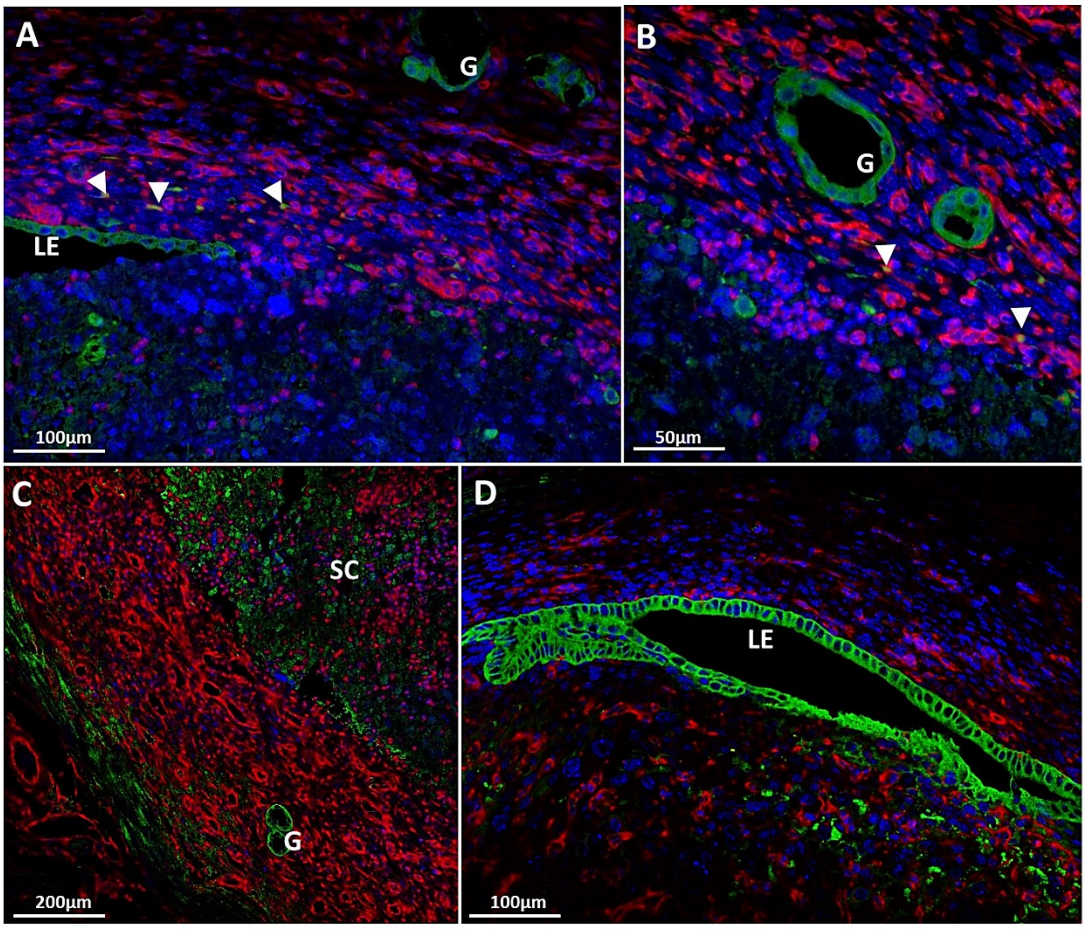

Figure 5-9: Evidence of MET in DHT treated tissues. Epithelial cell marker cytokeratin (green) and mesenchymal cell marker vimentin (red). Tissues recovered at the 24 hour time-point, two representative uteri are shown in A-C and D. A-D; Stromal cells in the basal layer are positively stained for vimentin. The luminal and glandular epithelium are positive for cytokeratin. Dual labelled cells (yellow) are identified by the white arrowheads. BL; basal layer, DS; decidualised stroma, LE; luminal epithelium, G; glandular epithelium. Images representative of 3 animals per time-point.

If treatment with DHT was merely delaying the normal onset of endometrial breakdown, as evidenced by histological examination, we might expect a rightward shift in mRNA concentrations for genes known to regulate MET. In contrast to this hypothesis, concentrations of *Wt1* mRNA were significantly up-regulated (Figure 5-10) in the DHT treated horns compared to the untreated horns at 8 hours ($p<0.001$) and 12 hours ($p<0.001$) after the withdrawal of progesterone. Concentrations of Snail (*Snai1)* mRNA were also up-regulated in the DHT treated horns when compared to their untreated time-points (4 hours; $p<0.001$, 8 hours; $p<0.001$, 12 hours; $p<0.01$, 24 hours; $p<0.001$).

Interestingly, mRNA concentrations of Slug (*Snai2*) were decreased in the DHT treatment animals in comparison to the untreated animals 4 hours after the withdrawal of progesterone (ns, $p>0.05$). Concentrations of Slug were increased at 12 hours ($p<0.001$). By 24 hours, no

difference in mRNA concentrations of Slug was detected between the DHT treated or untreated animals.

Concentrations for mRNAs for stromal cell markers *Cdh2* and vimentin were down-regulated in the DHT treated group when compared to the untreated time-points (Figure 5-11). *Cdh2* was down regulated at 4 hours ($p<0.01$) and 8 hours ($p<0.05$) after progesterone withdrawal. Concentrations for vimentin were down-regulated at 4 hours ($p<0.05$). Interestingly, mRNA concentrations for *Wnt4* were increased at 4 hours ($p<0.001$) and 8 hours ($p<0.05$) in the DHT group.

Concentrations for mRNAs for epithelial cell marker *Cdh1* were decreased at 4 hours, but started to increase at 8 hours, however no significant difference in mRNA concentrations were detected at any time-point (Figure 5-11). Similar patterns in mRNA concentrations were detected for *Wnt7a* and *Krt8*, where mRNAs were decreased at 4 hours, but slowly increased towards the 24 hour time-point.

Taken together these data were suggestive of profound disturbances in the regulation of cell identity as a result of DHT exposure following progesterone withdrawal.

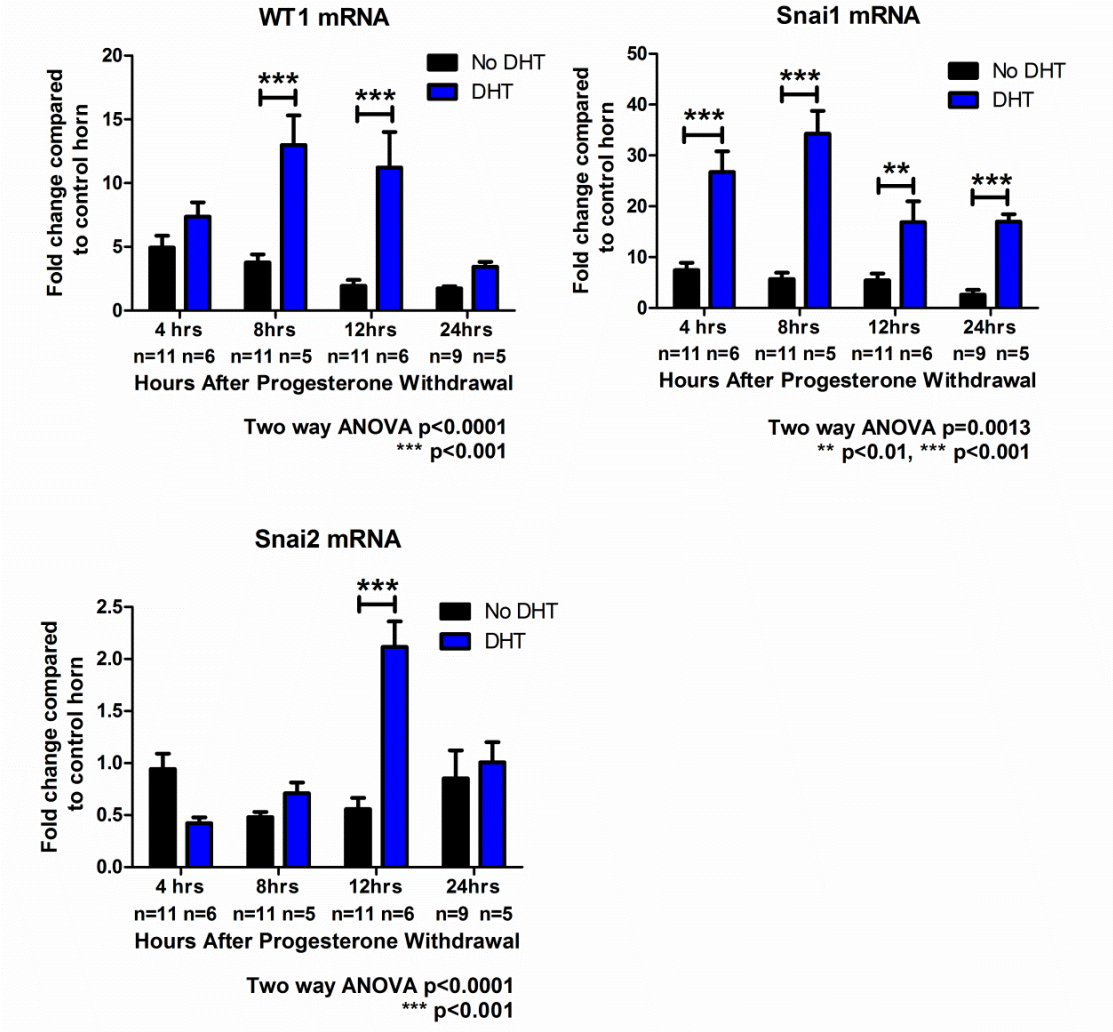

Figure 5-10: mRNA concentrations for candidate genes involved in mesenchymal to epithelial transition; *Wt1*, Snail (*Snai1*) and Slug (*Snai2*). mRNA expression for both untreated and DHT treated horns was normalised against non-decidualised 0 hour horn. Statistical analysis was performed by Two way ANOVA and Bonferroni post hoc testing, where * p<0.05, ** p<0.01 and *** p<0.001.

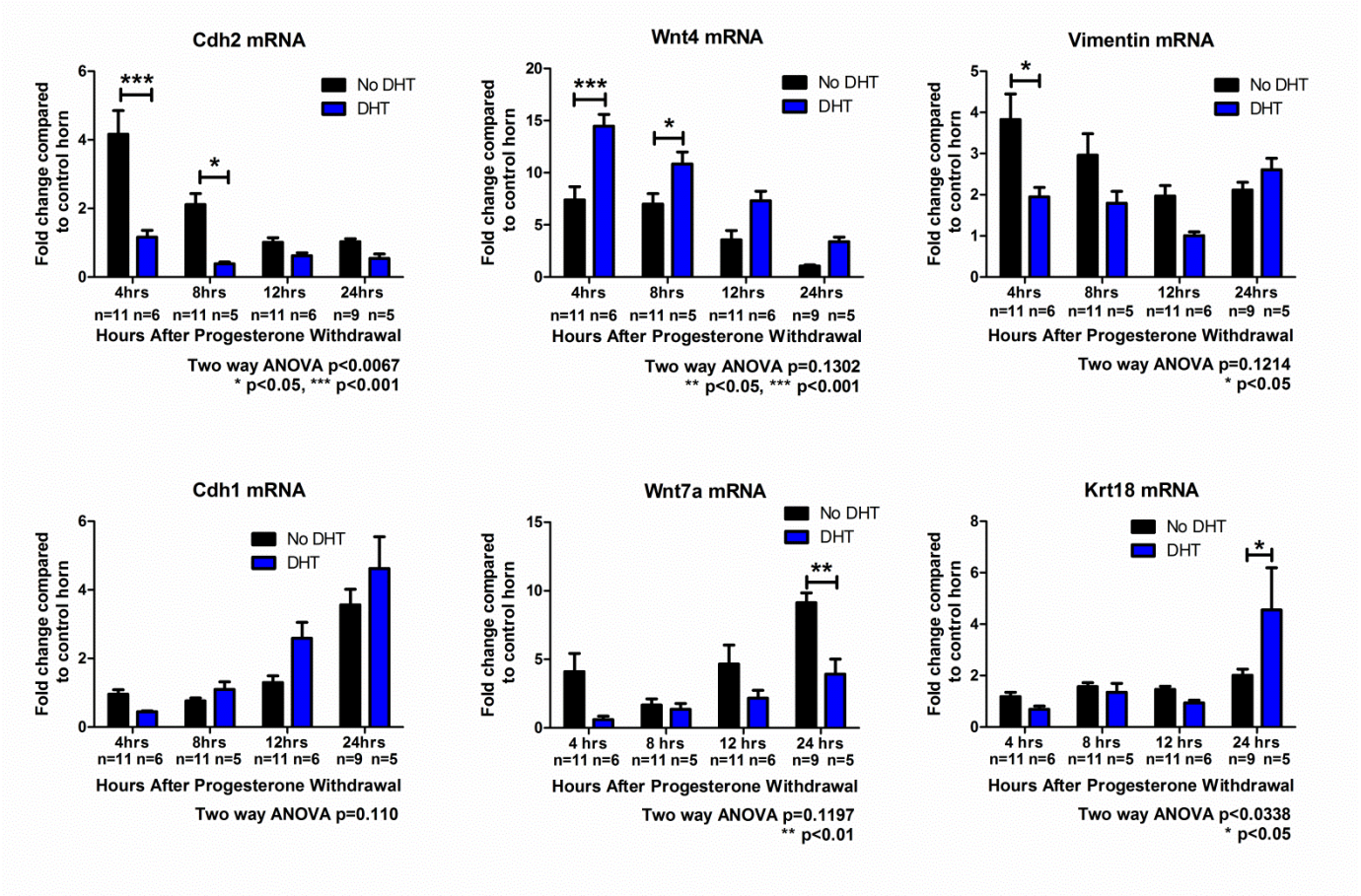

Figure 5-11: mRNA concentrations for candidate genes involved in mesenchymal to epithelial transition; *Cdh2, Wnt4*, vimentin, *Cdh1, Wnt7a* and keratin 8 (*Krt8*). mRNA expression for both untreated and DHT treated horns was normalised against the 0 hour non-decidualised horn. Statistical analysis was performed by Two way ANOVA and Bonferroni post hoc testing, where * p<0.05, ** p<0.01 and *** p<0.001.

5.3.5 Evidence for an effect of androgens on MET by array analysis

Additional evaluation of the impact of DHT on MET was investigated using a PCR array that profiles 84 key genes that are known to be involved in the EMT/MET pathway. The full gene list can be found in Supplementary Table 1. The array utilised uterine samples from mice with and without DHT treatment. Samples from the three key time-points (0 (-DHT only), 8 and 24 hours) were studied. The differences in fold regulation of gene expression were analysed using the ΔΔCT method, where the 8 hour and 24 hour time-points for both the untreated and DHT treated samples were compared to the untreated 0 hour time-point, uteri recovered at the point of full decidualisation. Additionally, the fold regulation between the untreated (-DHT) and DHT treated animals were also analysed e.g. 8 hours -DHT v 8 hours +DHT. Those genes in which a significant change in fold regulation was observed are shown in Table 5-1, Table 5-2 and Table 5-3.

Notably, a lower number of significant changes in gene expression were observed after treatment with DHT (0 v 8 hours -DHT; 24 changes; 0 v 8 hours +DHT; 9 changes, 0 v 24 hours -DHT; 48 changes, 0 v 24 hours +DHT; 37 gene changes).

Treatment with DHT resulted in a number of striking gene changes at the 8 hour time-point (0 v 8 hours -DHT/+DHT). Integrin beta 1, significantly up-regulated (1.5 fold increase) in the -DHT animals was significantly down-regulated after the addition of DHT (36.5 fold decrease). *Rgs2* (involved in G protein signalling) was decreased 2.7 fold in the -DHT set but decreased by 10.8 fold in the +DHT set. Another notable difference was in the regulation of *Wnt11*, 3.4 fold increased in the -DHT set but 19.9 fold increased in the +DHT set. Collagen 3a1, which was not detected to be significantly regulated in the -DHT set decreased 13.3 fold in the DHT treated animals.

At the 24 hour time-point (0 v24 hours -DHT/+DHT), keratin 19 expression decreased from a 7.5 fold increase in -DHT tissues to a 3.5 fold increase in the DHT treated animals. Similar changes were also detected in keratin 7, a 28 fold increase to a 7 fold increase and MMP3, a 61 fold increase to a 9.8 fold increase in the DHT treated group.

When direct comparisons between -DHT and +DHT animals were analysed a number of changes were detected in the 8 hours -DHT v 8 hour +DHT group. Collagens 1a2, 3a1 and 5a2 were all down-regulated (7.5 fold; 35 fold and 4 fold respectively). Integrin beta 1 was down-regulated 104 fold. Cell adhesion molecule osteopontin (*Spp1)* was down-regulated 25 fold. Molecules known to be involved in cell migration, moesin (*Msn*) and *Rac1* were also significantly down-regulated, 11 fold and 13 fold respectively. Notably, Snail was increased by 15.7 fold and *Notch1* by 10 fold.

At 24 hours, a notable gene change between -DHT and +DHT tissues was the down-regulation of *Mmp-3*, by 5 fold.

0hrs v 8hrs -DHT			0 v 8hrs +DHT		
Gene Name	**p value**	**Fold Regulation**	**Gene Name**	**p value**	**Fold Regulation**
Col5a2	0.014999	1.3733	*Col3a1*	0.004759	-13.3755
Fzd7	0.004084	2.112	*Itgb1*	0.029826	-36.5277
Gng11	0.027026	-2.0012	*Pppde2*	0.041858	1.8169
Igfbp4	0.007334	1.8312	*Rac1*	0.009679	-7.3429
Il1rn	0.000873	2.0872	*Rgs2*	0.001117	-10.8609
Ilk	0.027785	1.4167	*Sparc*	0.012026	-11.9256
Itgb1	0.001503	1.4681	*Tfpi2*	0.022356	-10.4001
Krt19	0.000383	1.9973	*Twist1*	0.029906	8.6303
Krt7	0.001239	4.8209	*Wnt11*	0.041917	19.9072
Mmp2	0.008265	2.0402	No. Genes Up Regulated		3
Mmp3	0.013284	3.0056	No. Genes Down Regulated		6
Mtap1b	0.021019	1.7783			
Pdgfrb	0.030445	2.1571			
Plek2	0.001445	2.1191			
Rgs2	0.001027	-2.7773			
Snai2	0.018714	-2.1138			
Snai3	0.006822	5.6312			
Spp1	0.001467	4.3785			
Stat3	0.001286	1.5821			
Steap1	0.000673	2.3442			
Tfpi2	0.008769	-1.8252			
Timp1	0.015419	1.6154			
Tmeff1	0.000078	2.3973			
Wnt11	0.000277	3.4224			
No. Genes Up Regulated		20			
No. Genes Down Regulated		4			

Table 5-1: Significant changes in gene expression 8 hours after progesterone withdrawal in both the untreated (left) and DHT treated (right) groups. Gene changes are displayed as up- or down-fold regulation when compared to the 0 hour group, n=6.

0hrs v 24hrs -DHT			0 v 24hrs +DHT		
Gene Name	**p value**	**Fold Regulation**	**Gene Name**	**p value**	**Fold Regulation**
Akt1	0.004507	1.6241	*Akt1*	0.021554	1.4004
Bmp1	0.001376	1.7233	*Bmp1*	0.004875	1.781
Bmp7	0.04878	1.8035	*Bmp7*	0.019901	1.5242
Cald1	0.006957	2.2812	*Cald1*	0.041718	1.9679
Camk2n1	0.04425	4.8329	*Camk2n1*	0.006771	2.4549
Cav2	0.03615	1.7465	*Cav2*	0.039747	1.4628
Cdh1	0	5.1764	*Cdh1*	0.012869	2.2448
Cdh2	0.046312	1.4957	*Col1a2*	0.035275	1.526
Dsc2	0.000383	4.734	*Dsc2*	0.038507	2.5695
Dsp	0.000257	9.5533	*Dsp*	0.002195	2.6723
Esr1	0.032215	1.5223	*Esr1*	0.015056	1.3194
Fn1	0.007739	3.0108	*Fgfbp1*	0.029242	2.4738
Fzd7	0.011578	2.2833	*Fn1*	0.021125	2.466
Gng11	0.016563	-2.7033	*Gsc*	0.013639	3.1905
Gsc	0.039591	2.8029	*Ilk*	0.040806	1.4629
Gsk3b	0.046881	1.4052	*Krt19*	0	3.526
Ilk	0.004121	1.8766	*Krt7*	0.00039	7.217
Itgb1	0.006007	1.6552	*Mmp2*	0.011524	1.9656
Jag1	0.002575	3.4856	*Mmp3*	0.026796	9.8823
Krt19	0.000053	7.5293	*Msn*	0.024717	1.4358
Krt7	0.000018	28.178	*Ocln*	0.008739	2.5191
Mitf	0.001484	-2.1751	*Pdgfrb*	0.032017	1.8664
Mmp2	0.00544	2.7303	*Rgs2*	0.00053	-3.4636
Mmp3	0.001871	61.2906	*Smad2*	0.026931	1.1826
Msn	0.000728	1.8437	*Snai2*	0.003658	-1.7138
Mtap1b	0.000492	2.1494	*Spp1*	0	13.5539
Notch1	0.031693	1.6165	*Stat3*	0.001796	1.7196
Ocln	0.005327	11.2243	*Steap1*	0.001172	3.1253
Pdgfrb	0.000015	4.5738	*Tcf7l1*	0.00401	-1.7737
Plek2	0.044301	1.6349	*Tgfb1*	0.00214	1.8677
Ptp4a1	0.002475	1.8968	*Timp1*	0.018738	1.9144

0hrs v 24hrs -DHT			0 v 24hrs +DHT		
Gene Name	**p value**	**Fold Regulation**	**Gene Name**	**p value**	**Fold Regulation**
Rgs2	0.001014	-4.2015	*Tmeff1*	0.015332	2.8142
Smad2	0.005844	1.3823	*Tspan13*	0.000588	1.8561
Snai3	0.011681	15.8243	*Twist1*	0.00685	1.9548
Spp1	0.000141	23.2021	*Vim*	0.007273	1.376
Stat3	0.00232	1.8157	*Wnt11*	0.001067	3.7167
Steap1	0.000283	4.6399	*Wnt5b*	0.021871	-1.4652
Tcf4	0.001468	1.4002	No. Genes Up Regulated		33
Tfpi2	0.002632	-2.1709	No. Genes Down Regulated		4
Tgfb1	0.004964	1.783			
Tgfb2	0.004658	-1.497			
Tmeff1	0.000001	4.1575			
Tmem132a	0.00069	2.8066			
Tspan13	0.00039	3.2687			
Twist1	0.00125	3.294			
Vim	0.001135	1.7446			
Vps13a	0.035245	1.5401			
Zeb1	0.000009	2.4496			
No. Genes Up Regulated		43			
No. Genes Down Regulated		5			

Table 5-2: Significant changes in gene expression 24 hours after progesterone withdrawal in both the untreated (left) and DHT treated (right) groups. Gene changes are displayed as up- or down-fold regulation when compared to the 0 hour group, n=6.

8hrs -DHT v 8hrs +DHT		
Gene Name	**p value**	**fold regulation**
Col1a2	0.000052	-7.5768
Col3a1	0.000385	-35.8022
Col5a2	0.044721	-4.6694
Itgb1	0.005316	-104.9922
Msn	0.006524	-11.4497
Notch1	0.023339	10.1191
Ocln	0.047584	2.4584
Rac1	0.018337	-13.8268
Serpine1	0.035952	-9.2519
Snai1	0.020913	15.7722
Snai2	0.030825	2.2587
Sparc	0.006405	-22.146
Spp1	0.003026	-25.388
No. Genes Up Regulated		4
No. Genes Down Regulated		9

24hrs -DHT v 24hrs +DHT		
Gene Name	**p value**	**fold regulation**
Bmp1	0.041058	1.2724
Cdh1	0.018099	-1.8729
Cdh2	0.048043	-1.6649
Dsp	0.005709	-2.9035
Egfr	0.037947	1.6062
Itga5	0.021464	2.1408
Jag1	0.013583	-2.2656
Krt7	0.028112	-3.1711
Mitf	0.028874	2.2192
Mmp3	0.030717	-5.0373
Ocln	0.02128	-3.6188
Pdgfrb	0.003909	-1.9904
Ptk2	0.007871	1.2553
Serpine1	0.017296	3.6066
Tfpi2	0.000242	3.0199
Wnt5b	0.040307	-1.7319
No. Genes Up Regulated		7
No. Genes Down Regulated		9

Table 5-3: Significant changes in gene expression when DHT groups are directly compared to their own control time-points at 8 hours (left) and 24 hours (right). Gene changes are displayed as up- or down- fold regulation when compared to the 0 hour group, n=6.

5.3.5.1 Network analysis of array and qRTPCR data

To understand the potential regulation of androgens on the MET pathway, the full gene list, qRTPCR candiates and the androgen receptor were input into MetaCore™ software. Using this software it was possible to identify which genes were known to be downstream of AR. The results of this analysis are depicted in Figure 5-12.

Notably, AR was shown to be upstream of β catenin, involved in the Wnt signalling pathway, as well as TGFβ, who along with the Wnts are key regulators of EMT and MET. Interestingly, AR is shown to have activatory actions on the epithelial marker keratin 7 whilst having inhibitory actions on another epithelial marker E cadherin, consistent with a decrease in mRNA concentrations at 4 hours (Figure 5-11).

AR has also been reported to exert activatory effects on extracellular matrix protein osteopontin, which is in contrast to the findings in the array where osteopontin (*Spp1*) was down-regulated in the DHT treated animals at 8 hours. Mesenchymal marker N cadherin has also been shown to be activated by AR, which correlates with an increase in mRNA concentrations for N cadherin after DHT treatment (Figure 5-11).

In order to determine a role for DHT and the AR in the regulation of tissue repair a list of potential AR-regulated candidates was identified for further investigation and is discussed in section 5.4.3.1.

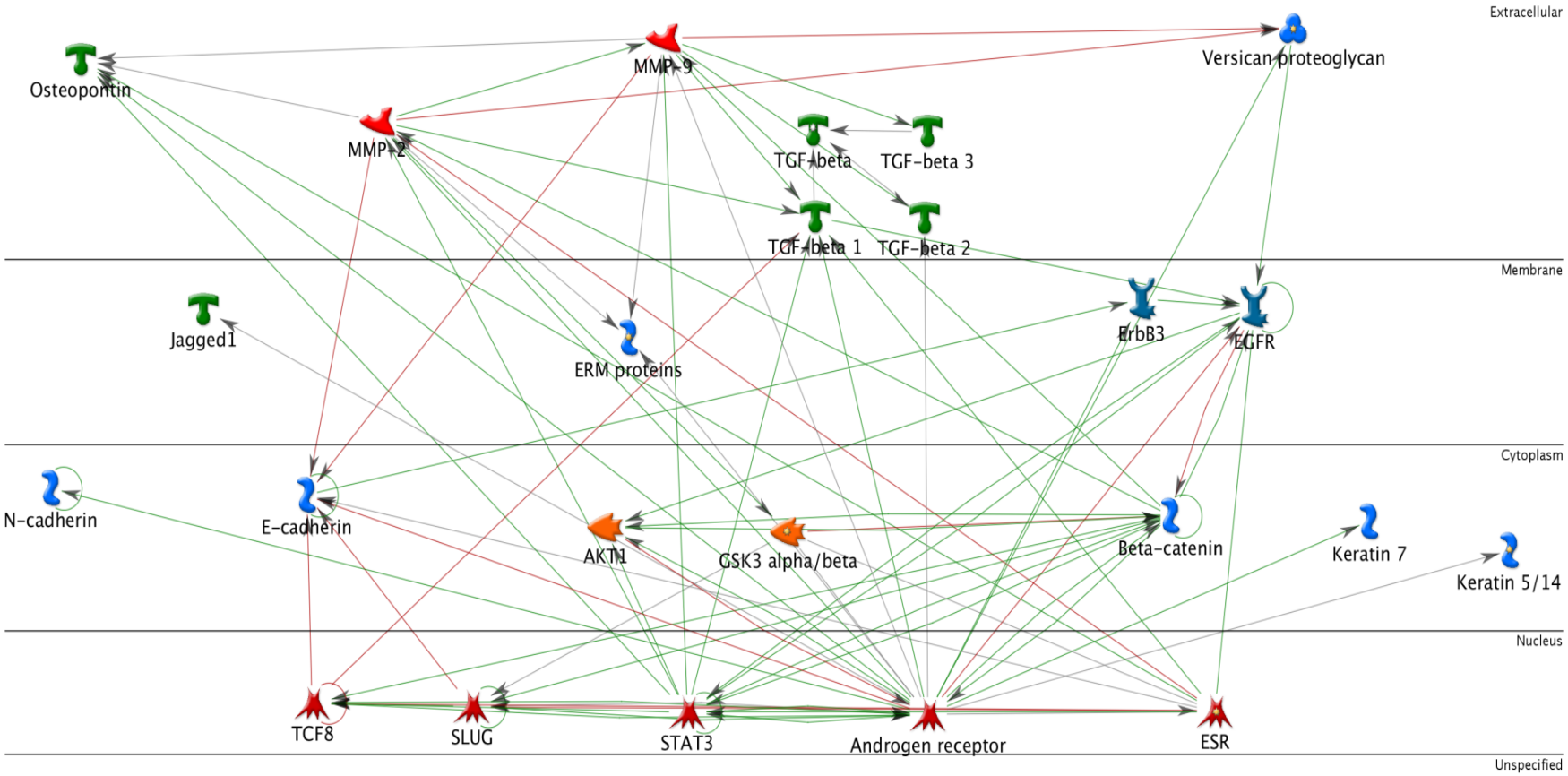

Figure 5-12: Known interactions of genes from the EMT array that are downstream of the androgen receptor. Arrows indicate direct effects on other genes in the pathway. Green arrows indicate activation, whereas red arrows show inhibitory action. Pathway generated using Metacore™ software.

5.3.6 DHT maintains the hypoxic response

Immunohistochemistry for hypoxia was carried out using the Hypoxyprobe® labelling system to investigate the effect of DHT on the hypoxic response during the window of breakdown and repair, as detailed in section 4.3.3. Hypoxia can be visualised by immunohistochemistry, where a brown stain indicates cells under hypoxic conditions. Strong staining is indicative of very low oxygen tensions and very hypoxic, weak staining indicates cells that are hypoxic, whereas an absence of staining indicates cells under normoxic conditions. In Overleaf, Figure 5-13 untreated (-DHT) animals (left) are compared to DHT animals (right), at 0, 4, 8 and 24 hours after the withdrawal of progesterone.

In the DHT group, 4 hours after progesterone withdrawal the beginnings of a hypoxic response are observed in the stromal cell compartment close to the lumen, which is similar to the immunopositive staining for hypoxia observed in the untreated 0 hour group. At both the 0 and 4 hour time-points, cells in the basal layer and myometrium are not stained for hypoxia. By 8 hours after progesterone withdrawal, the DHT treated animals display a phenotype similar to that observed in the 4 hour -DHT group, where the decidualised cell mass is strongly immunostained for hypoxia. Weak immunostaining is detected around the luminal epithelium at this time; however the basal layer and myometrium remained unstained suggesting they are under more normoxic conditions. By 24 hours, staining for hypoxia is restricted to the luminal epithelium and the shed cells in the lumen, similar to that seen in the untreated tissues, however invagination of the luminal epithelium has not occurred.

Overleaf, Figure 5-13: DHT attenuates the hypoxic response. Staining for hypoxia was carried out using Hypoxyprobe®. A delay in the breakdown of the endometrium of the DHT treated animals (right column) is observed when compared to the untreated (left column). Immunostaining for hypoxia shows that the hypoxia response is maintained in the DHT animals, with strong staining observed at 8 hours resembling the 4 hour -DHT group. By the 24 hour time-point, shed cells in the lumen and the luminal epithelium are positively stained for hypoxia, resembling the phenotype of the 8 hour -DHT section. Images representative of 2 animals per time-point.

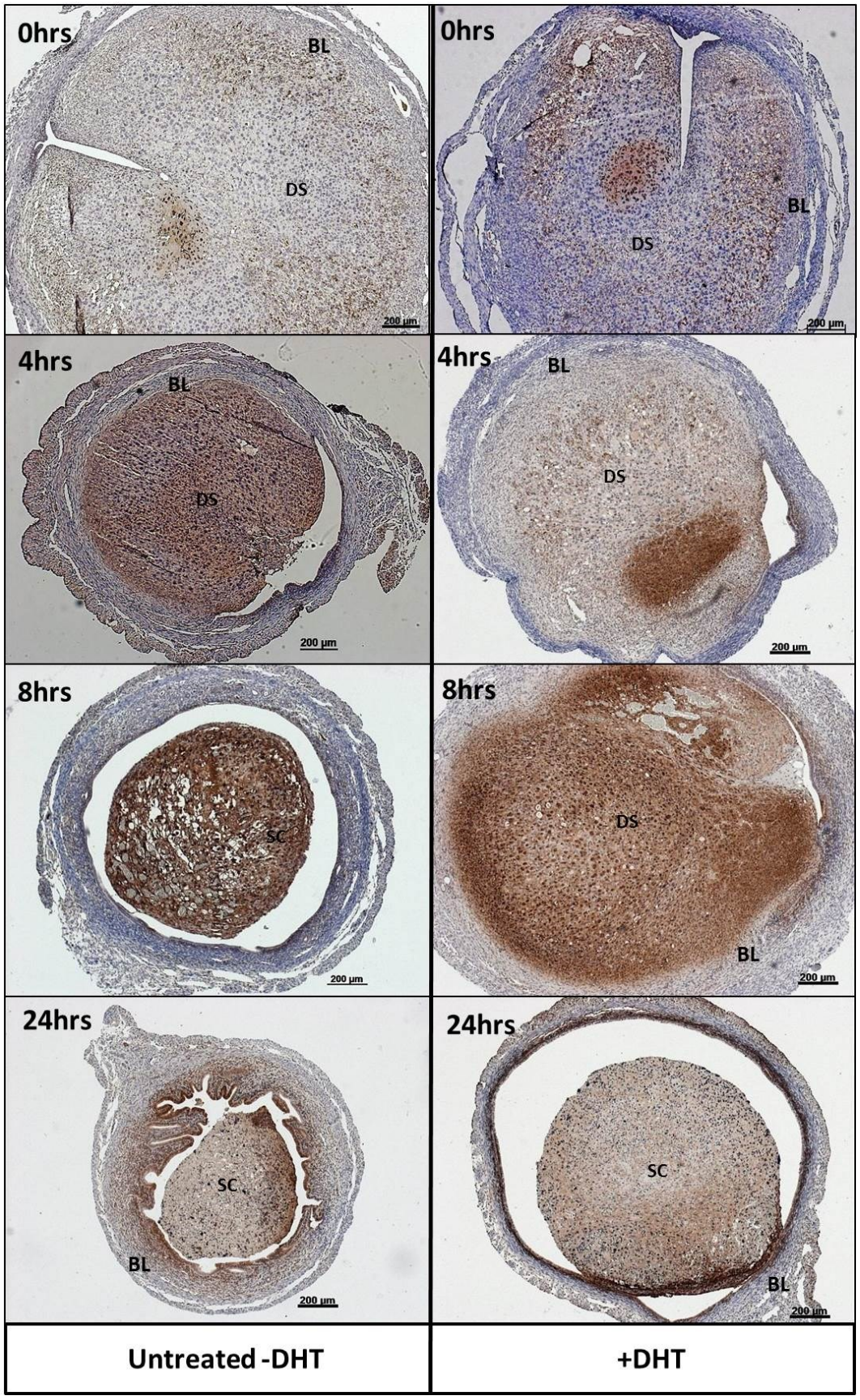
0hrs
BL
DS
200 µm
0hrs
BL
DS
200 µm
4hrs
BL
DS
200 µm
4hrs
BL
DS
200 µm
8hrs
SC
200 µm
8hrs
DS
BL
200 µm
24hrs
SC
BL
200 µm
24hrs
SC
BL
200 µm
Untreated -DHT
+DHT

5.3.7 DHT alters key genes involved in angiogenesis and endothelial cell stability

To investigate whether androgens have an impact on the expression of genes previously reported to be regulated by hypoxia *in vitro;* gene expression was quantified using qRTPCR of total tissue extracts (Figure 5-14).

Concentrations of mRNA encoding *Vegfa* were increased in the DHT treated group at 4, 8 and 12 hours after the withdrawal of progesterone, however no significant difference was detected. Concentrations then decreased back to levels of those seen in untreated tissues at the 24 hour time-point.

Notably, treatment with DHT attenuated the increase in mRNA concentrations for *Cxcl12* that occurred after progesterone withdrawal at 4 hours ($p<0.01$) and 24 hours ($p<0.001$). In DHT treated samples concentrations of mRNAs for *Pecam-1* were maintained at 4 hours, decreased at 8 hours ($p<0.05$) then were up-regulated at 24 hours ($p<0.001$) compared to their untreated time-points.

Interestingly, the pattern of expression of both angiopoietins 1 and 2 (*Angpt1/Angpt2*) was similar after treatment with DHT, with no change in expression at 4 and 8 hours when compared to the 0 hour time-point. However, significant increases in mRNA concentrations at 12 hours (*Angpt 1*, $p<0.05$, *Angpt 2*, $p<0.01$) and 24 hours (*Angpt1/2*, $p<0.001$) were detected when compared to the untreated samples.

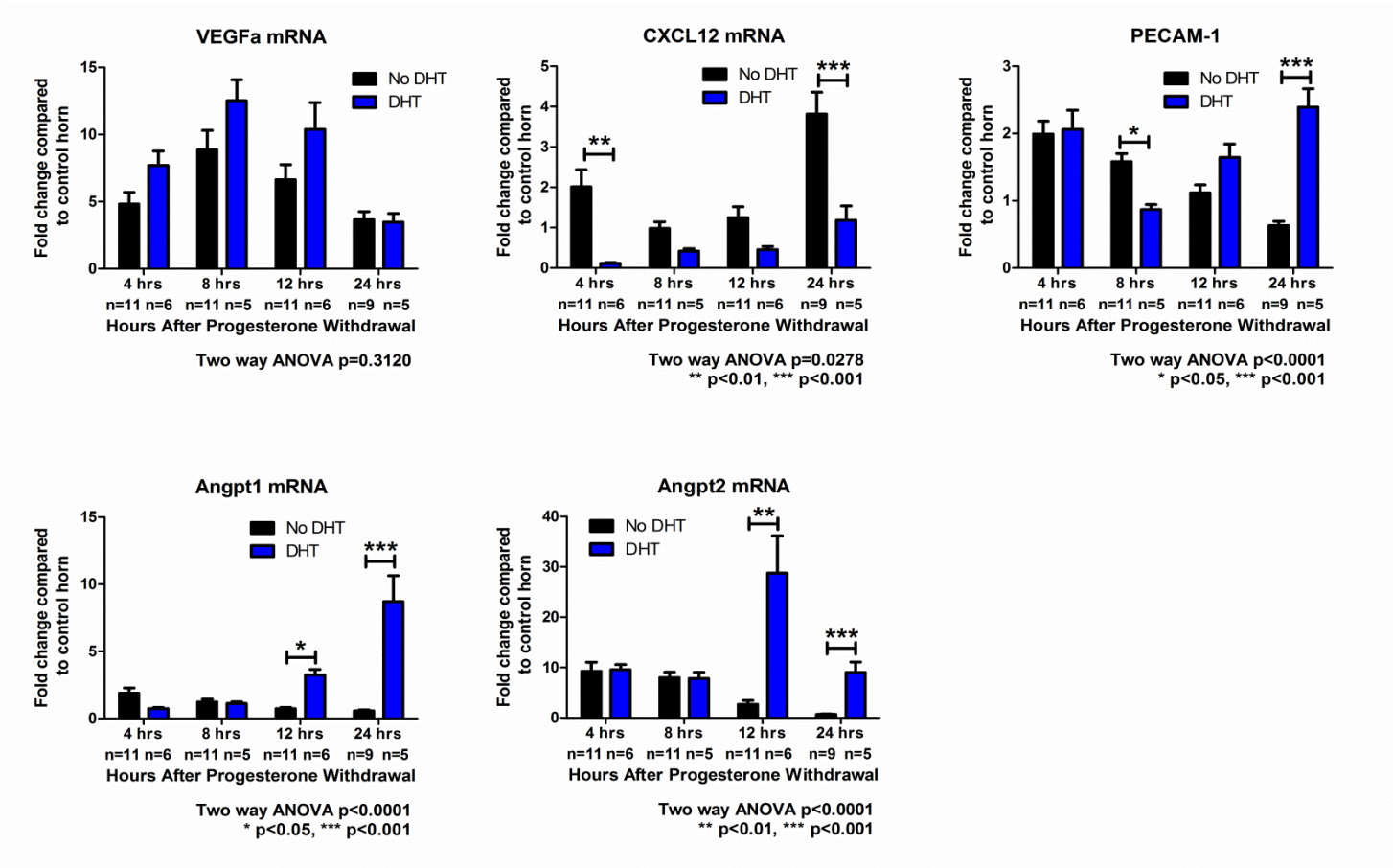

Figure 5-14: mRNA concentrations for candidate genes involved in angiogenesis; *Vegfa, Cxcl12, Pecam-1, Angpt1, Angpt2*. mRNA expression for both untreated and DHT treated horns was normalised against the 0 hour non-decidualised horn. Statistical analysis was performed by Two Way ANOVA and Bonferroni post hoc testing, where * p<0.05, ** p<0.01 and *** p<0.001.

5.3.8 Evidence for an effect of androgens on angiogenesis by array analysis

Additional evaluation of a role for androgens in vascular function was investigated using a PCR array that focuses on genes known to be involved in angiogenesis or vascular remodelling. The full gene list can be found in Supplementary Table 2. Samples from three time-points (0 hours, 8 hours and 24 hours) were studied as above. Those genes in which a significant change in fold regulation was observed are shown in Table 5-4, Table 5-5 and Table 5-6.

As previously noted using the EMT array, a lower number of significant gene changes were detected in uteri from mice that had been treated with DHT, (0 hours v 8 hours -DHT; 40 gene changes, 0 hours v 8 hours +DHT; 28 gene changes, 0 hours v 24 hours -DHT; 45 gene changes, 0 hours v 24 hours +DHT; 34 gene changes). In all cases the number of down-regulated genes exceeded that of the number of up-regulated genes at both time-points in the DHT group.

At the 8 hour time-point, similar fold changes were observed in both the 0 v -DHT and 0 v +DHT sets, for example angiopoietin 2 (*Angpt2*) ~5 fold decrease in -DHT and an ~6 fold decrease after DHT treatment. However, *Lect1* reported a 6 fold decrease in the untreated group but a 10 fold decrease in the +DHT group. Plasminogen (*Plg*) reported a 3 fold increase in the -DHT group but an 8 fold increase in the +DHT group.

Interestingly, at the 24 hour time-point differences appeared more striking between the -DHT and +DHT groups, suggesting that treatment with DHT at 0 hours exerted changes at the molecular level in a time-dependent manner.

When compared to the 0 hour reference sample, treatment with DHT appeared to reduce some responses to progesterone withdrawal; for example, *Angpt2* reported a 22 fold decrease in the -DHT group, but only a 2 fold decrease in the +DHT group; *Cxcl5* mRNA was reduced to a 2 fold increase in the DHT treated animals (10 fold increase in -DHT group); HIF2α (*Epas1*) was detected to decrease by 3.5 fold (~9 fold in the –DHT group); a 13 fold increase in *Tnf* was detected in the +DHT group; whilst a 24 fold increase had been reported in the -DHT set.

Stark differences were detected in relative changes in expression of *Lect1*, a 3 fold decrease detected in the 24 hour +DHT group (55 fold decrease in untreated samples) and *Mmp-9* was also differentially regulated, an ~7 fold increase was detected at 24 hours +DHT (28 fold increase in the -DHT set). Interleukin 1β was found to increase by 35 fold after the addition

of DHT however no significant change in fold regulation was detected in the -DHT set at the 24 hour time-point.

In direct time-point comparisons, (8 hours -DHT v 8 hours +DHT) only 5 genes were detected to be significantly different at 8 hours. All 5 genes were significantly up-regulated in the +DHT group. At the 24 hour time-point, (24 hours -DHT v 24 hours +DHT) 18 genes were differentially regulated in the DHT group compared to the -DHT time-point. *Angpt2, Lect1* and *Serpine1* were all up-regulated (8 fold, 16 fold and 5 fold respectively).

0hrs v 8hrs -DHT		
Gene Name	**p value**	**Fold Regulation**
Akt1	0.000137	-2.5842
Angpt2	0.00299	-4.9175
Bai1	0.048497	-2.5934
Cdh5	0.012848	-4.0682
Csf3	0.025896	2.5198
Cxcl1	0.004732	4.1928
Cxcl2	0.006045	4.4648
Efnb2	0.001374	-2.8566
Egf	0.005832	-3.4239
Eng	0.001554	-2.2298
Epas1	0.000331	-3.9733
Ephb4	0.00026	-1.8575
Erbb2	0.000141	-2.1867
Fgfr3	0.00048	-2.539
Flt1	0.009749	-1.804
Ifng	0.031845	-2.258
Igf1	0.000008	-3.1822
Il1b	0.00072	4.8631
Il6	0.041614	1.7567
Itgav	0.015424	-1.6608
Kdr	0.000342	-1.7111
Lect1	0.000234	-6.116
Mapk14	0.00171	-1.3964
Mmp9	0.001015	2.1744
Nos3	0.006183	-1.4661
Pecam1	0.0097	-1.5109
Plau	0.022668	2.7188
Plg	0.000315	3.5833
Ptgs1	0.000024	-1.6422
Ptk2	0.016074	-1.269
Sphk1	0.000006	-4.9733

0hrs v 8hrs +DHT		
Gene Name	**p value**	**Fold Regulation**
Akt1	0.000751	-1.5007
Angpt2	0.001059	-5.856
Cxcl1	0.022825	2.8975
Cxcl2	0.001759	5.4048
Edn1	0.000677	3.9095
Eng	0.001462	-1.5005
Epas1	0.002151	-2.6124
Ephb4	0.026111	-1.2138
Fgf6	0.041569	2.2572
Fgfr3	0.000333	-2.0865
Igf1	0	-3.7126
Il1b	0.008532	2.6909
Itgav	0.026512	-1.6079
Kdr	0.000029	-1.5762
Lect1	0.00015	-10.0228
Mapk14	0.004891	-1.4346
Mmp9	0.038474	1.8724
Nos3	0.006988	-1.4408
Plau	0.020667	2.1905
Plg	0.000746	8.048
Ptgs1	0.005573	-1.9106
Ptk2	0.001618	-1.429
Sphk1	0.000014	-5.9061
Tek	0.046092	-1.375
Tgfa	0.000035	-2.8412
Thbs1	0.021062	1.97
Tie1	0.002983	-1.3557
Vegfa	0.037623	1.6257
Number of genes significantly up-regulated		10
Number of genes significantly down-regulated		18

0hrs v 8hrs -DHT			0hrs v 8hrs +DHT		
Gene Name	**p value**	**Fold Regulation**	**Gene Name**	**p value**	**Fold Regulation**
Tek	0.000448	-1.4716			
Tgfa	0.000068	-3.4111			
Thbs1	0.010501	2.4701			
Tie1	0.006365	-1.4041			
Timp2	0.028328	-1.1885			
Tnf	0.003052	2.3139			
Vegfa	0.003885	2.1533			
Vegfb	0.038244	-1.2515			
Vegfc	0.004284	-1.8048			
Number of genes significantly up-regulated		11			
Number of genes significantly down-regulated		29			

Table 5-4: Significant changes in gene expression 8 hours after progesterone withdrawal in both the untreated (left) and DHT treated (right) groups. Gene changes are displayed as up- or down-fold regulation when compared to the 0 hour group, n=6.

0hrs v 24hrs -DHT			0hrs v 24 hrs +DHT		
Gene Name	**p value**	**Fold Regulation**	**Gene Name**	**p value**	**Fold Regulation**
Angpt1	0.046288	-1.7594	*Ang*	0.000879	3.8728
Angpt2	0.000001	-22.9351	*Angpt2*	0.004513	-2.7053
Ccl11	0.02758	2.2697	*Ctgf*	0.034871	2.3
Ccl2	0.032995	7.0443	*Cxcl5*	0.025513	2.7626
Cdh5	0.004155	-3.0425	*Edn1*	0.001502	12.8259
Csf3	0.01885	31.9636	*Efnb2*	0.001274	-2.7987
Ctgf	0.035697	1.9539	*Egf*	0.007205	-1.7551
Cxcl1	0.004845	56.8512	*Epas1*	0.000205	-3.5014
Cxcl5	0.001852	10.6539	*Ephb4*	0.012697	-5.1606
Edn1	0.006193	6.0435	*Erbb2*	0.000927	-1.8294
Efna1	0.043344	1.5754	*F2*	0.007101	2.8433
Efnb2	0.003062	-2.6326	*F3*	0.040744	2.9398
Egf	0.018678	-1.9777	*Fgf1*	0.014657	-1.9486
Eng	0.026026	-1.8363	*Fgfr3*	0.000086	-3.3566
Epas1	0.000012	-8.9365	*Igf1*	0.000141	-2.7399
Ephb4	0.041566	-1.7025	*Il1b*	0.045551	35.2507
F3	0.001286	4.2343	*Itgb3*	0.001196	2.1481
Fgfr3	0.000062	-3.4944	*Kdr*	0.008861	-1.6411
Flt1	0.006391	-2.0237	*Lect1*	0.001536	-3.0916
Hgf	0.006579	2.1842	*Mapk14*	0.00147	-1.6027
Igf1	0.000002	-3.1035	*Mmp9*	0.042146	6.8393
Il6	0.01492	1.9559	*Pgf*	0.000032	3.7586
Jag1	0.00324	1.6671	*Plau*	0.004478	4.2526
Kdr	0.00011	-2.471	*Plg*	0.000159	4.0777
Lect1	0.000004	-51.9476	*Ptgs1*	0.000002	-2.6375
Mapk14	0.011274	-1.4252	*Smad5*	0.043498	-1.4936
Mmp14	0.038408	1.4948	*Sphk1*	0.000005	-3.0822
Mmp9	0.00972	28.7339	*Tek*	0.022974	-1.5147
Nos3	0.003536	-2.0241	*Tgfa*	0.000008	-3.2086
Pdgfa	0.000588	2.8488	*Tgfb1*	0.026449	1.5808
Pecam1	0.000247	-2.0313	*Tgfb2*	0.007811	-1.4944
Plau	0.007907	3.6989	*Thbs1*	0.024226	3.0517

0hrs v 24hrs -DHT		
Gene Name	**p value**	**Fold Regulation**
Plg	0.00004	4.7103
Ptgs1	0.000002	-2.6514
Ptk2	0.013642	-1.5107
S1pr1	0.000788	-1.6036
Sphk1	0	-11.2585
Tek	0.010909	-2.0434
Tgfa	0.000001	-6.0818
Tgfb2	0.000026	-2.7031
Tgfb3	0.025882	-1.9838
Thbs2	0.000037	4.5008
Tie1	0.00304	-2.1991
Timp1	0.040893	-1.9155
Tnf	0.003514	24.461
Number of genes significantly up-regulated		19
Number of genes significantly down-regulated		26

0hrs v 24 hrs +DHT		
Gene Name	**p value**	**Fold Regulation**
Tnf	0.007213	13.5483
Vegfa	0.000016	3.0398
Vegfc	0.003747	-1.8746
Number of genes significantly up-regulated		16
Number of genes significantly down-regulated		19

Table 5-5: Significant changes in gene expression 24 hours after progesterone withdrawal in both the untreated (left) and DHT treated (right) groups. Gene changes are displayed as up- or down-fold regulation when compared to the 0 hour group, n=6.

8hrs -DHT v 8 hrs +DHT		
Gene Name	**p value**	**Fold Regulation**
Akt1	0.044221	1.8404
Efna1	0.02319	2.7301
Ephb4	0.028451	1.6355
Flt1	0.032444	1.4924
Plg	0.033616	2.4004
Number of genes significantly up-regulated		5
Number of genes significantly down-regulated		0

24hrs -DHT v 24hrs +DHT		
Gene Name	**p value**	**Fold Regulation**
Ang	0.049399	2.9463
Angpt2	0.022478	8.3268
Cxcl5	0.026708	-3.9265
Epas1	0.020464	2.5068
Hgf	0.017917	-2.2119
Itgb3	0.012049	2.0497
Jag1	0.029383	-2.124
Lect1	0.009679	16.5037
Nos3	0.035013	1.8536
Pecam1	0.038112	1.7283
S1pr1	0.002801	1.7741
Serpine1	0.006237	5.0798
Sphk1	0.000068	3.5877
Tgfa	0.007621	1.8617
Tgfb2	0.020672	1.7766
Thbs2	0.025847	-3.2965
Timp1	0.023128	2.6099
Vegfa	0.003424	3.3824
Number of genes significantly up-regulated		14
Number of genes significantly down-regulated		4

Table 5-6: Significant changes in gene expression when DHT groups are directly compared to their own untreated time-points at 8 hours (left) and 24 hours (right). Gene changes are displayed as up- or down- fold regulation when compared to the 0 hour group, n=6.

5.3.8.1 Network analysis of array and qRTPCR data

To investigate a possible role for direct regulation by androgens through the AR during angiogenesis, the full gene list, qRTPCR candidates and AR were input into MetaCore™ software to generate a network of known genes interacting with AR (Figure 5-15).

The network analysis highlighted MMP-9 as a possible downstream target of the AR, which would be consistent with the difference in fold regulation that was detected at the 24 hour time-point in the -DHT (28.3) and DHT group (6.83). Network analysis also highlights that

the AR may have an activatory effect on VEGFa, consistent with a 3 fold increase observed at the 24 hour time-point in the array.

Notably, those genes which were detected to have large differences in fold regulation after the addition of DHT, (*Lect1, Plg, Angpt2, Il1β, Tnf*) were absent from the network and therefore may not be directly regulated by androgens acting via direct binding of the AR to regulatory sequences in their promoters. Direct or indirect regulation would need to be confirmed by chromatin immunoprecipitation (chIP) or other methodology. These genes, *Lect1, Plg, Angpt2, Il1β, Tnf*, were all highlighted for further investigation and a role for these genes in AR-regulated tissue repair is discussed in section 5.4.3.1.

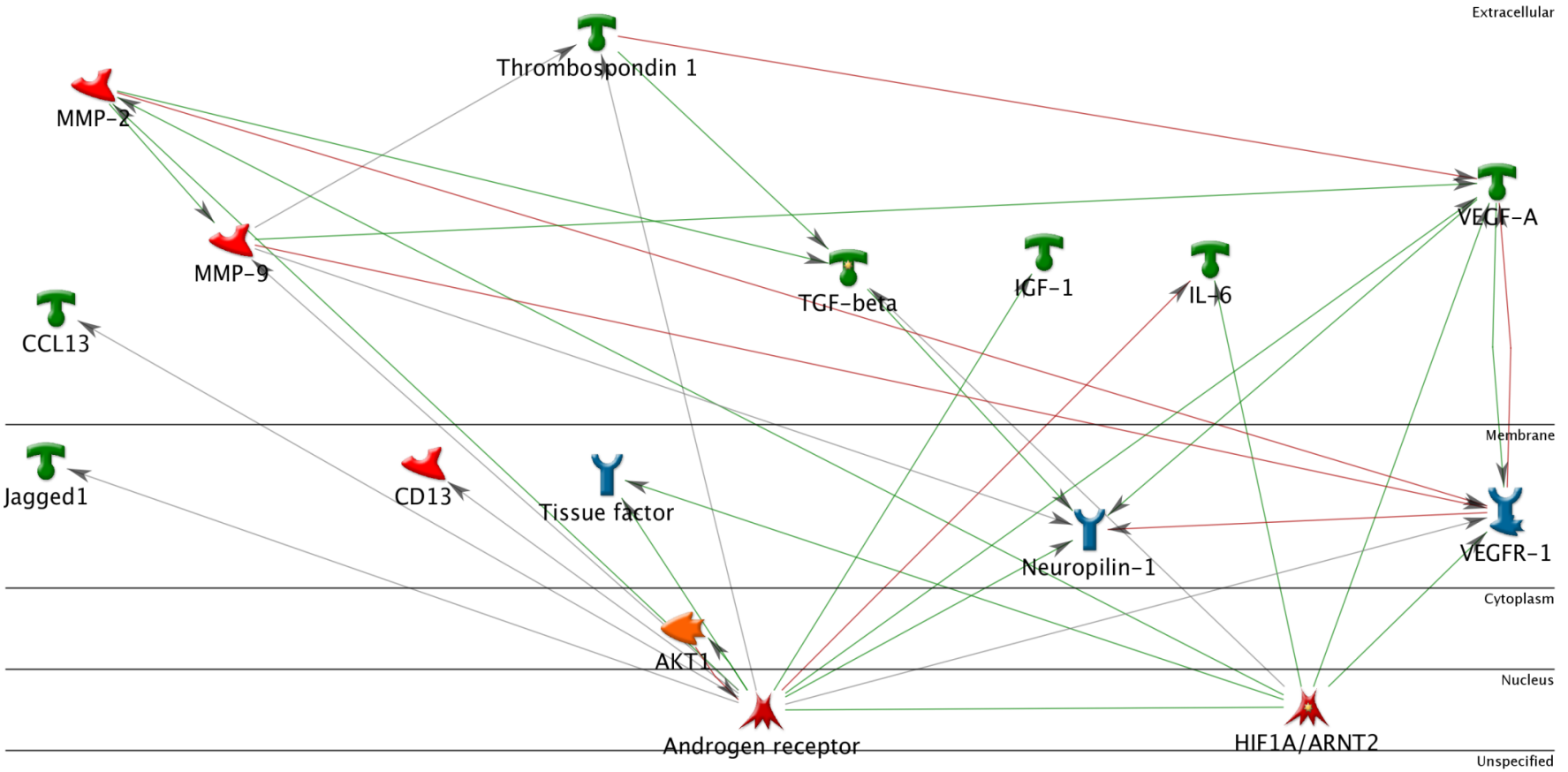

Figure 5-15: Known interactions of genes from the array that are downstream of the androgen receptor. Arrows indicate direct effects on other genes in the pathway. Green arrows indicate activation, whereas red arrows show inhibitory action. Pathway generated using MetaCore™ software.

5.3.9 Evidence that DHT alters factors associated with tissue breakdown and repair

To determine whether treatment with DHT had an effect on mechanisms that contribute to repair of the endometrium, additional qRTPCR was conducted to measure mRNAs for factors previously identified as being associated with wound healing and tissue remodelling (Figure 5-16).

In untreated (no DHT) tissues, mRNA concentrations of *Smad3*, previously shown to be involved in wound healing, did not change over the window of breakdown and repair (not shown). However, treatment with DHT resulted in an increase in total *Smad3* mRNA concentrations at each time-point with significant up-regulation observed at 8 hours ($p<0.001$) and 12 hours ($p<0.001$). The highest mRNA concentrations for *Smad3* were detected at the 8 hour time-point, by 24 hours they were no different to the untreated samples.

Striking changes were detected in mRNA concentrations of connective tissue growth factor (*Ctgf*) in response to DHT treatment, with 20-40 fold increases observed when compared to untreated tissues at all time-points (4 hours; $p<0.001$, 8 hours; $p<0.001$, 12 hours; $p<0.001$ and 24 hours $p<0.01$). Similarly to *Smad3* the highest mRNA concentration for *Ctgf* was at 8 hours, concentrations then decreased at 12 and 24 hours.

In contrast, mRNA concentrations for *Pdgfrb* were strikingly down-regulated at every time-point. In contrast to the untreated horns, where mRNA concentrations were increased at 24 hours, *Pdgfrb* was down-regulated at the 8 hour time-point ($p<0.001$) and concentrations remained low at 12 hours ($p<0.05$) and 24 hours ($p<0.001$). *Mmp-3* mRNA concentrations were also down-regulated at 24 hours ($p<0.01$) in comparison to their untreated group.

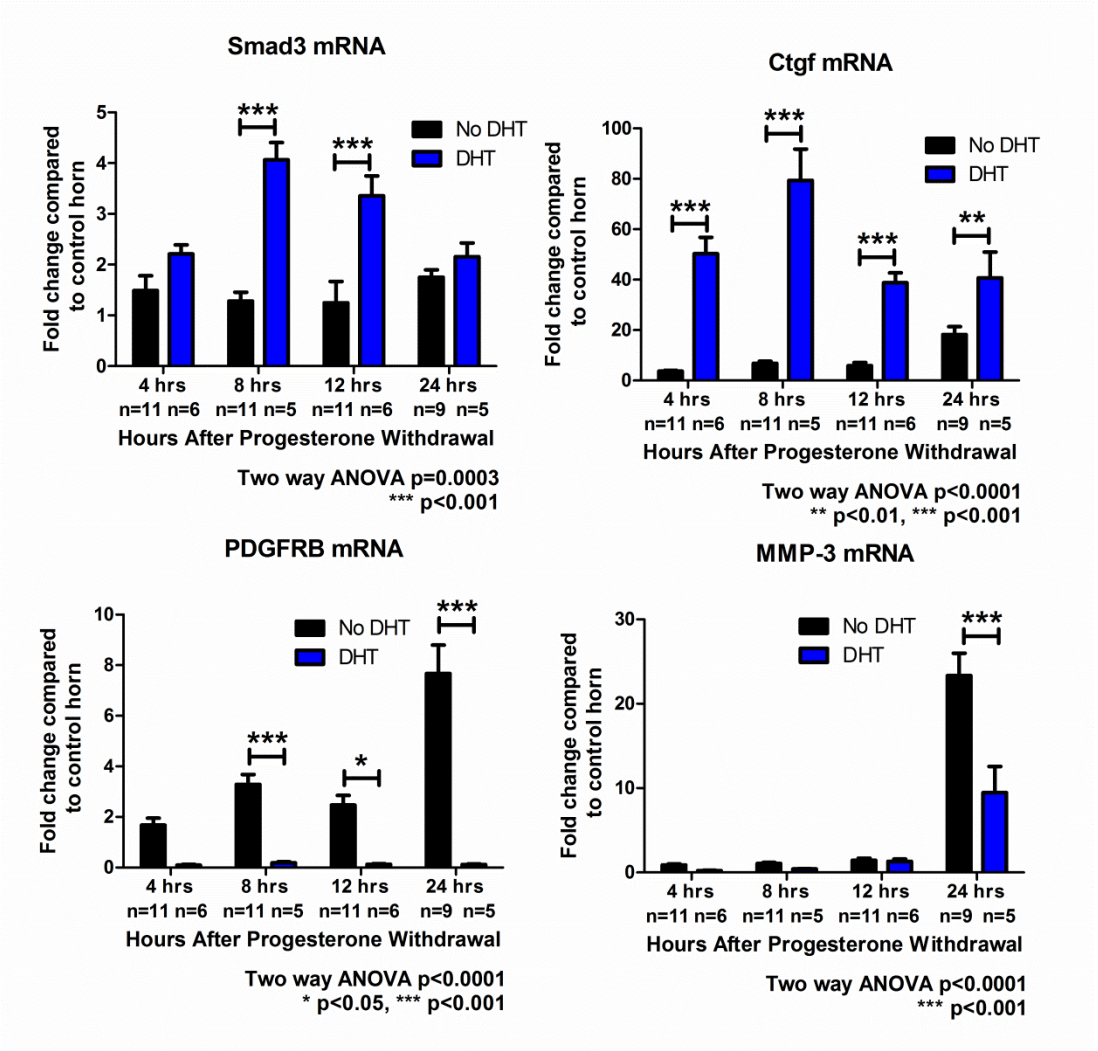

Figure 5-16: mRNA concentrations for candidate genes involved tissue remodelling; *Smad3, Ctgf, Pdgfrb, Mmp-3*. mRNA expression for both untreated and DHT treated horns was normalised against the 0 hour non-decidualised horn. Statistical analysis was performed by Two Way ANOVA and Bonferroni post hoc testing, where * p<0.05, ** p<0.01 and *** p<0.001.

5.4 Discussion

5.4.1 Administration of a single dose of DHT results in changes to normal tissue breakdown

In our refined mouse model, a single dose of DHT at the time of progesterone withdrawal was able to delay the onset of breakdown, whilst also delaying repair of the tissue, as evidenced by a delay in detachment of the functional layer from the underlying stroma (Figure 5-6).

5.4.1.1 DHT maintains the decidual response

The observation that DHT delayed the onset of breakdown of the tissue would be consistent with reports that androgens can alter decidual cell function and in mice will maintain the decidual response in the absence of progesterone (96, 146, 504). A role for androgens in maintenance of pregnancy (maintenance of the deciduoma) has been studied both *in vivo* and *in vitro* (96, 146, 504, 510). For example, in an *in vivo* mouse model, decidualisation following artificial stimulation was maintained by DHT in the absence of progesterone, this effect of DHT was abolished by the addition of flutamide (an AR antagonist) indicating that DHT was acting through the AR (146). *In vitro* studies using primary human endometrial stromal cells (hESCs) have also highlighted a role for androgens in decidualisation. Decidualisation can be induced in hESCs *in vitro* following treatment with 8-bromoadenosine 3'-5'-cyclic adenosine monophosphate (8-Br-cAMP) and progesterone. Addition of DHT, enhances the decidual response of these cells by increasing secretion of decidual marker prolactin (504).This increase in prolactin is consistent with data from our model where mRNA concentrations for prolactin (*Prl8*) were increased and levels maintained across the breakdown and repair window in the DHT treated animals (Figure 5-3).

The effects of DHT on decidualised stromal cell morphology have been investigated by transmission electron microscopy (TEM) (510). Decidualised stromal cells treated in combination with progesterone and DHT are reported to develop intracellular organelles, form lipid droplets and display cytoplasmic expansion, in comparison to decidualised stromal cells treated with progesterone only (510). This may account for the morphological differences in the uterine tissue between the untreated and DHT treated animals at the earlier time-points of 4 and 8 hours (Figure 5-5).

Maintenance of the decidual response, and therefore delay in breakdown, may also involve inhibition of apoptosis. Androgens have been proposed to play an anti-apoptotic role in the development of prostate cancer, as evidenced in *in vitro* models of the disease (536–538). A recent study has identified an anti-apoptotic role for DHT in the endometrium (144). When apoptosis was induced in primary endometrial stromal fibroblasts *in vitro*, DHT significantly reduced caspase activation (144). Further investigation, using our model, into genes that regulate apoptosis would complement the data reported; immunostaining for apoptotic markers such as caspase 3 would also determine if apoptosis is delayed in the DHT treated animals.

Injection of DHT at the time of progesterone withdrawal resulted in some significant changes in gene expression which were particularly striking at the 8 hour time-point. Notably, expression of genes associated with epithelial cell proliferation and adhesion (*Spp1*, integrinβ1) were down-regulated when compared to the control. In contrast, Snail and Slug, both of which are known to regulate EMT, were up-regulated following treatment with DHT which might have contributed to repression of E cadherin expression. An up-regulation of Notch at the 8 hour time-point (8 hours- DHT v 8 hours +DHT) may also contribute to active EMT. Activation of Notch is associated with tumour cell migration, and has been shown to regulate hypoxia-mediated tumour cell migration (539) in cervical, colon and ovarian cancer cell lines *in vitro.* Androgenic regulation of EMT has not previously been investigated in the endometrium.

Interestingly, a number of striking differences were detected in genes associated with cell morphology at the 8 hour time-point in animals treated with DHT. Cell adhesion molecule integrinβ1 was down-regulated by 36 fold, consistent with the phenotype of the decidualised cell mass at this time (Figure 5-6), where the tissue shows the beginning of breakdown next to areas of intact decidualised stroma. DHT has been previously shown to down-regulate cell adhesion molecules in *in vitro* models of prostate cancer (540, 541), whilst also activating Snail (542) which promotes cancer invasion and metastasis. Regulatory molecules for cell migration, cell shape and cellular remodelling were also down-regulated at the 8 hour time-point suggesting that DHT maintains the decidualised phenotype by inhibiting these molecules. This may result in an overall suppression of cellular remodelling that would normally occur in the absence of progesterone.

5.4.2 DHT has an effect on "normal" tissue repair mechanisms

MMPs play an integral role in endometrial tissue breakdown during menses as well as in tissue remodelling during repair phases (82, 224, 439, 543, 544). The addition of a single dose of DHT resulted in dramatic differences in concentrations of *Mmp-3 and Mmp-9* mRNAs in treated and untreated animals (*Mmp-3*; 61 fold v 9 fold; *Mmp-9*; 28 fold v 6 fold) at the 24 hour time-point. *Mmp-3* mRNA concentrations were further investigated by qRTPCR, which indicated that the addition of DHT decreased mRNA concentrations at 4, 8 and 24 hours relative to those females not exposed to DHT. In DHT treated animals mRNA concentrations of *Mmp-3* began to increase at 12 hours, with the highest concentration detected at 24 hours, where the beginnings of breakdown had been observed. However, concentrations were not as high as in untreated animals. This DHT induced decrease in MMP activity would be consistent with the observed delay in first the breakdown, and then

the detachment, of the endometrium by the 24 hour time-point in the DHT treated animals (Figure 5-). Differential regulation of MMPs by androgens have been reported in other tissues; in the prostate, expression of MMP-2 and MMP-13 are induced by androgens (545, 546); whilst in vascular smooth muscle cells DHT inhibits MMP-2 activity (547); whilst in the skin MMP-2 and MMP-9 were decreased at lower serum androgen concentrations (548). Network analysis by MetaCore™ identified both MMP-2 and MMP-9 as being potentially downstream of the androgen receptor, suggesting direct regulation of these genes although further studies are required to validate this in uterine cells.

Administration of DHT did not appear to affect the number of macrophages in the uterus observed at any time-point (not shown), however the function of macrophages may have been indirectly affected by DHT acting on adjacent cell types. For example, as detailed in section 4.4.1.3, macrophages have been reported to secrete factors such as tumour necrosis factor, osteopontin and VEGF (440, 452, 457), all of which were down-regulated in the +DHT group when compared to the -DHT group. Therefore, DHT may not have an effect on macrophage proliferation or recruitment but may inhibit secretion of factors that contribute to breakdown and repair of the tissue.

The skin itself is a site of androgen synthesis, and a role for androgens in cutaneous wound repair has been investigated (549–551). Much like the repair of the endometrium, cutaneous wound repair involves infiltration of immune cells, tissue remodelling and re-epithelialisation (552–554). A study using an AR knock-out mouse line, reported accelerated cutaneous wound healing, suggesting that AR suppresses wound healing activity (549). Furthermore, the authors report that in macrophage-specific AR knock-out mice healing and tissue remodelling were accelerated whilst re-epithelialisation was unaffected highlighting the potential for differential regulation of these two processes. Inhibition of 5α reductase accelerates cutaneous wound healing and leads to decreased inflammation in mice, implicating a role for DHT in delaying repair (551).

In the current study, a number of factors previously implicated in wound repair were investigated. Increased mRNA concentrations for *Smad3* were observed at all DHT treated time-points, this is consistent with a previous report, where Smad3 null mice exhibit accelerated cutaneous wound healing in comparison to wild type mice (555). Platelet derived growth factor beta (PDGFRβ) has also been proposed as a key regulatory factor in cutaneous wound repair (556, 557). A study in a mouse model, in which the activity of PDGFRβ was inhibited by imatinib mesylate, revealed a delay in wound closure and a decrease in collagen synthesis (556). This would be consistent with data reported in this chapter where mRNA

concentrations for collagens 1a2, 3a1 and 5a2 were significantly lower in the +DHT group compared to the -DHT group at 8 hours (Table 5-3), a time-point where *Pdgfrb* was also down-regulated in the +DHT set (Figure 5-16). In an *in vitro* model using *Cre* recombinase transfection, to knock out PDGFRβ from dermal fibroblasts, depletion of PDGFRβ led to a decrease in cell proliferation and migration (557). In the current study, the addition of DHT resulted in a significant decrease in mRNA concentrations for *Pdgfrb* at 8, 12 and 24 hours, suggesting that androgens may be suppressing PDGFRβ-mediated tissue repair, something that merits further investigation.

5.4.3 Androgens and angiogenesis

In our mouse model the decidualised cell mass is made up of decidualised stromal fibroblasts, immune cells and a proliferating vascular compartment (as demonstrated in

Overleaf, Figure 4-13). However, murine endometrial endothelial cells do not express androgen receptor (Simitsidellis, unpublished) which may suggest that DHT will not have a direct effect on endothelial cells in our model. DHT has also been shown to have no effect on the network formation of human endometrial endothelial cells *in vitro*, suggesting that androgens may not regulate endothelial cell migration or proliferation (Greaves, unpublished). However, as a number of genes in the angiogenesis array were differentially regulated by treatment with DHT in our mouse model, we suggest that DHT indirectly regulates endothelial cell stability rather than promoting proliferation and migration. DHT may act on AR positive stromal cells that may secrete angiogenic factors that promote endothelial cell stability. DHT mediated endothelial stability would also account for the delay in breakdown in DHT treated animals. Vessel stability is normally weakened upon progesterone withdrawal; therefore we propose a role for DHT in maintenance of the decidual stroma by promoting vessel stability. In support of this, mRNA concentrations of *Vegfa* and *Ctgf* were increased at 8 hours after treatment with DHT; both factors have been implicated in endothelial cell dynamics (558–560).

5.4.3.1 Direct or indirect regulation by androgens

Promoter regions of potential AR target genes, identified from the arrays, were assessed for putative transcription factor binding sites (TFBS) to investigate direct or indirect regulation by androgens. Using bioinformatic software (Mapper CHIP Bioinformatics (561)), promoter regions of candidate genes were investigated for the presence of consensus binding sites for specificity protein-1 (Sp-1) or activator protein-1 (Ap-1), as well as the androgen response element (ARE) outlined in Table 5-7.

Of the 27 genes investigated, 15 contained a potential ARE in their promoter, 22 had a Sp-1 site and only 3 had an Ap-1 site. Interleukin 1b (*Il1b*), plasminogen (*Plg*) and Angiopoietin 1 (*Angpt1*) did not contain either an ARE, Sp-1 or Ap-1 site despite a significant change in their expression after the addition of DHT and therefore may be indirectly regulated by androgens through another transcription factor, such as NFκB or via a more distant enhancer element (562, 563). The data gathered from the MAPPER search is by no means definitive and further analysis by chromatin immunoprecipitation (chIP) would be necessary to confirm whether AR is capable of direct binding or activation of gene expression.

Gene Name	Androgen Response Element	Sp-1 site	Ap-1 site
Angpt1	0	0	0
Angpt2	1	1	0
Col3a1	0	1	0
Ctgf	1	2	0
Cxcl12	1	5	0
Hif2α/Epas	1	4	0
Il1b	0	0	0
Itgb1	1	6	0
Krt19	2	7	0
Krt7	2	4	0
Lect1	0	2	0
Mmp-2	0	2	0
Mmp-3	1	0	1
Mmp-9	0	5	2
Notch	1	4	0
Pdgfrb	0	1	2
Plg	0	0	0
Rgs2	2	4	0
Smad3	0	3	0
Snai1	0	2	0
Snai2	1	0	0
Snai3	1	5	0
Spp1	1	2	0
Tnf	1	1	0
Vegfa	0	1	0
Wnt11	0	1	0
Wt1	1	3	0

Table 5-7: Putative transcription factor binding sites in the promoters of candidate genes in the mouse. Analysed using Mapper CHIP Bioinformatics (561).

5.4.4 Androgens as a self-limiting factor in "normal" endometrial function

Previous animal models of endometrial breakdown focussed solely on the contributions of oestradiol and progesterone in normal endometrial function, despite reports of relatively constant serum androgen levels across the human menstrual cycle (44, 45). In

ovariectomised mouse models only oestradiol and progesterone are replaced by exogenous injection or implant and to date no androgens have been administered, despite mice adrenals lacking 17α hydroxylase (CYP17) which means mice are unable to synthesise androgens. In ovariectomised macaque models of menses, oestradiol and progesterone are administered to induce artificial menstrual cycles. However, the effect of exogenous oestradiol and progesterone on adrenal androgen production has not been considered, despite recent data that demonstrates exogenous hormones increase adrenal secretion of DHEA and DHEAS in macaques in comparison to intact controls (564), which may have an effect on the endometrium during the artificial menstrual cycles.

The refined mouse model of breakdown described in this study exhibits rapid shedding, with re-epithelialisation complete, or almost so, by 24 hours after the withdrawal of progesterone. Previous studies have reported that uterine horns have returned to an ovariectomised, steroid depleted morphology by 48 hours (230, 233, 239). The addition of a single dose of DHT was enough to delay the onset of breakdown, and extend the breakdown phase, such that by the 24 hour time-point 100% of mice were bleeding (Figure 5-2), suggestive of a delay in the onset of repair mechanisms. Collection of tissues at later time-points (28, 32, 36 hours after progesterone withdrawal) would determine whether androgens also had an impact on the length of the bleed and therefore initiation of repair. Treating mice with tritiated DHT, would also allow analysis of the clearance of DHT by radioimmunoassay, to determine whether DHT could still be having an effect at the later time-points. It is important to consider, however, that peripheral concentrations of DHT are not a good measure of target tissue concentrations (565).

Despite these results suggesting that androgens such as DHT may delay onset of bleeding, and ultimately impact on repair processes, it is also possible that androgens normally present in women as a result of adrenal/peripheral site biosynthesis may play a role in limiting the severity of tissue destruction upon progesterone withdrawal. The most recent data shows that endometrial shedding occurs in a piecemeal process (169), with scanning electron microscopy of menstrual phase endometrium showing areas of shed tissue adjacent to areas of intact epithelium. Therefore, it is possible to speculate that circulating androgens at the time of menses may, in part, modulate the breakdown of the endometrium through regulation of MMPs to limit tissue destruction and through anti-apoptotic mechanisms to stabilise sections of the tissue. Also, it is possible that androgens may regulate immune cell dynamics and secretion of factors which contribute to digestion and breakdown of the functional layer

of the tissue. Thus, this "self-limiting" regulation may regulate the severity of breakdown and reduce blood loss.

5.4.5 Summary

In the current study, using our refined mouse model of endometrial breakdown and repair, a role for androgens during endometrial repair was investigated.

The addition of DHT at the time of progesterone withdrawal resulted in a delay in the onset of breakdown, whilst also delaying repair. Analysis of genes known to be involved in EMT and MET were investigated by a PCR array, dynamic changes were observed at both the 8 hour (breakdown) and 24 hour (repair) time-points after DHT treatment. An up-regulation in known EMT regulator Snail was observed at all time-points, whilst Slug was up-regulated at 12 hours, whilst cell adhesion markers such as integrinβ1 and osteopontin were down-regulated. MMPs, involved in breakdown, were also significantly down-regulated, as were a number of factors involved in wound repair.

Potential AR target genes were investigated for putative transcription factor binding sites to investigate direct or indirect regulation by androgens, however further analysis by chIP is necessary to confirm direct activation of gene expression.

From the results presented in this chapter it is evident that androgens (DHT) have an effect on endometrial function. However, the full impact of androgens on endometrial function and a possible role in endometrial pathologies including HMB awaits further elucidation.

Chapter 6 Final Discussion

6.1 Introduction

The human endometrium is a highly complex, multi-cellular tissue that lines the uterine cavity. The endometrium can be divided into two layers; the upper, functional layer and the underlying basal layer that is attached to the muscular myometrial layer. The luminal surface of the tissue is composed of a layer of epithelial cells, underneath of which is the multi-cellular stromal cell compartment that is composed of stromal fibroblasts, blood vessels lined by endothelial cells, and an immune cell population which contains macrophages, neutrophils and uterine natural killer cells. In women of reproductive age, the functional layer of the endometrium undergoes dynamic tissue remodelling in response to ovarian-derived sex steroid hormones, to maintain endometrial receptivity for the possible implantation of a blastocyst. Well defined phases of endometrial function have been described including; the oestrogen-dominant proliferative phase and the progesterone-dominant secretory phase which prepares the tissue for a possible pregnancy. In the absence of a blastocyst, progesterone levels fall which results in breakdown and clearance of the functional layer of the endometrium during menses. The endometrium undergoes tightly controlled remodelling resulting in a healed, scar-free tissue ready for the next cycle.

Endometrial repair occurs concurrently with tissue breakdown (148), at a time when both oestradiol and progesterone levels are low, termed a "steroid-depleted" environment. Although mice do not spontaneously decidualise or menstruate, regulation of uterine function mirrors that in women with cyclical episodes of proliferation. In addition, artificial "menstrual" cycles can be induced in the mouse (234), making mouse models an attractive model for studying aspects of endometrial function relevant to women's health. Notably, endometrial repair was reported to occur in the absence of oestrogen in a mouse model of endometrial breakdown (239). To date, mouse models have been used to study a number of factors involved in endometrial breakdown and regeneration (79, 188, 217, 230, 233, 235, 239, 318–320, 368), however these models have not considered simultaneous breakdown and repair, instead focussing on time-points where breakdown has already occurred and therefore these studies have investigated a later stage of repair.

The mechanisms that drive endometrial repair during this steroid-depleted state are not fully understood but contributions from the underlying basal glandular epithelium and the basal stromal cell compartment as two possible sources of new luminal epithelial cells have been suggested. Furthermore, despite low circulating levels of oestrogens and progesterone in

women, androgens are maintained across the cycle and therefore may contribute to repair of the tissue, either directly or following metabolism to other steroids.

In the current study we set out to challenge a number of dogmas that surround the study of endometrial function, by asking the following questions.

1. Is it possible to establish a model of menses in the mouse, which mimics menses in women, namely; can we model simultaneous breakdown and repair, overt menstruation, immune cell influx, tissue necrosis and re-epithelialisation?
2. Does the stromal cell compartment contribute to endometrial regeneration?
3. Is there a role, if any, for androgens during endometrial repair?

We hypothesised that a combination of mechanisms will contribute to re-epithelialisation and remodelling of the endometrium during the repair phase. We suggest that epithelial cell proliferation will occur but the stromal cell compartment will also contribute to repair, either directly through mesenchymal to epithelial transition of stromal fibroblasts or indirectly by factors produced by immune cells including tissue resident macrophages.

6.2 Key findings

6.2.1 Endometrial breakdown and repair can be broken down into three key phases

In Chapter 3, a previously described mouse model of menses (233) was refined in order to develop a model that more closely mimics menses in women. A number of novel findings were identified using our refined model. Firstly, collection of uterine tissues at time-points earlier than those previously published identified an “early” window of repair, one where both breakdown and repair mechanisms were initiated. Immunohistological and molecular analysis identified three phases of the repair process; tissue stabilisation, tissue restoration and tissue remodelling (outlined in Table 6-1).

4-8 hours PW/D	12 hours PW/D	24 hours PW/D onwards
Circulating progesterone falls to ~30%	Circulating progesterone falls to ~25%	Circulating progesterone falls to ≤10%
Stromal cell proliferation in basal layer	Increased epithelial cell proliferation	Basal gland epithelial cell proliferation
Endothelial cell proliferation in decidualised cell mass (4 hours)	Apoptotic shed cells.	Apoptotic shed cells
Exposed blood vessels adjacent to lumen (8 hours)	Blood vessels appear "sealed"	Endothelial cell proliferation in basal layer
Hypoxia localised to decidualised cells; increase in hypoxia-regulated VEGF	Hypoxia localised to shed cells and luminal epithelium	Hypoxia localised to shed cells and luminal epithelium
Increase in stromal cell markers	Decrease in stromal markers, increase in epithelial markers	Increase in epithelial markers
Genes associated with EMT up-regulated	Switch in markers associated with EMT to MET	Genes associated with MET up-regulated
MMPs suppressed by progesterone	Increase in MMPs associated with tissue breakdown	Increase in MMPs associated with tissue remodelling
Macrophages are identified in the decidualised stroma	Macrophages are associated with the luminal epithelium	Increase in no. of macrophages, localised to luminal epithelium & stroma
		Potential pericyte activation
Conditions favour stromal cell compartment	Stromal → Epithelial switch	Conditions favour epithelial cell compartment
Tissue Stabilisation	**Tissue Restoration**	**Tissue Remodelling**

Table 6-1: Three phases of endometrial breakdown and repair in a mouse model of menses. PW/D; progesterone withdrawal

6.2.2 Tissue stabilisation controls breakdown and initiates repair

Endometrial breakdown occurred within 4 hours of the withdrawal of progesterone, consistent with a 70% decrease in serum progesterone concentrations and evidence of blood in the vaginal smear. This is the first study to report breakdown and bleeding within 4 hours, suggesting that the mechanisms contributing to tissue breakdown are tightly regulated by progesterone and that the rapid fall in serum progesterone levels trigger initiation of tissue destruction. In a previously published mouse model of menses, a critical period of progesterone withdrawal precedes endometrial breakdown (235), this finding supports studies in the macaque (356) and the human (164, 566). In the mouse, replacement of progesterone after 12-16 hours was sufficient to reverse the effects of progesterone withdrawal. However, the authors do not report any evidence of endometrial bleeding until 12 hours after the withdrawal of progesterone, despite a reported drop in progesterone concentrations from ~128ng/ml to ~14ng/ml in the first 8 hours (235). Therefore, it is not the drop in progesterone that must trigger breakdown but a minimal threshold, once the level has dropped below it, recovery is not possible. For example, in our model, circulating progesterone concentrations are maximal prior to progesterone pellet removal at ~12ng/ml, bleeding is recorded at 4 hours when progesterone concentrations are ~3ng/ml. Therefore it is likely in our model that progesterone would have to be replaced by 4 hours to prevent the degree of tissue destruction observed at our 8 hour time-point.

In the first 8 hours after progesterone withdrawal, a large number of stromal cells in the basal compartment were positive for BrdU, indicative of stromal proliferation. In addition, endothelial cell proliferation in the decidual cell mass was also detected. Stromal cell markers and genes associated with EMT were increased as well as induction of hypoxia across the decidualised cell mass. The molecular and cellular dynamics observed at 4-8 hours after the withdrawal of progesterone suggest that the stromal cell compartment is favoured over the epithelial compartment. We believe that the molecular and cellular mechanisms that occur during this time frame (up to 8 hours after the withdrawal of progesterone), in response to falling progesterone concentrations, stabilise the tissue in preparation for endometrial shedding so that only the functional layer of the endometrium is shed. Shedding of the basal layer of the endometrium has been linked to the establishment of lesions in the pathology of endometriosis (567) and the mechanisms by which the endometrium only sheds its functional layer are unknown.

As the decidualised functional layer sheds, it is possible that it secretes factors that initiate repair. In our mouse model, progressive shedding of the decidualised functional stroma was

observed (8 hours after progesterone withdrawal); in addition to this, residual round luminal epithelial cells were observed to be lining the lumen adjacent to sites of newly exposed endometrium. We postulate that as the endometrium detaches from the underlying basal stroma, it secretes factors that promote repair. A study by Gaide-Chevronnay *et al.,* on human tissues, supports a role for the degenerating endometrium supporting its own repair; an increase in leukocyte chemokines, extracellular matrix (ECM) proteins and enzymes involved in prostaglandin synthesis were detected in the functional layer of menstrual phase tissue (462). Furthermore, an SEM study by Garry *et al.,* observed that immediately after shedding, a fibrinous matrix appears to "seal" the endometrium prior to re-epithelisation (148). In support of this finding a previous mouse model of breakdown has shown that extra-cellular matrix proteins were detected to be increased at the time of repair and were localised to the luminal edge of the uterine horn (79). We suggest that the shed material in our newly refined model may be supporting endometrial repair by secreting factors that promote the establishment of the ECM. The degenerating stroma is hypoxic and hypoxia has been shown to regulate immune cell function, and therefore may mediate macrophage migration to endometrium during remodelling (492, 496).

A role for the degenerating functional stroma in endometrial repair has not been widely studied. Although, it is tempting to speculate that it may play a role in the pathology of endometrial disorders. For example, women with heavy menstrual bleeding may have a dysfunctional stroma that does not secrete repair factors, resulting in delayed repair and a longer bleed. Or, in women with endometriosis, the functional layer could promote its own survival by secreting factors that enable establishment of lesions, such as ECM proteins, and therefore the dissociated, shed tissue observed in our model warrant further study.

Consistent with studies in human tissues, or in human cells *in vitro*, the cellular changes observed in our model by 8 hours are similar to those seen in women within the first 24 hours of progesterone withdrawal (148, 193, 237, 439, 544); where hypoxia-induced up-regulation of VEGF is observed (193), MMPs are still low (439, 544) and the beginnings of breakdown can be seen (148, 237).

6.2.3 Initiation of early repair mechanisms contributes to tissue restoration

By the 24 hour time-point, blood was not detected in the vaginal smear of any of the animals investigated. However, endometrial-like tissue was detected in the lumen of these animals upon dissection. These mice were considered to have ceased bleeding by this time, which suggests that stabilisation of the blood vessels in the underlying basal layer had occurred. Interestingly, as re-epithelialisation of the uterine horn was not observed in every animal at

this time-point, we suggest that vessel stabilisation occurs rapidly to reduce blood loss preceding completion of re-epithelialisation. This finding is consistent with SEM studies in menstruating women, where blood vessels appeared to be "sealed" prior to re-epithelialisation of the uterine surface (148).

In our model, tissue restoration was associated with an increase in epithelial cell proliferation and MMP expression. The decidualised functional stroma was apoptotic (detected by caspase 3, not shown) and was detected to no longer express steroid receptors (not shown), which would suggest that by this time-point it would not be capable of driving any further repair mechanisms and was not contributing to the overall mRNA concentrations detected in qRTPCR or PCR arrays. Hypoxia was localised to the shed cells, consistent with breakdown of blood vessels, and the luminal epithelium only. The underlying stromal cell compartment was under more "normoxic" conditions, suggesting that hypoxia may not regulate tissue restoration from the stroma but may play a key role in initiating early repair mechanisms during the tissue stabilisation period; this will be further discussed in section 6.2.5.

In our model, the addition of DHT at the time of progesterone withdrawal was associated with a delay in breakdown and also a delay in repair. Delayed repair mechanisms, either involving vessel stabilisation or re-epithelialisation, have been implicated in the aetiology of heavy menstrual bleeding (HMB). Furthermore, expression of a number of factors, including vascular endothelial growth factor (VEGF) and connective tissue growth factor (CTGF) (193, 423) have been investigated as potential regulators of normal repair. Women with HMB have lower levels of VEGF (275) and increased prostaglandin synthesis (568), which are thought to contribute to a delay in repair by inhibiting endothelial stability and increasing inflammatory mediators.

In our model, administration of DHT at the time of progesterone withdrawal significantly up-regulated *Ctgf* at all time-points, whilst also increasing mRNA concentrations of *Vegfa*, which suggests that despite delaying breakdown androgens may mediate initial repair mechanisms by encouraging vessel stability. Conversely, DHT administration resulted in increased Smad3 expression, which is associated with delayed wound repair in the skin (555). Danazol (an anti-oestrogenic, anti-progestagenic, androgenic compound) has been used to treat women with HMB (569), with the success of treatment attributed to its anti-proliferative effects, which may limit endometrial growth and therefore reduce the thickness of the tissue to be shed. However, it is also interesting to speculate that Danazol's androgenic and glucocorticoid effects may also aid endometrial repair by regulating repair mechanisms.

Endometrial tissues from women with HMB have been widely studied in the context of tissue repair factors (193, 423, 570) however, a possible role for androgens in regulating repair has not been studied. In women, circulating oestrogen concentrations fall during menopause resulting in an increased androgen to oestrogen ratio (571, 572), as observed during menses. Post-menopausal women report slower wound healing; topical application of exogenous oestrogens has been shown to aid wound repair (573–576). This would suggest that during the menstrual cycle, when oestrogen levels are greater than androgens this may aid repair and remodelling of the tissue, which would be consistent with the morphological changes observed in the endometrium during the early proliferative phase (previously described in section 1.6.1). It is possible that in "normal" women cyclical fluctuations in the androgen to oestrogen ratio are such that tissue repair proceeds unimpeded. However, in women with HMB there may be an imbalance in this ratio, as observed in post-menopausal women, which leads to dysfunctional repair and a delay in tissue remodelling. This would be consistent with women with PCOS, who have increased androgen levels, who report long and heavy menstrual periods. However, the impact of androgens on endometrial function and endometrial pathologies including HMB awaits further elucidation.

In our mouse model we report differential regulation of matrix metalloproteinases (MMPs). MMPs play an integral role in endometrial breakdown (219), and increased expression of MMPs has been detected during menses in women and during tissue breakdown in mouse models of menses (220, 221, 223, 227, 230, 544). Despite the significant drop in circulating progesterone levels during tissue stabilisation (4-8 hours), mRNA concentrations for *Mmp-2, Mmp-3* and *Mmp-9* do not increase dramatically at this time, suggesting that progesterone levels are still high enough to inhibit MMP activity. These results are consistent with reports in human tissues that identify a role for progesterone in MMP inhibition (425, 577–579). *Mmp-3* was significantly up-regulated at 8 hours, whilst the tissue was observed to be breaking down, consistent with reports of increased MMP-3 activity during tissue breakdown in women at menses (215, 222). A dramatic increase (61 fold) was detected in the PCR array at 24 hours suggesting that MMP-3 is also involved in tissue remodelling and re-epithelialisation. This dual role for MMP-3 has been previously reported with cells immunopositive for MMP-3 identified in both the decidualised stroma and in areas of re-epithelialisation in a mouse model of menses (230).

Interestingly, whilst *Mmp-9* was significantly up-regulated at 8 hours (2 fold) it was greatly increased at 24 hours (28 fold increase), consistent with previous data from Kaitu'u-Lino *et al.,* (230) who also detected a significant increase in *Mmp*-9 mRNA at this time. We suggest

that MMP-9 may play a role in tissue remodelling rather than tissue breakdown, consistent with data from wound healing studies where MMP-9 has been shown to be involved in keratinocyte migration and granulation tissue (580). MMP-9 knock-out mice display delayed wound healing due to delayed re-epithelialisation and an increase in fibrin clotting (580). Human endometrial expression of MMP-9 is at its highest during the mid-secretory phase of the menstrual cycle, where the tissue is undergoing decidualisation, consistent with a role for MMP-9 in tissue remodelling (226). A decrease in MMP-2 and MMP-9 expression has been associated with women with HMB (275), who are suspected to have deregulated repair mechanisms in comparison to normal women.

6.2.4 The stromal cell compartment contributes to tissue restoration and tissue remodelling

The basal glandular epithelium is considered to be the source of the new luminal epithelium (154, 201, 237, 241), and a label retaining study in a mouse model of breakdown supports this theory (318), suggesting that a "stem-like" population maintains the luminal epithelial layer. However, in our study, evidence of basal gland epithelial proliferation was only observed in a few animals and not until the 24 hour time-point; therefore we suggest that the basal gland contribution to regeneration is not an early repair mechanism.

A recent study, using human endometrium recovered during the menstrual phase, failed to detect any significant number of Ki-67 (proliferation marker) positive cells in either the stromal or epithelial cell compartments, which the authors suggest means that repair in women may not occur by mitotic division (169). Notably, these samples were taken from women with known gynaecological conditions (including adenomyosis and poor fertility) and therefore may not clearly represent the cellular dynamics in normal women. The evidence of both stromal and epithelial cell proliferation at all time-points in our mouse model implies that mitotic division does contribute to endometrial repair.

In Chapter 3, pan cytokeratin positive stromal cells were identified close to the luminal surface at the 24 hour time-point, suggesting that these cells were in a transition-like state and may contribute to the new luminal epithelium via mesenchymal to epithelial transition (MET). Further investigation presented in Chapter 4, identified dual labelled pan cytokeratin and vimentin (definitive epithelial and mesenchymal markers, respectively) cells in the stromal cell compartment at the endometrial-myometrial ridge, 12 hours after the withdrawal of progesterone, at a time where the tissue was still breaking down. Dual labelled cells were then identified at the luminal edge at the 24 hour time-point in tissues collected from animals where full re-epithelialisation was not yet complete, suggesting that these dual labelled cells

migrate from the endometrial-myometrial border to contribute to the luminal epithelium. However, as there is a 12 hour interval between the last two time-points investigated, it would be of interest to collect tissues at 16 and/or 20 hours after progesterone withdrawal to determine whether these cells do migrate and can be identified interspersed throughout the stromal cell compartment.

The possible contribution of the stromal cell compartment to endometrial function has been investigated in two models of post-partum repair (375, 376). Both models incorporated mesenchymal cell-labelled mouse lines, which were used for lineage tracing studies. In intact virgin mice, epithelial cells did not contain any cells that were of mesenchymal origin, however after three pregnancies both luminal and glandular epithelium contained cells that were mesenchymal-derived (375). The identification of mesenchymal-derived cells in the epithelium is in support with a pilot study in our lab, using PDGFRβ-GFP labelled mice (which labelled stromal fibroblasts), which has identified PDGFRβ positive cells in the epithelium of intact, cycling mice (Simitsidellis, unpublished). This would suggest that not only does the stromal cell compartment contribute to the extensive remodelling observed during post-partum repair in the mouse, but it also contributes to overall tissue function in a non-menstruating species, that displays endometrial resorption (315) instead of endometrial shedding. To investigate this further, the PDGFRβ-GFP labelled mouse line will be incorporated into our refined mouse model of breakdown to study stromal cell dynamics. PDGFRβ is expressed by stromal fibroblasts in the endometrium and has also been proposed as a marker for putative endometrial stem cells known as pericytes (251).

Re-epithelialisation of the endometrium by MET, has implications in the pathology of endometriosis, where endometrial tissue establishes itself outside of the uterine cavity (290, 581). A role for MET in the regulation of endometrial tissue has not been studied intensively, whereas EMT has been proposed as a mechanism in the pathogenesis of endometriosis. A study published in 2003, by Demir *et al.* (582), was the first to suggest a role for EMT during establishment of peritoneal lesions in endometriosis. In their study, menstrual effluent was found to have an effect on the expression of mesenchymal and epithelial markers in mesothelial cells *in vitro*. Up-regulation of mRNA concentrations of the mesenchymal marker vimentin and down-regulation of the epithelial marker E cadherin were observed. Furthermore, disruptions to cell-cell adhesion between mesothelial cells *in vitro* was reported, suggesting that factors in menstrual effluent may aid the manifestation of endometriotic lesions (582).

A more recent study in 2012, by Matsuzaki and Darcha, investigated a role for MET in the development of different types of endometriotic lesions, as cytokeratin has been reported in the stromal cell compartment of lesions from women with endometriosis (581). Deep infiltrating and "black" peritoneal lesions expressed increased levels of cytokeratin markers and lower levels of mesenchymal markers than normal endometrium, suggesting MET as a process that enables lesion establishment. However, "red" peritoneal lesions and ovarian endometriotic tissue expressed higher levels of mesenchymal markers when compared to normal endometrium. This suggests that EMT plays a role in the establishment of these types of lesions. In both cases, expression of all markers may simply reflect changes in proportions of cell types in the lesions when compared to eutopic endometrium.

The adult stem cell niche has been studied in a number of tissues; like the endometrium, the intestine is a highly regenerative tissue capable of rapid regeneration after injury meaning that the intestinal crypt has been extensively studied (244, 247–249). It is likely that the endometrium also contains a stem cell population which contributes to restoration of tissue integrity during each menstrual cycle. The clonogenicity of endometrial stroma and epithelial cells has been studied *in vitro* (257, 259), and putative endometrial stem cells have been investigated in mouse models of breakdown (318, 368), using a label retaining method, which identified stromal and epithelial label retaining cells suggestive of stem cell niches for each compartment.

Putative human endometrial stem cells have been identified using two markers CD146 and PDGFRβ, these dual labelled putative pericytes, once cell sorted, are multipotent and can differentiate into mesenchymal lineages (251, 461). CD146+ PDGFRβ+ cells have been identified at perivascular sites in the endometrium of intact mice (Simitsidellis, unpublished). The number of human endometrial pericytes is reported to be higher in the basal layer compared to the functional layer (583), and pericytes are reported to be essential for blood vessel formation and stabilisation (584) and therefore may be contributing to repair of the murine endometrium. *Pdgfrb* mRNA concentrations increase during the repair phase in control mice (24 hours after progesterone withdrawal, not shown) but were decreased after the addition of DHT, which may suggest that androgens regulate pericyte activation and their possible contribution to repair.

The contribution of bone marrow progenitors as a potential new source of epithelial cells has been investigated in mouse models (266, 267, 585) where GFP-labelled bone marrow from donor males was injected into female mice. GFP-labelled bone marrow derivatives were identified in both endometrial stromal and epithelial compartments of intact cycling mice. In

support of this theory, in our mouse model, a significant increase in mRNA concentrations for *Snai3* were detected in the array (5 fold at 8 hours, 15 fold at 24 hours). In contrast to Snai1 and Snai2, little is known about Snai3 however it is expressed in high concentrations in the thymus and is thought to regulate haematopoietic stem cell differentiation (586). Over expression of Snai3 is also thought to be associated with decreased lymphocyte development and increased myeloid cell development (precursors for granulocytes) (586, 587). The increase in *Snai3* observed in our model during tissue remodelling may be indicative of recruitment of bone marrow progenitors, and therefore may be an important factor for future study. The addition of DHT led to a decrease in mRNA concentration for *Snai3* at all time-points, which may implicate androgens as a regulator of stem cell recruitment. However, it is possible that due to the overall delay in breakdown and changes in other genes in the EMT pathway that this may be a downstream effect of DHT. Also, MAPPER analysis revealed that Snai3 does contain a putative androgen response element (561) so could be directly regulated by androgens. As Snai3 has not been investigated in the endometrium or widely studied in many other tissues, there is the potential to investigate a new candidate that could regulate repair. Identifying Snai3 protein in the endometrium, by immunohistochemistry or by western blot would be invaluable.

The presence and regulation of endometrial stem cells also has implications in endometriosis. It is postulated that endometriosis occurs through retrograde menstruation, where endometrial tissue is flushed into the peritoneal cavity, which adheres to the peritoneum (292). It is thought that women with endometriosis will shed some of the basal layer of the endometrium during menstruation (567, 588), and that this tissue will contain endometrial stem cells that will contribute to the establishment of lesions (589). Bone marrow progenitors have also been implicated as a contributor to lesion formation in endometriosis (266, 267), and therefore both potential mechanisms warrant further study.

6.2.5 Hypoxia as an initiator of repair mechanisms

In our mouse model, hypoxia was detected in the decidualised cell mass during breakdown and in the luminal epithelium, whilst the basal stromal compartment remained unstained and under more normoxic conditions. Hypoxia has been shown to regulate genes involved in angiogenesis *in vitro* (191, 193), consistent with these data, an increase in hypoxia was associated with an increase in VEGF and a decrease in CXCL12. Downstream targets of HIF1α, as identified by MetaCore™, were found to be significantly up- or down-regulated at 8 hours, when staining for hypoxia was at its strongest, suggesting direct regulation. A number of genes including *Cxcl1, Cxcl5, Lect1* were reported to be significantly regulated

between 8 and 24 hours, where hypoxia in the uterine horn was localised to the shed cell mass and the luminal epithelium. These genes had not been identified as downstream targets of HIF1α and therefore may be indirectly regulated by HIF1α or by a HIF1α-independent mechanism.

A potential role for hypoxia during endometrial repair has been investigated (188, 191, 193, 321, 439), however the debate over its importance as a driver of repair remains. Hypoxic regulation of endometrial neo-angiogenesis has been implicated (188, 191, 193, 439), however no evidence of hypoxia was detected in a xenograft mouse model, where human explants were exposed to repeated cycles of oestrogen and progesterone withdrawal (321). Hypoxia has been shown to suppress MMP expression in stromal cells *in vitro,* (439) where a return to normoxic conditions removed this inhibition, therefore this may account for increased MMP expression at the 8 and 24 hour time-points when the hypoxic response was not as strong as at 4 hours.

Whilst the debate over hypoxia mediated endometrial repair continues, hypoxia mediated metastasis has been widely studied in a number of tissues including the liver (590), the pancreas (591) and the breast (393). Whilst a role for hypoxia in proliferation of epithelial cells in endometrial carcinoma has recently been elucidated (464, 468), hypoxia has also been implicated in VEGF-dependent tumour angiogenesis in both the endometrium (592) and the ovary (470). Hypoxia has been reported to regulate EMT (and therefore cancer metastasis) by direct or indirect regulation of Snail, Slug and Twist (464, 590). Administration of androgens resulted in a maintenance of the decidual response and a prolonged exposure to hypoxic conditions that may have initiated the process of EMT, consistent with a 15 fold increase in Snail at 8 hours +DHT compared to 8 hours -DHT, and an 8 fold increase in Twist at 8 hours +DHT compared to the 0 hour -DHT group. Prolonged exposure to hypoxia- mediated EMT may account for the phenotypic differences observed during the 24 hour window between -DHT and +DHT groups.

A rat adenocarcinoma model highlights oxygen as a key regulator of EMT and MET, where tumours treated under hyperoxic conditions showed regression due to initiation of MET processes (593). This would suggest that a switch in oxygen tension is capable of suppressing EMT regulators and activating MET regulatory molecules, which would be consistent with the initiation of MET in our model as the uterus returns to more normoxic conditions. However, the rat model was carried out at very high oxygen concentrations, which are unlikely to have been replicated at any time-point in our model; furthermore this is the only study to link high oxygen concentrations to MET.

It is likely that hypoxia is a key initiator of endometrial breakdown, and may set in motion repair mechanisms that are observed at the later time-points in our model. However, the absence of immunostaining for hypoxia in the underlying basal stroma at all time-points suggests that it does not directly regulate the stromal cell compartment, although a role for hypoxia in endometrial mesenchymal stem cell differentiation has been postulated (461). Hypoxia was observed in the decidualised stroma during breakdown which suggests that if the functional stromal compartment does contribute to repair by secreting factors (462) that this may be regulated by hypoxia. Evidence of hypoxia in the repairing luminal epithelial may also be regulating repair of this cell type and therefore, further investigation is required.

Understanding the mechanisms of hypoxia-mediated endometrial breakdown, and whether it does contribute to repair, may also provide an insight into endometrial cancer, further work is needed to determine whether hypoxia regulates these mechanisms in a HIF-dependent or HIF-independent manner.

6.2.6 Androgens disrupt normal repair mechanisms

In our refined mouse model a single injection of DHT at the time of progesterone withdrawal delayed the onset of endometrial breakdown whilst delaying repair mechanisms so that these two processes did not occur concurrently. Collection of uterine tissues at 28, 32 and 36 hours after the withdrawal of progesterone (and addition of DHT) should identify a time-point where repair mechanisms are initiated in the DHT treated animals.

In the absence of progesterone, androgens were able to maintain the decidual cell mass to delay the onset of breakdown by regulating factors that drive EMT, evidenced by the up-regulation of *Wt1* and Snail and down-regulation of E cadherin. A number of genes known to be involved in MET/EMT and angiogenesis/inflammation were found to be differentially regulated following treatment with DHT. Further analysis using MAPPER identified putative androgen response elements, Sp-1 and Ap-1 binding sites in the promoters of 24 of the 27 candidate genes investigated.

At the time of menses, circulating testosterone and androstenedione levels are relatively high (44, 45). Evidence for strong immunostaining for 5α reductase in the human endometrium at the secretory phase (499) suggests that local synthesis of DHT is occurring during this time. These data suggest that androgens are present and are contributing to tissue function during menses. Further analysis of the impact of DHT on endometrial function is required.

Analysis of the uterine samples by chromatin immunoprecipitation would provide a more definitive list of androgen regulated genes. Incorporation of the PDGFRβ-GFP mice into the

mouse model and utilisation of *in vivo* imaging would allow investigation into the effects of DHT on pericyte migration.

6.3 Future studies

From the studies in this thesis it is evident that the stromal cell compartment contributes either directly or indirectly to endometrial repair and therefore there are a number of potential targets to focus on.

In this study, mRNA concentrations were determined from whole tissue lysates. Laser capture micro-dissection would allow for isolation of specific cell types, which would provide further insight into the dynamics of each cellular compartment. More specifically it would allow investigation into the regulation of MET regulated genes and those of cell identity at key time-points (8 hours and 24 hours).

A number of *in vitro* cell culture methods are available to study cellular dynamics. Utilising 3D co-culture models with primary endometrial epithelial and stromal cells will enable investigation of cell-cell interactions in a model that recapitulates the multi-cellular morphology of the human endometrium. It is evident that stromal cell compartment contributes to repair; manipulation of the stromal cell compartment in these models would allow elucidation of its effect on the epithelial cell compartment. *In vitro* studies using cell conditioned media would also allow investigation of how each cell type interacts with another, for example, whether decidualised stromal cells undergoing progesterone withdrawal have an effect on epithelial cell or immune cell dynamics.

In order to delineate a role for MET in epithelial repair, future work should focus on fate mapping studies to determine the presence and lineage of stromal cells undergoing MET. Labelled mouse lines and collection of tissues at more frequent time points (16, 20, 28 hours after progesterone withdrawal) would enable tracking of cells from the myometrial ridge to the luminal surface, if this is indeed the source of these cells. Recent acquisition of a PDGFRβ labelled mouse line will enable detection of cells that have/or are currently expressing the stromal cell marker. The effect of androgens, more specifically DHT, on breakdown and repair can also be studied in these mice using live *in vivo* imaging. DHT was shown to down-regulated PDGFRβ mRNA concentrations at all time-points and therefore, may be having an effect on the migration of cells.

It is possible that the degenerating functional stroma may also play a role in repair and utilising laser capture technology would enable investigation of candidate genes that may be secreted by the functional stroma, such as integrins, adherens, MMPs and chemokines. In

addition, *in vitro* cell culture using human stromal cell conditioned media in a wound healing assay, utilising primary human epithelial cells, would allow further investigation of potential stromal secreted factors during breakdown and how they affect epithelial cell proliferation or migration.

Neutralising antibodies to candidate targets would also maximise the output of this mouse model. For example, further investigation of MMP regulation in our refined model would confirm their role in the rapid onset of breakdown and tissue remodelling. DHT was shown to down-regulate *Mmp-3* mRNA concentrations consistent with a dealy in shedding and separation of the functional layer from the basal layer. Giving specific MMP inhibitors at the time of progesterone withdrawal would delineate potential roles for MMP-3 and MMP-9 at different points in the early repair process. Macrophages were shown to increase during tissue remodelling; inhibition of macrophages by neutralisation antibodies would delineate their importance in this process. *In vitro* culture of macrophages with conditioned media would also enhance our knowledge on the factors that may regulate their recruitment.

The mouse model focuses on a very short time frame, where repair mechanisms are initiated within 24 hours of progesterone withdrawal. In women, re-epithelialisation (in the absence of oestrogen) is complete by around day 3 of the average cycle, at this time ovarian derived oestrogen biosynthesis occurs to drive endometrial proliferation which contributes to overall remodelling of the tissue. One limitation of our model is that we have not investigated the effect of oestrogen on remodelling in our mouse model; administration of oestradiol at the 24 hour time-point would enable investigation of how it contributes to restoration of tissue integrity and overall tissue homeostasis.

Finally, androgens have been shown to have an effect on the “normal” breakdown and repair mechanisms in our mouse model and therefore their role at menses merits further study. Preliminary work, outlined in this thesis, has highlighted that a single dose of DHT is sufficient to disturb the dynamics of breakdown and repair. DHT appeared to maintain the decidual response; however it is unknown whether DHT is acting through the androgen receptor or through the progesterone receptor. Furthermore, it is unknown whether the changes in gene expression identified in Chapter 5 are through direct or indirect action of the androgen receptor. Utilising chromatin immunoprecipitation (chIP) will allow for identification of those genes which contain an androgen response element and therefore may be regulated directly or those that may be regulated indirectly through an Sp-1 or Ap-1 binding site (outlined in Table 5-7) or another transcription factor. The list of candidate

genes will also be investigated for the presence of a progesterone response element to provide further insight into how DHT may be regulating these genes.

6.4 Conclusions

The data presented in this thesis provides evidence of a more relevant mouse model where breakdown and repair occur simultaneously, as in women. A previously unrecognised role for mesenchymal to epithelial transition was investigated, along with a putative role for androgens during endometrial repair. The results presented in this thesis have implications for the treatment of endometrial disorders including heavy menstrual bleeding and endometriosis.

References

1. O'Rahilly R (1983) The timing and sequence of events in the development of the human reproductive system during the embryonic period proper. *Anat Embryol (Berl)* 166:247–61.
2. Hashimoto R (2003) Development of the human Müllerian duct in the sexually undifferentiated stage. *Anat Rec* 272:514–9.
3. Kobayashi A, Behringer RR (2003) Developmental genetics of the female reproductive tract in mammals. *Nat Rev Genet* 4:969–80.
4. Pietryga E, Woźniak W (1992) The growth and topography of the human fetal uterus. *Folia Morphol (Warsz)* 51:165–80.
5. Valdes-Dapena (1973) *The development of the uterus in late fetal life, infancy, and childhood. In: The Uterus*. ed Norris HJ, Hertig AT, Abell MR (ed). (Williams and Wilkins, Baltimore).
6. Koff A (1933) Development of the vagina in the human fetus. *Contrib Embryol* 24:59–90.
7. Bartol FF et al. (1999) Uterine differentiation as a foundation for subsequent fertility. *J Reprod Fertil Suppl* 54:287–302.
8. Van Campenhout E, Witschi E (1948) The interstitial tissue of a human hermaphrodite. *J Clin Endocrinol Metab* 8:271–4.
9. Molyneaux KA, Stallock J, Schaible K, Wylie C (2001) Time-lapse analysis of living mouse germ cell migration. *Dev Biol* 240:488–98.
10. Makabe S, Motta PM (1989) Migration of human germ cells and their relationship with the developing ovary: ultrastructural aspects. *Prog Clin Biol Res* 296:41–54.
11. Fujimoto T, Yoshinaga K, Kono I (1985) Distribution of fibronectin on the migratory pathway of primordial germ cells in mice. *Anat Rec* 211:271–8.
12. Freeman B (2003) The active migration of germ cells in the embryos of mice and men is a myth. *Reproduction* 125:635–643.
13. Bendsen E, Byskov AG, Andersen CY, Westergaard LG (2006) Number of germ cells and somatic cells in human fetal ovaries during the first weeks after sex differentiation. *Hum Reprod* 21:30–5.
14. Wartenberg H (1982) Development of the early human ovary and role of the mesonephros in the differentiation of the cortex. *Anat Embryol (Berl)* 165:253–80.
15. Lovell-Badge R, Robertson E (1990) XY female mice resulting from a heritable mutation in the primary testis-determining gene, Tdy. *Development* 109:635–46.
16. Falin LI (1969) The development of genital glands and the origin of germ cells in human embryogenesis. *Acta Anat (Basel)* 72:195–232.
17. Stoop H et al. (2005) Differentiation and development of human female germ cells during prenatal gonadogenesis: an immunohistochemical study. *Hum Reprod* 20:1466–76.
18. Gondos B (1985) Development of the reproductive organs. *Ann Clin Lab Sci* 15:363–73.

19. Rabinovici J, Jaffe RB (1990) Development and regulation of growth and differentiated function in human and subhuman primate fetal gonads. *Endocr Rev* 11:532–57.

20. Kurilo LF (1981) Oogenesis in antenatal development in man. *Hum Genet* 57:86–92.

21. Stopa EG, Sower SA, Svendsen CN, King JC (1988) Polygenic expression of gonadotropin-releasing hormone (GnRH) in human? *Peptides* 9:419–23.

22. Fernald RD, White RB (1999) Gonadotropin-releasing hormone genes: phylogeny, structure, and functions. *Front Neuroendocrinol* 20:224–40.

23. Bates GW, Bowling M (2013) Physiology of the female reproductive axis. *Periodontol 2000* 61:89–102.

24. Yen SS (1977) Regulation of the hypothalamic--pituitary--ovarian axis in women. *J Reprod Fertil* 51:181–91.

25. Conte FA, Grumbach MM, Kaplan SL (1975) A diphasic pattern of gonadotropin secretion in patients with the syndrome of gonadal dysgenesis. *J Clin Endocrinol Metab* 40:670–4.

26. Wildt L, Marshall G, Knobil E (1980) Experimental induction of puberty in the infantile female rhesus monkey. *Science (80-)* 207:1373–5.

27. Conn PM, Crowley WF (1994) Gonadotropin-releasing hormone and its analogs. *Annu Rev Med* 45:391–405.

28. Stojilkovic SS, Catt KJ (1995) Expression and signal transduction pathways of gonadotropin-releasing hormone receptors. *Recent Prog Horm Res* 50:161–205.

29. Hiller-sturmhöfel S, Bartke A (1998) The Endocrine System: An Overview. *Alcohol Horm* 22:153–164.

30. Marshall JC, Kelch RP (1986) Gonadotropin-releasing hormone: role of pulsatile secretion in the regulation of reproduction. *N Engl J Med* 315:1459–68.

31. Reame N, Sauder SE, Kelch RP, Marshall JC (1984) Pulsatile gonadotropin secretion during the human menstrual cycle: evidence for altered frequency of gonadotropin-releasing hormone secretion. *J Clin Endocrinol Metab* 59:328–37.

32. Tsutsumi R, Webster NJG (2009) GnRH pulsatility, the pituitary response and reproductive dysfunction. *J Endocrinol* 56:729–37.

33. Marshall JC et al. (1991) Gonadotropin-releasing hormone pulses: regulators of gonadotropin synthesis and ovulatory cycles. *Recent Prog Horm Res* 47:155–87; discussion 188–9.

34. Britt JH, Esbenshade KL, Ziecik AJ (1991) Roles of estradiol and gonadotropin-releasing hormone in controlling negative and positive feedback associated with the luteinizing hormone surge in ovariectomized pigs. *Biol Reprod* 45:478–85.

35. Moore CR, Price D (1932) Gonad hormone functions, and the reciprocal influence between gonads and hypophysis with its bearing on the problem of sex hormone antagonism. *Am J Anat* 50:13–71.

36. Hohlweg W, Junkmann K (1932) Die Hormonal-Nervöse Regulierung der Funktion des Hypophysenvorderlappens. *Klin Wochenschr* 11:321–323.

37. Knobil E (1988) The hypothalamic gonadotrophic hormone releasing hormone (GnRH) pulse generator in the rhesus monkey and its neuroendocrine control. *Hum Reprod* 3:29–31.

38. Krsmanovic LZ, Hu L, Leung P-K, Feng H, Catt KJ (2009) The hypothalamic GnRH pulse generator: multiple regulatory mechanisms. *Trends Endocrinol Metab* 20:402–8.

39. Glidewell-Kenney C et al. (2007) Nonclassical estrogen receptor alpha signaling mediates negative feedback in the female mouse reproductive axis. *Proc Natl Acad Sci U S A* 104:8173–7.

40. Naftolin F et al. (2007) Estrogen-induced hypothalamic synaptic plasticity and pituitary sensitization in the control of the estrogen-induced gonadotrophin surge. *Reprod Sci* 14:101–16.

41. Britt KL et al. (2004) Estrogen actions on follicle formation and early follicle development. *Biol Reprod* 71:1712–23.

42. Clarke IJ, Cummins JT (1984) Direct pituitary effects of estrogen and progesterone on gonadotropin secretion in the ovariectomized ewe. *Neuroendocrinology* 39:267–74.

43. Stocco C, Telleria C, Gibori G (2007) The molecular control of corpus luteum formation, function, and regression. *Endocr Rev* 28:117–49.

44. Abraham GE (1974) Ovarian and adrenal contribution to peripheral androgens during the menstrual cycle. *J Clin Endocrinol Metab* 39:340–6.

45. Massafra C et al. (2000) Effects of estrogens and androgens on erythrocyte antioxidant superoxide dismutase, catalase and glutathione peroxidase activities during the menstrual cycle. *J Endocrinol* 167:447–52.

46. Lunenfeld B, Kraiem Z, Eshkol A (1975) The function of the growing follicle. *J Reprod Fertil* 45:567–74.

47. Payne AH, Hales DB (2004) Overview of steroidogenic enzymes in the pathway from cholesterol to active steroid hormones. *Endocr Rev* 25:947–70.

48. Hu J, Zhang Z, Shen W-J, Azhar S (2010) Cellular cholesterol delivery, intracellular processing and utilization for biosynthesis of steroid hormones. *Nutr Metab (Lond)* 7:47.

49. Krisans SK (1996) Cell compartmentalization of cholesterol biosynthesis. *Ann N Y Acad Sci* 804:142–64.

50. Short R (1962) Steroids in the follicular fluid and the corpus luteum of the mare. A "two-cell type" theory of ovarian steroid synthesis. *J Endocrinol* 24:59–63.

51. Hillier SG, Whitelaw PF, Smyth CD (1994) Follicular oestrogen synthesis: the "two-cell, two-gonadotrophin" model revisited. *Mol Cell Endocrinol* 100:51–4.

52. Drummond AE (2006) The role of steroids in follicular growth. *Reprod Biol Endocrinol* 4:16.

53. Magoffin DA (2005) Ovarian theca cell. *Int J Biochem Cell Biol* 37:1344–9.

54. Marsh JM (1976) The role of cyclic AMP in gonadal steroidogenesis. *Biol Reprod* 14:30–53.

55. Chung B-C (1986) Human Cholesterol Side-Chain Cleavage Enzyme, P450scc: cDNA Cloning, Assignment of the Gene to Chromosome 15, and Expression in the Placenta. *Proc Natl Acad Sci* 83:8962–8966.

56. Moghrabi N, Andersson S (1998) 17β-Hydroxysteroid Dehydrogenases: Physiological Roles in Health and Disease. *Trends Endocrinol Metab* 9:265–270.

57. Labrie F et al. (1997) The key role of 17β-hydroxysteroid dehydrogenases in sex steroid biology. *Steroids* 62:148–158.

58. Sprengel R, Braun T, Nikolics K, Segaloff DL, Seeburg PH (1990) The testicular receptor for follicle stimulating hormone: Structure and functional expression of cloned cDNA. *Mol Endocrinol* 4:525–530.

59. Ryan K, Petro Z, Kaiser J (1968) Steroid formation by isolated and recombined ovarian granulosa and tehcal cells. *J Clin Endocrinol Metab* 28:355 – 8.

60. Hillier SG, van den Boogaard AM, Reichert LE, van Hall E V (1980) Intraovarian sex steroid hormone interactions and the regulation of follicular maturation: aromatization of androgens by human granulosa cells in vitro. *J Clin Endocrinol Metab* 50:640–7.

61. Niswender GD, Juengel JL, Silva PJ, Rollyson MK, McIntush EW (2000) Mechanisms controlling the function and life span of the corpus luteum. *Physiol Rev* 80:1–29.

62. Fraenkel L (1903) Die function des corpus luteum. *Arch Gynecol Obstet* 68:438–545.

63. Lachance Y et al. (1990) Characterization of human 3 beta-hydroxysteroid dehydrogenase/delta 5-delta 4-isomerase gene and its expression in mammalian cells. *J Biol Chem* 265:20469–20475.

64. Lorence MC, Corbin CJ, Kamimura N, Mahendroo MS, Mason JI (1990) Structural analysis of the gene encoding human 3 -hydroxysteroid dehydrogenase/ 5->4-isomerase. *Mol Endocrinol* 4:1850–1855.

65. Csapo AI, Pulkkinen M (1978) Indispensability of the human corpus luteum in the maintenance of early pregnancy. Luteectomy evidence. *Obstet Gynecol Surv* 33:69–81.

66. Duncan WC (1999) Steroidogenic enzyme expression in human corpora lutea in the presence and absence of exogenous human chorionic gonadotrophin (HCG). *Mol Hum Reprod* 5:291–298.

67. Csapo AI, Pulkkinen MO, Ruttner B, Sauvage JP, Wiest WG (1972) The significance of the human corpus luteum in pregnancy maintenance. I. Preliminary studies. *Am J Obstet Gynaecol* 112:1061–7.

68. Sheth AR, Vijayalakshmi S (1981) Selective suppression of FSH as a possible approach for fertility regulation. *Arch Androl* 7:109–15.

69. Kaneko H et al. (1997) Inhibin is involved in the suppression of FSH secretion in the growth phase of the dominant follicle during the early luteal phase in cows. *Domest Anim Endocrinol* 14:263–71.

70. De Ziegler D, Fanchin R, de Moustier B, Bulletti C (1998) The hormonal control of endometrial receptivity: estrogen (E2) and progesterone. *J Reprod Immunol* 39:149–66.

71. King AE, Critchley HOD, Kelly RW (2003) Innate immune defences in the human endometrium. *Reprod Biol Endocrinol* 1:116.

72. Jabbour HN, Kelly RW, Fraser HM, Critchley HOD (2006) Endocrine regulation of menstruation. *Endocr Rev* 27:17–46.

73. Finn CA, Martin L (1972) Endocrine control of the timing of endometrial sensitivity to a decidual stimulus. *Biol Reprod* 7:82–6.

74. Robel P, Mortel R, Baulieu E (1981) in *Reproductive Processes and Contraception*, ed McKerns KW (Springer US, Boston, MA), pp 257–280.

75. Moyer DL, Felix JC (1998) The effects of progesterone and progestins on endometrial proliferation. *Contraception* 57:399–403.

76. Hertz R (1965) Hormonal Relationships of the Endometrium in Animals. *Cancer Res* 25:1188–1189.

77. Hegele-Hartung C (1992) Luteal control of endometrial receptivity and its modification by progesterone antagonists. *Endocrinology* 131:2446–2460.

78. Salamonsen LA (2003) Review Tissue injury and repair in the female human reproductive tract. *Reproduction*:301–311.

79. Evans J, Kaitu'u-Lino T, Salamonsen LA (2011) Extracellular matrix dynamics in scar-free endometrial repair: perspectives from mouse in vivo and human in vitro studies. *Biol Reprod* 85:511–23.

80. Ludwig H, Spornitz UM (1991) Microarchitecture of the human endometrium by scanning electron microscopy: menstrual desquamation and remodeling. *Ann N Y Acad Sci* 622:28–46.

81. Tanner J (1962) *Growth at adolescence* (Blackwell). 2nd Ed.

82. Salamonsen LA (1998) Current concepts of the mechanisms of menstruation: a normal process of tissue destruction. *Trends Endocrinol Metab* 9:305–9.

83. King AE, Critchley HOD (2010) Oestrogen and progesterone regulation of inflammatory processes in the human endometrium. *J Steroid Biochem Mol Biol* 120:116–26.

84. Tabibzadeh S (1996) The signals and molecular pathways involved in human menstruation, a unique process of tissue destruction and remodelling. *Mol Hum Reprod* 2:77–92.

85. Jabbour HN, Sales KJ, Catalano RD, Norman JE (2009) Inflammatory pathways in female reproductive health and disease. *Reproduction* 138:903–19.

86. Maybin JA, Critchley HOD (2011) Progesterone: a pivotal hormone at menstruation. *Ann N Y Acad Sci* 1221:88–97.

87. Bartelmez G (1957) The phases of the menstrual cycle and their interpretation in terms of the pregnancy cycle. *Am J Obstet Gynaecol* 74:931–55.

88. Bartelmez GW (1951) in *Contributions to embryology*, p 144.

89. Noyes RW, Hertig AT, Rock J (1950) Dating the endometrial biopsy. *Fertil Steril* 1:325.

90. McLennan CE, Rydell AH (1965) Extent of endometrial shedding during normal menstruation. *Obstet Gynecol* 26:605–621.

91. Gargett CE, Masuda H (2011) Adult stem cells in the endometrium. *Mol Hum Reprod* 16:818–834.

92. Fujimoto K (1995) Pericyte-endothelial gap junctions in developing rat cerebral capillaries: a fine structural study. *Anat Rec* 242:562–5.

93. Chantrain CF et al. (2006) Mechanisms of pericyte recruitment in tumour angiogenesis: a new role for metalloproteinases. *Eur J Cancer* 42:310–8.

94. Thiruchelvam U, Dransfield I, Saunders PTK, Critchley HOD (2013) The importance of the macrophage within the human endometrium. *J Leukoc Biol* 93:217–25.

95. Berbic M, Fraser IS (2013) Immunology of normal and abnormal menstruation. *Women's Heal* 9:387–95.

96. Cloke B et al. (2008) The androgen and progesterone receptors regulate distinct gene networks and cellular functions in decidualizing endometrium. *Endocrinology* 149:4462–4474.

97. Groothuis PG, Dassen HHNM, Romano A, Punyadeera C (2007) Estrogen and the endometrium: lessons learned from gene expression profiling in rodents and human. *Hum Reprod Update* 13:405–17.

98. Critchley HO, Saunders PT (2009) Hormone receptor dynamics in a receptive human endometrium. *Reprod Sci* 16:191–199.

99. Wahli W, Martinez E (1991) Superfamily of steroid nuclear receptors: positive and negative regulators of gene expression. *FASEB J* 5:2243–2249.

100. Krust A et al. (1986) The chicken oestrogen receptor sequence: homology with v-erbA and the human oestrogen and glucocorticoid receptors. *EMBO J* 5:891–7.

101. Brinkmann AO et al. (1989) Structure and function of the androgen receptor. *Urol Res* 17:87–93.

102. Gibson DA, Saunders PTK (2012) Estrogen dependent signaling in reproductive tissues - a role for estrogen receptors and estrogen related receptors. *Mol Cell Endocrinol* 348:361–72.

103. Cork DMW, Lennard TWJ, Tyson-Capper AJ (2008) Alternative splicing and the progesterone receptor in breast cancer. *Breast Cancer Res* 10:207.

104. Kumar R, Thompson EB (1999) The structure of the nuclear hormone receptors. *Steroids* 64:310–9.

105. Danielian PS, White R, Lees JA, Parker MG (1992) Identification of a conserved region required for hormone dependent transcriptional activation by steroid hormone receptors. *EMBO J* 11:1025–33.

106. Nilsson S et al. (2001) Mechanisms of estrogen action. *Physiol Rev* 81:1535–65.

107. Green S, Chambon P (1988) Nuclear receptors enhance our understanding of transcription regulation. *Trends Genet* 4:309–14.

108. Evans RM (1988) The steroid and thyroid hormone receptor superfamily. *Science (80-)* 240:889–95.

109. Sartorius CA et al. (1994) A third transactivation function (AF3) of human progesterone receptors located in the unique N-terminal segment of the B-isoform. *Mol Endocrinol* 8:1347–60.

110. Brinkmann AO (2001) Lessons to be learned from the androgen receptor. *Eur J Dermatol* 11:301–3.

111. Smith SK (1998) Angiogenesis, vascular endothelial growth factor and the endometrium. *Hum Reprod Update* 4:509–19.

112. Gibson DA, McInnes KJ, Critchley HOD, Saunders PTK (2013) Endometrial Intracrinology--Generation of an Estrogen-dominated Microenvironment in the Secretory Phase of Women. *J Clin Endocrinol Metab* 98:E1802–6.

113. Huhtinen K et al. (2012) Endometrial and endometriotic concentrations of estrone and estradiol are determined by local metabolism rather than circulating levels. *J Clin Endocrinol Metab* 97:4228–35.

114. Huhtinen K, Ståhle M, Perheentupa A, Poutanen M (2012) Estrogen biosynthesis and signaling in endometriosis. *Mol Cell Endocrinol* 358:146–54.

115. Bukulmez O et al. (2008) Androstenedione up-regulation of endometrial aromatase expression via local conversion to estrogen: potential relevance to the pathogenesis of endometriosis. *J Clin Endocrinol Metab* 93:3471–7.

116. Huet YM, Dey SK (1987) Role of early and late oestrogenic effects on implantation in the mouse. *J Reprod Fertil* 81:453–8.

117. Huet-Hudson YM, Andrews GK, Dey SK (1989) Cell type-specific localization of c-myc protein in the mouse uterus: modulation by steroid hormones and analysis of the periimplantation period. *Endocrinology* 125:1683–90.

118. Simón C et al. (1998) Increasing uterine receptivity by decreasing estradiol levels during the preimplantation period in high responders with the use of a follicle-stimulating hormone step-down regimen. *Fertil Steril* 70:234–9.

119. Dey SK et al. (2004) Molecular cues to implantation. *Endocr Rev* 25:341–73.

120. Lim H et al. (2002) Molecules in blastocyst implantation: uterine and embryonic perspectives. *Vitam Horm* 64:43–76.

121. Saunders P, Critchley H (2003) Estrogen receptor subtypes in the female reproductive tract. *Reprod Med Rev* 10:149–164.

122. Cooke PS et al. (1997) Stromal estrogen receptors mediate mitogenic effects of estradiol on uterine epithelium. *Proc Natl Acad Sci U S A* 94:6535–40.

123. Critchley HO et al. (2001) Estrogen receptor beta, but not estrogen receptor alpha, is present in the vascular endothelium of the human and nonhuman primate endometrium. *J Clin Endocrinol Metab* 86:1370–1378.

124. Collins F et al. (2009) Expression of oestrogen receptors, ERalpha, ERbeta, and ERbeta variants, in endometrial cancers and evidence that prostaglandin F may play a role in regulating expression of ERalpha. *BMC Cancer* 9:330.

125. Kastner P et al. (1990) Two distinct estrogen-regulated promoters generate transcripts encoding the two functionally different human progesterone receptor forms A and B. *EMBO J* 9:1603–14.

126. Rousseau-Merck MF, Misrahi M, Loosfelt H, Milgrom E, Berger R (1987) Localization of the human progesterone receptor gene to chromosome 11q22-q23. *Hum Genet* 77:280–2.

127. Lessey BA et al. (1988) Immunohistochemical analysis of human uterine estrogen and progesterone receptors throughout the menstrual cycle. *J Clin Endocrinol Metab* 67:334–340.

128. Press M, Greene G (1988) Localization of Progesterone Receptor with Monoclonal Antibodies to the Human Progestin Receptor. *Endocrinology* 122:1165–1175.

129. Bergeron C (2000) Morphological changes and protein secretion induced by progesterone in the endometrium during the luteal phase in preparation for nidation. *Hum Reprod* 15 Suppl 1:119–28.

130. Satyaswaroop PG, Wartell DJ, Mortel R (1982) Distribution of progesterone receptor, estradiol dehydrogenase, and 20 alpha-dihydroprogesterone dehydrogenase activities in human endometrial glands and stroma: progestin induction of steroid dehydrogenase activities in vitro is restricted to the glandul. *Endocrinology* 111:743–9.

131. Girling JE, Lederman FL, Walter LM, Rogers PA (2007) Progesterone, but not estrogen, stimulates vessel maturation in the mouse endometrium. *Endocrinology* 148:5433–5441.

132. Slayden OD, Brenner RM (2004) Hormonal regulation and localization of estrogen, progestin and androgen receptors in the endometrium of nonhuman primates: effects of progesterone receptor antagonists. *Arch Histol Cytol* 67:393–409.

133. Lydon JP et al. (1995) Mice lacking progesterone receptor exhibit pleiotropic reproductive abnormalities. *Genes Dev* 9:2266–78.

134. Mulac-Jericevic B, Conneely OM (2004) Reproductive tissue selective actions of progesterone receptors. *Reproduction* 128:139–46.

135. Conneely OM (2002) Reproductive Functions of Progesterone Receptors. *Recent Prog Horm Res* 57:339–355.

136. Zouboulis CC (2009) The skin as an endocrine organ. *Dermatoendocrinol* 1:250–2.

137. Zouboulis CC, Degitz K (2004) Androgen action on human skin -- from basic research to clinical significance. *Exp Dermatol* 13 Suppl 4:5–10.

138. Labrie F (1997) Physiological Changes in Dehydroepiandrosterone Are Not Reflected by Serum Levels of Active Androgens and Estrogens But of Their Metabolites: Intracrinology. *J Clin Endocrinol Metab* 82:2403–2409.

139. Dawood MY, Saxena BB (1976) Plasma testosterone and dihydrotestosterone in ovulatory and anovulatory cycles. *Am J Obstet Gynaecol* 126:430–5.

140. Davison SL, Bell R, Donath S, Montalto JG, Davis SR (2005) Androgen levels in adult females: changes with age, menopause, and oophorectomy. *J Clin Endocrinol Metab* 90:3847–53.

141. Brown CJ et al. (1989) Androgen receptor locus on the human X chromosome: regional localization to Xq11-12 and description of a DNA polymorphism. *Am J Hum Genet* 44:264–9.

142. Walters KA, Allan CM, Handelsman DJ (2008) Androgen actions and the ovary. *Biol Reprod* 78:380–9.

143. Mertens Heineman, M.J., Koudstaal, J., Theunissen, P., Evers, J.L.H. HJMM (1996) Androgen receptor content in human endometrium. *Eur J Obstet Gynecol Reprod Biol* 70:11–13.

144. Marshall E et al. (2011) In silico analysis identifies a novel role for androgens in the regulation of human endometrial apoptosis. *J Clin Endocrinol Metab* 96:E1746–55.

145. Narvekar N (2004) Low-Dose Mifepristone Inhibits Endometrial Proliferation and Up-Regulates Androgen Receptor. *J Clin Endocrinol Metab* 89:2491–2497.

146. Zhang X, Croy B a (1996) Maintenance of decidual cell reaction by androgens in the mouse. *Biol Reprod* 55:519–24.

147. Hitschmann, F & Adler L (1908) Der Bu der Uterusschleimhaut des geschlechtsreifen Weibes mit besonderer Berucksichtigung der Menstruation. *Monatscchr Geburtshilfe Gynaekol* 27:1–82.

148. Garry R, Hart R, Karthigasu KA, Burke C (2009) A re-appraisal of the morphological changes within the endometrium during menstruation: a hysteroscopic, histological and scanning electron microscopic study. *Hum Reprod* 24:1393–1401.

149. Petracco RG, Kong A, Grechukhina O, Krikun G, Taylor HS (2012) Global gene expression profiling of proliferative phase endometrium reveals distinct functional subdivisions. *Reprod Sci* 19:1138–45.

150. Ruiz-Alonso M, Blesa D, Simón C (2012) The genomics of the human endometrium. *Biochim Biophys Acta*.

151. Gambino LS (2002) Angiogenesis occurs by vessel elongation in proliferative phase human endometrium. *Hum Reprod* 17:1199–1206.

152. Gleeson N, Jordan M, Sheppard B, Bonnar J (1993) Cyclical variation in endometrial oestrogen and progesterone receptors in women with normal menstruation and dysfunctional uterine bleeding. *Eur J Obstet Gynecol Reprod Biol* 48:207–14.

153. Thornburgh I, Anderson MC (1997) The endometrial deficient secretory phase. *Histopathology* 30:11–5.

154. Ferenczy A, Bertrand G, Gelfand MM (1979) Proliferation kinetics of human endometrium during the normal menstrual cycle. *Am J Obstet Gynaecol* 133:859–67.

155. Punyadeera C et al. (2006) Expression and regulation of vascular endothelial growth factor ligands and receptors during menstruation and post-menstrual repair of human endometrium. *Mol Hum Reprod* 12:367–75.

156. Agarwal AK, Durani S, Setty BS (1982) Dose dependent modulation of receptor dynamics and uterine growth in immature rat by estradiol: importance of an additional nuclear binding at 24 hr for long-term (72 hr) uterine growth. *Endokrinologie* 79:235–41.

157. Irwin JC, de las Fuentes L, Dsupin BA, Giudice LC (1993) Insulin-like growth factor regulation of human endometrial stromal cell function: coordinate effects on insulin-like growth factor binding protein-1, cell proliferation and prolactin secretion. *Regul Pept* 48:165–77.

158. Watson H, Franks S, Bonney RC (1996) Regulation of epidermal growth factor receptor synthesis by ovarian steroids in human endometrial cells in culture. *J Reprod Fertil* 107:199–205.

159. Nelson KG, Takahashi T, Bossert NL, Walmer DK, McLachlan JA (1991) Epidermal growth factor replaces estrogen in the stimulation of female genital-tract growth and differentiation. *Proc Natl Acad Sci U S A* 88:21–5.

160. Taketani Y, Mizuno M (1988) Cyclic changes in epidermal growth factor receptor in human endometrium during menstrual cycle. *Endocrinol Jpn* 35:19–25.

161. Ferenczy A, Bergeron C (1991) Histology of the human endometrium: from birth to senescence. *Ann N Y Acad Sci* 622:6–27.

162. Motta PM, Andrews PM (1976) Scanning electron microscopy of the endometrium during the secretory phase. *J Anat* 122:315–22.

163. Campbell S et al. (1988) Expression of a secretory product by microvillous and ciliated cells of the human endometrial epithelium in vivo and in vitro. *Hum Reprod* 3:927–34.

164. Kelly RW, King AE, Critchley HOD (2001) Cytokine control in human endometrium. *Reproduction* 121:3–19.

165. Huang J, Tseng L, Bischof P, Janne O (1987) Regulation of prolactin production by progestin, estrogen, and relaxin in human eEndometrial stromal cells. *Endocrinology* 121:2011–2017.

166. Lockwood CJ, Krikun G, Hausknecht V, Wang EY, Schatz F (1997) Decidual cell regulation of hemostasis during implantation and menstruation. *Ann N Y Acad Sci* 828:188–93.

167. Wang H, Critchley HO, Kelly RW, Shen D, Baird DT (1998) Progesterone receptor subtype B is differentially regulated in human endometrial stroma. *Mol Hum Reprod* 4:407–412.

168. Gargett CE, Chan RWS, Schwab KE (2008) Hormone and growth factor signaling in endometrial renewal: role of stem/progenitor cells. *Mol Cell Endocrinol* 288:22–9.

169. Garry R, Hart R, Karthigasu K, Burke C (2010) Structural changes in endometrial basal glands during menstruation. *BJOG* 117:1175–85.

170. Salker M et al. (2010) Natural selection of human embryos: impaired decidualization of endometrium disables embryo-maternal interactions and causes recurrent pregnancy loss. *PLoS One* 5:e10287.

171. Lessey BA (2000) Endometrial receptivity and the window of implantation. *Baillieres Best Pract Res Clin Obstet Gynaecol* 14:775–88.

172. Van Mourik MSM, Macklon NS, Heijnen CJ (2008) Embryonic implantation: cytokines, adhesion molecules, and immune cells in establishing an implantation environment. *J Leukoc Biol* 85:4–19.

173. Psychoyos A (1973) Hormonal control of ovoimplantation. *Vitam Horm* 31:201–56.

174. Acosta AA et al. (2000) Endometrial dating and determination of the window of implantation in healthy fertile women. *Fertil Steril* 73:788–798.

175. Martel D, Monier MN, Roche D, Psychoyos A (1991) Hormonal dependence of pinopode formation at the uterine luminal surface. *Hum Reprod* 6:597–603.

176. Riesewijk A et al. (2003) Gene expression profiling of human endometrial receptivity on days LH+2 versus LH+7 by microarray technology. *Mol Hum Reprod* 9:253–64.

177. Kao LC et al. (2002) Global gene profiling in human endometrium during the window of implantation. *Endocrinology* 143:2119–38.

178. Felix JC, Farahmand S (1997) Endometrial glandular proliferation and estrogen receptor content during the normal menstrual cycle. *Contraception* 55:19–22.

179. Aplin JD, Charlton AK, Ayad S (1988) An immunohistochemical study of human endometrial extracellular matrix during the menstrual cycle and first trimester of pregnancy. *Cell Tissue Res* 253:231–40.

180. Church HJ, Vićovac LM, Williams JD, Hey NA, Aplin JD (1996) Laminins 2 and 4 are expressed by human decidual cells. *Lab Invest* 74:21–32.

181. Bell SC, Jackson JA, Ashmore J, Zhu HH, Tseng L (1991) Regulation of Insulin-Like Growth Factor-Binding Protein-1 Synthesis and Secretion by Progestin and Relaxin

in Long Term Cultures of Human Endometrial Stromal Cells. *J Clin Endocrinol Metab* 72:1014–1024.

182. Matsumoto H, Sakai K, Iwashita M (2008) Insulin-like growth factor binding protein-1 induces decidualization of human endometrial stromal cells via alpha5beta1 integrin. *Mol Hum Reprod* 14:485–9.

183. Gargett CE, Nguyen HPT, Ye L (2012) Endometrial regeneration and endometrial stem/progenitor cells. *Rev Endocr Metab Disord*.

184. Lockwood CJ, Krikun G, Hickey M, Huang SJ, Schatz F (2009) Decidualized human endometrial stromal cells mediate hemostasis, angiogenesis, and abnormal uterine bleeding. *Reprod Sci* 16:162–70.

185. Salamonsen L., Woolley D. (1999) Menstruation: induction by matrix metalloproteinases and inflammatory cells. *J Reprod Immunol* 44:1–27.

186. Markee JE (1940) Menstruation in intraocular endometrial transplants in the rhesus monkey. *Contrib Embryol* 28:219–318.

187. Pawitan JA (2001) Mechanism of normal menstruation and abnormality associated with menorrhagia. *Med J Indones* 10.

188. Fan X et al. (2008) VEGF blockade inhibits angiogenesis and reepithelialization of endometrium. *FASEB J* 22:3571–80.

189. Semenza GL (1998) Hypoxia-inducible factor 1: master regulator of O2 homeostasis. *Curr Opin Genet Dev* 8:588–94.

190. Critchley HOD et al. (2006) Hypoxia-inducible factor-1alpha expression in human endometrium and its regulation by prostaglandin E-series prostanoid receptor 2 (EP2). *Endocrinology* 147:744–53.

191. Tsuzuki T et al. (2012) Hypoxic stress simultaneously stimulates vascular endothelial growth factor via hypoxia-inducible factor-1α and inhibits stromal cell-derived factor-1 in human endometrial stromal cells. *Hum Reprod* 27:523–30.

192. Maybin JA, Hirani N, Jabbour HN, Critchley HOD (2011) Novel roles for hypoxia and prostaglandin E2 in the regulation of IL-8 during endometrial repair. *Am J Pathol* 178:1245–56.

193. Maybin JA, Hirani N, Brown P, Jabbour HN, Critchley HOD (2011) The regulation of vascular endothelial growth factor by hypoxia and prostaglandin $F_2\alpha$ during human endometrial repair. *J Clin Endocrinol Metab* 96:2475–83.

194. Finn CA, Pope M (1986) Control of leucocyte infiltration into the decidualized mouse uterus. *J Endocrinol* 110:93–6.

195. Riley SC, Poyser NL (1987) Effects of oestradiol, progesterone, hydrocortisone and oxytocin on prostaglandin output from the guinea-pig endometrium maintained in tissue culture. *Prostaglandins* 34:535–51.

196. Kelly RW, Smith SK (1987) Glucocorticoids do not share with progesterone the potent inhibitory action on prostaglandin synthesis in human proliferative phase endometrium. *Prostaglandins* 33:919–29.

197. Schatz F, Markiewicz L, Barg P, Gurpide E (1985) In vitro effects of ovarian steroids on prostaglandin F2 alpha output by human endometrium and endometrial epithelial cells. *J Clin Endocrinol Metab* 61:361–7.

198. Cane EM, Villee CA (1975) The synthesis of prostaglandin F by human endometrium in organ culture. *Prostaglandins* 9:281–8.

199. Hapangama DK, Critchley HOD, Henderson TA, Baird DT (2002) Mifepristone-induced vaginal bleeding is associated with increased immunostaining for cyclooxygenase-2 and decrease in prostaglandin dehydrogenase in luteal phase endometrium. *J Clin Endocrinol Metab* 87:5229–34.

200. Jensen D V, Andersen KB, Wagner G (1987) Prostaglandins in the menstrual cycle of women. A review. *Dan Med Bull* 34:178–82.

201. Ferenczy A (1976) Studies on the cytodynamics of human endometrial regeneration. II. Transmission electron microscopy and histochemistry. *Am J Obstet Gynaecol* 124:582–95.

202. Gleeson NC (1994) Cyclic changes in endometrial tissue plasminogen activator and plasminogen activator inhibitor type 1 in women with normal menstruation and essential menorrhagia. *Am J Obstet Gynaecol* 171:178–83.

203. Skjødt P, Albrechtsen OK (1965) Coagulation and Fibrinolysis in Uterine Blood: (Post-partum, during Menstruation, and during Abnormal Uterine Bleeding). *Acta Obstet Gynecol Scand* 44:416–436.

204. Salvatore CA (1969) Identification of fibrin in menstrual endometrium. *Am J Obstet Gynaecol* 103:537–43.

205. Jones RL, Kelly RW, Critchley HO (1997) Chemokine and cyclooxygenase-2 expression in human endometrium coincides with leukocyte accumulation. *Hum Reprod* 12:1300–6.

206. Zhang J, Lathbury LJ, Salamonsen LA (2000) Expression of the chemokine eotaxin and its receptor, CCR3, in human endometrium. *Biol Reprod* 62:404–11.

207. Lathbury LJ (2000) In-vitro studies of the potential role of neutrophils in the process of menstruation. *Mol Hum Reprod* 6:899–906.

208. Hampton AL, Rogers P, Affandi B, Salamonsen LA (2001) Expression of the chemokines, monocyte chemotactic protein (MCP)-1 and MCP-2 in endometrium of normal women and Norplant users, does not support a central role in macrophage infiltration into endometrium. *J Reprod Immunol* 49:115–32.

209. Jeziorska M (1995) Mast cell and eosinophil distribution and activation in human endometrium throughout the menstrual cycle. *Biol Reprod* 53:312–320.

210. King A, Loke YW (1991) On the nature and function of human uterine granular lymphocytes. *Immunol Today* 12:432–5.

211. King A, Gardner L, Loke YW (1999) Co-stimulation of human decidual natural killer cells by interleukin-2 and stromal cells. *Hum Reprod* 14:656–63.

212. Pace D, Morrison L, Bulmer JN (1989) Proliferative activity in endometrial stromal granulocytes throughout menstrual cycle and early pregnancy. *J Clin Pathol* 42:35–9.

213. Carson W, Caligiuri M (1996) Natural Killer Cell Subsets and Development. *Methods* 9:327–343.

214. Salamonsen LA, Zhang J, Brasted M (2002) Leukocyte networks and human endometrial remodelling. *J Reprod Immunol* 57:95–108.

215. Jeziorska M, Nagase H, Salamonsen LA, Woolley DE (1996) Immunolocalization of the matrix metalloproteinases gelatinase B and stromelysin 1 in human endometrium throughout the menstrual cycle. *Reproduction* 107:43–51.

216. Cornillie F et al. (1991) Lysosomal enzymes in the human endometrium: a biochemical study in untreated and levonorgestrel-treated women. *Contraception* 43:387–400.

217. Kaitu'u-Lino TJ, Morison NB, Salamonsen LA (2007) Neutrophil depletion retards endometrial repair in a mouse model. *Cell Tissue Res* 328:197–206.

218. Xu XB, He B, Wang JD (2007) Menstrual-like changes in mice are provoked through the pharmacologic withdrawal of progesterone using mifepristone following induction of decidualization. *Hum Reprod* 22:3184–91.

219. Marbaix E et al. (1996) Menstrual breakdown of human endometrium can be mimicked in vitro and is selectively and reversibly blocked by inhibitors of matrix metalloproteinases. *Proc Natl Acad Sci U S A* 93:9120–5.

220. Goffin F et al. (2003) Expression pattern of metalloproteinases and tissue inhibitors of matrix-metalloproteinases in cycling human endometrium. *Biol Reprod* 69:976–84.

221. Vassilev V et al. (2005) Response of matrix metalloproteinases and tissue inhibitors of metalloproteinases messenger ribonucleic acids to ovarian steroids in human endometrial explants mimics their gene- and phase-specific differential control in vivo. *J Clin Endocrinol Metab* 90:5848–57.

222. Hampton AL, Salamonsen LA (1994) Expression of messenger ribonucleic acid encoding matrix metalloproteinases and their tissue inhibitors is related to menstruation. *J Endocrinol* 141:R1–3.

223. Rodgers WH et al. (1994) Patterns of matrix metalloproteinase expression in cycling endometrium imply differential functions and regulation by steroid hormones. *J Clin Invest* 94:946–53.

224. Freitas S et al. (1999) Expression of Metalloproteinases and Their Inhibitors in Blood Vessels. 1082:1070–1082.

225. Rigot V, Marbaix E, Lemoine P, Courtoy PJ, Eeckhout Y (2001) In vivo perimenstrual activation of progelatinase B (proMMP-9) in the human endometrium and its dependence on stromelysin 1 (MMP-3) ex vivo. *Biochem J* 358:275–80.

226. Skinner JL, Riley SC, Gebbie AE, Glasier AF, Critchley HO (1999) Regulation of matrix metalloproteinase-9 in endometrium during the menstrual cycle and following administration of intrauterine levonorgestrel. *Hum Reprod* 14:793–9.

227. Rodgers WH et al. (1993) Expression and localization of matrilysin, a matrix metalloproteinase, in human endometrium during the reproductive cycle. *Am J Obstet Gynaecol* 168:253–60.

228. Lockwood CJ, Krikun G, Hausknecht VA, Papp C, Schatz F (1998) Matrix metalloproteinase and matrix metalloproteinase inhibitor expression in endometrial stromal cells during progestin-initiated decidualization and menstruation-related progestin withdrawal. *Endocrinology* 139:4607–13.

229. Henriet P et al. (2002) Circulating ovarian steroids and endometrial matrix metalloproteinases (MMPs). *Ann N Y Acad Sci* 955:119–38; discussion 157–8, 396–406.

230. Kaitu'u TJ, Shen J, Zhang J, Morison NB, Salamonsen LA (2005) Matrix metalloproteinases in endometrial breakdown and repair: functional significance in a mouse model. *Biol Reprod* 73:672–80.

231. Brenner RM, Rudolph L, Matrisian L, Slayden OD (1996) Non-human primate models; artificial menstrual cycles, endometrial matrix metalloproteinases and s.c. endometrial grafts. *Hum Reprod* 11 Suppl 2:150–64.

232. Kaiserman-Abramof IR, Padykula HA (1989) Angiogenesis in the postovulatory primate endometrium: the coiled arteriolar system. *Anat Rec* 224:479–89.

233. Brasted M, White CA, Kennedy TG, Salamonsen LA (2003) Mimicking the events of menstruation in the murine uterus. *Biol Reprod* 69:1273–1280.

234. Finn CA, Pope M (1984) Vascular and cellular changes in the decidualized endometrium of the ovariectomized mouse following cessation of hormone treatment: a possible model for menstruation. *J Endocrinol* 100:295–300.

235. Wang Q et al. (2013) A criticial period of progesterone withdrawal precedes endometrial breakdown and shedding in a mouse menstrual-like model. *Hum Reprod* 28:1670–1678.

236. Girling JE, Rogers PAW (2009) Regulation of endometrial vascular remodelling: role of the vascular endothelial growth factor family and the angiopoietin-TIE signalling system. *Reproduction* 138:883–93.

237. Ferenczy A (1976) Studies on the cytodynamics of human endometrial regeneration. 1. Scanning electron microscopy. *Am J Obstet Gynaecol* 124:64–73.

238. Critchley HO et al. (1998) Morphological and functional features of endometrial decidualization following long-term intrauterine levonorgestrel delivery. *Hum Reprod* 13:1218–24.

239. Kaitu'u-Lino TJ, Morison NB, Salamonsen LA (2007) Estrogen is not essential for full endometrial restoration after breakdown: Lessons from a mouse model. *Endocrinology* 148:5105–5111.

240. Matsuura-Sawada R et al. (2005) Reproduction of menstrual changes in transplanted human endometrial tissue in immunodeficient mice. *Hum Reprod* 20:1477–1484.

241. Novak E, Te Linde R (1924) in *Collected papers of members of the Gynecological Department of the Johns Hopkins Hospital and University : 1922 to 1928* (The journal of the American medical Association), pp 900–906.

242. Baggish MS, Pauerstein CJ, Woodruff JD (1967) Role of stroma in regeneration of endometrial epithelium. *Am J Obstet Gynaecol* 99:459–65.

243. Prianishnikov VA (1978) On the concept of stem cell and a model of functional morphological structure of the endometrium. *Contraception* 18:213–223.

244. Wright NA, Al-Nafussi A (1982) The kinetics of villus cell populations in the mouse small intestine. II. Studies on growth control after death of proliferative cells induced by cytosine arabinoside, with special reference to negative feedback mechanisms. *Cell Tissue Kinet* 15:611–21.

245. Potten CS, Loeffler M (1990) Stem cells: attributes, cycles, spirals, pitfalls and uncertainties. Lessons for and from the crypt. *Development* 110:1001–1020.

246. Bach SP, Renehan a G, Potten CS (2000) Stem cells: the intestinal stem cell as a paradigm. *Carcinogenesis* 21:469–76.

247. Booth C, Potten CS (2000) Gut instincts: thoughts on intestinal epithelial stem cells. *J Clin Invest* 105:1493–1499.

248. Barker N, van de Wetering M, Clevers H (2008) The intestinal stem cell. *Genes Dev* 22:1856–64.

249. Takeda N et al. (2011) Interconversion between intestinal stem cell populations in distinct niches. *Science (80-)* 334:1420–4.

250. Lipschutz J et al. (1999) Clonality of urogenital organs as determined by analysis of chimeric mice. *Cells Tissues Organs* 165:57–66.

251. Schwab K, Hutchison P, Gargett C (2008) Identification of surface markers for prospective isolation of human endometrial strom colony-forming cells. *Hum Reprod* 23:934–943.

252. Schofield R (1978) The relationship between the spleen colony-forming cell and the haemopoietic stem cell. *Blood Cells* 4:7–25.

253. Li Xie, T. L (2005) Stem cell niche: structure and function. *Annu Rev Cell Dev Biol* 21:605–631.

254. Shen Q et al. (2004) Endothelial cells stimulate self-renewal and expand neurogenesis of neural stem cells. *Science (80-)* 304:1338–1340.

255. Cotsarelis G, Sun TT, Lavker RM (1990) Label-retaining cells reside in the bulge area of pilosebaceous unit: implications for follicular stem cells, hair cycle, and skin carcinogenesis. *Cell* 61:1329–1337.

256. Calvi LM et al. (2003) Osteoblastic cells regulate the haematopoietic stem cell niche. *Nature* 425:841–846.

257. Chan R, Schwab K, Gargett C (2004) Clonogenicity of human endometrial epithelial and stromal cells. *Biol Reprod* 24:1738–1750.

258. Goodell MA, Brose K, Paradis G, Conner AS, Mulligan RC (1996) Isolation and functional properties of murine hematopoietic stem cells that are replicating in vivo. *J Exp Med* 183:1797–806.

259. Cervelló I et al. (2010) Human endometrial side population cells exhibit genotypic, phenotypic and functional features of somatic stem cells. *PLoS One* 5:e10964.

260. Cervelló I et al. (2011) Reconstruction of endometrium from human endometrial side population cell lines. *PLoS One* 6:e21221.

261. Schwab KE, Gargett CE (2007) Co-expression of two perivascular cell markers isolates mesenchymal stem-like cells from human endometrium. *Hum Reprod* 22:2903–11.

262. Masuda H, Anwar SS, Bühring H-J, Rao JR, Gargett CE (2012) A novel marker of human endometrial mesenchymal stem-like cells. *Cell Transplant* 21:2201–14.

263. Theise ND et al. (2000) Liver from bone marrow in humans. *Hepatology* 32:11–6.

264. Mezey E et al. (2003) Transplanted bone marrow generates new neurons in human brains. *Proc Natl Acad Sci U S A* 100:1364–9.

265. Nemeth K et al. (2012) Analyses of donor-derived keratinocytes in hairy and nonhairy skin biopsies of female patients following allogeneic male bone marrow transplantation. *Stem Cells Dev* 21:152–7.

266. Du H, Taylor HS (2007) Contribution of bone marrow-derived stem cells to endometrium and endometriosis. *Stem Cells* 25:2082–6.

267. Taylor HS (2004) Endometrial cells derived from donor stem cells in bone marrow transplant recipients. *JAMA* 292:81–5.

268. Cervelló I et al. (2012) Bone marrow-derived cells from male donors do not contribute to the endometrial side population of the recipient. *PLoS One* 7:e30260.

269. Report SA (2012) National heavy menstrual bleeding audit.

270. Hallberg L, Nilsson L (1964) Determination of menstrual blood loss. *Scand J Clin Lab Invest* 16:244–8.

271. Hallberg L, Högdahl AM, Nilsson L, Rybo G (1966) Menstrual blood loss--a population study. Variation at different ages and attempts to define normality. *Acta Obstet Gynecol Scand* 45:320–51.

272. Fraser I, Warner P, Marantos P (2001) Estimating menstrual blood loss in women with normal and excessive menstrual fluid volume. *Obstet Gynecol* 98:806–814.

273. Smith OPM, Jabbour HN, Critchley HOD (2007) Cyclooxygenase enzyme expression and E series prostaglandin receptor signalling are enhanced in heavy menstruation. *Hum Reprod* 22:1450–6.

274. Smith SK, Abel MH, Kelly RW, Baird DT (1981) Prostaglandin synthesis in the endometrium of women with ovular dysfunctional uterine bleeding. *Br J Obstet Gynaecol* 88:434–42.

275. Malik S, Day K, Perrault I, Charnock-Jones DS, Smith SK (2006) Reduced levels of VEGF-A and MMP-2 and MMP-9 activity and increased TNF-alpha in menstrual endometrium and effluent in women with menorrhagia. *Hum Reprod* 21:2158–66.

276. About Womb Cancer- A Quick Guide (2013) *Cancer Res UK's Patient Inf Website*:1–3. Available at: www.cruk.org/cancerhelp [Accessed July 27, 2013].

277. Bokhman J V (1983) Two pathogenetic types of endometrial carcinoma. *Gynecol Oncol* 15:10–7.

278. Hecht JL, Mutter GL (2006) Molecular and pathologic aspects of endometrial carcinogenesis. *J Clin Oncol* 24:4783–91.

279. Prat J, Gallardo A, Cuatrecasas M, Catasús L (2007) Endometrial carcinoma: pathology and genetics. *Pathology* 39:72–87.

280. Lax SF, Kendall B, Tashiro H, Slebos RJ, Hedrick L (2000) The frequency of p53, K-ras mutations, and microsatellite instability differs in uterine endometrioid and serous carcinoma: evidence of distinct molecular genetic pathways. *Cancer* 88:814–24.

281. Lax SF, Pizer ES, Ronnett BM, Kurman RJ (1998) Clear cell carcinoma of the endometrium is characterized by a distinctive profile of p53, Ki-67, estrogen, and progesterone receptor expression. *Hum Pathol* 29:551–8.

282. Beiner ME et al. (2007) The risk of endometrial cancer in women with BRCA1 and BRCA2 mutations. A prospective study. *Gynecol Oncol* 104:7–10.

283. Spruck CH et al. (2002) hCDC4 gene mutations in endometrial cancer. *Cancer Res* 62:4535–9.

284. Sherbet G V, Patil D (2003) Genetic abnormalities of cell proliferation, invasion and metastasis, with special reference to gynaecological cancers. *Anticancer Res* 23:1357–71.

285. Wallace AE, Gibson DA, Saunders PTK, Jabbour HN (2010) Inflammatory events in endometrial adenocarcinoma. *J Endocrinol* 206:141–57.

286. Giudice L (2010) Endometriosis. *N Engl J Med* 362:2389–2398.

287. Giudice L, Kao L (2004) Endometriosis. *Lancet* 364:1789–99.

288. Wang Y, Leng J, Shi J, Li X, Lang J (2010) Relationship between pain and nerve fibers distribution in multiple endometriosis lesions. *Zhonghua Fu Chan Ke Za Zhi* 45:260–3.

289. Dai Y, Leng J-H, Lang J-H, Li X-Y, Zhang J-J (2012) Anatomical distribution of pelvic deep infiltrating endometriosis and its relationship with pain symptoms. *Chin Med J (Engl)* 125:209–13.

290. Stratton P, Berkley KJ (2011) Chronic pelvic pain and endometriosis: translational evidence of the relationship and implications. *Hum Reprod Update* 17:327–46.

291. Fauconnier A, Chapron C (2005) Endometriosis and pelvic pain: epidemiological evidence of the relationship and implications. *Hum Reprod Update* 11:595–606.

292. Sampson JA (1927) Metastatic or Embolic Endometriosis, due to the Menstrual Dissemination of Endometrial Tissue into the Venous Circulation. *Am J Pathol* 3:93–110.43.

293. Jelihovsky T, Grant AF (1968) Endometriosis of the lung. *Thorax* 23:434–7.

294. Ichida M et al. (1993) A case of cerebral endometriosis causing catamenial epilepsy. *Neurology* 43:2708–2708.

295. Martin JD, Hauck AE (1985) Endometriosis in the male. *Am Surg* 51:426–30.

296. Starzinski-Powitz A, Zeitvogel A, Schreiner A, Baumann R (2003) Endometriosis--a stem cell disease? *Zentralbl Gynakol* 125:235–8.

297. Young VJ, Brown JK, Saunders PTK, Horne AW (2013) The role of the peritoneum in the pathogenesis of endometriosis. *Hum Reprod Update*.

298. Hull ML et al. (2008) Endometrial-peritoneal interactions during endometriotic lesion establishment. *Am J Pathol* 173:700–15.

299. Polson DW, Wadsworth J, Adams J, Franks S (1988) Polycystic ovaries- a common finding in normal women. *Lancet* 331:870–872.

300. Adams J, Polson DW, Franks S (1986) Prevalence of polycystic ovaries in women with anovulation and idiopathic hirsutism. *BMJ* 293:355–359.

301. Clayton RN et al. (1992) How common are polycystic ovaries in normal women and what is their significance for the fertility of the population? *Clin Endocrinol (Oxf)* 37:127–34.

302. Farquhar CM, Birdsall M, Manning P, Mitchell JM, France JT (1994) The prevalence of polycystic ovaries on ultrasound scanning in a population of randomly selected women. *Aust N Z J Obstet Gynaecol* 34:67–72.

303. Eden JA et al. (1989) The diagnosis of polycystic ovaries in subfertile women. *Br J Obstet Gynaecol* 96:809–15.

304. Kousta E, White DM, Cela E, McCarthy MI, Franks S (1999) The prevalence of polycystic ovaries in women with infertility. *Hum Reprod* 14:2720–3.

305. Sharpless JL (2003) Polycystic ovary syndrome and the metabolic syndrome. *Clin Diabetes* 21:154–161.

306. Carmina E (2006) Metabolic syndrome in polycystic ovary syndrome. *Minerva Ginecol* 58:109–14.

307. Dunaif A (1997) Insulin Resistance and the Polycystic Ovary Syndrome: Mechanism and Implications for Pathogenesis. *Endocr Rev* 18:774–800.

308. Gambineri A, Pelusi C, Vicennati V, Pagotto U, Pasquali R (2002) Obesity and the polycystic ovary syndrome. *Int J Obes Relat Metab Disord* 26:883–96.

309. Rebar RW, Connolly H V (1990) Clinical features of young women with hypergonadotropic amenorrhea. *Fertil Steril* 53:804–10.

310. Gilling-Smith C, Willis DS, Beard RW, Franks S (1994) Hypersecretion of androstenedione by isolated thecal cells from polycystic ovaries. *J Clin Endocrinol Metab* 79:1158–65.

311. Garrett A, Quinn MA (2008) Hormonal therapies and gynaecological cancers. *Best Pract Res Clin Obstet Gynaecol* 22:407–21.

312. Zhu M-L, Kyprianou N (2010) Role of androgens and the androgen receptor in epithelial-mesenchymal transition and invasion of prostate cancer cells. *FASEB J* 24:769–77.

313. Levine A et al. (1998) Androgens induce the expression of vascular endothelial growth factor in human fetal prostatic fibroblasts. *Endocrinology* 139:4672–8.

314. Finn CA (1987) Why Do Women And Some OTher Primates Mesntruate? . *Perspect Biol Med* 30:566–574.

315. Emera D et al. (2012) Convergent evolution of endometrial prolactin expression in primates, mice, and elephants through the independent recruitment of transposable elements. *Mol Biol Evol* 29:239–47.

316. Rasweiler J (1991) Spontaneous decidual reactions and menstruation in the black mastiff bat, Molossus ater. *Am J Anat* 191:1–22.

317. Strassmann BI (1996) The evolution of endometrial cycles and menstruation. *Q Rev Biol* 71:181–220.

318. Kaitu'u-Lino TJ, Ye L, Gargett CE (2010) Reepithelialization of the uterine surface arises from endometrial glands: Evidence from a functional mouse model of breakdown and repair. *Endocrinology* 151:3386–3395.

319. Kaitu'u-Lino TJ, Phillips DJ, Morison NB, Salamonsen LA (2009) A new role for activin in endometrial repair after menses. *Endocrinology* 150:1904–1911.

320. Fan X et al. (2012) Dynamic regulation of Wnt7a expression in the primate endometrium: implications for postmenstrual regeneration and secretory transformation. *Endocrinology* 153:1063–9.

321. Coudyzer P et al. (2013) Hypoxia is not required for human endometrial breakdown or repair in a xenograft model of menstruation. *FASEB J*.

322. Guo Y, He B, Xu X, Wang J (2011) Comprehensive analysis of leukocytes, vascularization and matrix metalloproteinases in human menstrual xenograft model. *PLoS One* 6:e16840.

323. Satyaswaroop PG, Tabibzadeh S (2000) Progestin regulation of human endometrial function. *Hum Reprod* 15 Suppl 1:74–80.

324. Masuda H et al. (2007) Noninvasive and real-time assessment of reconstructed functional human endometrium in NOD/SCID/gamma c(null) immunodeficient mice. *Proc Natl Acad Sci U S A* 104:1925–30.

325. Guo Y, He B, Xu X, Wang J (2011) Comprehensive analysis of leukocytes, vascularization and matrix metalloproteinases in human menstrual xenograft model. *PLoS One* 6:e16840.

326. Van Esch E, Cline JM, Buse E, Weinbauer GF (2008) The Macaque Endometrium, with Special Reference to the Cynomolgus Monkey (Macaca fascicularis). *Toxicol Pathol* 36:67S–100S.

327. Cao W, Mah K, Carroll RS, Slayden OD, Brenner RM (2007) Progesterone withdrawal up-regulates fibronectin and integrins during menstruation and repair in the rhesus macaque endometrium. *Hum Reprod* 22:3223–31.

328. Nayak NR, Brenner RM (2002) Vascular proliferation and vascular endothelial growth factor expression in the rhesus macaque endometrium. *J Clin Endocrinol Metab* 87:1845–55.

329. Slayden OD, Brenner RM (2006) A critical period of progesterone withdrawal precedes menstruation in macaques. *Reprod Biol Endocrinol* 4 Suppl 1:S6.

330. Fata JE, Chaudhary V, Khokha R (2001) Cellular turnover in the mammary gland is correlated with systemic levels of progesterone and not 17beta-estradiol during the estrous cycle. *Biol Reprod* 65:680–688.

331. Finn CA, Keen PM (1963) The induction of deciduoma in the rat. *J Embryol Exp Morphol* 11:673–82.

332. Finn C, Hinchliffe J (1964) Reaction of the mouse uterus during implantation and deciduoma formation as demonstrated by changes in the distribution of alkaline phosphatase. *J Reprod Fertil* 8:331–8.

333. Milligan SR, Cohen PE (1994) Silastic implants for delivering physiological concentrations of progesterone to mice. *Reprod Fertil Dev* 6:235–9.

334. Menning A et al. (2012) Granulocytes and vascularization regulate uterine bleeding and tissue remodeling in a mouse menstruation model. *PLoS One* 7:e41800.

335. Xu XB, He B, Wang JD (2007) Menstrual-like changes in mice are provoked through the pharmacologic withdrawal of progesterone using mifepristone following induction of decidualization. *Hum Reprod* 22:3184–91.

336. Rudolph M et al. (2012) Induction of overt menstruation in intact mice. *PLoS One* 7:e32922.

337. Mettus R V, Rane SG (2003) Characterization of the abnormal pancreatic development, reduced growth and infertility in Cdk4 mutant mice. *Oncogene* 22:8413–8421.

338. Stanley ER et al. (1997) Biology and action of colony--stimulating factor-1. *Mol Reprod Dev* 46:4–10.

339. Xie Y, Chen C, Hume DA (2001) Transcriptional regulation of c-fms gene expression. *Cell Biochem Biophys* 34:1–16.

340. Yue X, Favot P, Dunn TL, Cassady a I, Hume DA (1993) Expression of mRNA encoding the macrophage colony-stimulating factor receptor (c-fms) is controlled by a constitutive promoter and tissue-specific transcription elongation. *Mol Cell Biol* 13:3191–201.

341. Sasmono RT et al. (2003) A macrophage colony-stimulating factor receptor-green fluorescent protein transgene is expressed throughout the mononuclear phagocyte system of the mouse. *Blood* 101:1155–63.

342. Sasmono RT, Williams E (2012) Leucocytes. 844:157–176.

343. Gibson NJ (2006) The use of real-time PCR methods in DNA sequence variation analysis. *Clin Chim Acta* 363:32–47.

344. Taylor CR (1979) Immunohistologic studies of lymphomas. New methodology yields new information and poses new problems. *J Histochem Cytochem* 27:1189–91.

345. Suurmeijer AJ, Boon ME (1993) Notes on the application of microwaves for antigen retrieval in paraffin and plastic tissue sections. *Eur J Morphol* 31:144–50.

346. Shi SR, Key ME, Kalra KL (1991) Antigen retrieval in formalin-fixed, paraffin-embedded tissues: an enhancement method for immunohistochemical staining based on microwave oven heating of tissue sections. *J Histochem Cytochem* 39:741–748.

347. Evers P, Uylings HBM (1994) Effects of microwave pretreatment on immunocytochemical staining of vibratome sections and tissue blocks of human cerebral cortex stored in formaldehyde fixative for long periods. *J Neurosci Methods* 55:163–172.

348. Shi SR, Imam SA, Young L, Cote RJ, Taylor CR (1995) Antigen retrieval immunohistochemistry under the influence of pH using monoclonal antibodies. *J Histochem Cytochem* 43:193–201.

349. Prenant A (1898) La valeur morphologique du corps jaune. Son action physiologique et therapeutique possible. *Rev Gen Sci Pures Appl Bull Assoc Fr Av Sci* 9:646–650.

350. Morison NB, Kaitu'u-Lino TJ, Fraser IS, Salamonsen LA (2008) Stimulation of epithelial repair is a likely mechanism for the action of mifepristone in reducing duration of bleeding in users of progestogen-only contraceptives. *Reproduction* 136:267–74.

351. Schäfer WR et al. (2011) Critical evaluation of human endometrial explants as an ex vivo model system: a molecular approach. *Mol Hum Reprod* 17:255–65.

352. Catalano RD et al. (2003) The effect of RU486 on the gene expression profile in an endometrial explant model. *Mol Hum Reprod* 9:465–73.

353. Shively CA, Register TC, Grant KA, Johnson JL, Cline JM (2004) Effects of social status and moderate alcohol consumption on mammary gland and endometrium of surgically postmenopausal monkeys. *Menopause* 11:389–99.

354. Schild LJ et al. (2003) Formation of tamoxifen-DNA adducts in multiple organs of adult female cynomolgus monkeys dosed with tamoxifen for 30 days. *Cancer Res* 63:5999–6003.

355. Brenner RM, Slayden OD (2012) Molecular and functional aspects of menstruation in the macaque. *Rev Endocr Metab Disord* 13:309–18.

356. Slayden OD, Chwalisz K, Brenner RM (2001) Reversible suppression of menstruation with progesterone antagonists in rhesus macaques. *Hum Reprod* 16:1562–74.

357. Fazleabas AT (2006) A baboon model for inducing endometriosis. *Methods Mol Med* 121:95–9.

358. Fazleabas AT, Brudney A, Gurates B, Chai D, Bulun S (2002) A modified baboon model for endometriosis. *Ann N Y Acad Sci* 955:308–17; discussion 340–2, 396–406.

359. Hastings JM, Fazleabas AT (2006) A baboon model for endometriosis: implications for fertility. *Reprod Biol Endocrinol* 4 Suppl 1:S7.

360. MacKenzie WF, Casey HW (1975) Animal model of human disease. Endometriosis. Animal model: endometriosis in rhesus monkeys. *Am J Pathol* 80:341–4.

361. Rier SE, Martin DC, Bowman RE, Dmowski WP, Becker JL (1993) Endometriosis in rhesus monkeys (Macaca mulatta) following chronic exposure to 2,3,7,8-tetrachlorodibenzo-p-dioxin. *Fundam Appl Toxicol* 21:433–41.

362. Rier SE, Martin DC, Bowman RE, Becker JL (1995) Immunoresponsiveness in endometriosis: implications of estrogenic toxicants. *Environ Health Perspect* 103 Suppl:151–6.

363. VandeBerg JL, Williams-Blangero S (1997) Advantages and limitations of nonhuman primates as animal models in genetic research on complex diseases. *J Med Primatol* 26:113–9.

364. Smith L (2011) Good planning and serendipity: exploiting the Cre/Lox system in the testis. *Reproduction* 141:151–61.

365. De Feo VJ (1966) Vaginal-cervical vibration: a simple and effective method for the induction of pseudopregnancy in the rat. *Endocrinology* 79:440–2.

366. Finn CA, Martin L (1971) The onset of progesterone secretion during pregnancy in the mouse. *J Reprod Fertil* 25:299–300.

367. Jabbour HN, Critchley HO (2001) Potential roles of decidual prolactin in early pregnancy. *Reproduction* 121:197–205.

368. Kaitu'u-Lino TJ, Ye L, Salamonsen LA, Girling JE, Gargett CE (2012) Identification of label-retaining perivascular cells in a mouse model of endometrial decidualization, breakdown, and repair. *Biol Reprod*.

369. Cousins FL et al. (2014) Evidence from a Mouse Model That Epithelial Cell Migration and Mesenchymal-Epithelial Transition Contribute to Rapid Restoration of Uterine Tissue Integrity during Menstruation. *PLoS One* 9:e86378.

370. Lim J, Thiery JP (2012) Epithelial-mesenchymal transitions: insights from development. *Development* 139:3471–3486.

371. Kalluri R, Weinberg RA (2009) Review series The basics of epithelial-mesenchymal transition. 119.

372. Hao L, Ha JR, Kuzel P, Garcia E, Persad S (2012) Cadherin Switch from E- to N-Cadherin in Melanoma Progression is regulated by the PI3K/PTEN Pathway through TWIST and SNAIL. *Br J Dermatol* 166:1184–1197.

373. Craene B De, Berx G (2012) Regulatory networks defining EMT during cancer initiation and progression. *Nat Rev Cancer* 13:97–110.

374. Brabletz T (2012) EMT and MET in metastasis: where are the cancer stem cells? *Cancer Cell* 22:699–701.

375. Huang C-C, Orvis GD, Wang Y, Behringer RR (2012) Stromal-to-epithelial transition during postpartum endometrial regeneration. *PLoS One* 7:e44285.

376. Patterson AL, Zhang L, Arango NA, Teixeira J, Pru JK (2013) Mesenchymal-to-epithelial transition contributes to endometrial regeneration following natural and artificial decidualization. *Stem Cells Dev* 22:1–11.

377. Humtsoe JO et al. (2012) Transcriptional profiling identifies upregulated genes following induction of epithelial-mesenchymal transition in squamous carcinoma cells. *Exp Cell Res* 318:379–90.

378. Stemmer V, de Craene B, Berx G, Behrens J (2008) Snail promotes Wnt target gene expression and interacts with beta-catenin. *Oncogene* 27:5075–80.

379. Casas E et al. (2011) Snail2 is an essential mediator of Twist1-induced epithelial mesenchymal transition and metastasis. *Cancer Res* 71:245–54.

380. Gargett CE, Schwab KE, Zillwood RM, Nguyen HPT, Wu D (2009) Isolation and culture of epithelial progenitors and mesenchymal stem cells from human endometrium. *Biol Reprod* 80:1136–45.

381. Zhang W-B et al. (2012) A study in vitro on differentiation of bone marrow mesenchymal stem cells into endometrial epithelial cells in mice. *Eur J Obstet Gynecol Reprod Biol* 160:185–90.

382. Bratincsák A et al. (2007) CD45-positive blood cells give rise to uterine epithelial cells in mice. *Stem Cells* 25:2820–6.

383. Masuda H et al. (2010) Stem cell-like properties of the endometrial side population: implication in endometrial regeneration. *PLoS One* 5:e10387.

384. Tsuji S et al. (2008) Side population cells contribute to the genesis of human endometrium. *Fertil Steril* 90:1528–37.

385. Chan RWS, Gargett CE (2006) Identification of label-retaining cells in mouse endometrium. *Stem Cells* 24:1529–38.

386. Cervelló I, Martínez-Conejero JA, Horcajadas JA, Pellicer A, Simón C (2007) Identification, characterization and co-localization of label-retaining cell population in mouse endometrium with typical undifferentiated markers. *Hum Reprod* 22:45–51.

387. Gargett CE (2006) Identification and characterisation of human endometrial stem/progenitor cells. *Aust N Z J Obstet Gynaecol* 46.

388. Greenburg G, Hay ED (1982) Epithelia suspended in collagen gels can lose polarity and express characteristics of migrating mesenchymal cells. *J Cell Biol* 95:333–9.

389. Hay ED (1990) Role of cell-matrix contacts in cell migration and epithelial-mesenchymal transformation. *Cell Differ Dev* 32:367–75.

390. Hay ED (2005) The mesenchymal cell, its role in the embryo, and the remarkable signaling mechanisms that create it. *Dev Dyn* 233:706–20.

391. Nakaya Y, Kuroda S, Katagiri YT, Kaibuchi K, Takahashi Y (2004) Mesenchymal-epithelial transition during somitic segmentation is regulated by differential roles of Cdc42 and Rac1. *Dev Cell* 7:425–38.

392. Lu T et al. (2012) Targeting androgen receptor to suppress macrophage-induced EMT and benign prostatic hyperplasia (BPH) development. *Mol Endocrinol* 26:1707–15.

393. Lundgren K, Nordenskjöld B, Landberg G (2009) Hypoxia, Snail and incomplete epithelial-mesenchymal transition in breast cancer. *Br J Cancer* 101:1769–81.

394. Jang TJ, Jeon KH, Jung KH (2009) Cyclooxygenase-2 expression is related to the epithelial-to-mesenchymal transition in human colon cancers. *Yonsei Med J* 50:818–24.

395. Kim NH et al. (2011) A p53/miRNA-34 axis regulates Snail1-dependent cancer cell epithelial-mesenchymal transition. *J Cell Biol* 195:417–33.

396. Scherbakov AM, Andreeva OE, Shatskaya VA, Krasil'nikov MA (2012) The relationships between snail1 and estrogen receptor signaling in breast cancer cells. *J Cell Biochem* 113:2147–55.

397. Fuxe J, Karlsson MCI (2012) TGF-β-induced epithelial-mesenchymal transition: A link between cancer and inflammation. *Semin Cancer Biol*:1–7.

398. Winter E, Gittenberger-de Groot A (2007) Epicardium-derived cells in cardiogenesis and cardiac regeneration. *Cell Mol Life Sci* 64:692–703.

399. Von Gise A et al. (2011) WT1 regulates epicardial epithelial to mesenchymal transition through β-catenin and retinoic acid signaling pathways. *Dev Biol* 356:421–31.

400. Chai J et al. (2010) CCN1 induces a reversible epithelial-mesenchymal transition in gastric epithelial cells. *Lab Investig a J Tech methods Pathol* 90:1140–51.

401. Macneil S (2009) Research article Co-culture of intestinal epithelial and stromal cells in 3D collagen-based environments research article. 4:397–406.

402. Leong KG et al. (2007) Jagged1-mediated Notch activation induces epithelial-to-mesenchymal transition through Slug-induced repression of E-cadherin. *J Exp Med* 204:2935–48.

403. Li B, Zheng Y-W, Sano Y, Taniguchi H (2011) Evidence for mesenchymal-epithelial transition associated with mouse hepatic stem cell differentiation. *PLoS One* 6:e17092.

404. Martínez-Estrada OM et al. (2010) Wt1 is required for cardiovascular progenitor cell formation through transcriptional control of Snail and E-cadherin. *Nat Genet* 42:89–93.

405. Thiery JP, Sleeman JP (2006) Complex networks orchestrate epithelial-mesenchymal transitions. *Nat Rev Mol Cell Biol* 7:131–42.

406. Chau Y-Y, Hastie ND (2012) The role of Wt1 in regulating mesenchyme in cancer, development, and tissue homeostasis. *Trends Genet* 28:515–24.

407. Scholz H, Kirschner KM (2011) Oxygen-dependent gene expression in development and cancer: Lessons learned from the Wilms' tumor gene, WT1. *Front Mol Neurosci* 4:4.

408. Discenza MT, Pelletier J (2004) Insights into the physiological role of WT1 from studies of genetically modified mice. *Physiol Genomics* 16:287–300.

409. Chau Y-Y et al. (2011) Acute multiple organ failure in adult mice deleted for the developmental regulator Wt1. *PLoS Genet* 7:e1002404.

410. Kreidberg JA et al. (1993) WT-1 is required for early kidney development. *Cell* 74:679–91.

411. Cano A et al. (2000) The transcription factor snail controls epithelial-mesenchymal transitions by repressing E-cadherin expression. *Nat Cell Biol* 2:76–83.

412. Batlle E et al. (2000) The transcription factor snail is a repressor of E-cadherin gene expression in epithelial tumour cells. *Nat Cell Biol* 2:84–9.

413. Bolos V (2002) The transcription factor Slug represses E-cadherin expression and induces epithelial to mesenchymal transitions: a comparison with Snail and E47 repressors. *J Cell Sci* 116:499–511.

414. Troxell M et al. (2000) Inhibiting cadherin function by dominant mutant E-cadherin expression increases the extent of tight junction assembly. *J Cell Sci* 113 (Pt 6:985–96.

415. Zeisberg M, Shah AA, Kalluri R (2005) Bone morphogenic protein-7 induces mesenchymal to epithelial transition in adult renal fibroblasts and facilitates regeneration of injured kidney. *J Biol Chem* 280:8094–100.

416. Plisov SY et al. (2000) Mesenchymal-epithelial transition in the developing metanephric kidney: gene expression study by differential display. *Genesis* 27:22–31.

417. Tunggal JA et al. (2005) E-cadherin is essential for in vivo epidermal barrier function by regulating tight junctions. *EMBO J* 24:1146–56.

418. Nelson WJ (2009) Remodeling epithelial cell organization: transitions between front-rear and apical-basal polarity. *Cold Spring Harb Perspect Biol* 1:a000513.

419. Babischkin JS et al. (2009) Estrogen stimulates the human endometrium to express a factor(s) that promotes vascular smooth muscle cell migration as an early step in microvessel remodeling. *Endocrine* 35:81–8.

420. Huang JC, Liu DY, Dawood MY (1998) The expression of vascular endothelial growth factor isoforms in cultured human endometrial stromal cells and its regulation by 17beta-oestradiol. *Mol Hum Reprod* 4:603–7.

421. Gargett CE, Lederman FL, Lau TM, Taylor NH, Rogers P (1999) Lack of correlation between vascular endothelial growth factor production and endothelial cell proliferation in the human endometrium. *Hum Reprod* 14:2080–8.

422. Smith WL, Marnett LJ (1991) Prostaglandin endoperoxide synthase: structure and catalysis. *Biochim Biophys Acta* 1083:1–17.

423. Maybin JA et al. (2012) The presence and regulation of connective tissue growth factor in the human endometrium. *Hum Reprod* 27:1112–21.

424. Kamat BR, Isaacson PG (1987) The immunocytochemical distribution of leukocytic subpopulations in human endometrium. *Am J Pathol* 127:66–73.

425. Salamonsen LA, Butt AR, Hammond FR, Garcia S, Zhang J (1997) Production of endometrial matrix metalloproteinases, but not their tissue inhibitors, is modulated by progesterone withdrawal in an in vitro model for menstruation. *J Clin Endocrinol Metab* 82:1409–15.

426. Froberg K, Brown RE, Gaylord H, Manivel C (1998) Intra-abdominal desmoplastic small round cell tumor: immunohistochemical evidence for up-regulation of autocrine and paracrine growth factors. *Ann Clin Lab Sci* 28:386–93.

427. Jiang MC, Liao CF, Lee PH (2001) Aspirin inhibits matrix metalloproteinase-2 activity, increases E-cadherin production, and inhibits in vitro invasion of tumor cells. *Biochem Biophys Res Commun* 282:671–7.

428. Jing S-W et al. (2012) HIF-1α contributes to hypoxia-induced invasion and metastasis of esophageal carcinoma via inhibiting E-cadherin and promoting MMP-2 expression. *Acta Med Okayama* 66:399–407.

429. Cowden Dahl KD et al. (2008) Matrix metalloproteinase 9 is a mediator of epidermal growth factor-dependent e-cadherin loss in ovarian carcinoma cells. *Cancer Res* 68:4606–13.

430. Sancéau J, Truchet S, Bauvois B (2003) Matrix metalloproteinase-9 silencing by RNA interference triggers the migratory-adhesive switch in Ewing's sarcoma cells. *J Biol Chem* 278:36537–46.

431. Bosco MC et al. (2004) Hypoxia selectively inhibits monocyte chemoattractant protein-1 production by macrophages. *J Immunol* 172:1681–90.

432. Azuma C et al. (1990) Steroid hormones induce macrophage colony-stimulating factor (MCSF) and MCSF receptor mRNAs in the human endometrium. *J Mol Endocrinol* 5:103–8.

433. Azuma C et al. (1991) The gene expressions of macrophage colony-stimulating factor (MCSF) and MCSF receptor in the human myometrium during pregnancy: regulation by sex steroid hormones. *J Steroid Biochem Mol Biol* 39:883–8.

434. Werner F et al. (2000) Transforming growth factor-beta 1 inhibition of macrophage activation is mediated via Smad3. *J Biol Chem* 275:36653–8.

435. Feinberg MW et al. (2004) Essential role for Smad3 in regulating MCP-1 expression and vascular inflammation. *Circ Res* 94:601–8.

436. Michelotti GA et al. (2013) Smoothened is a master regulator of adult liver repair. *J Clin Invest* 123:2380–2394.

437. Herrera MB et al. (2004) Mesenchymal stem cells contribute to the renal repair of acute tubular epithelial injury. *Int J Mol Med* 14:1035–41.

438. Jones RL (2004) Identification of Chemokines Important for Leukocyte Recruitment to the Human Endometrium at the Times of Embryo Implantation and Menstruation. *J Clin Endocrinol Metab* 89:6155–6167.

439. Zhang J, Salamonsen LA (2002) Expression of hypoxia-inducible factors in human endometrium and suppression of matrix metalloproteinases under hypoxic conditions do not support a major role for hypoxia in regulating tissue breakdown at menstruation. *Hum Reprod* 17:265–74.

440. Cakarova L et al. (2009) Macrophage tumor necrosis factor-alpha induces epithelial expression of granulocyte-macrophage colony-stimulating factor: impact on alveolar epithelial repair. *Am J Respir Crit Care Med* 180:521–32.

441. Murdoch C, Giannoudis A, Lewis CE (2004) Mechanisms regulating the recruitment of macrophages into hypoxic areas of tumors and other ischemic tissues. *Blood* 104:2224–34.

442. Carr MW (1994) Monocyte Chemoattractant Protein 1 Acts as a T-Lymphocyte Chemoattractant. *Proc Natl Acad Sci* 91:3652–3656.

443. Bischoff SC, Krieger M, Brunner T, Dahinden CA (1992) Monocyte chemotactic protein 1 is a potent activator of human basophils. *J Exp Med* 175:1271–5.

444. Allavena P et al. (1994) Induction of natural killer cell migration by monocyte chemotactic protein-1, -2 and -3. *Eur J Immunol* 24:3233–6.

445. Negus RP et al. (1995) The detection and localization of monocyte chemoattractant protein-1 (MCP-1) in human ovarian cancer. *J Clin Invest* 95:2391–6.

446. Arici A, Senturk LM, Seli E, Bahtiyar MO, Kim G (1999) Regulation of monocyte chemotactic protein-1 expression in human endometrial stromal cells by estrogen and progesterone. *Biol Reprod* 61:85–90.

447. Brenner RM, Nayak NR, Slayden OD, Critchley HOD, Kelly RW (2002) Premenstrual and menstrual changes in the macaque and human endometrium: relevance to endometriosis. *Ann N Y Acad Sci* 955:60–74; discussion 86–8, 396–406.

448. Leonard EJ, Yoshimura T (1990) Human monocyte chemoattractant protein-1 (MCP-1). *Immunol Today* 11:97–101.

449. King AE et al. (2001) Cd40 expression in uterine tissues: a key regulator of cytokine expression by fibroblasts. *J Clin Endocrinol Metab* 86:405–12.

450. Li M-Q et al. (2012) Chemokine CCL2 enhances survival and invasiveness of endometrial stromal cells in an autocrine manner by activating Akt and MAPK/Erk1/2 signal pathway. *Fertil Steril* 97:919–29.

451. Arici A, MacDonald PC, Casey ML (1995) Regulation of monocyte chemotactic protein-1 gene expression in human endometrial cells in cultures. *Mol Cell Endocrinol* 107:189–197.

452. Anton K, Banerjee D, Glod J (2012) Macrophage-associated mesenchymal stem cells assume an activated, migratory, pro-inflammatory phenotype with increased IL-6 and CXCL10 secretion. *PLoS One* 7:e35036.

453. Igarashi A, Okochi H, Bradham DM, Grotendorst GR (1993) Regulation of connective tissue growth factor gene expression in human skin fibroblasts and during wound repair. *Mol Biol Cell* 4:637–45.

454. Uzumcu M et al. (2000) Localization of connective tissue growth factor in human uterine tissues. *Mol Hum Reprod* 6:1093–8.

455. Grotendorst GR, Duncan MR (2005) Individual domains of connective tissue growth factor regulate fibroblast proliferation and myofibroblast differentiation. *FASEB J* 19:729–38.

456. Lee CH, Shah B, Moioli EK, Mao JJ (2010) CTGF directs fibroblast differentiation from human mesenchymal stem/stromal cells and defines connective tissue healing in a rodent injury model. *J Clin Invest* 120:3340–9.

457. White FJ et al. (2006) Secreted phosphoprotein 1 (osteopontin) is expressed by stromal macrophages in cyclic and pregnant endometrium of mice, but is induced by estrogen in luminal epithelium during conceptus attachment for implantation. *Reproduction* 132:919–29.

458. Aiuti A (1997) The chemokine SDF-1 is a chemoattractant for human CD34+ hematopoietic progenitor cells and provides a new mechanism to explain the mobilization of CD34+ progenitors to peripheral blood. *J Exp Med* 185:111–120.

459. Kim CH, Broxmeyer HE (1998) In vitro behavior of hematopoietic progenitor cells under the influence of chemoattractants: stromal cell-derived factor-1, steel factor, and the bone marrow environment. *Blood* 91:100–10.

460. Asahara T et al. (1999) VEGF contributes to postnatal neovascularization by mobilizing bone marrow-derived endothelial progenitor cells. *EMBO J* 18:3964–3972.

461. Spitzer TLB et al. (2011) Perivascular human endometrial mesenchymal stem cells express pathways relevant to self-renewal, lineage specification, and functional phenotype. *Biol Reprod* 86:1–16.

462. Gaide Chevronnay HP et al. (2009) Spatiotemporal coupling of focal extracellular matrix degradation and reconstruction in the menstrual human endometrium. *Endocrinology* 150:5094–105.

463. Lu X, Kang Y (2010) Hypoxia and hypoxia-inducible factors: master regulators of metastasis. *Clin Cancer Res* 16:5928–35.

464. Feng Z et al. (2013) Aberrant expression of hypoxia-inducible factor 1α, TWIST and E-cadherin is associated with aggressive tumor phenotypes in endometrioid endometrial carcinoma. *Jpn J Clin Oncol* 43:396–403.

465. Martin SK et al. (2010) Hypoxia-inducible factor-2 is a novel regulator of aberrant CXCL12 expression in multiple myeloma plasma cells. *Haematologica* 95:776–84.

466. Keith B, Simon MC (2007) Hypoxia-inducible factors, stem cells, and cancer. *Cell* 129:465–72.

467. Larsen M et al. (2008) Hypoxia-induced secretion of macrophage migration-inhibitory factor from MCF-7 breast cancer cells is regulated in a hypoxia-inducible factor-independent manner. *Cancer Lett* 265:239–49.

468. Catalano RD et al. (2011) Hypoxia and prostaglandin E receptor 4 signalling pathways synergise to promote endometrial adenocarcinoma cell proliferation and tumour growth. *PLoS One* 6:e19209.

469. Kryczek I, Wei S, Keller E, Liu R, Zou W (2007) Stroma-derived factor (SDF-1/CXCL12) and human tumor pathogenesis. *Am J Physiol Cell Physiol* 292:C987–95.

470. Kryczek I et al. (2005) CXCL12 and vascular endothelial growth factor synergistically induce neoangiogenesis in human ovarian cancers. *Cancer Res* 65:465–72.

471. Sharkey A et al. (2000) Vascular endothelial growth factor expression in human endometrium is regulated by hypoxia. *J Clin Endocrinol Metab* 85:402–9.

472. Sivridis E, Giatromanolaki A, Gatter KC, Harris AL, Koukourakis MI (2002) Association of hypoxia-inducible factors 1a and 2a with activated angiogenic pathways and prognosis in patients with endometrial carcinoma. *Cancer* 95:1055–1063.

473. Gospodarowicz D, Abraham J a, Schilling J (1989) Isolation and characterization of a vascular endothelial cell mitogen produced by pituitary-derived folliculo stellate cells. *Proc Natl Acad Sci U S A* 86:7311–5.

474. Maisonpierre PC et al. (1997) Angiopoietin-2, a natural antagonist for Tie2 that disrupts in vivo angiogenesis. *Science (80-)* 277:55–60.

475. Hewett P et al. (2002) Down-regulation of angiopoietin-1 expression in menorrhagia. *Am J Pathol* 160:773–80.

476. Pichiule P, Chavez JC, LaManna JC (2004) Hypoxic regulation of angiopoietin-2 expression in endothelial cells. *J Biol Chem* 279:12171–80.

477. Krikun G et al. (2005) Endometrial endothelial cell steroid receptor expression and steroid effects on gene expression. *J Clin Endocrinol Metab* 90:1812–8.

478. Simon M-P, Tournaire R, Pouyssegur J (2008) The angiopoietin-2 gene of endothelial cells is up-regulated in hypoxia by a HIF binding site located in its first intron and by the central factors GATA-2 and Ets-1. *J Cell Physiol* 217:809–18.

479. Pichiule P, Chavez JC, LaManna JC (2004) Hypoxic regulation of angiopoietin-2 expression in endothelial cells. *J Biol Chem* 279:12171–80.

480. Sánchez-Martín L et al. (2011) The chemokine CXCL12 regulates monocyte-macrophage differentiation and RUNX3 expression. *Blood* 117:88–97.

481. Karin N (2010) The multiple faces of CXCL12 (SDF-1alpha) in the regulation of immunity during health and disease. *J Leukoc Biol* 88:463–73.

482. Schioppa T et al. (2003) Regulation of the chemokine receptor CXCR4 by hypoxia. *J Exp Med* 198:1391–402.

483. Tsutsumi A et al. (2011) Estrogen induces stromal cell-derived factor 1 (SDF-1/CXCL12) production in human endometrial stromal cells: a possible role of endometrial epithelial cell growth. *Fertil Steril* 95:444–7.

484. Virgintino D et al. (2012) CXCL12/CXCR4/CXCR7 axis regulates microvessel growth in human developing cerebral cortex. *Ital J Anat Embryol* 117:199.

485. Li W et al. (2013) Peripheral nerve-derived CXCL12 and VEGF-A regulate the patterning of arterial vessel branching in developing limb skin. *Dev Cell* 24:359–71.

486. Zernecke A et al. (2005) SDF-1alpha/CXCR4 axis is instrumental in neointimal hyperplasia and recruitment of smooth muscle progenitor cells. *Circ Res* 96:784–91.

487. Harwood RJ, Lewis CE, Biswas SK (2012) in *Tumour Microenvironment and Myelomonocytic cells*, ed Biswas S, pp 89–111.

488. Murdoch C, Muthana M, Lewis CE (2005) Hypoxia regulates macrophage functions in inflammation. *J Immunol* 175:6257–6263.

489. Mojsilovic-Petrovic J et al. (2007) Hypoxia-inducible factor-1 (HIF-1) is involved in the regulation of hypoxia-stimulated expression of monocyte chemoattractant protein-1 (MCP-1/CCL2) and MCP-5 (Ccl12) in astrocytes. *J Neuroinflammation* 4:12.

490. Salvesen HB, Akslen LA (1999) Significance of tumour-associated macrophages, vascular endothelial growth factor and thrombospondin-1 expression for tumour angiogenesis and prognosis in endometrial carcinomas. *Int J Cancer* 84:538–43.

491. Ohno S et al. (2004) Correlation of histological localization of tumor-associated macrophages with clinicopathological features in endometrial cancer. *Anticancer Res* 24:3335–42.

492. Sica A et al. (2000) Defective expression of the monocyte chemotactic protein-1 receptor CCR2 in macrophages associated with human ovarian carcinoma. *J Immunol* 164:733–8.

493. Turner L, Scotton C, Negus R, Balkwill F (1999) Hypoxia inhibits macrophage migration. *Eur J Immunol* 29:2280–7.

494. Ueno T et al. (2000) Significance of macrophage chemoattractant protein-1 in macrophage recruitment, angiogenesis, and survival in human breast cancer. *Clin Cancer Res* 6:3282–9.

495. Baay-guzman GJ et al. (2012) HIF-1 expression is associated with CCL2 chemokine expression in airway inflammatory cells : implications in allergic airway inflammation. *Respir Res* 13:1–11.

496. Kobayashi H et al. (2012) Myeloid cell-derived hypoxia-inducible factor attenuates inflammation in unilateral ureteral obstruction-induced kidney injury. *J Immunol* 188:5106–15.

497. Bruchovsky N, Wilson JD (1968) The Conversion of Testosterone to 5agr-Androstan-17{beta}-ol-3-one by Rat Prostate in Vivo and in Vitro. *J Biol Chem* 243:2012–2021.

498. Russell DW, Wilson JD (1994) Steroid 5 alpha-reductase: two genes/two enzymes. *Annu Rev Biochem* 63:25–61.

499. Ito K et al. (2002) Expression of androgen receptor and 5alpha-reductases in the human normal endometrium and its disorders. *Int J Cancer* 99:652–7.

500. Serafini P et al. (1986) Acute modulation of the hypothalamic-pituitary axis by intravenous testosterone in normal women. *Am J Obstet Gynaecol* 155:1288–92.

501. McEwan IJ (2009) Nuclear receptors: one big family. *Methods Mol Biol* 505:3–18.

502. Horie K, Takakura K, Imai K, Liao S, Mori T (1992) Immunohistochemical localization of androgen receptor in the human endometrium, decidua, placenta and pathological conditions of the endometrium. *Hum Reprod* 7:1461–6.

503. Slayden OD et al. (2001) Progesterone antagonists increase androgen receptor expression in the rhesus macaque and human endometrium. *J Clin Endocrinol Metab* 86:2668–79.

504. Kajihara T et al. (2012) Androgen signaling in decidualizing human endometrial stromal cells enhances resistance to oxidative stress. *Fertil Steril* 97:185–91.

505. Narukawa S et al. (1994) Androgens induce prolactin production by human endometrial stromal cells in vitro. *J Clin Endocrinol Metab* 78:165–8.

506. Miller N, Bédard YC, Cooter NB, Shaul DL (1986) Histological changes in the genital tract in transsexual women following androgen therapy. *Histopathology* 10:661–9.

507. Chadha S, Pache TD, Huikeshoven JM, Brinkmann AO, van der Kwast TH (1994) Androgen receptor expression in human ovarian and uterine tissue of long-term androgen-treated transsexual women. *Hum Pathol* 25:1198–204.

508. Futterweit W, Deligdisch L (1986) Histopathological effects of exogenously administered testosterone in 19 female to male transsexuals. *J Clin Endocrinol Metab* 62:16–21.

509. Zang H, Sahlin L, Masironi B, Eriksson E, Linden Hirschberg A (2007) Effects of testosterone treatment on endometrial proliferation in postmenopausal Women. *J Clin Endocrinol Metab* 92:2169–2175.

510. Kajihara T et al. (2013) Androgens modulate the morphological characteristics of human endometrial stromal cells decidualized in vitro. *Reprod Sci*.

511. Okon M (1998) Serum androgen levels in women who have recurrent miscarriages and their correlation with markers of endometrial function. *Fertil Steril* 69:682–690.

512. Apparao KBC, Lovely LP, Gui Y, Lininger RA, Lessey BA (2002) Elevated endometrial androgen receptor expression in women with polycystic ovarian syndrome. *Biol Reprod* 66:297–304.

513. Lethaby A et al. (2000) Hormone replacement therapy in postmenopausal women: endometrial hyperplasia and irregular bleeding. *Cochrane database Syst Rev*:CD000402.

514. Navaratnarajah R, Pillay OC, Hardiman P (2008) Polycystic ovary syndrome and endometrial cancer. *Semin Reprod Med* 26:62–71.

515. Fogle RH, Stanczyk FZ, Zhang X, Paulson RJ (2007) Ovarian androgen production in postmenopausal women. *J Clin Endocrinol Metab* 92:3040–3.

516. Adashi EY (1994) The climacteric ovary as a functional gonadotropin-driven androgen-producing gland. *Fertil Steril* 62:20–7.

517. Ala-Fossi SL, Mäenpää J, Aine R, Punnonen R (1998) Ovarian testosterone secretion during perimenopause. *Maturitas* 29:239–45.

518. Bulun SE, Economos K, Miller D, Simpson ER (1994) CYP19 (aromatase cytochrome P450) gene expression in human malignant endometrial tumors. *J Clin Endocrinol Metab* 79:1831–4.

519. Koivisto-Korander R, Butzow R, Koivisto A-M, Leminen A (2011) Immunohistochemical studies on uterine carcinosarcoma, leiomyosarcoma, and endometrial stromal sarcoma: expression and prognostic importance of ten different markers. *Tumour Biol* 32:451–9.

520. Moinfar F, Regitnig P, Tabrizi AD, Denk H, Tavassoli FA (2004) Expression of androgen receptors in benign and malignant endometrial stromal neoplasms. *Virchows Arch* 444:410–4.

521. Lovely LP, Appa Rao KB., Gui Y, Lessey BA (2000) Characterization of androgen receptors in a well-differentiated endometrial adenocarcinoma cell line (Ishikawa). *J Steroid Biochem Mol Biol* 74:235–241.

522. Chamberlain NL, Driver ED, Miesfeld RL (1994) The length and location of CAG trinucleotide repeats in the androgen receptor N-terminal domain affect transactivation function. *Nucleic Acids Res* 22:3181–6.

523. Tilley WD, Marcelli M, Wilson JD, McPhaul MJ (1989) Characterization and expression of a cDNA encoding the human androgen receptor. *Proc Natl Acad Sci U S A* 86:327–31.

524. Kuiper GG et al. (1989) Structural organization of the human androgen receptor gene. *J Mol Endocrinol* 2:R1–4.

525. Schildkraut JM et al. (2007) Trinucleotide repeat polymorphisms in the androgen receptor gene and risk of ovarian cancer. *Cancer Epidemiol Biomarkers Prev* 16:473–80.

526. Mifsud A, Ramirez S, Yong EL (2000) Androgen receptor gene CAG trinucleotide repeats in anovulatory infertility and polycystic ovaries. *J Clin Endocrinol Metab* 85:3484–8.

527. Ibáñez L et al. (2003) Androgen receptor gene CAG repeat polymorphism in the development of ovarian hyperandrogenism. *J Clin Endocrinol Metab* 88:3333–8.

528. Jääskeläinen J, Korhonen S, Voutilainen R, Hippeläinen M, Heinonen S (2005) Androgen receptor gene CAG length polymorphism in women with polycystic ovary syndrome. *Fertil Steril* 83:1724–8.

529. Sasaki M, Sakuragi N, Dahiya R (2003) The CAG repeats in exon 1 of the androgen receptor gene are significantly longer in endometrial cancer patients. *Biochem Biophys Res Commun* 305:1105–8.

530. McGrath M et al. (2006) Androgen receptor polymorphisms and endometrial cancer risk. *Int J Cancer* 118:1261–8.

531. Yang HP et al. (2009) Genetic variation in the androgen receptor gene and endometrial cancer risk. *Cancer Epidemiol Biomarkers Prev* 18:585–9.

532. Ju W, Kim SC (2007) Polymorphisms in CAG active allele length of the androgen receptor gene are not associated with increased risk of endometrial cancer. *Cancer Genet Cytogenet* 172:178–9.

533. Barbieri RL, Evans S, Kistner RW (1982) Danazol in the treatment of endometriosis: analysis of 100 cases with a 4-year follow-up. *Fertil Steril* 37:737–46.

534. Selak V, Farquhar C, Prentice A, Singla A (2007) Danazol for pelvic pain associated with endometriosis. *Cochrane database Syst Rev*:CD000068.

535. Daly DC, Maslar IA, Riddick DH (1983) Prolactin production during in vitro decidualization of proliferative endometrium. *Am J Obstet Gynaecol* 145:672–8.

536. Rokhlin OW et al. (2005) Androgen regulates apoptosis induced by TNFR family ligands via multiple signaling pathways in LNCaP. *Oncogene* 24:6773–84.

537. Lorenzo PI, Saatcioglu F (2008) Inhibition of apoptosis in prostate cancer cells by androgens is mediated through downregulation of c-Jun N-terminal kinase activation. *Neoplasia* 10:418–28.

538. Choudhary V et al. (2011) Novel role of androgens in mitochondrial fission and apoptosis. *Mol Cancer Res* 9:1067–77.

539. Sahlgren C, Gustafsson M V, Jin S, Poellinger L, Lendahl U (2008) Notch signaling mediates hypoxia-induced tumor cell migration and invasion. *Proc Natl Acad Sci U S A* 105:6392–7.

540. Evangelou A (2002) Androgen modulation of adhesion and antiadhesion Molecules in PC-3 prostate cancer cells expressing androgen receptor. *Endocrinology* 143:3897–3904.

541. Nightingale J et al. (2003) Ligand activation of the androgen receptor downregulates E-cadherin-mediated cell adhesion and promotes apoptosis of prostatic cancer cells. *Neoplasia* 5:347–61.

542. Zhu M-L, Kyprianou N (2010) Role of androgens and the androgen receptor in epithelial-mesenchymal transition and invasion of prostate cancer cells. *FASEB J* 24:769–77.

543. Henriet P, Gaide Chevronnay HP, Marbaix E (2012) The endocrine and paracrine control of menstruation. *Mol Cell Endocrinol* 358:197–207.

544. Gaide Chevronnay HP et al. (2012) Regulation of matrix metalloproteinases activity studied in human endometrium as a paradigm of cyclic tissue breakdown and regeneration. *Biochim Biophys Acta* 1824:146–56.

545. Li B-Y et al. (2007) Dual androgen-response elements mediate androgen regulation of MMP-2 expression in prostate cancer cells. *Asian J Androl* 9:41–50.

546. Pang S-T et al. (2004) Regulation of matrix metalloproteinase 13 expression by androgen in prostate cancer. *Oncol Rep* 11:1187–92.

547. Mountain DJH et al. (2013) Androgens regulate MMPs and the cellular processes of intimal hyperplasia. *J Surg Res*.

548. Gilliver SC, Ruckshanthi JPD, Atkinson SJ, Ashcroft GS (2007) Androgens influence expression of matrix proteins and proteolytic factors during cutaneous wound healing. *Lab Invest* 87:871–81.

549. Lai J-J et al. (2009) Monocyte/macrophage androgen receptor suppresses cutaneous wound healing in mice by enhancing local TNF-alpha expression. *J Clin Invest* 119:3739–51.

550. Ashcroft GS, Mills SJ (2002) Androgen receptor-mediated inhibition of cutaneous wound healing. *J Clin Invest* 110:615–24.

551. Gilliver SC, Ashworth JJ, Mills SJ, Hardman MJ, Ashcroft GS (2006) Androgens modulate the inflammatory response during acute wound healing. *J Cell Sci* 119:722–32.

552. Wilgus TA (2008) Immune cells in the healing skin wound: influential players at each stage of repair. *Pharmacol Res* 58:112–6.

553. Midwood KS, Williams LV, Schwarzbauer JE (2004) Tissue repair and the dynamics of the extracellular matrix. *Int J Biochem Cell Biol* 36:1031–7.

554. Laplante AF, Germain L, Auger FA, Moulin V (2001) Mechanisms of wound reepithelialization: hints from a tissue-engineered reconstructed skin to long-standing questions. *FASEB J* 15:2377–89.

555. Ashcroft GS, Roberts AB (2000) Loss of Smad3 modulates wound healing. *Cytokine Growth Factor Rev* 11:125–31.

556. Rajkumar VS et al. (2006) Platelet-derived growth factor-beta receptor activation is essential for fibroblast and pericyte recruitment during cutaneous wound healing. *Am J Pathol* 169:2254–65.

557. Gao Z et al. (2005) Deletion of the PDGFR-beta gene affects key fibroblast functions important for wound healing. *J Biol Chem* 280:9375–89.

558. Babic AM, Chen CC, Lau LF (1999) Fisp12/mouse connective tissue growth factor mediates endothelial cell adhesion and migration through integrin alphavbeta3, promotes endothelial cell survival, and induces angiogenesis in vivo. *Mol Cell Biol* 19:2958–66.

559. Plouët J, Schilling J, Gospodarowicz D (1989) Isolation and characterization of a newly identified endothelial cell mitogen produced by AtT-20 cells. *EMBO J* 8:3801–6.

560. Ferrara N, Henzel WJ (1989) Pituitary follicular cells secrete a novel heparin-binding growth factor specific for vascular endothelial cells. *Biochem Biophys Res Commun* 161:851–8.

561. Marinescu VD, Kohane IS, Riva A (2005) MAPPER: a search engine for the computational identification of putative transcription factor binding sites in multiple genomes. *BMC Bioinformatics* 6:79.

562. Shang Y, Myers M, Brown M (2002) Formation of the Androgen Receptor Transcription Complex. *Mol Cell* 9:601–610.

563. Zentner GE, Scacheri PC (2012) The chromatin fingerprint of gene enhancer elements. *J Biol Chem* 287:30888–96.

564. Conley AJ et al. (2013) Modulation of higher-primate adrenal androgen secretion with estrogen-alone or estrogen-plus-progesterone intervention. *Menopause* 20:322–8.

565. Horton R (1992) Dihydrotestosterone is a peripheral paracrine hormone. *J Androl* 13:23–7.

566. Critchley HOD, Kelly RW, Baird DT, Brenner RM (2006) Regulation of human endometrial function: mechanisms relevant to uterine bleeding. *Reprod Biol Endocrinol* 4 Suppl 1:S5.

567. Leyendecker G (2002) Endometriosis results from the dislocation of basal endometrium. *Hum Reprod* 17:2725–2736.

568. Smith O, Jabbour H, Critchley H (2007) Cyclooxygenase enzyme expression and E series prostaglandin receptor signalling are enhanced in heavy menstruation. *Hum Reprod* 22:1450–1456.

569. Beaumont H, Augood C, Duckitt K, Lethaby A (2002) Danazol for heavy menstrual bleeding. *Cochrane database Syst Rev*:CD001017.

570. Maybin JA et al. (2011) The expression and regulation of adrenomedullin in the human endometrium: a candidate for endometrial repair. *Endocrinology* 152:2845–56.

571. Vermeulen A (1976) The hormonal activity of the postmenopausal ovary. *J Clin Endocrinol Metab* 42:247–53.

572. Grönroos M, Klemi P, Salmi T, Rauramo L, Punnonen R (2012) Ovarian production of estrogens in postmenopausal women. *Int J Gynaecol Obstet* 18:93–8.

573. Ashcroft GS, Greenwell-Wild T, Horan MA, Wahl SM, Ferguson MW (1999) Topical estrogen accelerates cutaneous wound healing in aged humans associated with an altered inflammatory response. *Am J Pathol* 155:1137–46.

574. Engeland CG, Sabzehei B, Marucha PT (2009) Sex hormones and mucosal wound healing. *Brain Behav Immun* 23:629–35.

575. Campbell L et al. (2010) Estrogen promotes cutaneous wound healing via estrogen receptor beta independent of its antiinflammatory activities. *J Exp Med* 207:1825–33.

576. McCarthy M (1997) Oestrogen accelerates wound healing in postmenopausal women. *Lancet* 350:1301.

577. Marbaix E, Donnez J, Courtoy PJ, Eeckhout Y (1992) Progesterone regulates the activity of collagenase and related gelatinases A and B in human endometrial explants. *Proc Natl Acad Sci U S A* 89:11789–93.

578. Marbaix E et al. (1995) The expression of interstitial collagenase in human endometrium is controlled by progesterone and by oestradiol and is related to menstruation. *Biochem J* 305 (Pt 3:1027–30.

579. Schatz F, Papp C, Toth-Pal E, Lockwood CJ (1994) Ovarian steroid-modulated stromelysin-1 expression in human endometrial stromal and decidual cells. *J Clin Endocrinol Metab* 78:1467–72.

580. Salo T, Mäkelä M, Kylmäniemi M, Autio-Harmainen H, Larjava H (1994) Expression of matrix metalloproteinase-2 and -9 during early human wound healing. *Lab Invest* 70:176–82.

581. Matsuzaki S, Darcha C (2012) Epithelial to mesenchymal transition-like and mesenchymal to epithelial transition-like processes might be involved in the pathogenesis of pelvic endometriosis. *Hum Reprod* 27:712–21.

582. Demir AY (2004) Menstrual effluent induces epithelial-mesenchymal transitions in mesothelial cells. *Hum Reprod* 19:21–29.

583. Smith SK (2001) Regulation of angiogenesis in the endometrium. *Trends Endocrinol Metab* 12:147–151.

584. Armulik A, Abramsson A, Betsholtz C (2005) Endothelial/pericyte interactions. *Circ Res* 97:512–23.

585. Morelli SS, Rameshwar P, Goldsmith LT (2013) Experimental evidence for bone marrow as a source of nonhematopoietic endometrial stromal and epithelial compartment cells in a murine model. *Biol Reprod* 89:7.

586. Dahlem T, Cho S, Spangrude GJ, Weis JJ, Weis JH (2012) Overexpression of Snai3 suppresses lymphoid- and enhances myeloid-cell differentiation. *Eur J Immunol* 42:1038–43.

587. Pioli PD, Dahlem TJ, Weis JJ, Weis JH (2013) Deletion of snai2 and snai3 results in impaired physical development compounded by lymphocyte deficiency. *PLoS One* 8:e69216.

588. Anaf V (2000) Smooth muscles are frequent components of endometriotic lesions. *Hum Reprod* 15:767–771.

589. Maruyama T, Yoshimura Y (2012) Stem cell theory for the pathogenesis of endometriosis. *Front Biosci* 4:2854–63.

590. Zhang L et al. (2013) Hypoxia induces epithelial-mesenchymal transition via activation of SNAI1 by hypoxia-inducible factor -1α in hepatocellular carcinoma. *BMC Cancer* 13:108.

591. Salnikov A V et al. (2012) Hypoxia induces EMT in low and highly aggressive pancreatic tumor cells but only cells with cancer stem cell characteristics acquire pronounced migratory potential. *PLoS One* 7:e46391.

592. Ozbudak IH, Karaveli S, Simsek T, Erdogan G, Pestereli E (2008) Neoangiogenesis and expression of hypoxia-inducible factor 1alpha, vascular endothelial growth factor, and glucose transporter-1 in endometrioid type endometrium adenocarcinomas. *Gynecol Oncol* 108:603–8.

593. Moen I et al. (2009) Hyperoxic treatment induces mesenchymal-to-epithelial transition in a rat adenocarcinoma model. *PLoS One* 4:e6381.

594. Birmachu W et al. (2007) Transcriptional networks in plasmacytoid dendritic cells stimulated with synthetic TLR 7 agonists. *BMC Immunol* 8:26.

Appendix

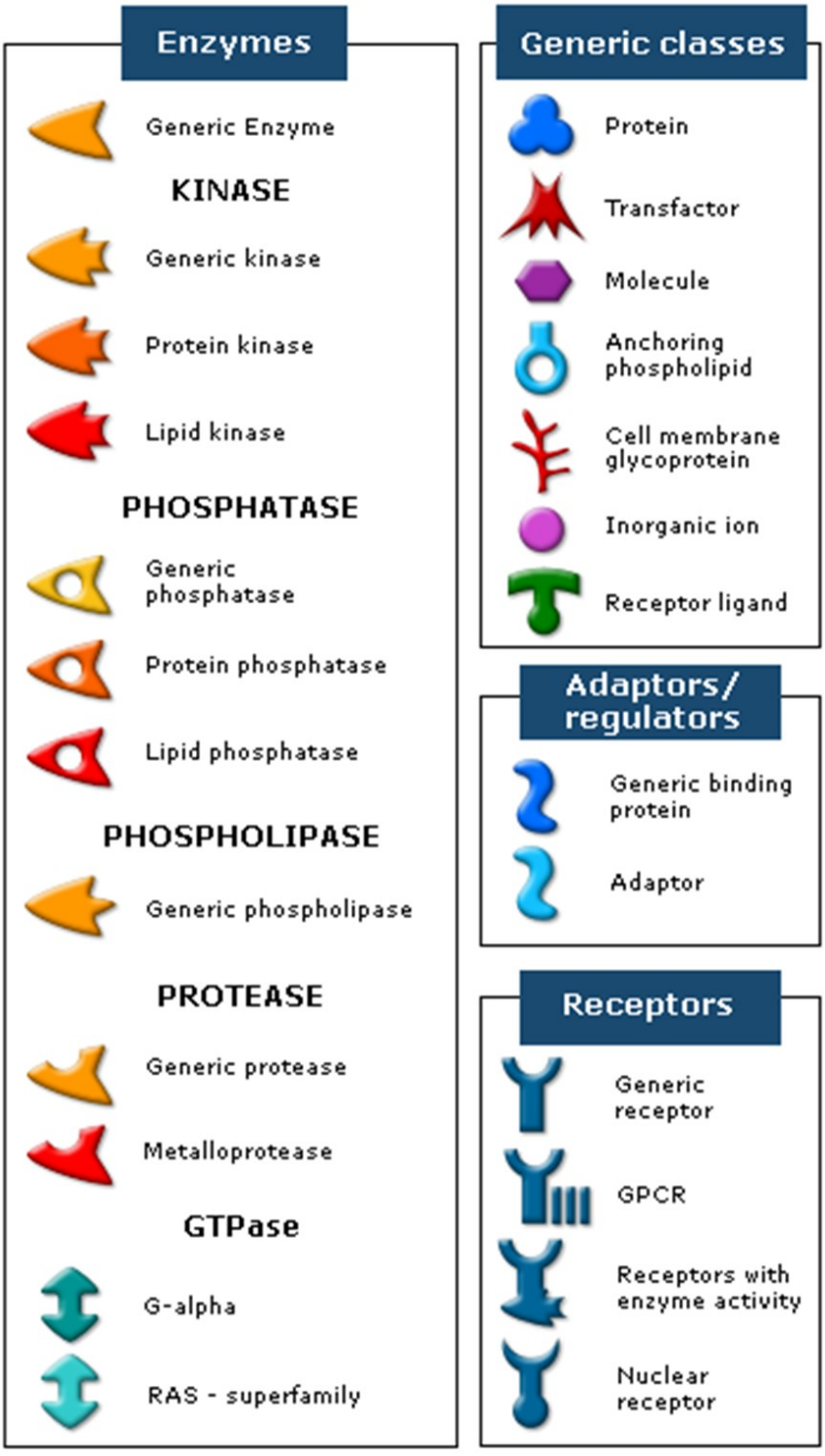

Supplementary Figure 1. Metacore network symbols. Adapted from (594).

Appendix.

Symbol	Description	Gene names	Gene Name used in Metacore™ analysis	Unigene	Refseq
Ahnak	AHNAK nucleoprotein (desmoyokin)	1110004P15Rik/2310047C17Rik/AA589382/AV091586/DY6	-	Mm.203866	NM_001039959
Akt1	Thymoma viral proto-oncogene 1	Akt/PKB/PKB/Akt/PKBalpha/Rac	AKT(PKB)	Mm.6645	NM_009652
Bmp1	Bone morphogenetic protein 1	Pcp/Tld	BMP1	Mm.27757	NM_009755
Bmp7	Bone morphogenetic protein 7	OP1	BMP7	Mm.595	NM_007557
Cald1	Caldesmon 1	4833423D12Rik/AI195384/AV071549/AW536160/C920027I18Rik/MGC30319	-	Mm.308134	NM_145575
Camk2n1	Calcium/calmodulin-dependent protein kinase II inhibitor 1	1810006K23Rik/AI848599/AI891706	-	Mm.41603	NM_025451
Cav2	Caveolin 2	AI447843	-	Mm.396075	NM_016900
Cdh1	Cadherin 1	AA960649/Ecad/L-CAM/MGC107495/UVO/Um	E-cadherin	Mm.35605	NM_009864
Cdh2	Cadherin 2	CDHN/N-cadherin/Ncad	N-cadherin	Mm.257437	NM_007664
Col1a2	Collagen, type I, alpha 2	AA960264/AI325291/Col1a-2/Cola-2/Cola2/oim	Collagen I	Mm.277792	NM_007743
Col3a1	Collagen, type III, alpha 1	AW550625/Col3a-1/KIAA4231/MMS10-W/Ms10w/mKIAA4231	Collagen III	Mm.249555	NM_009930
Col5a2	Collagen, type V, alpha 2	1110014L14Rik/D230017N05	Collagen V	Mm.10299	NM_007737
Ctnnb1	Catenin (cadherin associated protein), beta 1	Bfc/Catnb/Mesc	β-catenin	Mm.291928	NM_007614
Dsc2	Desmocollin 2	AW228162/Dsc2a/Dsc2b	-	Mm.280547	NM_013505
Dsp	Desmoplakin	2300002E22Rik/5730453H04Rik/AA407887/AA407888/AW109828/DP	-	Mm.355327	NM_023842

Appendix.

Symbol	Description	Gene names	Gene Name used in Metacore™ analysis	Unigene	Refseq
Egfr	Epidermal growth factor receptor	9030024J15Rik/AI552599/Erbb/Errp/Wa5/wa-2/wa2	EGFR	Mm.8534	NM_007912
Erbb3	V-erb-b2 erythroblastic leukemia viral oncogene homolog 3 (avian)	C76256/Erbb-3/Erbb3r/Her3/MGC117742	-	Mm.373043	NM_010153
Esr1	Estrogen receptor 1 (alpha)	AA420328/AU041214/ER-alpha/ER[a]/ERa/ERalpha/ESR/Estr/Estra/Nr3a1	ESR	Mm.9213	NM_007956
F11r	F11 receptor	9130004G24/AA638916/ESTM33/JAM/JAM-1/JAM-A/Jcam/Jcam1/Ly106	-	Mm.294882	NM_172647
Fgfbp1	Fibroblast growth factor binding protein 1	FGF-BP	-	Mm.46053	NM_008009
Fn1	Fibronectin 1	E330027I09/Fn/Fn-1/MGC117493	Fibronectin	Mm.193099	NM_010233
Foxc2	Forkhead box C2	Fkh14/Hfhbf3/MFH-1/Mfh1	FOXC1/2	Mm.14092	NM_013519
Fzd7	Frizzled homolog 7 (Drosophila)	Fz7	Frizzled	Mm.297906	NM_008057
Gng11	Guanine nucleotide binding protein (G protein), gamma 11	0610037B21Rik	-	Mm.25547	NM_025331
Gsc	Goosecoid homeobox	-	-	Mm.129	NM_010351
Gsk3b	Glycogen synthase kinase 3 beta	7330414F15Rik/8430431H08Rik/C86142/GSK-3/GSK-3beta/GSK3	-	Mm.394930	NM_019827
Igfbp4	Insulin-like growth factor binding protein 4	AI875747/Deb2/IGFBP-4	-	Mm.233799	NM_010517
Il1rn	Interleukin 1 receptor antagonist	F630041P17Rik/IL-1ra	-	Mm.882	NM_031167
Ilk	Integrin linked kinase	AA511515/ESTM24	ILK	Mm.274846	NM_010562

Appendix.

Symbol	Description	Gene names	Gene Name used in Metacore™ analysis	Unigene	Refseq
Itga5	Integrin alpha 5 (fibronectin receptor alpha)	Cd49e/Fnra/VLA5	-	Mm.16234	NM_010577
Itgav	Integrin alpha V	1110004F14Rik/2610028E01Rik/CD51/D430040G12Rik	-	Mm.227	NM_008402
Itgb1	Integrin beta 1 (fibronectin receptor beta)	4633401G24Rik/AA409975/AA960159/CD29/ENSMUSG00000051907/Fnrb/Gm9863/gpIIa	alpha-8/beta-1 integrin	Mm.263396	NM_010578
Jag1	Jagged 1	Htu/Ozz/Ser-1	Jagged1	Mm.22398	NM_013822
Krt14	Keratin 14	AI626930/K14/Krt-1.14/Krt1-14	-	Mm.439898	NM_016958
Krt19	Keratin 19	AI663979/EndoC/K19/Krt-1.19/Krt1-19/MGC25344	Keratin 19	Mm.439699	NM_008471
Krt7	Keratin 7	D15Wsu77e/K7/Krt2-7/MGC11625	-	Mm.289377	NM_033073
Mitf	Microphthalmia-associated transcription factor	Bhlhe32/MGC124309/MGC124310/Vitiligo/Wh/bw/mi/vit	MITF	Mm.333284	NM_008601
Mmp2	Matrix metallopeptidase 2	Clg4a/GelA/MMP-2	MMP-2	Mm.29564	NM_008610
Mmp3	Matrix metallopeptidase 3	SLN-1/SLN1/STR-1/Stmy1/Str1	Stromelysin-1	Mm.4993	NM_010809
Mmp9	Matrix metallopeptidase 9	AW743869/B/MMP9/Clg4b/MMP-9/pro-MMP-9	MMP-9	Mm.4406	NM_013599
Msn	Moesin	C78546	-	Mm.138876	NM_010833
Mst1r	Macrophage stimulating 1 receptor (c-met-related tyrosine kinase)	CD136/CDw136/Fv-2/Fv2/PTK8/Ron/STK	-	Mm.3901	NM_009074
Mtap1b	Microtubule-associated protein 1B	A230055D22/AI843217/LC1/MAP1B/MAP5/MGC169657/MGC169658/Mtap-5/Mtap5	-	Mm.4173	NM_008634

Appendix.

Symbol	Description	Gene names	Gene Name used in Metacore™ analysis	Unigene	Refseq
Nodal	Nodal	Tg.413d	NODAL	Mm.57195	NM_013611
Notch1	Notch gene homolog 1 (Drosophila)	9930111A19Rik/Mis6/Tan1/lin-12	Notch (and Notch1 receptor)	Mm.290610	NM_008714
Nudt13	Nudix (nucleoside diphosphate linked moiety X)-type motif 13	4933433B15Rik	-	Mm.317636	NM_026341
Ocln	Occludin	AI503564/Ocl	Occludin	Mm.4807	NM_008756
Pdgfrb	Platelet derived growth factor receptor, beta polypeptide	AI528809/CD140b/Pdgfr	PDGF receptor	Mm.4146	NM_008809
Plek2	Pleckstrin 2	-	-	Mm.103380	NM_013738
Pppde2	PPPDE peptidase domain containing 2	AI427858/AI850401/D15Wsu75e/Fam152b	-	Mm.474453	NM_134095
Ptk2	PTK2 protein tyrosine kinase 2	FAK/FRNK/Fadk/KIAA4203/mKIAA4203	FAK1	Mm.254494	NM_007982
Ptp4a1	Protein tyrosine phosphatase 4a1	AA415290/AU019864/C130021B01/MGC10 2117/MGC25304/Prl-1	-	Mm.374437	NM_011200
Rac1	RAS-related C3 botulinum substrate 1	AL023026/D5Ertd559e	Rac1	Mm.292510	NM_009007
Rgs2	Regulator of G-protein signaling 2	GOS8		Mm.28262	NM_009061
Serpine1	Serine (or cysteine) peptidase inhibitor, clade E, member 1	PAI-1/PAI1/Planh1	-	Mm.250422	NM_008871
Sip1	Survival of motor neuron protein interacting protein 1	1700012N19Rik/Gemin2	SIP1 (ZFHX1B)	Mm.35353	NM_025656
Smad2	MAD homolog 2 (Drosophila)	Madh2/Madr2	SMAD2	Mm.391091	NM_010754
Snai1	Snail homolog 1 (Drosophila)	AI194338/Sna/Sna1/Snail/Snail1	SNAIL1	Mm.2093	NM_011427

Appendix.

Symbol	Description	Gene names	Gene Name used in Metacore™ analysis	Unigene	Refseq
Snai2	Snail homolog 2 (Drosophila)	Slug/Slugh/Snail2	SLUG	Mm.4272	NM_011415
Snai3	Snail homolog 3 (Drosophila)	AI643946/Smuc/Zfp293	-	Mm.103673	NM_013914
Sox10	SRY-box containing gene 10	Dom/Sox21	-	Mm.276739	NM_011437
Sparc	Secreted acidic cysteine rich glycoprotein	AA517111/BM-40	Osteonectin	Mm.291442	NM_009242
Spp1	Secreted phosphoprotein 1	2AR/Apl-1/BNSP/BSPI/Bsp/ETA-1/Eta/OP/Opn/Opnl/Ric/Spp-1	Osteopontin	Mm.288474	NM_009263
Stat3	Signal transducer and activator of transcription 3	1110034C02Rik/AW109958/Aprf	-	Mm.249934	NM_011486
Steap1	Six transmembrane epithelial antigen of the prostate 1	2410007B19Rik/Prss24/Steap	-	Mm.85429	NM_027399
Tcf4	Transcription factor 4	5730422P05Rik/ASP-I2/E2-2/E2.2/ITF-2/ITF-2b/ITF2/ME2/MITF-2A/MITF-2B/SEF-2/SEF2/SEF2-1/TFE/Tcf-4/bHLHb19	ITF2	Mm.4269	NM_013685
Tcf7l1	Transcription factor 7-like 1 (T-cell specific, HMG box)	Tcf-3/Tcf3/bHLHb21	-	Mm.440067	NM_009332
Tfpi2	Tissue factor pathway inhibitor 2	AV000670/PP5/TFPI-2	TFPI-2	Mm.25612	NM_009364
Tgfb1	Transforming growth factor, beta 1	TGF-beta1/TGFbeta1/Tgfb/Tgfb-1	TGF Beta	Mm.248380	NM_011577
Tgfb2	Transforming growth factor, beta 2	BB105277/Tgf-beta2/Tgfb-2	TGF beta	Mm.18213	NM_009367
Tgfb3	Transforming growth factor, beta 3	MGC118722/Tgfb-3	TGF beta	Mm.3992	NM_009368
Timp1	Tissue inhibitor of metalloproteinase 1	Clgi/MGC7143/TIMP-1/Timp	TIMP1	Mm.8245	NM_011593

Appendix.

Symbol	Description	Gene names	Gene Name used in Metacore™ analysis	Unigene	Refseq
Tmeff1	Transmembrane protein with EGF-like and two follistatin-like domains 1	A830033E11/M7365/Tr1	-	Mm.422686	NM_021436
Tmem132a	Transmembrane protein 132A	6720481D13Rik/Hspa5bp1/Orai1/R74613	-	Mm.27387	NM_133804
Tspan13	Tetraspanin 13	1100001I23Rik/NET-6/Tm4sf13	-	Mm.254663	NM_025359
Twist1	Twist homolog 1 (Drosophila)	AA960487/M-Twist/MGC103391/Pde/Ska10/Ska<m10Jus>/Twist/bHLHa38/pdt	TWIST1	Mm.3280	NM_011658
Vcan	Versican	5430420N07Rik/9430051N09/Cspg2/DPEAAE/NG2/PG-M/PG-M(V0)/PG-M(V1)/hdf	Versican proteoglycan	Mm.158700	NM_001081249
Vim	Vimentin	MGC102095	Vimentin	Mm.268000	NM_011701
Vps13a	Vacuolar protein sorting 13A (yeast)	4930425F11/4930516E05Rik/4930543C13Rik/9930023P20/CHAC/D330038K10Rik/KIAA0986/chorein/mKIAA0986	-	Mm.211963	NM_173028
Wnt11	Wingless-related MMTV integration site 11	-	WNT	Mm.22182	NM_009519
Wnt5a	Wingless-related MMTV integration site 5A	8030457G12Rik/Wnt-5a	WNT	Mm.287544	NM_009524
Wnt5b	Wingless-related MMTV integration site 5B	AW545702/Wnt-5b	WNT	Mm.321818	NM_009525
Zeb1	Zinc finger E-box binding homeobox 1	3110032K11Rik/AREB6/BZP/MEB1/Nil2/Tcf18/Tcf8/ZEB/Zfhep/Zfhx1a/Zfx1a/Zfx1ha/[delta]EF1	TCF8	Mm.3929	NM_011546
Zeb2	Zinc finger E-box binding homeobox 2	9130203F04Rik/D130016B08Rik/SIP1/Zfhx1b/Zfx1b/Zfxh1b/mKIAA0569	-	Mm.440702	NM_015753

Supplementary Table 1: EMT array gene list.

Appendix.

Symbol	Description	Gene Names	Gene Name used in Metacore™ analysis	Unigene	Refseq
Akt1	Thymoma viral proto-oncogene 1	Akt/PKB/PKB/Akt/PKBalpha/Rac	AKT (PKB)	Mm.6645	NM_009652
Ang	Angiogenin, ribonuclease, RNase A family, 5	AI385586/Ang1/Rnase5/Rnase5a	-	N/A	NM_007447
Angpt1	Angiopoietin 1	1110046O21Rik/Ang-1/Ang1	Angiopoietin 1	Mm.309336	NM_009640
Angpt2	Angiopoietin 2	Agpt2/Ang-2/Ang2	Angiopoietin 2	Mm.439874	NM_007426
Anpep	Alanyl (membrane) aminopeptidase	Apn/Cd13/Lap-1/Lap1/P150	-	Mm.4487	NM_008486
Bai1	Brain-specific angiogenesis inhibitor 1	B830018M07Rik/KIAA4089/R75078/mKIAA4089	-	Mm.43133	NM_174991
Ccl11	Chemokine (C-C motif) ligand 11	Scya11/eotaxin	Eotaxin	Mm.4686	NM_011330
Ccl2	Chemokine (C-C motif) ligand 2	AI323594/HC11/JE/MCAF/MCP-1/MCP1/SMC-CF/Scya2/Sigje	-	Mm.290320	NM_011333
Cdh5	Cadherin 5	7B4/AA408225/Cd144/VE-Cad/VECD/VEcad/Vec	VE-cadherin	Mm.21767	NM_009868
Col18a1	Collagen, type XVIII, alpha 1	-	Endostatin	Mm.4352	NM_009929
Col4a3	Collagen, type IV, alpha 3	[a]3(IV)/alpha3(IV)	Collagen IV	Mm.389135	NM_007734
Csf3	Colony stimulating factor 3 (granulocyte)	Csfg/G-CSF/MGI-IG	-	Mm.1238	NM_009971
Ctgf	Connective tissue growth factor	Ccn2/Fisp12/Hcs24/fisp-12	CTGF	Mm.390287	NM_010217
Cxcl1	Chemokine (C-X-C motif) ligand 1	Fsp/Gro1/KC/Mgsa/N51/Scyb1/gro	-	Mm.21013	NM_008176
Cxcl2	Chemokine (C-X-C motif) ligand 2	CINC-2a/GROb/Gro2/MIP-2/MIP-2a/Mgsa-b/Mip2/Scyb/Scyb2	GRO-2	Mm.4979	NM_009140

Appendix.

Symbol	Description	Gene Names	Gene Name used in Metacore™ analysis	Unigene	Refseq
Cxcl5	Chemokine (C-X-C motif) ligand 5	AMCF-II/ENA-78/GCP-2/LIX/Scyb5/Scyb6	-	Mm.4660	NM_009141
Edn1	Endothelin 1	ET-1/preproET	Endothelin-1	Mm.14543	NM_010104
Efna1	Ephrin A1	AI325262/B61/Efl1/Epl1/Eplg1/Lerk1	-	Mm.15675	NM_010107
Efnb2	Ephrin B2	ELF-2/Epl5/Eplg5/Htk-L/LERK-5/Lerk5/NLERK-1	-	Mm.209813	NM_010111
Egf	Epidermal growth factor	AI790464	-	Mm.252481	NM_010113
Eng	Endoglin	AI528660/AI662476/CD105/S-endoglin	Endoglin	Mm.225297	NM_007932
Epas1	Endothelial PAS domain protein 1	HIF-2alpha/HIF2A/HLF/HRF/MOP2/bHLHe73	EPAS1/ARNT	Mm.1415	NM_010137
Ephb4	Eph receptor B4	AI042935/Htk/MDK2/Myk1/Tyro11	-	Mm.34533	NM_010144
Erbb2	V-erb-b2 erythroblastic leukemia viral oncogene homolog 2, neuro/glioblastoma derived oncogene homolog (avian)	Erbb-2/HER-2/HER2/Neu/c-erbB2/c-neu/mKIAA3023	-	Mm.290822	NM_001003817
F2	Coagulation factor II	Cf-2/Cf2/FII/thrombin	Thrombin	Mm.89048	NM_010168
F3	Coagulation factor III	AA409063/CD142/Cf-3/Cf3/TF	Tissue Factor	Mm.273188	NM_010171
Fgf1	Fibroblast growth factor 1	Dffrx/Fam/Fgf-1/Fgfa	FGF1	Mm.241282	NM_010197
Fgf2	Fibroblast growth factor 2	Fgf-2/Fgfb/bFGF	FGF2	Mm.473689	NM_008006

Appendix.

Symbol	Description	Gene Names	Gene Name used in Metacore™ analysis	Unigene	Refseq
Fgf6	Fibroblast growth factor 6	Fgf-6/HSTF-2	-	Mm.3403	NM_010204
Fgfr3	Fibroblast growth factor receptor 3	CD333/FR3/Fgfr-3/Flg-2/HBGFR/Mfr3/sam3	FGFR3	Mm.6904	NM_008010
Figf	C-fos induced growth factor	AI325264/VEGF-D/Vegfd	VEGF-D	Mm.297978	NM_010216
Flt1	FMS-like tyrosine kinase 1	AI323757/Flt-1/VEGFR-1/VEGFR1/sFlt1	VEGFR1	Mm.389712	NM_010228
Fn1	Fibronectin 1	E330027I09/Fn/Fn-1/MGC117493	Fibronectin	Mm.193099	NM_010233
Hgf	Hepatocyte growth factor	C230052L06Rik/HGF/SF/NK1/NK2/SF/HGF	HGF	Mm.267078	NM_010427
Hif1a	Hypoxia inducible factor 1, alpha subunit	AA959795/HIF1alpha/MOP1/bHLHe78	HIF1A/ARNT2	Mm.3879	NM_010431
Ifng	Interferon gamma	IFN-g/Ifg	-	Mm.240327	NM_008337
Igf1	Insulin-like growth factor 1	C730016P09Rik/Igf-1/Igf-I	IGF-1	Mm.268521	NM_010512
Il1b	Interleukin 1 beta	IL-1beta/Il-1b	-	Mm.222830	NM_008361
Il6	Interleukin 6	Il-6	IL-6	Mm.1019	NM_031168
Itgav	Integrin alpha V	1110004F14Rik/2610028E01Rik/CD51/D430040G12Rik	Alpha-V/beta-1 integrin	Mm.227	NM_008402
Itgb3	Integrin beta 3	CD61/GP3A/INGRB3/MGC159221/MGC159223	-	Mm.87150	NM_016780
Jag1	Jagged 1	Htu/Ozz/Ser-1	Jagged1	Mm.22398	NM_013822
Kdr	Kinase insert domain protein receptor	6130401C07/Flk-1/Flk1/Krd-1/Ly73/VEGFR-2/VEGFR2/sVEGFR-2	VEGFR2	Mm.285	NM_010612

Appendix.

Symbol	Description	Gene Names	Gene Name used in Metacore™ analysis	Unigene	Refseq
Lect1	Leukocyte cell derived chemotaxin 1	ChM-I	-	Mm.46561	NM_010701
Lep	Leptin	ob/obese	-	Mm.277072	NM_008493
Mapk14	Mitogen-activated protein kinase 14	CSBP2/Crk1/Csbp1/MGC102436/Mxi2/PRKM14/PRKM15/p38/p38-alpha/p38MAPK/p38a/p38alpha	p38 MAPK	Mm.311337	NM_011951
Mdk	Midkine	MK/Mek	-	Mm.906	NM_010784
Mmp14	Matrix metallopeptidase 14 (membrane-inserted)	AI325305/MT-MMP-1/MT1-MMP	MMP-14	Mm.280175	NM_008608
Mmp19	Matrix metallopeptidase 19	MGC123370	MMP-19	Mm.131266	NM_021412
Mmp2	Matrix metallopeptidase 2	Clg4a/GelA/MMP-2	MMP-2	Mm.29564	NM_008610
Mmp9	Matrix metallopeptidase 9	AW743869/B/MMP9/Clg4b/MMP-9/pro-MMP-9	MMP-9	Mm.4406	NM_013599
Nos3	Nitric oxide synthase 3, endothelial cell	2310065A03Rik/Nos-3/eNOS/ecNOS	eNOS	Mm.258415	NM_008713
Nrp1	Neuropilin 1	C530029I03/NP-1/NPN-1/Npn1/Nrp	Neuropilin	Mm.271745	NM_008737
Nrp2	Neuropilin 2	1110048P06Rik/Np-2/Np2/Npn-2/Npn2	-	Mm.266341	NM_010939
Pdgfa	Platelet derived growth factor, alpha	-	-	Mm.2675	NM_008808
Pecam1	Platelet/endothelial cell adhesion molecule 1	C85791/Cd31/MGC102160/PECAM-1/Pecam	PECAM-1	Mm.343951	NM_008816
Pgf	Placental growth factor	AI854365/PIGF/Plgf	PLGF	Mm.4809	NM_008827
Plau	Plasminogen activator, urokinase	u-PA/uPA	PLAU (UPA)	Mm.4183	NM_008873

Appendix.

Symbol	Description	Gene Names	Gene Name used in Metacore™ analysis	Unigene	Refseq
Plg	Plasminogen	AI649309/Pg	Plasminogen	Mm.971	NM_008877
Ptgs1	Prostaglandin-endoperoxide synthase 1	COX1/Cox-1/Cox-3/Pghs1	-	Mm.275434	NM_008969
Ptk2	PTK2 protein tyrosine kinase 2	FAK/FRNK/Fadk/KIAA4203/mKIAA4203	FAK1	Mm.254494	NM_007982
S1pr1	Sphingosine-1-phosphate receptor 1	AI849002/Edg1/Lpb1/S1p/S1p1	S1P1 receptor	Mm.982	NM_007901
Serpine1	Serine (or cysteine) peptidase inhibitor, clade E, member 1	PAI-1/PAI1/Planh1	-	Mm.250422	NM_008871
Serpinf1	Serine (or cysteine) peptidase inhibitor, clade F, member 1	AI195227/EPC-1/Pedf/Pedfl/Sdf3	-	Mm.2044	NM_011340
Smad5	MAD homolog 5 (Drosophila)	1110051M15Rik/AI451355/Dwf-C/Madh5/MusMLP	SMAD5	Mm.272920	NM_008541
Sphk1	Sphingosine kinase 1	1110006G24Rik/Sk1/Spk1	SPHK1	Mm.20944	NM_025367
Tbx1	T-box 1	-	-	Mm.295194	NM_011532
Tek	Endothelial-specific receptor tyrosine kinase	AA517024/Cd202b/Hyk/Tie2/tie-2	Tie2	Mm.14313	NM_013690
Tgfa	Transforming growth factor alpha	wa-1/wa1	-	Mm.137222	NM_031199
Tgfb1	Transforming growth factor, beta 1	TGF-beta1/TGFbeta1/Tgfb/Tgfb-1	TGF-beta	Mm.248380	NM_011577
Tgfb2	Transforming growth factor, beta 2	BB105277/Tgf-beta2/Tgfb-2	TGF-beta	Mm.18213	NM_009367
Tgfb3	Transforming growth factor, beta 3	MGC118722/Tgfb-3	TGF-beta	Mm.3992	NM_009368
Tgfbr1	Transforming growth factor, beta receptor I	ALK5/AU017191/Alk-5/TbetaR-I/TbetaRI	TGF-beta receptor type 1	Mm.197552	NM_009370

Appendix.

Symbol	Description	Gene Names	Gene Name used in Metacore™ analysis	Unigene	Refseq
Thbs1	Thrombospondin 1	TSP-1/TSP1/Thbs-1/tbsp1	Thrombospondin 1	Mm.4159	NM_011580
Thbs2	Thrombospondin 2	TSP2/Thbs-2	-	Mm.26688	NM_011581
Tie1	Tyrosine kinase with immunoglobulin-like and EGF-like domains 1	D430008P04Rik/TIE/tie-1	TIE	Mm.4345	NM_011587
Timp1	Tissue inhibitor of metalloproteinase 1	Clgi/MGC7143/TIMP-1/Timp	TIMP1	Mm.8245	NM_011593
Timp2	Tissue inhibitor of metalloproteinase 2	D11Bwg1104e/Timp-2	TIMP2	Mm.206505	NM_011594
Tnf	Tumor necrosis factor	DIF/MGC151434/TNF-alpha/TNFSF2/TNFalpha/Tnfa/Tnfsf1a	-	Mm.1293	NM_013693
Tnfsf12	Tumor necrosis factor (ligand) superfamily, member 12	Apo3l/Dr3l/Dr3lg/Tweak	-	Mm.344820	NM_011614
Tymp	Thymidine phosphorylase	2900072D10Rik/Ecgf1/PD-ECGF/PDECGF/Pdgfec	-	Mm.287977	NM_138302
Vegfa	Vascular endothelial growth factor A	Vegf/Vegf120/Vegf164/Vegf188/Vpf	VEGF-A	Mm.282184	NM_009505
Vegfb	Vascular endothelial growth factor B	VEGF-B/Vrf	VEGF-B	Mm.15607	NM_011697
Vegfc	Vascular endothelial growth factor C	AW228853/VEGF-C	VEGF-C	Mm.1402	NM_009506

Supplementary Table 2: Angiogenesis array gene list.